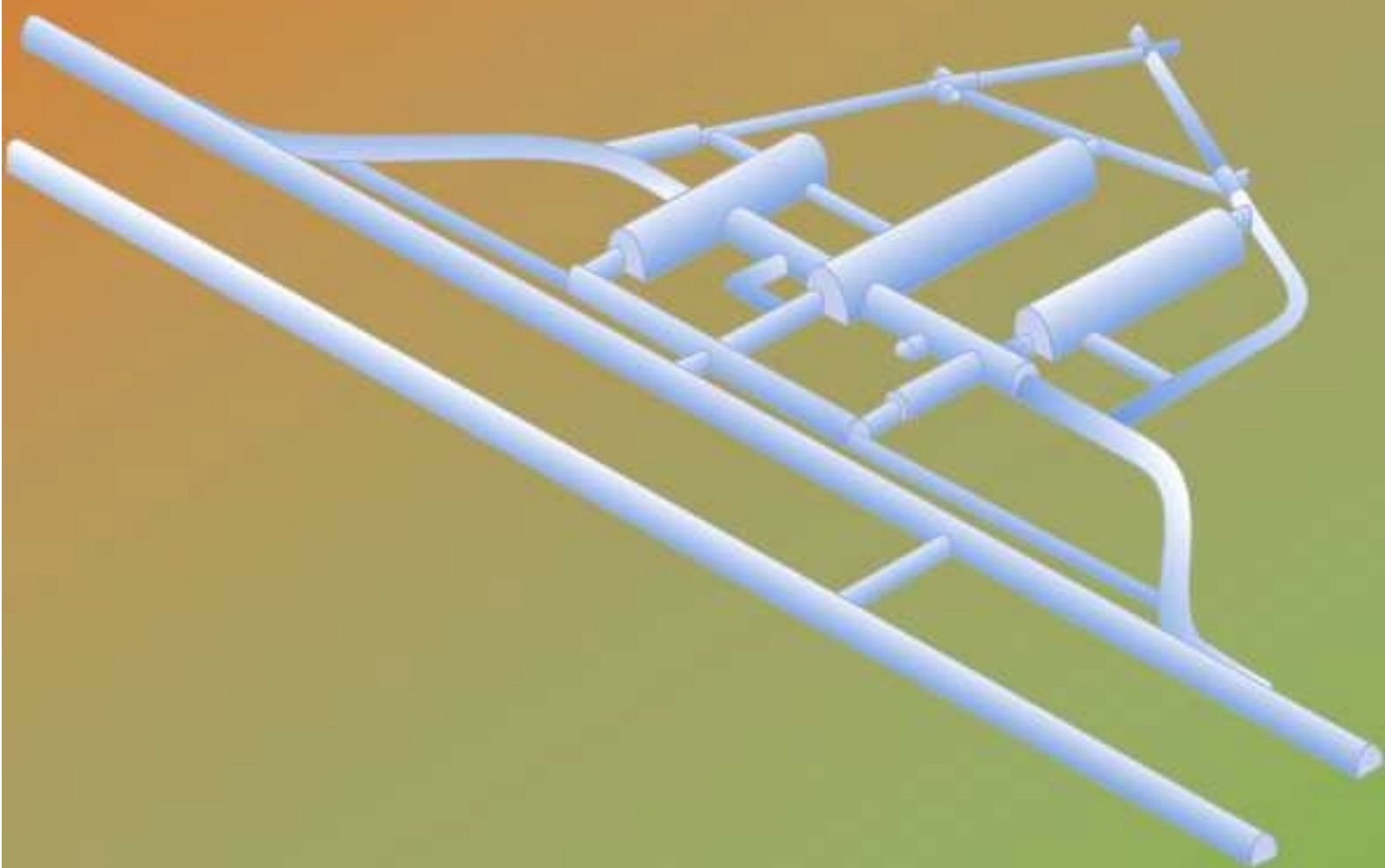# INFN - LNGS

## Laboratori Nazionali del Gran Sasso

# Annual Report 1998

# The Gran Sasso National Laboratory

The Gran Sasso National Laboratory (LNGS) is one of four INFN Laboratories. It is the largest underground laboratory in the world for experiments in particle and nuclear astrophysics and it is used as a world-wide facility by scientists (presently 450 in number) from 13 nations. The Laboratory is close to the town of L'Aquila, about 120 km from Rome. The underground laboratories are located near a ten kilometres long freeway tunnel crossing the Gran Sasso mountain. They consist of three large experimental halls, each about 100 m long, 20 m wide and 20 m high and service tunnels for a total volume of about 180,000 cubic meters. The average 1,400 m rock coverage (corresponding to 4,000 m.w.e.) gives a reduction factor of one million times in the cosmic ray flux.

The mission of the Laboratory is to host experiments that require a low background environment. In the field of particle and nuclear astrophysics their purpose are the following:
- Study of the basic constituents of matter and their interactions by non-accelerator and accelerator means;
- Study of nuclear and particle properties and processes of astrophysical interest in the Universe;
- Study of the sources, acceleration mechanism and propagation of high energy particles in the Universe.
The Laboratory hosts experiments in other disciplines, mainly geology and biology, that require low background conditions. Main research topics of the present program are: solar neutrinos physics, neutrino oscillations with solar neutrinos, neutrino oscillations with atmospheric neutrinos, search for neutrinos from stellar collapses, rare decays (double beta decay, proton decay, etc.), dark matter search, small cross section nuclear reactions of astrophysical interest, high energy cosmic rays, search for exotics (monopoles, wimps, etc.).

A complementary facility at Campo Imperatore at 2,000 m height on the mountain hosts an extensive air shower experiment (EAS-TOP) aimed toward the study of the cosmic radiation especially around the "knee" of the spectrum both in its own and in coincidence with two large underground detectors, LVD and MACRO.

During 1997 the GALLEX experiment concluded its extremely successful life. This experiment collected data for seven years. For the first time amongst the experiments of its type GALLEX was calibrated (twice) with an artificial source of neutrinos of known activity. The experiment definitely proved that the thermonuclear fusion is the mechanism producing the energy in the Sun and showed a relevant deficit in the solar neutrino flux at low energy. It is extremely difficult now, after the GALLEX results, to avoid the conclusion that neutrinos oscillate, and as a consequence have non zero masses. If

confirmed, this will be the first evidence of physics beyond the standard theory. Solar neutrino physics will be further studied at the laboratory with GNO, BOREXINO and ICARUS. GNO has started data taking. It uses the Gallex technique and mainly its apparatus will continue the research of Gallex for a long period, gradually improving the resolution. Borexino is dedicated mainly to the measure of the Be line component of the solar neutrino spectrum; a large fraction of the resources of the laboratory has been dedicated to the construction of this experiment during 1998.

The standard solar model is based on data and extrapolations; in particular the thermonuclear cross sections of the involved reactions are not measured in the relevant energy range but rather extrapolated from higher energies. The direct measurements are made very difficult by the very low values of the cross sections; LUNA is continuing its experimental program to cover this field in the low activity environment of the laboratory. The cross section of a relevant reaction has been measured. LUNA will be completed in 1999. Its successor LUNA2 has been approved and the construction of its 400 KeV accelerator started.

If neutrinos are massive, part of (or all) their mass might be of the Majorana type. The Laboratory hosts experiments employing different and complementary techniques: the Heidelberg-Moscow experiment with a sensitive mass of 11 kg of enriched Ge is the most sensitive experiment in the world; the Mibeta experiment has produced an array of 20 thermal detectors, based on $TeO_2$ crystals (340 g natural tellurium each), and is now taking data. Two other experiments DBGS and DBA are running in the laboratories.

In the search for dark matter, DAMA is collecting data and has already reached a sensitivity level unmatched by other experiments; the cryogenic experiment CRESST has concluded its R&D phase.

MACRO is a very large multi-purpose experiment, which has been systematically collecting data for several years. The limits on monopoles flux are steadily improving well below the Parker limit, many interesting data have been collected on cosmic rays. Particularly interesting are the muons originated by muon-neutrino interactions from below, in other words from neutrinos produced in the atmosphere that have crossed a large fraction of the earth and interacted in the rock under the detector. Evidence for muon neutrino oscillations has been reported, confirming the results of the SuperKamiokande experiment in Japan. LVD has continued towards the completion of the apparatus having now more than two towers working; the experiment would collect a few hundred events from a supernova explosion in the centre of the Galaxy. Interesting data on the penetrating component of the cosmic rays are continuously collected.

GIGS is a laser interferometer for geophysical purposes operating since 1994. Analysis of the data has shown interesting signals of strain episodes that are similar to the so called slow earthquakes.

A number of first generation experiments at the Gran Sasso Laboratory are approaching their closure and the scientific program for the next period must be definited. In the next phase the problem of neutrino masses will be affronted. The oscillation phenomenon must be definitely confirmed, the types of oscillations established, the masses and the mixing parameters must be determinated. The following approaches will be followed:
1) Experiments on a neutrino beam produced at CERN and aimed to detectors at Gran Sasso. The beam design has been completed by a joint INFN-CERN group; proposals for

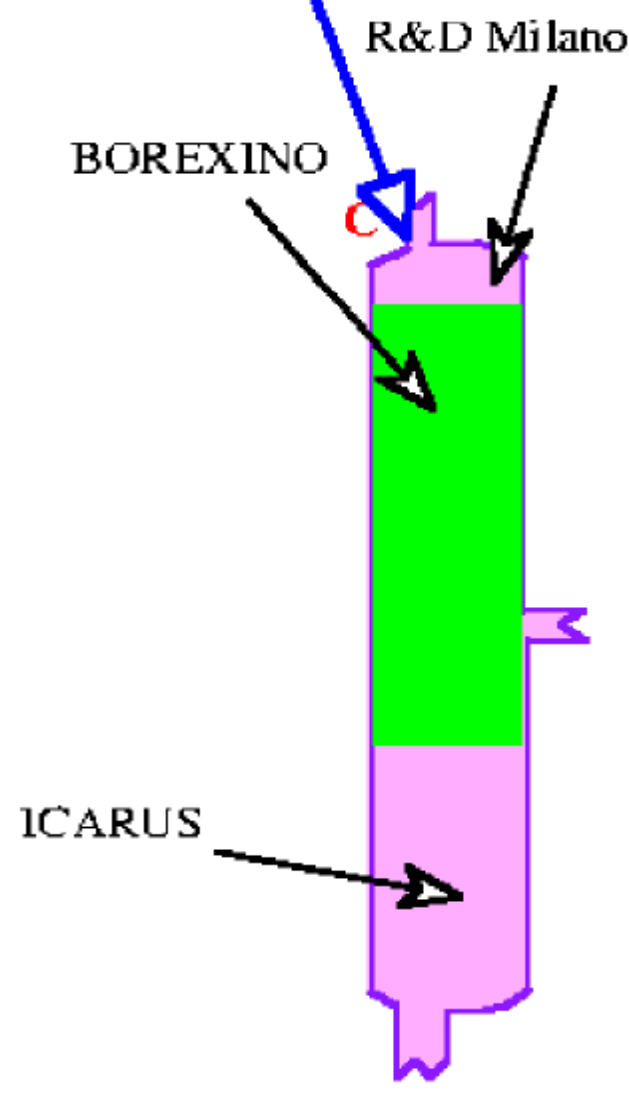appearance experiments are being prepared;
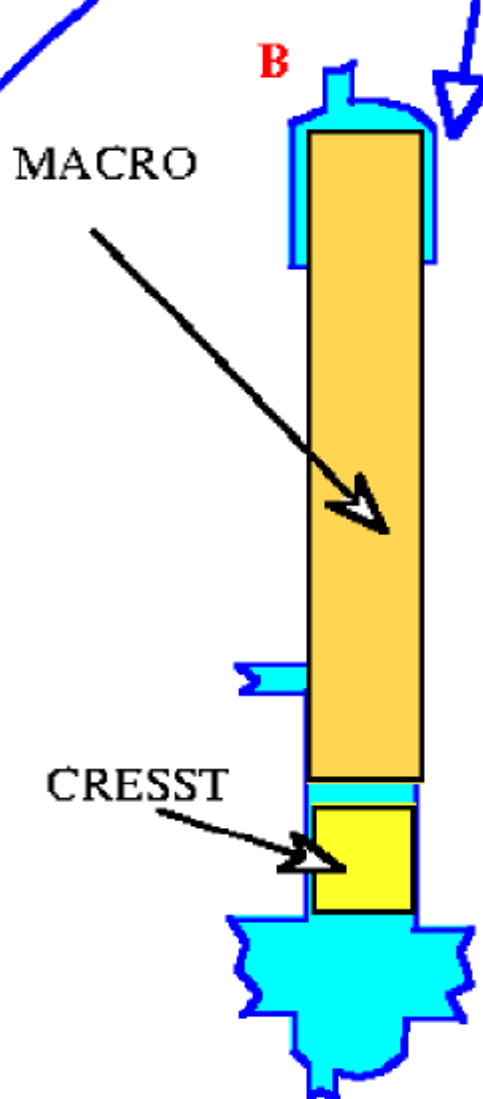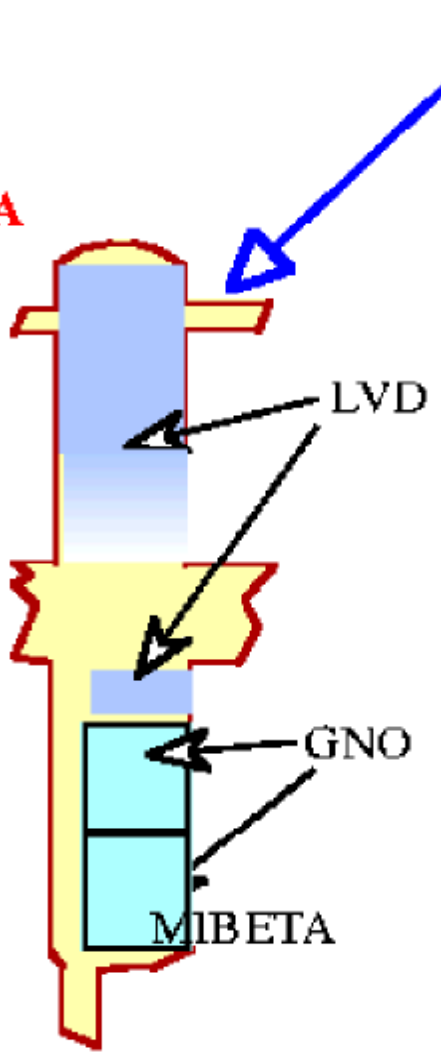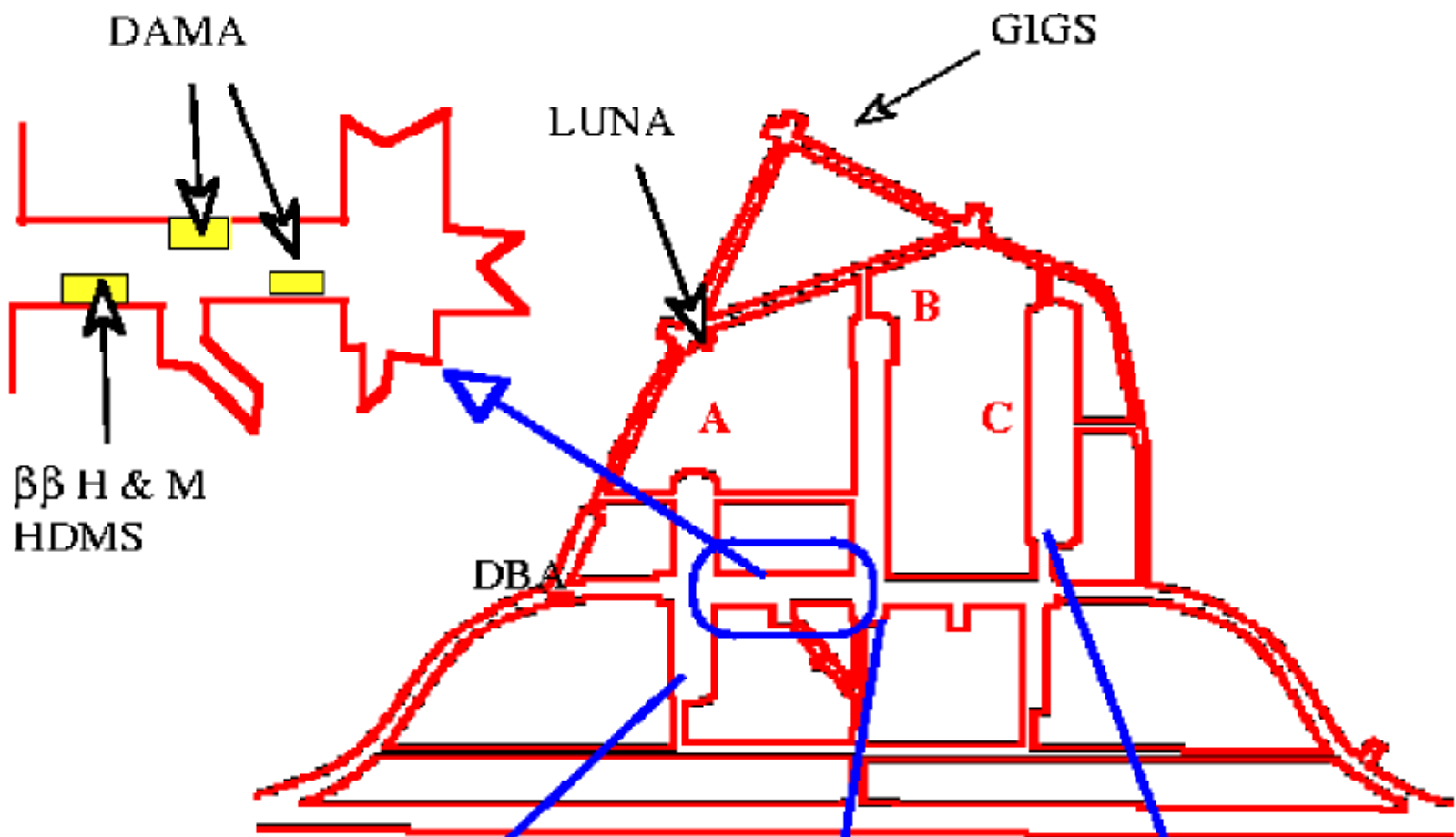2) Next generation atmospheric neutrinos experiments;
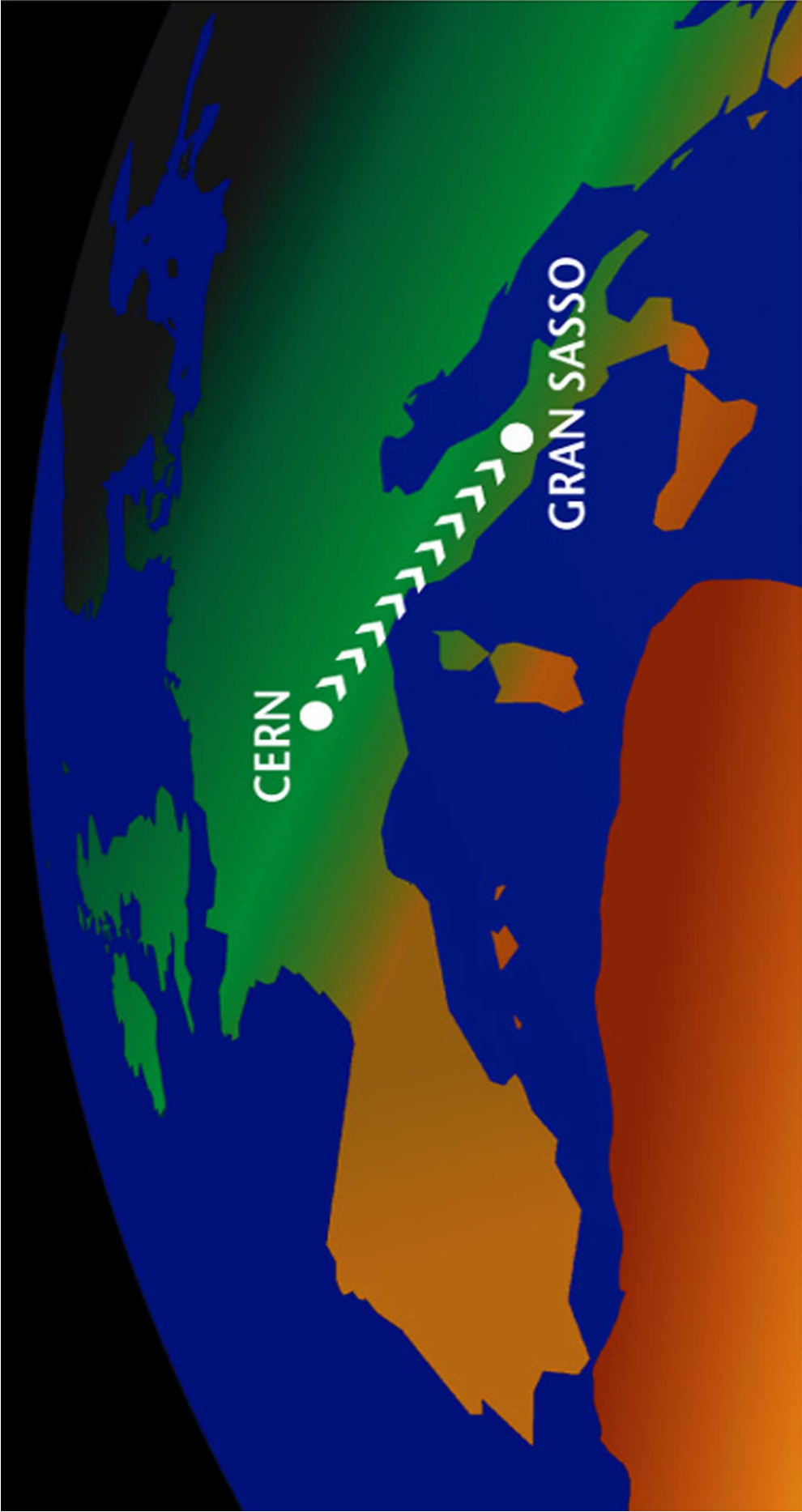3) Solar neutrino spectroscopy experiments;
4) Next generation searches for Majorana neutrino mass.

All the services and the personnel of the lab have contributed to the planning of the next phases of activity ranging from the decommissioning of some large experiments, to the preparation of the infrastructures needed for the next experiments and to the rigorous definition of the safety rules, procedures and infrastructures. In co-operation with ANAS (the Italian body responsible for freeway construction) a group of experts has been appointed to complete the project for the civil engineering and basic infrastructures of new facilities, consisting in a service tunnel and two new experimental halls, which have been already funded by the Italian Parliament. The project has been approved by the competent Ministerial body in July 1998.


Gran Sasso, July 1999.




The Director of the Laboratory
Prof. Alessandro Bettini

DAMA

GIGS

LUNA

B

A

C

DBA

ββ H & M
HDMS

R&D Milano

MACRO

BOREXINO

B

A

C

LVD

GNO

CRESST

ICARUS

MIBETA

# Contents

# BOREXINO. Solar Neutrino Physics

G. Alimonti[a], C. Arpesella[b], M. Balata[b], G. Bellini[a], J. Benziger[c],

S. Bonetti[a], A. Brigatti[a], B. Caccianiga[a], L. Cadonati[d], F.P. Calaprice[d],

G. Cecchet,[e], M. Chen,[d], L. Cser,[k], M. Deutsch[f], R. Dossi[a],

R. Eiseistein[d], F. Elisei[g], F. von Feilitzsch[h], R. Fernholz[d], R. Ford[b],

B. Freudiger[j], C. Galbiati[a], A. Garagiola[a], F. Gatti[i], S. Gazzana[b],

M.G. Giammarchi[a], D. Giugni[a], T. Goldbrunner[h], A. Golubchikov[a], A. Goretti[a],

C. Hagner[h], T. Hagner[h], W. Hampel[j], J. Handt[j], F.X. Hartmann[a],

R. von Hentig[h], G. Heusser[j], A. Ianni,[d], J. Jochum,[h], E. Kellner[h],

J. Kiko[j], T. Kirsten[j], D. Kiss[k], M. Koehler[p], G. Korga[a],

G. Korschinek[h], H. de Kerret[o], D. Kryn[o], V. Lagomarsino[i], P. LaMarche[d],

M. Laubenstein[b], F. Loeser[d], P. Lombardi[a], S. Magni[a], S. Malvezzi[a],

I. Manno[k], J. Maneira[a], G. Manuzio[i], G. Marx[k], F. Masetti[g],

U. Mazzucato[g], E. Meroni[a], P. Musico[i], H. Neder[j], M. Neff[b],

S. Nisi[b], L. Oberauer[h], M. Obolensky[o], M. Pallavicini[i], R. Parsells[d],

A. Pocar[d], L. Perasso[i], A. Perotti[e], G. Pieri[a], R.S. Raghavan[l],

G. Ranucci[a], W. Rau[j], A. Razeto[i], E. Resconi,[i], P. Saggese[a],

C. Salvo,[i], R. Scardaoni[a], S. Schönert[h], K.H. Schubeck[h], T. Shutt[d],

O. Smirnov[m], A. Sotnikov[m], R. Tartaglia,[b], G. Testera[i], B. Vogelaar[n],

S. Vitale[i], R. Walls[d], W. Wojcik[q], Y. Zakharov[j], O. Zaimidoroga[m]

[a]Dip. di Fisica dell'Università and Infn Milano - Italy

[b]Laboratori Nazionali del Gras Sasso, Assergi (Aq) - Italy

[c]Dep.t of Chemical Engineering, Princeton University - NJ USA

[d]Dep.t of Physics, Princeton University - NJ USA

[e]Dip. di Fisica dell'Università and Infn Pavia - Italy

[f]Dep.t of Physics, Massachusetts Institute of Technology - MA USA

[g]Dip. di Chimica dell'Università and Infn Perugia - Italy

[h]Technische Universität München - Germany

[i]Dip. di Fisica dell'Università and Infn Genova - Italy

[j]Max Planck Inst. für Kernphysik, Heidelberg - Germany

[k]KFKI-RMKI Research Institute for Particle & Nuclear Physics, Budapest - Hungary

[l]Bell Laboratories, Lucent Technologies, Murray Hill - NJ USA

[m]J.I.N.R. Dubna - Russia

[n]Dep.t of Physics, Virginia Polytechnic Institute - VA USA

[o]Laboratoire de Physique Corpusculaire et Cosmologie, Paris - France

[p]I.R.R.M. - EURATOM, Geel - Belgium

[q]Institute of Physics, Jagellonian University, Kracov - Poland

**Abstract**

This report describes the status of the BOREXINO experiment and summarizes the main 1998 activies. An overview of BOREXINO and of the Counting Test Facility is also given.

# 1   Introduction

BOREXINO is a low background real time detector for solar neutrino physics; it consists of a well shielded, large mass, scintillation counter. The detector sensitive volume consists of 300 tonnes of a high radiopurity liquid scintillator. The main experimental goal is the detection of the 0.862 MeV $^7$Be solar neutrino component through the $\nu e^- \rightarrow \nu e^-$ electroweak scattering reaction.

The first phase of the project consisted in the construction and operation of a Counting Test Facility (CTF) to test the BOREXINO design concept in a large scale (4.3 tonnes sensitive volume) underground detector. Special emphasis was put on the radiopurity needed to operate at the experimental threshold of 250 keV. This is required for the detection of the recoil electron spectrum generated by $^7$Be solar neutrinos [1].

---

[1]The so-called Neutrino Window of BOREXINO extends from 250 keV and 700 keV. The maximum energy of the recoil electron is 664 keV.

# 2 The Counting Test Facility

In the CTF detector 4.3 tonnes of liquid scintillator are shieldied by 1000 tonnes of high purity water and viewed by 100 photomultipliers located on a support steel structure (see fig. 1). The scintillator - a mixture of an aromatic solvent (pseudocumene, PC) and 1.5 $g/l$ of PPO as a fluor - is contained in a 0.5 $mm$ thick nylon balloon. The apparatus is coupled to a water purification system, to produce the low radioactivity water shield and to a scintillator purification system. The scintillator is purified via water extraction, distillation and gas stripping.

Finally, a 1.8 $m^2$ muon detector has been positioned on the top of the tank so as to test the muon identification capability of the CTF detection system.
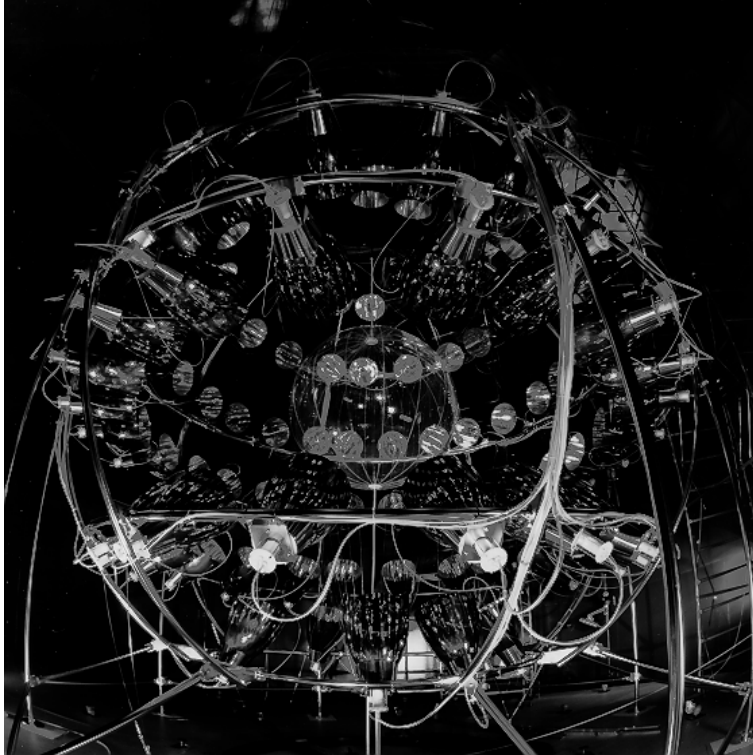


Figure 1: *The Counting Test Facility experimental setup viewed from inside the water tank. The scintillator is contained in the (1.05 m radius) nylon balloon at the center.*

The CTF experimental activities started in 1994 (installation) and continued through '95 (data taking) and '96 (source calibration program). The results of the CTF in terms of U,Th and $^{14}$C contamination (internal background of the scintillator), discussed in [2] [3], indicate that the radiopurity goals of the experiment have been reached, namely:

- Uranium chain contamination (more appropriately $^{226}$Ra) has been measured to be at most $3.5 \pm 1.3 \times 10^{-16}$ $g/g$.

3

- Thorium contamination was found to be $4.4^{+1.5}_{-1.2} \times 10^{-16}$ $g/g$.

- Carbon-14 contamination was measured to be $1.94 \pm 0.09 \times 10^{-18}$ ($^{14}C/^{12}C$). This contamination poses a special case, since Carbon is a constituent of the scintillator itself, which contains $^{12}C$. The measured value is compatible with the BOREXINO requirements for a low energy threshold of 250 keV.

To summarize, the results of the Counting Test Facility indicate that high radiopurity can be reached and that BOREXINO can be used as a solar neutrino telescope with sensitivity down to 250 keV. The information obtained with the Counting Test Facility, summarized in ref. [1],[2],[3],[4], were used to finalize the design of the BOREXINO detector, whose construction started at the end of 1996.

In Summer 1997 the Counting Test Facility was temporarily shut down and its photomultiplier system dismounted. The detector is currently being upgraded; a new PMT assembly will be used and a Radon-blocking nylon barrier will be installed between the PMT system and the scintillator containment vessel. The CTF is scheduled to be restarted in 1999.

# 3   The construction of BOREXINO

BOREXINO is an unsegmented liquid detector featuring 300 tonnes of well shielded ultrapure scintillator viewed by 2200 photomultipliers (fig. 2). The detector core is a transparent spherical vessel (Nylon Sphere, 100 $\mu$m thick), 8.5 $m$ of diameter, filled with 300 tonnes of liquid scintillator and surrounded by 1000 tonnes of a high-purity buffer liquid. The scintillator mixture is PC and PPO (1.5 $g/l$) as a fluor (as in the CTF), while the buffer liquid will be PC alone (with the possible addition of a light quencher, DMP). The photomultipliers are supported by a Stainless Steel Sphere (SSS) which also separates the inner part of the detector from the external shielding, provided by 2400 tonnes of pure water (water buffer). An additional containment vessel (Nylon film Radon barrier) is interposed between the Scintillator Nylon Sphere and the photomultipliers, with the goal of reducing Radon diffusion towards the internal part of the detector.

The outer water shield is instrumented with 200 outward-pointing photomultipliers serving as a veto for penetrating muons, the only significant remaining cosmic ray background at the Gran Sasso depth (about 3500 meters of water equivalent). In addition the 2200 photomultipliers viewing the internal part of the detector are divided in two sets: 1800 photomultipliers are equipped with light cones so that they see light only from the Nylon Sphere region, while the remaining 400 PMT's are sensitive to the total volume of the stainless steel sphere. This design greatly increases the capability of the system to identify muons crossing the PC buffer (and not the scintillator).

The BOREXINO design is based on the concept of a *graded shield* of progressively lower intrinsic radioactivity as one approaches the sensitive volume of the detector; this culminates in the use of 200 tonnes of the low background scintillator to shield the 100 tonnes innermost Fiducial Volume. In these conditions, the ultimate background will be dominated by the intrinsic contamination of the scintillator, while all backgrounds from the construction materials and external shieldings are negligible.
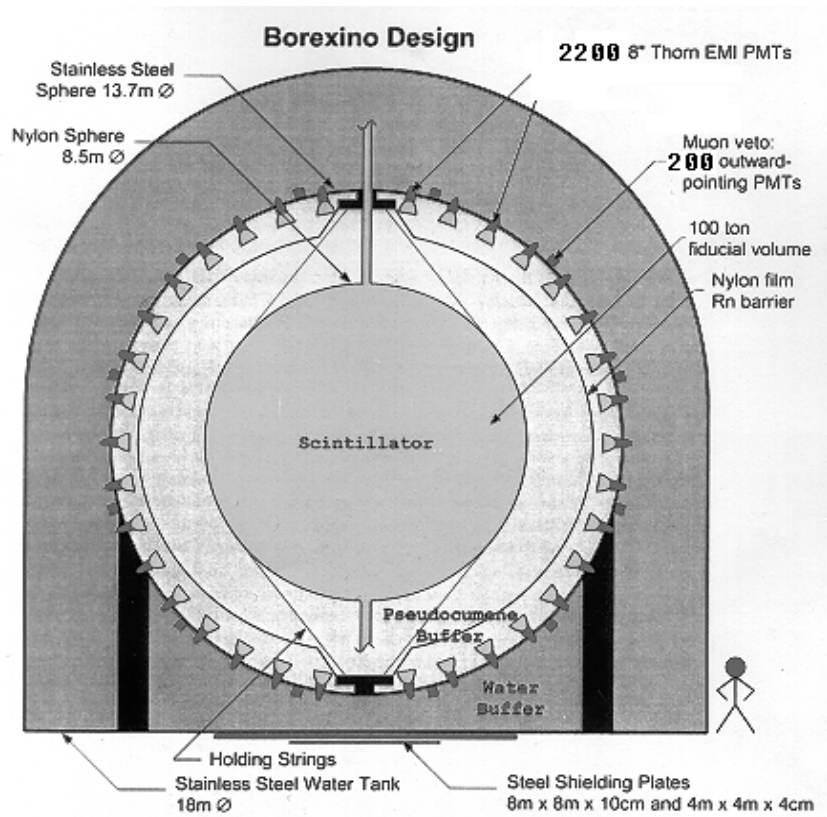
Figure 2: *Schematics of the BOREXINO detector. See text.*

In addition to the purity of the construction material and the predicted rejection efficiency of the muon system, the detection of the $^7$Be signal in the 100 tonnes of the BOREXINO Fiducial Volume requires that the intrinsic radiopurity of the scintillator be below $5 \times 10^{-16}$ $g/g$ of U,Th equivalent.

# 4   Summary of 1998 activities

During 1998 the Borexino construction has significantly moved forward and the design of most of the experiment sub-systems have been brought to completion.

- The external tank construction has been completed: during the last months of the year it has also been hydrostatically tested.

- The 93 plates which constitutes the Stainless Steel Sphere (SSS) have been cut and the holes for the PMT feedthroughs have been drilled. The surface of the plates is ready for the final treatment (pickling and passivation) before the assembling of the sphere.

- The nitrogen plant has been built at the Hall C entrance location. It allows the production of (low Radon) nitrogen for blanketing and scintillator sparging.

- The project for the so called "Big Building" (the structure surrounding the detector and containing all the ancillary facilities) has been finalized and the work has been commissioned.

- The PMT sealing design has been thoroughly studied: extensive ageing tests together with simulations have been performed in order to determine the optimum configuration. Three possible designs have been sorted out: an "open design" in which the pseudocumene is allowed to reach the electric pins while a resin prevents the contact with water and two "closed designs" in which both water and PC are kept out of the core of the PMT. These three configurations are still under test. In August 1998 a tank has been installed in preparation for a final test (the so called "two-liquid test") which will be performed on the first 50 PMTs of the chosen Borexino design. The tank consists of two concentrical cylinders, the innermost of which will contain 7 m$^3$ of pseudocumene, while the outermost will contain water. 50 PMTs will be mounted at the interface bewteen the two liquids thus simulating on a small scale the experimental conditions of Borexino.

- During 1998, the front-end electronics design for Borexino has been finalized and commissioned. Furthermore, the DAQ board first prototypes have been tested: the full production will start early in 1999. In 1998, cables for the PMTs have also been ordered.

- Extensive studies on the long term effects of materials on the transparency of pseudocumene have been carried out by the chemical laboratory at the Chemistry Department of the University in Perugia. The results of this work have indicated pickling and passivation as the best treatment for the surface of the sphere containing the PC buffer and has suggested the need for a coating layer on the PMT $\mu$-metal surface: a teflon-based covering or a phenolic resin-based painting are currently under study.

- The design of the 4 storage vessels for the pseudocumene has been brought to completion and the job has been commissioned. Moreover,important parts of the scintillator handling system have been designed. As far as pseudocumene procurement is concerned, schedule and procedures have been thoroughly discussed with ENICHEM. It was decided that the ENICHEM plant in Sarroch be modified to include a new loading station to be used by the Borexino collaboration.

- An extensive campaign of radioactivity measurements has been carried on both with the Germanium counters at the LNGS and with the Neutron activation technique in Munich. As far as the NAA is concerned, a significant upgrade of the apparatus has been realized leading to a sensitivity for Uranium down to $10^{-16}$g/g.

- During 1998, the fiber system for the PMT timing calibration has been designed. The energy calibration system (which foresees the use of radioactive sources) and

the detector stability monitoring system (which includes the possibility of using laser light at different wavelenghts to monitor the pseudocumene transparency) has been studied with the help of Montecarlo simulation programs.

- A significant effort has also been put in the optimization of the software codes for Montecarlo simulation, tracking (done with the use of GEANT4 code) and reconstruction.

# 5   List of Publications

The BOREXINO publications consist of the papers quoted in the Reference. In addition the following presentations at 1998 conferences were given:

- M. G. Giammarchi. BOREXINO: a Real Time Detector for Low Energy Solar Neutrinos. International Symposium on Lepton and Baryon Number Violation, Trento (Italy), April 1998. IoP publishing.

- E. Meroni. BOREXINO and solar neutrino physics. Frontier objects in astrophysics and particle physics. Vulcano (Italy), May 1998.

- G. Ranucci. BOREXINO: the detector and the Physics program. New Era in Neutrino Physics Symposium. Tokyo (Japan), June 1998. Ed. by Universal Academy Press.

- J. Benziger. A Scintillator Purification System for a Large Scale Solar Neutrino Experiment. $6^{th}$ International Conference on advanced technology and particle physics. Como (Italy), October 1998.

- L. Oberauer. Status of the BOREXINO Solar Neutrino Experiment. International Neutrino 98 Conference. Takayama (Japan), June 1998.

- J. C. Maneira. Sensitivity of BOREXINO to seasonal variations of the solar neutrino flux. Second Meeting on New Worlds in Astroparticle Physics. Faro (Portugal), September 1998.

- B.Caccianiga. BOREXINO and more future solar neutrino projects. $17^{th}$ International Workshop on Weak Interactions and Neutrinos. Cape Town (South Africa), January 1999.

# References

[1] G. Alimonti et al. (BOREXINO Collaboration), A large-scale low background liquid scintillator detector: the counting test facility at Gran Sasso, *N.I.M. A*, 406 (1998) 411.

[2] G. Alimonti et al. (BOREXINO Collaboration), Ultralow background measurements in a large volume underground detector, *Astroparticle Physics*, 8 (1998) 141.

[3] G. Alimonti et al. (BOREXINO Collaboration), Measurement of the $^{14}$C abundance in a low-background liquid scintillator, *Phys. Lett. B*, 422 (1998) 349.

[4] G. Alimonti et al. (BOREXINO collaboration), Light propagation in a large volume liquid scintillator, *Submitted to NIM*

# CRESST. Dark Matter Search

M. Bravin [a], M. Bruckmayer [a], C. Bucci [d], S. Cooper [c],
F.v.Feilitzsch [b], S. Giordano [a], J. Höhne [b], J. Jochum [b], V. Jörgens [d],
R. Keeling [c], H. Kraus [c], M. Loidl [a], J. Lush [a],
J. Marchese [c], O. Meier [a], P. Meunier [a], U. Nagel [b], T. Nüssle [b],
F. Pröbst [a], Y. Ramachers [c], M.L. Sarsa [b], H. Schnagl [b], W. Seidel [a*],
I. Sergeyev [a], M. Sisti [a], L. Stodolsky [a], S. Uchaikin [a], L. Zerle [a]

[a] Max-Planck-Institut für Physik, Föhringer Ring 6, D-80805 Munich, Germany
[b] Technische Universität München, Physik Department, D-85747 Munich, Germany
[c] University of Oxford, Physics Department, Oxford OX1 3RH, UK
[d] Laboratori Nazionali del Gran Sasso, I-67010 Assergi, Italy

### Abstract

We are preparing the CRESST (**C**ryogenic **R**are **E**vent **S**earch with **S**uper-conducting **T**hermometers) experiment to search for dark matter WIMPs using cryogenic detectors. In the first phase of the experiment we are using four 262 g sapphire detectors with thresholds of about 0.5 keV. In 1998 we have replaced the prototype cold box with one made of clean copper to provide low-background conditions and started the first low background run.

## 1  Introduction

The nature of the missing mass of our Universe is one of the most intriguing open questions of our time. Our theoretical understanding of the evolution of the Universe indicates that its density should be equal to the critical density ($\Omega = 1$) giving us a "closed" Universe, whereas the mass that we can observe in the form of stars, dust, and gas corresponds to only about $\Omega \sim 0.01$, leaving the other 99% as "'missing" or "dark matter". Independent of these theoretical considerations, various astronomical observations indicate that at most $\sim 10\%$ of the mass of spiral galaxies like our own is visible, with the rest then being attributed to dark matter.

---

*speaker

The theoretical study of elementary particle physics offers several hypothetical particles as candidates to make up the dark matter: axions, light but not massless neutrinos, and WIMPs (Weakly Interacting Massive Particles). However theory cannot tell us enough about any of these hypothetical particles to decide which, if any, are the dark matter. For example the WIMP is usually discussed in the framework of the minimal supersymmetric standard model (MSSM), but this model has not yet been proven to be the correct description of nature, and even within the model there are various free parameters.

Given the significance of the dark matter problem, we feel it is important that experiments are performed to search for the various candidates for the dark matter. The initial emphasis of our experiment is on low-mass WIMPs ($2 - 10\,\text{GeV}$), which are inaccessible to other experiments due to their higher threshold (see [1] and references therein). In a second step we will start a search for medium and high mass WIMPs. Due to a newly developed detector technique (simultaneous detection of scintillation light and phonons for background suppression) we may achieve an extremely high sensitivity in this mass range.

## 2 Technique for Detection of WIMPs

WIMPs could be detected via their elastic scattering on nuclei, giving nuclear recoil energies of about a keV for WIMP masses of a few GeV. We already know from previous experimental limits that WIMP scattering rates are low, less than about $1\,\text{event}$ per day in a $1\,\text{keV}$ bin in a $1\,\text{kg}$ detector. This is a very challenging experimental problem, requiring very sensitive detectors with masses in the kg range, as well as a very high purity and good shielding to reduce background from local radioactivity, with the cosmic ray background being eliminated by performing the experiment in an underground laboratory such as Gran Sasso.

Since low energy nuclei are very inefficient at producing ionization or scintillation, a low-threshold detector needs to act as a calorimeter, detecting the full nuclear recoil energy. At the Max Planck Institute of Physics and the Technical University of Munich we have developed cryogenic calorimeters using superconducting phase transition thermometers. The thermometer is a small thin film of a superconducting material (tungsten) evaporated onto the surface of a sapphire crystal. The detector is run at a temperature ($\sim 15\,\text{mK}$) where the thermometer is in the middle of its transition between the normal and superconducting phases. Here its resistance is very sensitive to the small rise in temperature caused by a recoiling nucleus. In our Munich laboratory we have been able to detect $1.5\,\text{keV}$ X-rays in a $32\,\text{g}$ sapphire crystal with a resolution of $100\,\text{eV}$ FWHM; the same type of readout gave $230\,\text{eV}$ FWHM in a $262\,\text{g}$ detector [2]. As reported below this resolution has now been improved using thermal feedback.

## 3 Detector tests

The model we have developed to describe the behaviour of our detectors indicates that we are detecting non-thermal phonons in our thermometer, before complete thermalization
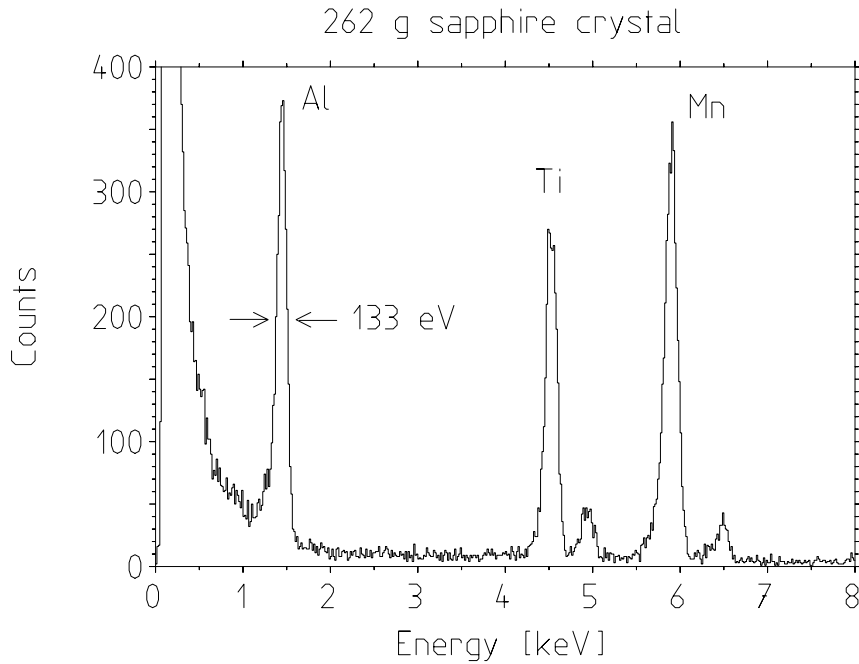
Figure 1: Uncut pulse height spectrum of one of the 262 g CRESST detectors with an X-ray fluorescence source. The rise in the spectrum at low energies is due to Auger-electrons escaping from the X-ray fluorescence source.

of the deposited energy in the sapphire absorber. This allows us to increase the absorber size without proportional loss in resolution. This has now been demonstrated. Our initial detector development was with a 32 g sapphire crystal, with which we achieved a FWHM of 100 eV for 1.5 keV X-rays. Larger detectors could not be satisfactorily tested above ground because of the high background rate. With our setup in Gran Sasso, we have been able to test our 262 g detectors. The detectors tested in 1997 had FWHM resolutions better than 300 eV for 1.5 keV X-rays and the best had 230 eV.

In order to improve long–term stability in a search for dark matter we now implemented a thermal feedback readout and introduced heater pulses for calibration. In our initial readout scheme a constant current is fed through a circuit in which the W film is in parallel with the input coil of a SQUID. When energy is deposited in the detector, the temperature and thus the resistance of the W film increases, so that a larger fraction of the current flows through the SQUID input coil, and it is this increase that is seen as the signal. In 1998 we developed a new thermal feedback scheme which keeps the W film at constant temperature. In the steady–state a constant heating power is applied to the film via an electric heater. When the W films resistance starts to rise, as in the onset of a pulse, this heating is reduced to hold the resistance constant. The signal is then the applied reduction in the heater power. With this scheme we have now achieved a resolution of 133 eV for 1.5 keV X–rays with a 262 g detector.

To allow monitoring of the detector stability we have implemented heater pulses in our readout scheme. In addition to the feedback heating, a short heat pulse can be applied to the W film and is then detected in the usual way. This will allow us to monitor the detectors performance without a source installed inside the cryostat. The
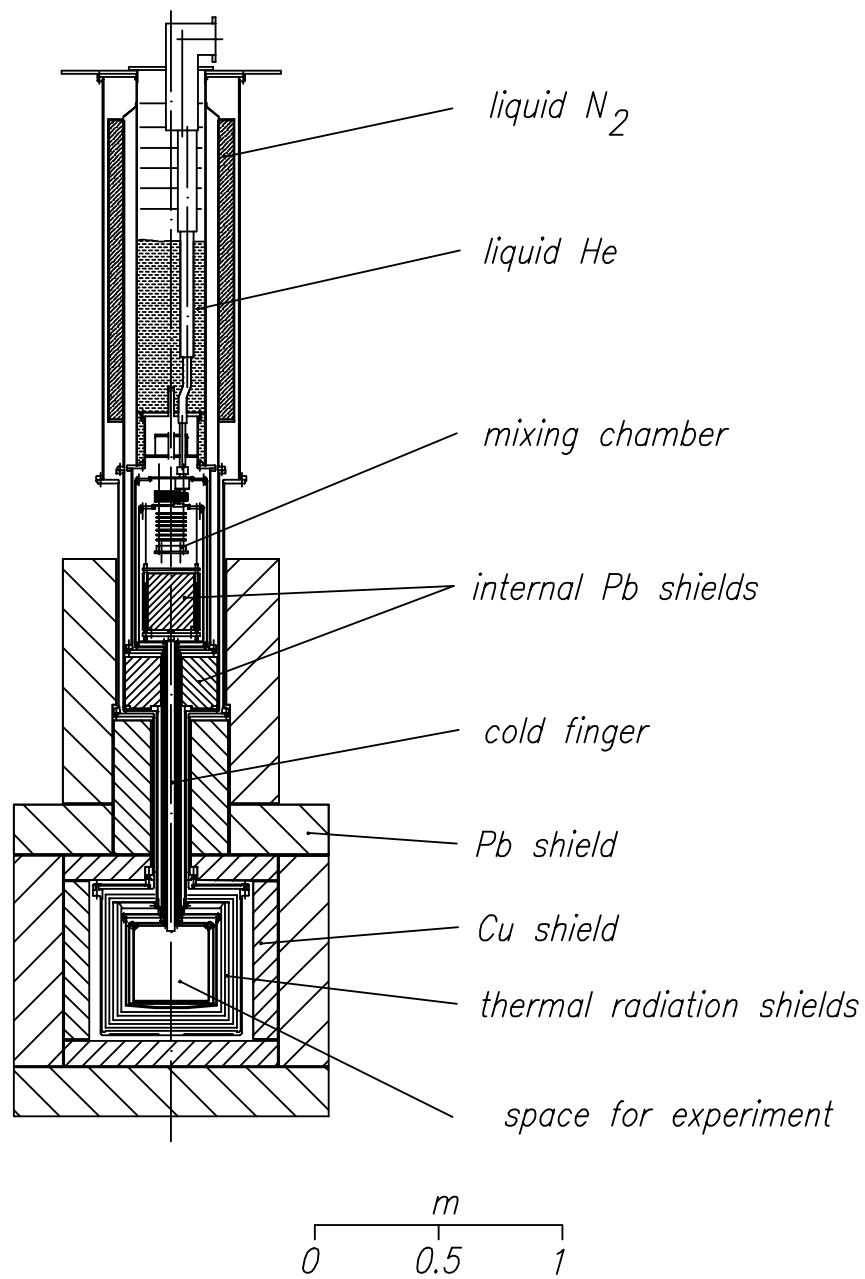
liquid N$_2$

liquid He

mixing chamber

internal Pb shields

cold finger

Pb shield

Cu shield

thermal radiation shields

space for experiment

m

0          0.5          1

Figure 2: Layout of dilution refrigerator and cold box.

equivalent energy scale of this heater pulse can be checked periodically with an external [57]Co source introduced temporarily through a plug in the shielding. Additionally, the trigger efficiencies of the individual detectors can be measured. This is already part of the preparations for future directions of the experiment, i.e. the setup of considerably more than four detectors in the cold box.

# 4   CRESST Setup in Gran Sasso

For a dark matter search experiment we need to combine the requirements of our detector (an operating temperature of $\sim 15\,\mathrm{mK}$, provided by a dilution refrigerator) with the requirements of a low-background experiment (elimination of radioactivity). Since a standard dilution refrigerator is made with various materials (stainless steel, indium vacuum seals) which are by far too radioactive, we have separated the dilution refrigerator from the detector, as shown in Fig. 2. The detectors are placed in the "cold box", which hangs from the dilution refrigerator. This cold box is large enough to accommodate up to 100 kg of sapphire. As shown in the figure, the cold box is surrounded by room-temperature shielding comprised of a 14 cm layer of high-purity copper and a 20 cm layer of lead. The low temperature is transmitted into the cold box by the 3 cm thick, 1 m long copper rod (cold finger).

It is not sufficient to use high-purity materials. Their surfaces must also be kept clean during use, and we have taken care to design our facilities in Gran Sasso to make this possible. The Faraday cage which surrounds the experiment was chosen large enough so that all work on the low-background components of the experiment can be performed inside the cage. It is divided into two levels, with the upper level allowing access to the top of the cryostat and to the electronics. The lower level of the cage is equipped as a clean room to protect the low-background components. The external lead and copper shields are in two closely fitting halves, each supported on a "wagon" so that the shielding can be opened without handling the individual pieces. In its retracted position (shown in Fig. 3) the shielding is outside the dilution refrigerator support structure but still inside the clean room. Sufficient room is then available to disassemble the cold box which, since it consists of 5 shells, requires considerably more space as individual pieces. Entrance to the clean room is through a changing room external to the Faraday cage. Our counting room is placed on top of the Faraday cage. All of this equipment is inside a building supplied for us by LNGS in Hall B. This situation of a second generation cryostat in a high quality clean room, deep underground in the LNGS, presently makes this instrument unique in the world.

First detector tests were done using our prototype cold box, which was intended mainly as a test of the cryogenic techniques, and no attempt was made to limit the cosmic ray exposure or surface contamination. In 1998 a new cold box has been fabricated using clean procedures similar to those used for the shielding. The installation is now complete and entering into full operation. The system demonstrated its high reliability by running for more than a year with the prototype cold box. Runs with a new low background cold box in the fall of 1998 showed stable operation over months. At present our four 262 g detectors are in the experimental volume, performing first measurements under low
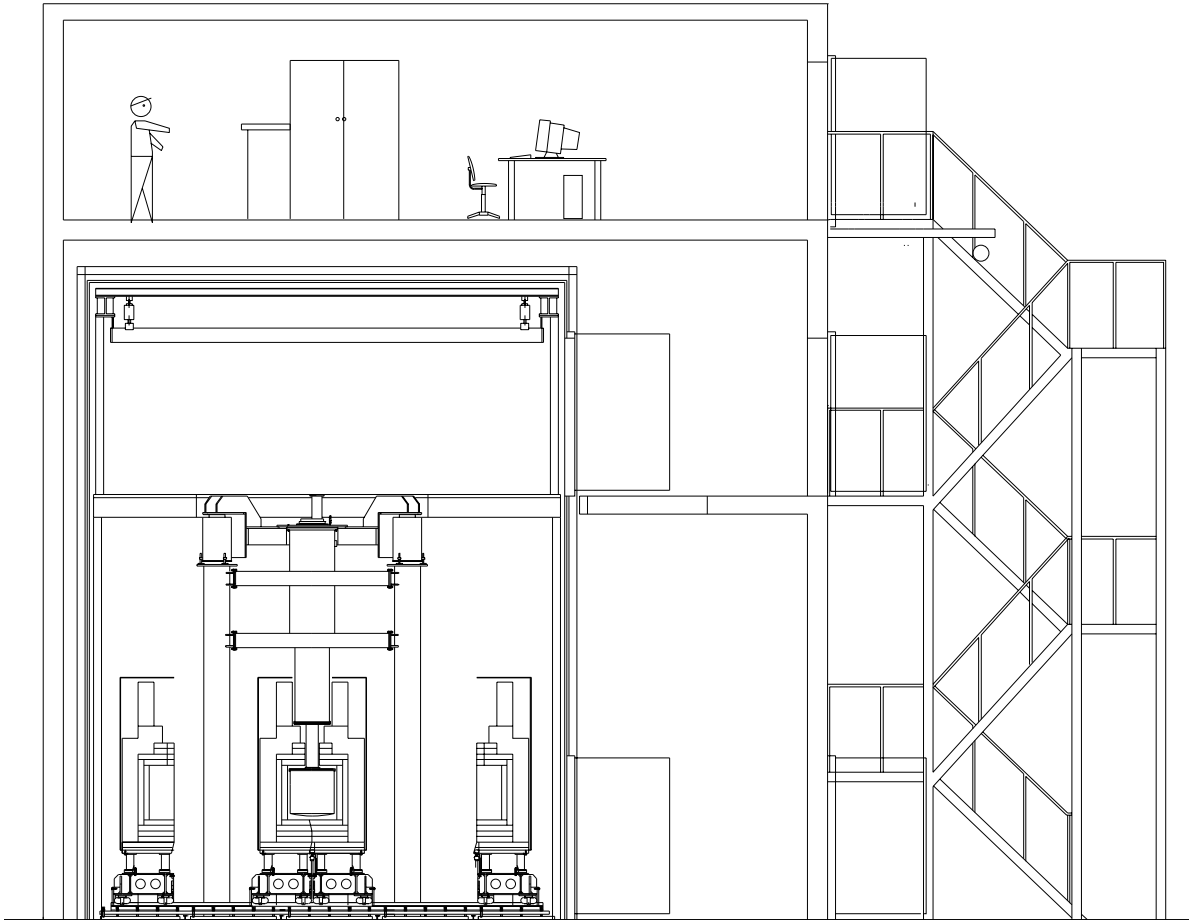
Figure 3: Cross section of CRESST building in Hall B.

background conditions. First results of this run have shown that at energies above 30 keV, the counting rate is of the order of a few counts/(kg keV day) and above 100 keV below 1 count/(kg keV day). There are strong indications that the low energy part of the spectrum was dominated by external disturbances such as mechanical vibrations or electromagnetic interferences. We are working to correct this for future runs.

As soon as we have measured significant data using our four sapphire crystals, we plan to start first measurements using the cryogenic scintillator setup which consists of a $CaWO_4$ scintillating crystal and a light detector made of sapphire. This new development has been tested so far in Munich in a surface laboratory and not under low background conditions [3]. The prospects for this active discrimination detector are very promising since already after the first non-optimised measurements, a nuclear recoil – electron recoil discrimination factor of better than 99.7% above 15 keV has been measured.

# 5    List of Publications

1. G. Safran, M. Loidl, O. Meier, G. Angloher, F. Pröbst and W. Seidel, "Switching device for the Superconducting Phase Transition Measurements of Thin W Films using a Single SQUID", submitted to J. Appl. Phys., Aug. 1998

2. P. Meunier, M. Bravin, M. Bruckmayer, S. Giordano, M. Loidl, O. Meier, F. Pröbst, W. Seidel, M. Sisti, L. Stodolsky, S. Uchaikin and L. Zerle, "Discrimination between Nuclear Recoils and Electron Recoils by Simultaneous Detection of Phonons and Scintillation Light", submitted to Appl. Phys. Lett., Nov. 1998

3. S. Cooper et al., "CRESST Dark Matter Search", Proceedings of the 2nd Int. Workshop on the Identification of Dark Matter (IDM98), Buxton, England, 7-11 1998, ed. N. Spooner

4. M. Bravin et al., "CRESST Dark Matter Search", submitted to Astropart. Phys., 1998

# References

[1] S. Cooper et al., see Ref. 3 from above.

[2] M. Sisti et al., Proc. 7th Int. Workshop on Low Temperature Detectors (LTD-7), July 27 - August 2, 1997, Munich, Germany, publ. by MPI Physik, avail. from urg@mppmu.mpg.de, p. 232

[3] P. Meunier et al., see Ref. 2 from above.

# DAMA. Dark Matter Search

P. Belli[a], R. Bernabei[a], C.J. Dai[d], W. Di Nicolantonio[b],
L.K. Ding[d], G. Ignesti[b,c], A. Incicchitti[b],
H.H. Kuang[d], J.M. Ma[d], F. Montecchia[a], D. Prosperi[b]

*and*

*in the neutron measurements:* M.Angelone[e], P.Batistoni[e], M.Pillon[e]

*in the measurements with* $^{106}Cd$ *samples:* C. Arpesella[c],V.V. Kobychev[f], O.A. Ponkratenko[f], V.I. Tretyak[f], Yu.G. Zdesenko[f]

*in studies for possible future experiments by using low radioactive NaI(Tl):* I.R. Barabanov[g] and collaborators

*+ technical staff:* A. Bussolotti[a], A. Mattei[b]

[a]Dip. di Fisica, Universita' di Roma "Tor Vergata" and INFN, sez. Roma2, Italy; [b]Dip. di Fisica, Universita' di Roma "La Sapienza" and INFN, sez. Roma, Italy; [c]Laboratorio Nazionale del Gran Sasso, INFN, Assergi(Aq), Italy; [d]IHEP, Chinese Academy, P.O. Box 918/3, Beijing 100039, China; [e]ENEA - C. R. Frascati, P.O. Box 65, I-00044 Frascati, Italy; [f]Institute for Nuclear Research, 252650 Kiev, Ukraine; [g]Institute for Nuclear Research, Moscow, Russia.

## Abstract

DAMA is searching for particle Dark Matter deep underground in the Gran Sasso National Laboratory by using several kinds of scintillators as target-detectors. In particular, the $\simeq$ 100 kg highly radiopure NaI(Tl) set-up allows to effectively investigate the WIMP annual modulation signature. Only the major results achieved during 1998 are described here. A new statistics of 14962 kg·day (DAMA/NaI-2 running period) has been analysed, giving a result consistent with the one previously achieved by using a statistics of 4549 kg·day (DAMA/NaI-1 running period). A maximum likelihood analysis of the combined two data sets (total statistics of 19511 kg·day) favours at 99.6% C.L. the hypothesis of presence of an annual modulation of the rate in the energy region of interest for Dark Matter direct detection. As regards the LXe experiment new results have been achieved by exploiting the pulse shape discrimination of the events to reject the electromagnetic background contribution. A full experiment has been also carried out in the R&D installation

to study the $\beta^+\beta^+$ decay channels of the $^{106}$Cd. Measurements have been carried out with a second CaF$_2$(Eu) BICRON prototype. Samples measurements have been realized with Ge detector deep underground and in Ispra, in the framework of the new R&D having the purpose to realize higher radiopure NaI(Tl) detectors. Further studies on possible measurements to be carried out with larger mass higher radiopurity NaI(Tl) set-up have been also performed.

# 1  Introduction

DAMA is searching for Dark Matter particles, WIMPs, with masses from few GeV to several hundreds GeV and cross sections equal or smaller than the electroweak ones (both for spin-independent, SI, and spin-dependent, SD, coupling) by detecting their elastic scattering on scintillator target-nuclei. This search is worthwhile due to the possibility of building very low radioactive — large mass — detectors that can point out a Dark Matter signal by detecting the annual modulation of the rate.

Several results are also achieved profiting of data taken in higher parts of the energy spectra or of particular data taking in the installation mainly devoted to R&D qualification.

In the following only the main activities performed during 1998 will be summarized.

# 2  The $\simeq$ 100 kg highly radiopure NaI(Tl) set-up

## 2.1  Generalities

The main aspects of the competitiveness of the $\simeq$ 100 kg low-radioactive DAMA NaI(Tl) set-up are: 1) sensitivity to WIMP interaction depending and not depending on spin, 2) sensitivity to "small" (due to Na) and "large" (due to I) WIMP masses, 3) clear knowledge of the energy threshold by calibrating down to the keV range with $\gamma$ sources (through a low Z window on the crystal housing) and with keV range Compton electrons, 4) suitable signal/noise discrimination profiting of the relatively high available number of photoelectrons/keV and of the different timing structures of the PMT noise pulses (single fast photoelectrons) with respect to the NaI(Tl) scintillation pulses (time distribution with time decay of order of hundreds ns), 5) absence of microphonic noise, 6) quenching factors well measured in a crystal from the same growth by irradiating a detector with neutrons to induce recoils in the whole sensitive volume, 7) electromagnetic background rejection by pulse shape discrimination (PSD) and by annual modulation analysis, 8) annual modulation signature well explorable with large statistics and monitoring of several parameters. The experiment is taking data from single photoelectron threshold to several MeV (being the optimization done for the lowest energy region). Additional triggers are active to obtain also some "by-product" results.

The main purpose of this set-up is the search for the WIMP annual modulation signature, induced by the Earth's motion around the Sun[1, 2]. We note that this signature is quite strong, requiring the satisfaction of all the following characteristics: i) presence in the rate of a modulated part varying as a cosine function, ii) with a proper period

(1 year), iii) with a proper phase (about June $2^{nd}$), iv) presence only in a defined low energy region, v) single "hit" events[1], vi) modulated amplitude in the region of maximal sensitivity $\lesssim 7\%$.

## 2.2  New results on the WIMP annual modulation signature

A new statistics of 14962 kg·day (DAMA/NaI-2 running period) has been analysed. These data have been collected from november $cos\omega(t_i - t_0) = -0.989$, until the subsequent july, $cos\omega(t_i - t_0) = 0.543$ (where $\omega = 2\pi/T$ with T = 1 year and $t_0 \simeq 2^{nd}$ June, when the Earth speed in the galactic halo is at maximum). Considering that the minimum of the effect is expected around December $2^{nd}$ and the maximum around June $2^{nd}$, it results that this data set allows to significantly verify the i) to vi) requirements mentioned above. The results achieved here are consistent with the ones obtained in the first period[2] and a combined analysis of the two data sets has been also performed.

A pre-print containing a detailed description of the set-up and its performances has been released in 1998 (see the publication list). We recall that the detectors can be calibrated by external $\gamma$ sources down to few keV and by low energy Compton electrons; in long term running conditions, the proper knowledge of the energy scale is assured by periodical calibrations with external $^{241}$Am source (performed in the same conditions as the production data, with no contact with external air) and by monitoring the position and resolution of the $^{210}$Pb peak present at level of few cpd/kg in the energy distributions collected by our detectors, mainly because of a surface contamination by environmental Radon during the first period of the underground detectors storage. Moreover, as regards the rejection of the residual noise above the energy threshold, we profit of the different timing structure between the noise (PMT fast signals with decay times of order of tens ns) and the scintillation (signals with decay times of order of hundreds ns) pulses, recorded over 3250 ns by a Lecroy Transient Digitizer (see the preprints 98 for details). As regards the general set-up working conditions, several parameters are monitored and acquired by CAMAC with the production data. In particular, the background stability has been investigated by monitoring the stability of the total hardware counting rate above the single photoelectron level (that is, from noise to "infinity") and by verifying the absence of significant variation of the background in the higher energy part of the spectrum (where only background can be present). In fact — being the background in the low energy region (from Compton electrons, from X-ray and/or Auger electrons, from muons, etc.) strictly correlated with events in higher energy parts of the spectrum — if a variation in the lowest energy region would be due to a variation of the background, an equal or larger (sometimes much larger) variation would be present at higher energies. Moreover, the

---

[1]When searching for Dark Matter particles with a multi-detector set-up, the quoted rates are always referred (as e.g. in [3, 4], see also the recent preprint on the set-up performances for details) to events where only one detector is firing (single "hit" events), being negligible the probability that a WIMP will interact in more than one of them.

[2]We recall that the discussion on the sensitivity of the DAMA/NaI-1 running period in ref. [5] is obviously wrong being based on the *false* statement that we extracted the signal from the rate *integrated* between 2 and 20 keV, while as it is evident from the formal description [3] we extracted it from the *differential* rate between 2 and 20 keV using 1 keV energy intervals. The two approaches — as it can be easily verified — have significantly different sensitivities.

counting rate stability just above the region of interest for the possible signal is also verified. Quantitative investigations of systematic effects credit a percentage systematic error $\lesssim 10^{-3}$ from variations in the light response along the year and $\lesssim 10^{-4}$ — in the region of maximal interest — from calibration uncertainties. Moreover, from the analysis of high energy data, an overall background variation is excluded even at more stringent level.

The possible presence in the rate of a contribution having the typical features of a WIMP with a dominant SI scalar interaction (as the most favoured Cold Dark Matter candidate, the neutralino [6]) can be effectively tested searching for the existence of a modulated component with peculiar features. To achieve the highest sensitivity in the extraction of the possible signal from the data, we perform the time correlation analysis by using the maximum likelihood method grouping the data collected in the 2-20 keV energy region in ijk cells, where i identifies the time interval (1 day each one), k the energy bin ($\Delta E = 1$ keV each one) and j the considered detector (see papers for details).

For the data of the DAMA/NaI-2 running period, the minimum value of the $y$ function ($y = -2ln(\mathbf{L}) - const$, where $\mathbf{L}$ is the maximum likelihood function) is obtained for $M_w = (59^{+22}_{-14})$ GeV and $\xi\sigma_p = (7.0^{+0.4}_{-1.7})10^{-6}$ pb, being $M_w$ the WIMP mass, $\xi = \frac{\rho_{WIMP}}{\rho_0}$ with $\rho_0 = 0.3$ GeVcm$^{-3}$ and $\sigma_p$ the WIMP cross section on proton. The test of the maximum likelihood ratio favours the hypothesis of the presence of a modulation with the given $M_w$ and $\xi\sigma_p$ at 98.5 % C.L.. Several careful analyses, using different statistical consistency tests, have been performed (see the preprint 98), achieving always consistent results. The region pointed out in fig. 1 at 2 $\sigma$ C.L. in the $\xi\sigma_p$ and $M_w$ plane by the DAMA/NaI-2 results is fully embedded in the one preliminarily determined at 90% C.L. in ref. [3] (fig. 1 - dotted contour). It is also well embedded in the Minimal Supersymmetric Standard Model (MSSM) estimates for neutralino [6]. The SI 90% C.L. exclusion plot obtained in ref. [4] by the same experiment is also shown there[3].

Analysing the two data sets together with the maximum likelihood method for a total statistics of 19511 kg·day, the minimum value of the $y$ function is found at $M_w = (59^{+17}_{-14})$ GeV and $\xi\sigma_p = (7.0^{+0.4}_{-1.2})10^{-6}$ pb and the test of the maximum likelihood favours now the hypothesis of the presence of a modulation with the given $M_w$ and $\xi\sigma_p$ at 99.6 % C.L.. In fig. 1 the dashed contour represents the region allowed at 2 $\sigma$ C.L. — for a SI coupled candidate — for the combined analysis of the two running periods. Possible implications of these results have been discussed e.g. in ref. [8].

Finally, let us note that crucial investigations to definitely clarify the nature of the observed effect are the verification of its repetitivity over several cycles and the exclusion of possible different physical processes able to satisfy the i) to vi) requirements of sec. 2.1. Up to now the effect was present in both the two considered running periods and the $\xi\sigma_p$ versus $M_w$ allowed region is significantly shrinked according to the increase of the statistics. No concurrent physical processes, which would satify the i) to vi) conditions, have been found. In particular, we recall here that the effect induced by the muon modulation reported in ref. [9] would generally fail at least the iv) requirement and would account

---

[3]We note that possible systematic uncertainties on it resulted negligible with respect to the statistical ones, as it is evident in fig. 7 of ref. [4]. Moreover, in this particular case, the exclusion plot would be substancially similar even in case the results of the pulse shape analysis would not be considered, as it has been extensively discussed in [7].

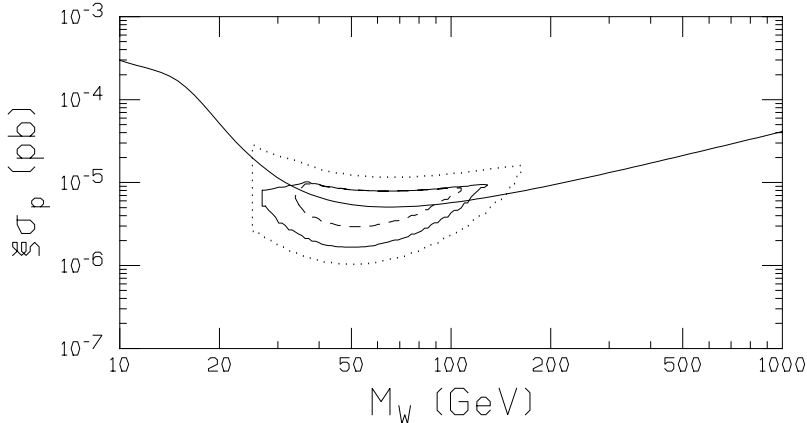only for modulated amplitudes $<< 10^{-4}$ cpd/kg/keV (that is much lower than the one pointed out here).



Figure 1: The continuous contour represents the region allowed at $2\sigma$ C.L. — for a SI coupled candidate — by the present analysis on the DAMA/NaI-2 data. It is compared with the 90% C.L. contour achieved in DAMA/NaI-1 (dotted contour). The dashed contour represents the region allowed at $2\sigma$ C.L. by the combined analysis of these two data taking periods. The SI 90% C.L. exclusion plot obtained in ref. [4] by the same experiment is also shown.

Further investigations are in progress.

# 3    The LXe set-up

The LXe detector is filled with about 2 l liquid Kr-free Xenon enriched at 99.5% in $^{129}$Xe. Its features have been described elsewhere.

In 1998 an experimental determination of the Xenon quenching factor ($q_{Xe}$) in pure liquid Xenon scintillator has been set. A 40 cc LXe scintillator (specially built for neutron measurements) has been used to perform both measurements with Am-B neutron source and with neutron beam at the ENEA Frascati Neutron Generator. This facility produces neutrons at $\simeq 14.7$ MeV via the reaction $^2$H + $^3$H $\rightarrow$ n + $^4$He. The measurements with Am-B source quote a $q_{Xe}$ value equal to (0.65±0.10), including systematic uncertainties which result not negligible with respect to the statistical ones when using a similar detector (see the paper). The measurements at the ENEA Frascati Neutron Generator (where $q_{Xe}$ is determined by tagging the scattered neutrons at a fixed angle with a NE213 detector and comparing the detected energy of Xenon recoil with the kinematical calculated one) give a $q_{Xe}$ value equal to (0.45 ± 0.12), still including the systematic uncertainties not negligible in this case. This last value is obtained by combining the results obtained at two different scattering angles $90^0$ and $76^0$. The combined final result is $q_{Xe} = (0.55 \pm 0.11)$. To be conservative the value 0.44 (mean value minus the maximal error) has been,

then, used in the evaluation of the exclusion plots (see later). Further measurements at neutron beam are foreseen.

From measurements with the Am-B neutron source and from the "Compton" calibrations the possibility of a pulse shape discrimination between recoils and electromagnetic background has been quantified following the method described in [4]. The discrimination quality factor — defined here $DQF = \left[\frac{\tau_{comp} - \tau_{rec}}{\tau_{comp}}\right]$ — as a function of the energy has been determined, being $\tau$ the first momentum of the time distribution of each recoil (rec) or "Compton" (comp) "reference pulse".

A statistics of 1763.2 kg·day, collected before fall 96, has been then analysed by investigating the pulse shape of the events to reject the contribution of the electromagnetic background. For each energy bin, the "reference pulses" from the "production" and from the "Compton-like" (induced in situ data by $\gamma$ source) have been built and, then, the corresponding $\tau_{data}$ and $\tau_{comp}$ have been computed. The recoil fraction, x, present in the data for each energy bin has been then evaluated as: x $= \frac{1 - \tau_{data}/\tau_{comp}}{DQF}$. The hypothesis that the x fractions normally fluctuate around zero gives a probability of $\simeq 13\%$ to get a worse $\chi^2$ only by statistical fluctuations, therefore, upper limits at 90% C.L. on the recoil fraction for each energy bin have been calculated. This also credits the possible systematic contribution as negligible with respect to the present statistical uncertainties (see the paper). The obtained residual recoil rates are shown in fig. 2 (continuous line).
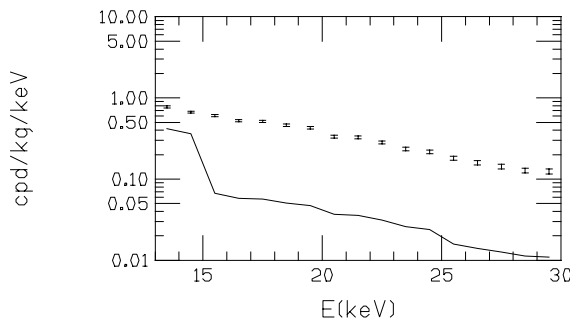


Figure 2: Low energy distribution collected with the $\simeq 2$ liters pure LXe scintillator deep underground (statistics of 1763.2 kg·day - DAMA/Xe-2 period); the rate is already corrected for the needed efficiency. The continuous line represents the upper limits at 90% C.L. on the recoil fractions.

The limit cross-sections versus WIMP mass have been then derived from the quoted recoil fractions (see fig. 3). The results for the SI case have been obtained using the Helm SI form factor, while for the SD case we have used — for Xenon, Iodine and Sodium — the recently published Ressell et al. nuclear form factors for Bonn-A potential and pure $Z^0$ coupling. For Fluorine indeed the effect due to the form factor is considered safely negligible. Note that, while the Helm expression for the coherent form factor has a general
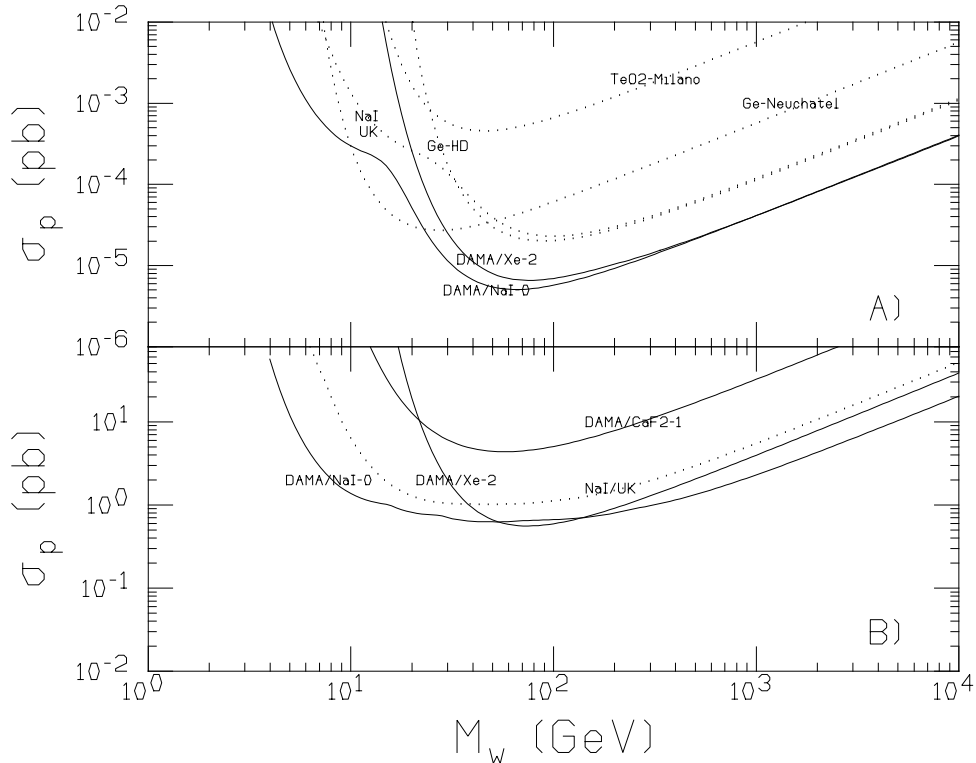
22

Figure 3: Limit elastic cross-sections on nucleon as a function of WIMP mass at 90% C.L.: A) SI interaction; B) SD interaction, considering here for the SD Xe, I and Na nuclear form factors recent calculations by Ressell et al. [10]. Note that the present poorer SD exclusion plot with respect to the DAMA/Xe-0 result — in spite of the present reduced rate — is very slightly affected by the used $q_{Xe}$ value, while it is greatly affected by the different form factor considered here. This gives a more favourable SD exclusion plot for NaI and a less favourable one for LXe. Exclusion plots from the data of other authors — evaluated in consistent manner — are also shown. Here $\rho_{WIMP} = 0.3$ GeV cm$^{-3}$.

character, the SD one is strongly dependent on nuclear properties of the target nucleus and on the neutralino composition.

A sensitivity similar to the one of ref. [4] has been reached here. Note that if the less conservative $q_{Xe}$ mean value (0.55) would be used, no substancially different results would be obtained; in particular, this would be still largely consistent with the annual modulation results previously discussed. We take this opportunity to remark that obviously an exclusion plot at given C.L. does not exclude completely the possible presence of a signal in the enclosed region (mainly near the borders) and that significant intrinsic uncertainties are present when comparing exclusion plots from different experiments (mainly when different experimental techniques are used), as briefly commented e.g. in [11, 12]. This points out the relevance of performing experiments with their own clear signature for Dark Matter particles.

23

# 4 R&D developments and by products

In the barrack, where the $\simeq 100$ kg NaI(Tl) set-up is installed, a set-up (mainly devoted to test new scintillator prototypes and to perform small scale experiments) is also running. There a sealed low radioactive copper box to house the detectors is installed inside a multi-component low radioactive shield, which is enclosed in an external sealed plexiglass box. The boxes are fluxed with high purity Nitrogen gas.

## 4.1 The second $CaF_2(Eu)$ prototype

During 1998 in the R&D installation data have been collected — in the whole energy spectrum — with a second $CaF_2(Eu)$ prototype detector by Bicron company. The data analysis is in progress.

## 4.2 Results on the double positron decay of the $^{106}Cd$

In 1998 the analysis of the data previouly collected in this installation to study the double positron decay of $^{106}Cd$ ($\beta^+\beta^+$, $\beta^+/EC$ or $EC/EC$) has been completed.

Table 1: Experimental half-life limits for the $2\beta^+$ decay processes of $^{106}Cd$

| Decay mode (transition) | $T_{1/2}$ limit (90% C.L.) years |
|---|---|
| $\beta^+/EC$ (2$\nu$) g.s. $\rightarrow$ g.s. | $4.1 \cdot 10^{20}$ |
| $\beta^+/EC$ (0$\nu$+0$\nu$M) g.s. $\rightarrow$ g.s. | $3.7 \cdot 10^{20}$ |
| $\beta^+/EC$ (0$\nu$ + 2$\nu$ + 0$\nu$M) g.s. $\rightarrow$ $0_1^+$ (1134 keV) | $1.1 \cdot 10^{20}$ |
| $\beta^+/EC$ (0$\nu$ + 2$\nu$ + 0$\nu$M) g.s. $\rightarrow$ $2_1^+$ (512 keV) | $2.6 \cdot 10^{20}$ |
| $\beta^+/EC$ (0$\nu$ + 2$\nu$ + 0$\nu$M) g.s. $\rightarrow$ $2_2^+$ (1128 keV) | $1.4 \cdot 10^{20}$ |
| $2\beta^+$ (0$\nu$ + 2$\nu$ + 0$\nu$M) g.s. $\rightarrow$ g.s. | $2.4 \cdot 10^{20}$ |
| $2\beta^+$ (0$\nu$ + 2$\nu$ + 0$\nu$M) g.s. $\rightarrow$ $2_1^+$ (512 keV) | $1.6 \cdot 10^{20}$ |
| $EC/EC$ (0$\nu$) g.s.$\rightarrow$ 1,2$^+$ (2741 keV) | $3.0 \cdot 10^{19}$ |
| $EC/EC$ (2$\nu$ + 0$\nu$M) g.s. $\rightarrow$ $0_1^+$ (1134 keV) | $7.3 \cdot 10^{19}$ |
| $EC/EC$ (2$\nu$ + 0$\nu$M) g.s. $\rightarrow$ $2_2^+$ (1128 keV) | $4.9 \cdot 10^{19}$ |

The low background set-up, installed in the R&D shield, was realized by two $\simeq 4$ kg NaI(Tl) detectors and by metallic Cadmium samples (total mass $\simeq 154$ g), enriched in $^{106}$Cd at 68%. Part of $^{106}$Cd, $\simeq 109$ g, were purified twice by the method of vacuum distillation and $\simeq 45$ g were purified only once. The source was placed between the two low background NaI(Tl) detectors; the energy spectra for each detector separately and two-dimension coincidence spectra have been obtained. The measurements were carried out during 4321 h. The two-dimension coincidence spectrum shows the peaks from $^{214}$Bi ($E_1 = 609$ keV, $E_2 = 1120$ keV) and from $^{208}$Tl ($E_1 = 583$ keV, $E_2 = 2614$ keV) which allow to check the energy scale and resolution of both detectors during the whole experiment and to determine the contents of the Th and U contamination in the enriched Cadmium samples with the aim of building up a model for the background. Coincidence spectra from the $^{232}$Th, $^{226}$Ra and $^{40}$K decays in the enriched Cadmium samples and in both PMTs were simulated by using the GEANT3.21 package, while to describe the initial kinematics of the events, the event generator DECAY4 was used.

The study of the residual energy spectrum — difference between the experimental distribution and the one evaluated by the model from $^{232}$Th and $^{226}$Ra contamination of the $^{106}$Cd samples — has allowed the determination of new limits for the different $\beta^+\beta^+$, $\beta^+/EC$ and $EC/EC$ decay channels in $^{106}$Cd. They are reported in table 1 and are significantly higher (by a factor 6 to 60) than those already published for this nuclide. Further measurements are foreseen using only the higher radiopure 109 g of Cadmium and slightly improving the set-up.

## 4.3   The new R&D for higher radiopure NaI(Tl)

A new R&D program is in progress with Crismatec in order to explore the possibility to increase the radiopurity of the NaI(Tl) detectors, testing new purification procedures. In particular, if the R&D program with Crismatec will be successful, it will be possible to increase the total mass in the present installation up to 250 kg. This will complete the goals of the present DAMA/NaI experiment.

The residual radioactivity in the needed samples has been measured both deep underground with Ge detector and at ISPRA with mass spectrometer during 1998. Moreover, further studies on possible applications of larger mass higher radiopure NaI(Tl) set-up have been also carried out during 1998 (see in the publication list 1998).

# 5   Conclusions

Interesting results have been obtained by the DAMA experiments and all the activities are producing results. In particular, the $\simeq 100$ kg NaI(Tl) set-up continuously runs to investigate the WIMP annual modulation signature.

Some upgradings of these set-ups are in preparation.

# 6 List of Publications during 1998

1. R. Bernabei for: I.R. Barabanov, P. Belli, R. Bernabei, C.J. Dai, L.K. Ding, W. Di Nicolantonio, V. I.Gurentzov, E.A. Janovich, A. Incicchitti, V.E. Janz, V.N. Kornoukhov, H.H. Kuang, J.M. Ma, F.Montecchia, I.V. Orekhov, C.V. Danshin, D. Prosperi, "Perspectives for a search of neutrino magnetic moment deep underground", Nucl.Phys. B (Proc. Sup.), 66 (1998), 222.

2. R. Bernabei, P. Belli, F. Montecchia, W. Di Nicolantonio, A. Incicchitti, D. Prosperi, C. Bacci, C.J. Dai , L.K. Ding, H.H. Kuang, J.M. Ma "WIMPs search by scintillators: possible strategy for annual modulation search with large-mass highly-radiopure NaI(Tl)", Nucl.Phys. B (Proc. Sup.), 70 (1999), 79.

3. P. Belli for DAMA coll., "Most recent DAMA results", in the volume *COSMO97*, L. Roszkowski ed., World Sc. pub. (1998), 179.

4. R. Bernabei for DAMA coll., "Particle Dark Matter search with scintillators at Gran Sasso: status and perspectives", Proceed. of *DM Italia-97*, Studio Fiorentino ed. (1998), 29.

5. R. Bernabei, P. Belli, F. Montecchia, W. Di Nicolantonio, A. Incicchitti, D. Prosperi, C. Bacci, C.J. Dai, L.K. Ding, H.H. Kuang, J.M. Ma, "Searching for WIMPs by the annual modulation signature", Phys. Lett. B424 (1998), 195.

6. R. Bernabei, P. Belli, F. Montecchia, W. Di Nicolantonio, A. Incicchitti, D. Prosperi, C.J. Dai, L.K. Ding, H.H. Kuang, J.M. Ma, M. Angelone, P. Batistoni, M. Pillon, "The DAMA experiments at Gran Sasso", proceedings of DM98 to appear on *Phys. Rep.*

7. R. Bernabei for the DAMA coll. "Recent result from the DAMA experiment", to appear on the Proc. of the Int. Workshop VULCANO98, Vulcano may 1998

8. P. Belli, R. Bernabei, C. J. Dai, L.K. Ding, W. Di Nicolantonio, G. Ignesti, A. Incicchitti, H.H. Kuang, J. M. Ma, F. Montecchia, D. Prosperi, M. Angelone, P. Batistoni, M. Pillon, "The DAMA experiments: status report", to appear in the Proc. of the Int. Workshop *DARK98*, Heidelberg july 1998.

9. R. Bernabei, P. Belli, A. Incicchitti, D. Prosperi, C.J. Dai, "Improved limits on neutrinoless double beta decays of 46Ca and 130Ba by using scintillators as source-detectors", Il Nuovo Cimento A111 (1998), 347 & N. Cim. A, oct. 1998.

10. P. Belli, R. Bernabei, A. Incicchitti, C. Arpesella, V.V. Kobychev, O.A. Ponkratenko, V.I. Tretyak, Yu.G. Zdesenko "New limits on $2\beta^+$ decay processes in $^{106}Cd$", pre-print ROM2F/98/12 to appear on Astrop. Phys.

11. R. Bernabei, P. Belli, F. Montecchia, W. Di Nicolantonio, A. Incicchitti, D. Prosperi, C.J. Dai, M. Angelone, P. Batistoni, M. Pillon, "New limits on particle dark matter search with liquid Xenon target-scintillator", Phys. Lett. B436 (1998), 379.

12. I.R. Barabanov, R. Bernabei, P. Belli, V. I. Gurentsov, V. N. Kornukhov, O. G. Miranda, V. B. Semikoz, J. W. F. Valle "Testing for New Physics with Low-Energy Anti-Neutrino Sources: LAMA as a Case Study", hep-ph/9808297 to appear on Nucl. Phys.

13. R. Bernabei, P. Belli, F. Montecchia, W. Di Nicolantonio, G. Ignesti, A. Incicchitti, D. Prosperi, C.J. Dai, L.K. Ding, H.H. Kuang, J.M. Ma, "Performances of the $\simeq$ 100 kg NaI(Tl) set-up of the DAMA experiment at Gran Sasso", pre-print ROM2F/98/27 and INFN/AE-98/23 submitted for publication

14. R. Bernabei, P. Belli, F. Montecchia, W. Di Nicolantonio, G. Ignesti, A. Incicchitti, D. Prosperi, C.J. Dai, L.K. Ding, H.H. Kuang, J.M. Ma, "On a further search for a yearly modulation of the rate in particle Dark Matter direct search", pre-print ROM2F/98/34 and INFN/AE-98/20 to appear on Phys. Lett. B.

15. P. Belli et al., "New DAMA results on annual modulation searches", to appear in the Proc. of the Int. Workshop IDM98, Buxton-UK Sept. 1998.

16. P. Belli et al., "Direct search for Dark Matter particles deep underground", to appear in the Proc. of the Int. Workshop 3k-Cosmology, Rome, oct. 1998.

# References

[1] Drukier, et al., *Phys. Rev.* **D33**, 3495 (1986).

[2] Freese, K., et al., *Phys. Rev.* **D37**, 3388 (1988).

[3] Bernabei, R., et al., *Phys. Lett.* **B424**, 195 (1998).

[4] Bernabei, R., et al., *Phys. Lett.* **B389**, 757 (1996).

[5] Hasenbalg, F., *astro-ph/9806198* on Astrop. Phys. 9 (1998), 325.

[6] Bottino, A., et al., *Phys. Lett.* **B402**, 113 (1997); Bottino, A., et al., *Phys. Lett.* **B423**, 109 (1998).

[7] Belli, P., talk at *DM98 Int. workshop* and discussion at *1-day satellite workshop on Detailed Techniques in the Direct Detection of Dark Matter at DM98*, USA, February 1998.

[8] Bottino, A., et al., *hep-ph/9808456* to appear on Phys. Rev. D; *hep-ph/9808459* to appear on Phys. Rev. D and *hep-ph/9809239* to appear on Astrop. Phys.

[9] Ambrosio, M., et al., *Astropart. Phys.* **7**, 109 (1997).

[10] M.T.Ressell and D.J.Dean, Phys. Rev. C56 (1997), 535.

[11] R. Bernabei, "Competitiveness of a very low radioactive ton scintillator for particle Dark matter search", in *The identification of Dark Matter*, World Sc. Pub., Singapore (1997), 574.

[12] R. Bernabei, La Rivista del Nuovo Cimento, n. 5 (1995).

[13] R. Bernabei et al., Astrop. Phys. vol.4 (1995), 45.

# DBA. Search for double beta decay of $^{100}$Mo with liquid argon ionization chamber

V.D. Ashitkov[1], A.S. Barabash[1], S.G. Belogurov[1], G. Carugno[2],
S.I. Konovalov[1], F.Massera[4], I.O. Pilugin[1], G. Puglierin[2], R.R. Saakyan[1,3],
V.N. Stekhanov[1], V.I. Umatov[1], I.A. Vanushin[1]

[1]Institute of Theoretical and Experimental Physics, B. Cheremushkinskaya 25,
117259 Moscow, Russia
[2]Dipartimento di Fisica e INFN, Universita di Padova, via Marzolo 8,
I-35131 Padova, Italy
[3]Laboratori Nazionali del Gran Sasso dell'INFN, I-67010 Assergi (L'Aquila), Italy
[4]INFN, Sezione di Bologna, 40126, via Berti Pichat, 6/2 (Bologna), Italy

### Abstract

The experiment is located in the Gran Sasso Underground Laboratory (3500 m w.e.). Full weight of $^{100}$Mo under investigation is 138.7 g. Three measurement runs were done ( 202 h, 238 h and 313h). As a result the limits on half-lives for $0\nu$- and $0\nu\chi^0$-decays of $^{100}$Mo were obtained $3.5 \cdot 10^{21}$ y and $1.2 \cdot 10^{20}$ y, respectively, at 90% CL. Some extra events in the $(1.6-3)$ MeV energy region lead for preliminary value on $2\nu\beta\beta$ decay of $^{100}$Mo, $\sim 8.5 \cdot 10^{18}$ y. As a by-product the limit on the content of radioactive $^{42}$Ar in the natural Ar was obtained, $6 \cdot 10^{-21}$. We plan to improve the background conditions of the experiment and increase the sensitivity to $(1-2) \cdot 10^{23}$ y for $0\nu$ decay mode and to $(1-2) \cdot 10^{22}$ y for $0\nu\chi^0$ decay. In addition we hope to investigate $2\nu$ decay mode of $^{100}$Mo with an accuracy of $\sim 10\%$.

## 1 Introduction

At present time, the neutrinoless double beta decay $(0\nu\beta\beta)$ is one of the best probe for physics beyond the standard model of electroweak interactions. Its existence deals with the fundamental aspects of particle physics:

- the lepton number non-conservation;
- the existence and nature of neutrino mass;
- the existence of right-handed currents in the electroweak interaction;

29

- the existence of Majoron;
- the structure of Higgs' sector;
- the supersymmetry;
- the leptoquarks;
- the sterile neutrino existence.

At the moment only lower limits on half-lives ($T_{1/2}$) have been obtained experimentally. These limits are used to deduce upper limits on the Majorana neutrino mass, the right-handed current admixture parameter, the Majoron-Majorana neutrino coupling constant etc. One of the most important uncertainties in above analysis is the evaluation of the nuclear matrix elements. In connection with the $0\nu\beta\beta$ decay, the detection of double beta decay with the emission of two neutrinos ($2\nu\beta\beta$) which is an allowed process of second order in the Standard Model enables the experimental determination of nuclear matrix elements involved in the double beta decay processes. This leads to the development of theoretical schemes for nuclear matrix element calculations both connected with the $2\nu\beta\beta$ decays as with the $0\nu\beta\beta$ decays. In order to search for the double beta decay with a new technique a multisectional liquid argon ionization chamber was suggested [1] (see also [2-4]). For the first step of the experiment we have selected a nucleus with sufficiently large $2\beta$-transition energy, $^{100}$Mo (E=3033 keV).

# 2  Experimental setup

The experiment is located in the Gran Sasso Undeground Laboratory (3500 m w.e.). The experimental setup consists of a liquid Ar ionization chamber placed in a lead passive shielding, gas system and manual crane for assembling and disassembling the liquid Ar chamber . All this equipment was put on the special concrete platform with dimensions 4 m × 6 m × 0.6 m. To reduce mechanical vibrations the platform was placed on a rubber layer. The special house was set up around the passive shielding in order to prevent the influence of high humidity to the equipment. The electronics and data acquisition system for the liquid argon chamber were placed in the separate "house" at the distance of 2 m from the platform.

## 2.1  Liquid argon ionization chamber

The main construction material of the chamber is titanium. Practically all insulators are made of teflon. The scheme of the detector is shown in the Fig.1. The chamber is cooled by liquid nitrogen getting into the "nitrogen" volume (2). The "nitrogen" volume is isolated from the air by the "vacuum" one (3). The "nitrogen" volume (2) is connected with the volume (4) in which there is a volume (1) with the liquid argon. The temperature of liquid argon is regulated by the heaters (5) which are on the outside surface of (1). The electrode system forming the chamber sensitive volume is placed in the vessel (1) with inner volume $\phi 40 \times 70$ cm$^3$. The registration part of the chamber is composed of
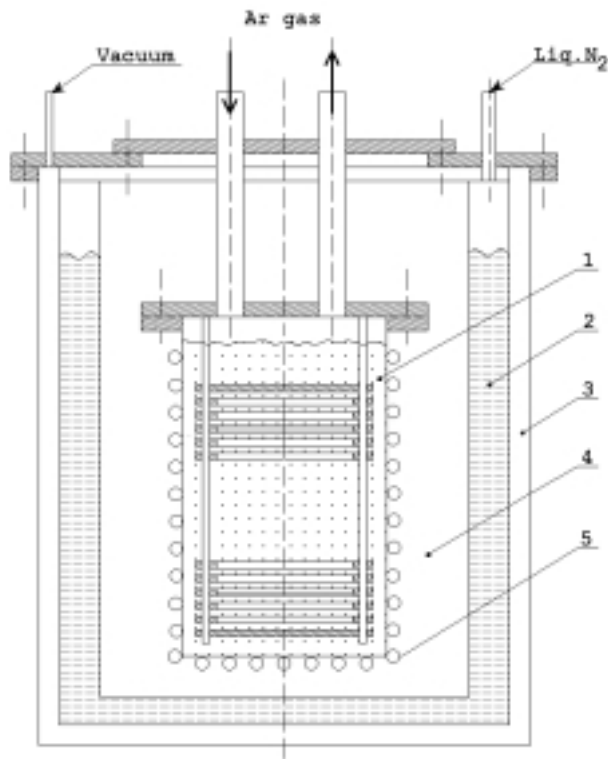
Figure 1: Schematic view of the ionization chamber. 1 – vessel with inner volume $\phi 40 \times 70$ cm$^3$; 2 – "liquid nitrogen" volume; 3 – vacuum casing; 4 – "vapour nitrogen" volume; 5 – heaters.

identical measuring sections. Each section consists of two paired flat ionization chambers with screening grids and common cathode. The cathode is made of material containing the isotope under study (molybdenum). The sensitive volume diameter is 30 cm and its height is 56 cm. The chamber contains 14 cathodes, 15 anodes and 28 screening grids. The grid-anode distance is 5.5 mm and grid-cathode one is 14.5 mm.

### 2.1.1 Isotopes

The chamber cathodes are made of molybdenum foil of $\sim 50$ mg/cm$^2$ thick. During last three runs (202h, 238h and 313h) 4 cathodes made of enriched molybdenum (98,35% of $^{100}$Mo) were used. These cathodes were located in the centre of the electrode system. The total mass of $^{100}$Mo under investigation was 138.7 g.

## 2.2 Gas system

The gas system consists of 22 40-th liter stainless steel cylinders for argon gas, a purification and purity control system (Fig.2). Six cylinders are put into stainless steel dewars in order to use them as a cryogenic pump for removing liquid Ar from the chamber into these cylinders in the end of experimental run. The Ti-sponge purification system has been chosen because of the low radioactivity. A single pass of argon gas through the
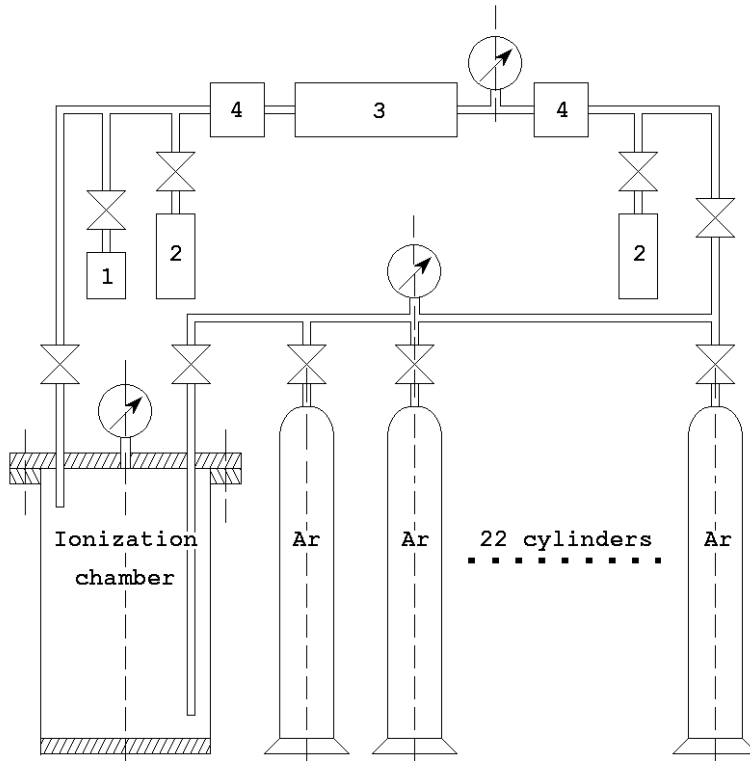
31

Figure 2: Gas supply system. 1 – purity control detector; 2 – cryogenic pump; 3 – Ti-sponge purification system; 4 – filters.

reactor at a temperature of 850°C provides an impurity content of $1.9 \cdot 10^{-9}$ eqv. $O_2$ [2, 3].

## 2.3   Passive shielding

The passive shielding of lead has been mounted on the concrete platform. The thickness of lead is 15 cm. It should be noted that the radon contamination in the air near our installation has been measured and found quite high, $\sim$200 Bq/m$^3$ (for comparison, about 40 Bq/m$^3$ in other halls of the Gran Sasso Underground Laboratory). To avoid the influence of air radon we have reduced the splits in the passive shielding with the poliuretan scume, used nitrogen vapour evaporated from the detector during the experimental run to flush the internal volume of the passive shielding and we had put the plastic boxes inside the passive shielding to reduce its internal volume. As a result we have managed to suppress the background from $^{222}$Rn around the detector up to $\sim$ 2 Bq/m$^3$ ($\sim$50 Bq/m$^3$ during the first run).

## 2.4   Electronics and data acquisition

The electronics and data acquisition are 15 measuring channels. Each channel consists of a charge-sensitive preamplifier, an amplifier and a flash ADC where signal is digitized

with sampling time of 50 ns. We use 30 ADC since each channel output has two types of signals: shaped and unshaped. The trigger for data collection requires that the signal exceeds the threshold at least on one of the anodes ($\sim$600 keV during the run). In this case the digitized signals from all channels are written to data tape.

# 3  Experimental results

The chamber has been assembled with four cathods containing enriched $^{100}$Mo and ten cathods with natural molybdenum. The enriched cathodes have been put in the center of the detector so that the natural Mo and $^{100}$Mo alternated each other. This configuration is used to provide background subtraction for two-neutrino double beta decay measurement. The measurements have been done at the following electrical fields: 1.93 kV/cm for cathode-grid gap, and 4 kV/cm for anode-grid gap. The chamber filled with liquid Ar has been irradiated by $^{22}$Na radioactive source (E=1.275 MeV). The energy resolution is 18% at the electron energy of 1 MeV which corresponds 6% at 3 Mev. The total measurement time was 753h. We select the signals in two neighbouring channels with time difference between the maxima of the pulses to be $< 0.6\mu$s.



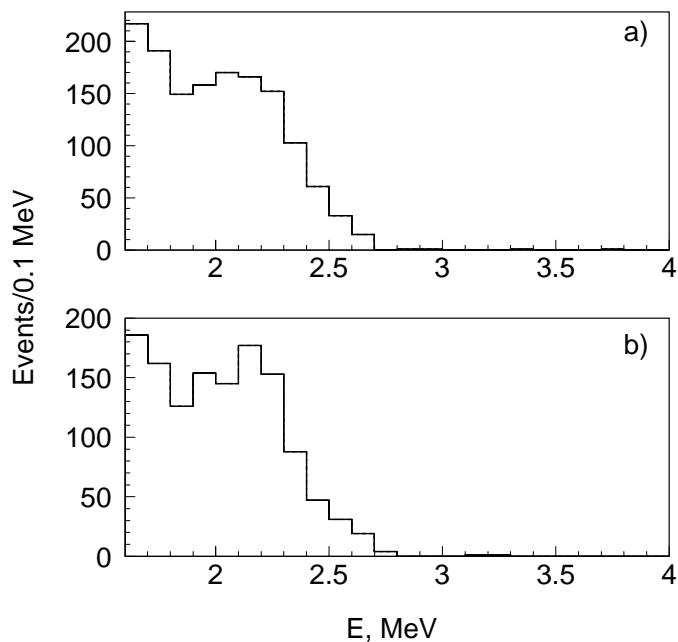Figure 3: Double electrons energy spectra for enriched and natural foils

$0\nu$-decay. Data for 753 hours were analysed. Only two events in enriched foils and 4 events in natural ones in energy interval (2.7–3) MeV were detected. Taking into account the efficiency (23.4%) we can obtain the limit on $0\nu$-decay of $^{100}$Mo, $T_{1/2} > 6.7(3.5) \cdot 10^{21}$ y at 68%(90%)CL.

$0\nu\chi^0$-decay. Data for 753 hours were analysed. The energy interval (2.3–3.0) MeV was

investigated. 214 events in enriched and 188 events in natural foils were found. Using the efficiency value of 5.7% the following limit was obtained, $T_{1/2} > 1.2 \cdot 10^{20}$ y at (90%)CL.

$2\nu$-decay. Data for 753 hours were analysed. The (1.6–3) MeV energy region was investigated because of quite high background at low energy. 1417 and 1292 events were detected in 4 enriched and 4 natural foils, respectively. The difference is $(125 \pm 52)$ events. If all 152 events are connected with $2\nu$-decay of $^{100}$Mo then the half-life is equal to $\sim 8.5 \cdot 10^{18}$ y which is in argeement with the last NEMO result [6].

The limit on $^{42}$Ar radioactive isotope contamination in natural argon using in the working volume was obtained. This limit is less than $6 \cdot 10^{-21}$ parts of $^{42}$Ar per part of $^{nat}$Ar at 90% CL [9].

# 4  Discussion and perspectives

In [10] it was noted the difference in the decay rate in $2\beta2\nu$ process at 'present' (direct counter experiment) and in the 'past' (geochemical experiment). It was proposed that this discrepances can be explaned by the time variation of the weak interaction constant. It was pointed out that the $^{100}$Mo is one of the best candidate to check this hypothesis because it has the maximum rate of decay and quite high concentration of the $^{100}$Mo (9,6%) in the natural molibdenum. In addition, the $^{100}$Ru arised due to the $2\beta$-decay of $^{100}$Mo well kept in minerals. Therefore measuring the half-life of the $2\beta2\nu$ decay of $^{100}$Mo with high accuracy for both direct and geochemical experiments is very interesting. At present the total mass of $^{100}$Mo in our detector is increased up to $\sim$300 g. This quantity is optimal to investigate the $2\beta2\nu$ mode with "differential method" when the electrode system is assembled with alternating cathods made of natural Mo and $^{100}$Mo. In addition we plan to improve the passive shielding (to add antineuteron shielding and 10 cm of copper). As a result the half-life for the $2\nu\beta\beta$ decay of $^{100}$Mo will be measured with accuracy of $\sim$10%, sensitivity to $0\nu$- and $0\nu\chi^0$-modes will be increased to the level of $\sim (1-2) \cdot 10^{23}$ y and $\sim (1-2) \cdot 10^{22}$ y, respectively. In the future the mass of $^{100}$Mo can be increased up to $\sim$500 g.

# 5  Acknowledgements

# 6  Publications and Conferences in 1998

1. V.D. Ashitkov et al., Nucl. Phys. B (Procl. Suppl.) 70 (1999) 233.

2. V.D. Ashitkov et al., Physics of Atomic Nuclei 61 No.6 (1998) 1002-1006.

3.V.N.Stekhanov, talk at conference 'Foundamental interactions of elementary particls', December 16-20, 1998, ITEP, Moscow, Russia

# References

[1] A.S. Barabash et al., preprint ITEP-154 (1986).

[2] A.S. Barabash, V.N. Stekhanov, Nucl. Inst. Meth. A316 (1992) 51.

[3] A.S. Barabash, V.N. Stekhanov, Nucl. Inst. Meth. A327 (1993) 168.

[4] A.S. Barabash et al., Nucl. Phys. B (Proc. Suppl.) 35 (1994) 384.

[5] C. Arpesella et al., preprint LNGS-92/27 (1992).

[6] D. Dassie et al., Phys. Rev. D 51 (1995) 2090.

[7] A.S.Barabash and A.I.Bolozdunya, Liquid Ionization Detectors, Moscow, Energoatomizdat, 1993.

[8] H. Ejiri et al., Nucl. Phys. A611 (1996) 85.

[9] V.D. Ashitkov et al., Nucl. Instr. Meth. A416 (1998) 179.

[10] A.S. Barabash, JETP Lett., 68 (1998) 1.

# DBGS. Search for double beta decay to excited states

C. Arpesella[a], E. Bellotti[b], N. Ferrari[a], L. Zanotti[b]

[a] INFN-LNGS
[b] University of Milano and INFN

**Abstract**

The search for double beta decay to excited states of daughter nuclei continues with the selection of samples with higher purity and some preliminary measurements with Molibdenum and Tellurium. The status is here presented

## 1   Introduction

Double beta decay of nuclei has been extensively investigated since many years, mainly to search for possible violation of the lepton number conservation rule.

Up to now, neutrinoless decay has never been observed; the experimental limits on the half-lives allow to set limits on the Majorana mass of the neutrinos and on the amplitude of right-handed currents.

The allowed decay with the emission of two neutrinos has been observed in a limited number of cases, both in the geochemical and in direct experiments. It is well known that the theoretical predictions on the half-lives were inaccurate also by large factors and only recently theoretical estimates are in agreement with the measured values. The difficulties arise essentially from the nuclear part of the process, namely from the evaluation of the nuclear matrix element.

We have considered, instead of the g.s.$\rightarrow$ g.s. transition, the decay to excited states of the daughter nucleus:

$$(A, Z) \rightarrow (A, Z + 2)^* + 2e(+2\nu)$$
$$\downarrow$$
$$(A, Z) + \gamma's$$
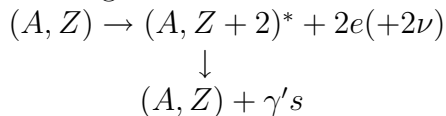
If only gamma rays are observed, the measured value or limit on the half-life is inclusive.

The technique is quite simple, cheap in term of money and manpower, if compared with the search based on the measurement of the two electron and, together with the information of the decay to the ground state, allows to evaluate the nuclear matrix elements of the transition. In addition, transition to $2^+$ excited state in neutrinoless double beta decay is a hint for right-handed coupling existence.

37

Half-life for $(2\nu)\beta\beta$ decay to the first excited states for nuclei with large transition energies ($^{96}Zr$, $^{100}Mo$, $^{150}Nd$) have been predicted [1] to be of the order of $10^{20} - 10^{21}$ years: the search in these lifetime ranges can be performed with high efficient, low intrinsic background Ge detectors, which are nowadays available.

Recent results on the decay of $^{100}Mo$ to excited states of $^{100}Ru$ [2], estimating a half life of the order of $7.10^{20}$ y, but in disagreement with previous published limits [3], indicate that the investigation with such a technique is of actuality but needs confirmation.

DBGS experiment performed measurements on $^{96}Zr$ and $^{150}Nd$ isotopes and the best lower limits on half-life of the decay to excited states have been already presented. The residual contaminations of radioactive contaminants in the analysed samples did not allow to continue the measurements without a further purification (see previous report).

Samples of Molibdenum and Tellurium are under investigation: a measurement of the $^{100}Mo$ decay is foreseen as a calibration test of the set-up system and to investigate a controversial situation; $^{130}Te$ decay to excited states of $^{130}Xe$ has been suggested by Annola and Suhonen [4].

The isotopic abundances of the candidate nuclei for such a $\beta\beta$ decay search allow to consider natural samples rather than enriched ones, thus reducing the prices of the provided materials.

# 2  Status of the experiment

During 1998, measurements have been performed to select a sample of Tellurium from the point of view of radioactivity. We have measured two samples of natural Tellurium from Strem Chemical, respectively of 250 g and 524 g. From few hundreds hours of acquisition, it appears that the two samples are quite pure: we consider very interesting to measure a sample of few Kg in order to estimate the level of radioactive contaminants.

Short measurements of natural Molibdenum samples have been carried on.

The samples showed a quite high level of contamination from radioactive elements; therefore we decide not to continue the measurements.

In any case we obtained the following limits:

$^{92}Mo : T_{1/2} > 5.10^{19} y (90\% C.L.)$

To our knowledge, no value has been reported in literature for this transition.

$^{100}Mo : T_{1/2}(0^+ \to 0_1^+) > 5.10^{19} y (90\% C.L.)$

$\qquad\quad T_{1/2}(0^+ \to 2^+) > 3.10^{19} y (90\% C.L.)$

Our sensitivity is about one order of magnitude worse than what needed to detect the decay.

We remind that we measured two samples of 6 Kg of natural Neodymium: for both samples, the result was a lower limit on the half-life of the decay to the first $0^+$ excited state: $T_{1/2}(0^+ \to 0^{+1}) > 10^{20} y (90\% C.L.)$, even if a factor 4 on background reduction was obtained in the energy region of interest for the more recent sample of Nd. With this purer sample, a small excess of counts above background was present in the energy region for double beta decay search, but it is not significant at 3 s level: we cannot exclude the possibility of a statistical fluctuation of the background and the limit for the transition $0^+ \to 0^{+1}$ was not increased.

# 3   Perspectives

In 1999 we plan to measure Te sample for radioactivity studies and with the mass today available ($\sim$3 Kg), with one year of measurements we could reach a sensitivity of the order of $10^{21}$ years.

For Neodymium and Molibdenum, selection of new samples in which the radioactive contamination, namely for the Thorium chain, are reduced by a factor 5-10, continues, in order to reach a sensitivity of $10^{20} - 10^{21}$ years.

# References

[1]  A.S. Barabash Sov. Phys. JEPT **51** (1990) 207

[2]  A.S. Barabash, presentation at WEIN98

[3]  D. Dassiè et al. Phys. Rev. D **51** (1995) 2090

[4]  M. Annola and J. Suhonen Nucl. Phys. A **206**  (1996) 133

# EAS-TOP. Cosmic Rays Experiment

M. Aglietta[a,b], B. Alessandro[b], P. Antonioli[c], F. Arneodo[d],
L. Bergamasco[b,e], M. Bertaina[b,e], C. Castagnoli[a,b],
A. Castellina[a,b], A. Chiavassa[b,e],G. Cini Castagnoli[b,e],
B. D'Ettorre Piazzoli[f], G. Di Sciascio[f], W. Fulgione[a,b],
P. Galeotti[b,e], P.L. Ghia[a,b], M. Iacovacci[f], G. Mannocchi[a,b],
C. Morello[a,b], G. Navarra[b,e], O. Saavedra[b,e], G. C. Trinchero[a,b],
P. Vallania[a,b], S. Vernetto[a,b], C. Vigorito[b,e]

[a] Istituto di Cosmo-Geofisica del CNR, Torino, Italy
[b] Istituto Nazionale di Fisica Nucleare, Sezione di Torino, Italy
[c] Istituto Nazionale di Fisica Nucleare, Sezione di Bologna, Italy
[d] Istituto Nazionale di Fisica Nucleare, LNGS, Assergi, L'Aquila, Italy
[e] Dipartimento di Fisica Generale dell'Università di Torino, Italy
[f] Dipartimento di Scienze Fisiche dell' Università and INFN, Sezione di Napoli, Italy

### Abstract

The status of the EAS-TOP experiment, the activity of the collaboration, and the main results obtained in 1998 are summarized. For a more complete view of the experiment's outputs refer also to the 1996 and 1997 Annual Reports.

# 1 Introduction

## 1.1 Aims of the experiment

Main aims of the EAS-TOP experiment (Campo Imperatore, 2000 m a.s.l., above the underground Gran Sasso laboratories) are of:

- contributing to construct the experimental knowledge of cosmic radiation in the energy range $10^{13} - 10^{17}$ eV (i.e. around the "knee" of the primary spectrum), through all the available observables: spectra, composition, anisotropies, gamma-ray primaries;

- performing multiparametric analysis, also exploiting the unique possibility of surface and deep underground measurements, which is essential for the debugging of the "interaction-composition-fluctuation" problem in the understanding of EAS data, through the interpretation of a subset of individual events;

- checking the main features of the high energy hadron interactions relevant for the interpretation, and the extrapolation to higher energies of the models elaborated from the accelerator data;

- providing significant informations to interpret the deep underground data.

The experiment results from a collaboration between INFN and CNR (Istituto di Cosmo-Geofisica, Torino).

Improving the statistics on the different items of interest is of main importance at this stage of the experiment. In 1998 the measurements of full detector have therefore been running, together with systematic calibration runs.

The analysis work has been mainly devoted: a) to systematic observations of the "knee" in different EAS components; b) to verifications of the hadronic interaction models used for data analysis using the different observables (that represent a necessary step towards the definition of primary composition); c) concerning astronomical studies, to improve the statistics, completing the searches for transients and "unexpected" gamma-ray sources; d) developing the anisotropy measurements.

Results have been presented to the 10th ISVHECRI (LNGS, July 12-17), Vulcano Workshop (May 25-30), 32nd COSPAR Scientific Assembly (Nagoya, July 12-19), Rome Gamma Ray Bursts Workshop (November 3-6).
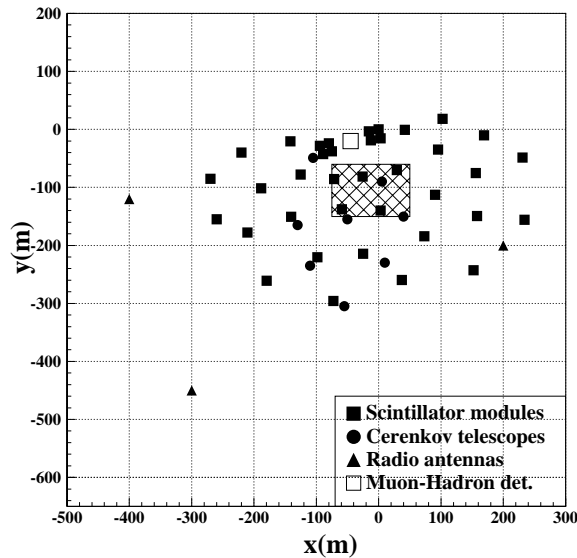


Figure 1: *The EAS-TOP array. The shaded area shows the core location region used for the shower size spectrum measurement.*
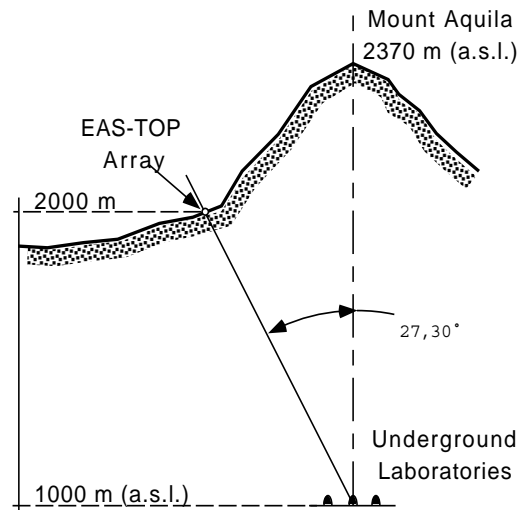


Figure 2: *The EAS-TOP array location with respect to the underground Gran Sasso laboratories.*

## 1.2 The experimental apparatus

The EAS-TOP array (see figs. 1, 2) is operating with:

- the e.m. detector: 35 modules of scintillators, 10 m² each (8 of them equipped with vertical scintillators, to improve the response to Horizontal Air Showers), fully efficient for $N_e > 10^5$;

- the muon-hadron detector: 140 m² calorimeter with 9 layers of 13 cm iron absorbers and streamer tubes as active elements, operating for hadron calorimetry at $E_h > 50$ $GeV$ (an enlargement of the dynamic range has been achieved by reducing the HV power supply of the chambers, increasing the gain on the ADC "low signal", and reducing the gain of the "high signal"), and for muon counting at $E_\mu > 1$ $GeV$ (two vertical walls made of streamer tubes operate at the North and South sides of the detector to provide a trigger to nearly horizontal muons and to help in their reconstruction; 130 m² scintillator muon detectors are distributed in the field ), and 24 $m^2$ RPC muon detector below the bottom layer, for timing measurements (to test the "Time Track Compatibilty" method for reconstructing the EAS longitudinal profile, in collaboration with M. Ambrosio et al.);

- the Cherenkov light detector: 8 telescopes with tracking capabilities equipped with imaging photomultipliers and wide angle optics, with full opening angles: 15 and 60 degrees (the latter in cooperation with the TUNKA group);

- three radio antennas for EAS radio emission measurements;

- moreover it operates in coincidence with the underground MACRO and LVD muon detectors ($E_\mu > 1.3$ $TeV$; full area $A_\mu^{TeV} \approx 1000$ $m^2$).

## 2 The studies of the *knee*

Shower size spectra observed at different zenith angles in the region of the knee are shown in fig. 3.

Table 1: *Results obtained from the fits to the Ne and Nμ spectra measured in different bins of zenith angle (1,2 = below, above the knee).*

| $\Delta \sec \theta$ | $\gamma_1$ | $\gamma_2$ | $I(> Ne_k, N\mu_k) \times 10^7$ $m^{-2}s^{-1}sr^{-1}$ | $Log(Ne_k, N\mu_k)$ |
|---|---|---|---|---|
| e 1.00 − 1.05 | 2.56 ± 0.02 | 2.99 ± 0.09 | 0.99 ± 0.2 | 6.09 ± 0.05 |
| 1.05 − 1.10 | 2.55 ± 0.02 | 2.93 ± 0.11 | 1.01 ± 0.3 | 6.02 ± 0.07 |
| 1.10 − 1.15 | 2.55 ± 0.03 | 2.85 ± 0.12 | 0.93 ± 0.4 | 5.97 ± 0.08 |
| 1.15 − 1.20 | 2.56 ± 0.03 | 2.81 ± 0.16 | 0.80 ± 0.4 | 5.93 ± 0.14 |
| 1.20 − 1.25 | 2.59 ± 0.03 | 2.91 ± 0.26 | 0.52 ± 0.3 | 5.95 ± 0.11 |
| 1.25 − 1.30 | 2.55 ± 0.07 | 2.80 ± 0.11 | 1.30 ± 0.6 | 5.63 ± 0.12 |
| μ 1.00 - 1.05 | 3.12 ± 0.1 | 3.52 ± 0.1 | 1.0 ± 0.2 | 4.72 ± 0.1 |
| 1.10 - 1.15 | 3.07 ± 0.1 | 3.52 ± 0.1 | 0.7 ± 0.2 | 4.77 ± 0.1 |

It has been proved that the break is observed at decreasing shower size with increasing atmospheric depth (i.e. zenith angle), and at constant intensity (see tab. 1; for this first observation of EAS-TOP see previous Reports). The absorbtion length of EAS particles
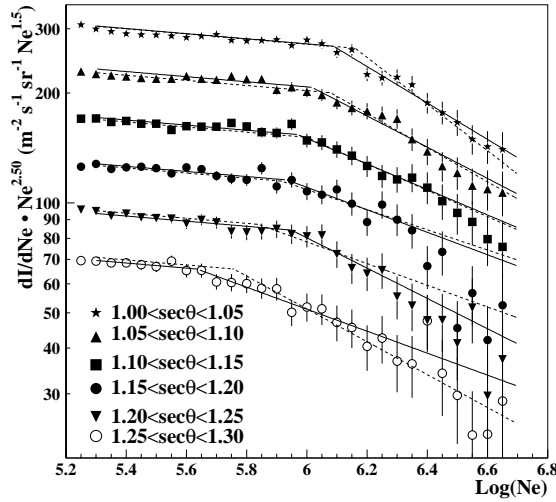
Figure 3: *Differential shower size spectra measured at different atmospheric depths. The solid lines show the results of the fitting procedure with 3 free parameters per spectrum; dashed lines those of the procedure requiring constant integral flux above the knee.*
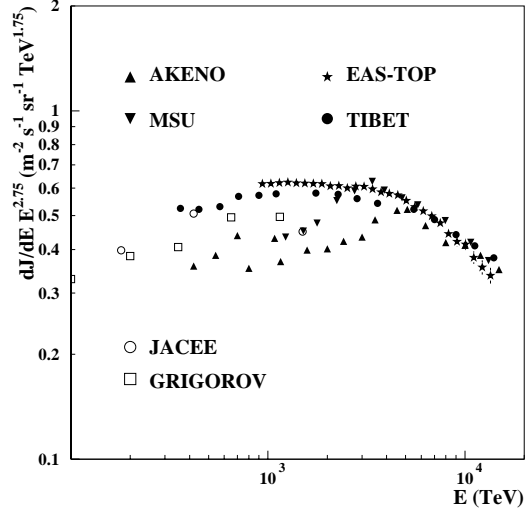


Figure 4: *The all particle energy spectrum obtained from the EAS-TOP shower size data, compared with the results of other experiments operating outside the atmosphere or at ground level.*

at the knee (i.e. $Ne_k$) is $\Lambda_k = 220 \pm 3$ g cm$^{-2}$, in agreement with the measurements obtained from the "constant intensity cut" technique ($\Lambda_{EAS} = 217 \pm 3$ g cm$^{-2}$).

The all particle energy spectrum, as obtained from the conversion of the size spectrum, is shown in fig. 4 (the value of $< A >$ as resulting from the extrapolation of the direct measurements, and a rigidity dependent knee are used; all conversions and comparisons with expectations are performed by using the CORSIKA-HDPM model). The data are well connected with the direct measurements, and agree with other EAS measurements at the knee and above.

Muon number spectra as observed at two different atmospheric depths are shown in fig. 5 ($N_\mu^{GeV}$ being obtained from the reconstructed number of muon tracks in the muon-hadron detector, and the experimental muon l.d.f.; see 1996 and 1997 Reports). Further comparison of the knee parameters as measured in the e.m. and muon components at different atmospheric depths are shown in tab. 1, and in fig. 6 concerning the relation between the exponents of the $N_e$ and $N_\mu^{GeV}$ spectra, which also demonstrate good consistency and agreement with the predictions of the hadron interaction models.

The scatter plot of a sample of vertical and inclined ($\approx 25$ deg) events in the $N_e - N_\mu^{GeV}$ observables are shown in figs. 7 and 8. On the same plots, the position of the knee as independently identified in $N_e$ and $N_\mu^{GeV}$ is shown. At both zenith angles (in agreement with consistent absorption properties of EAS at the knee), the knee error box is inside the distribution of the experimental points, far from the upper and lower edges, which
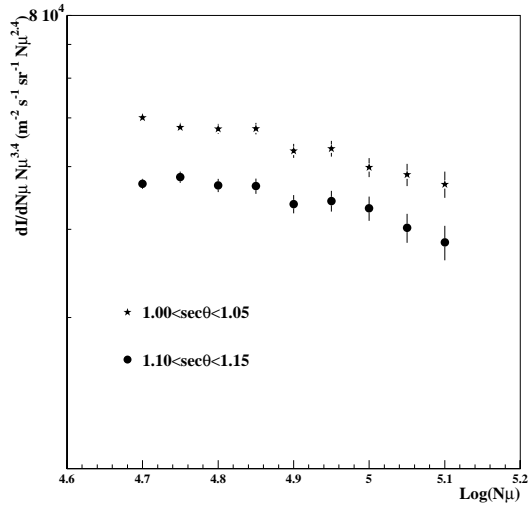
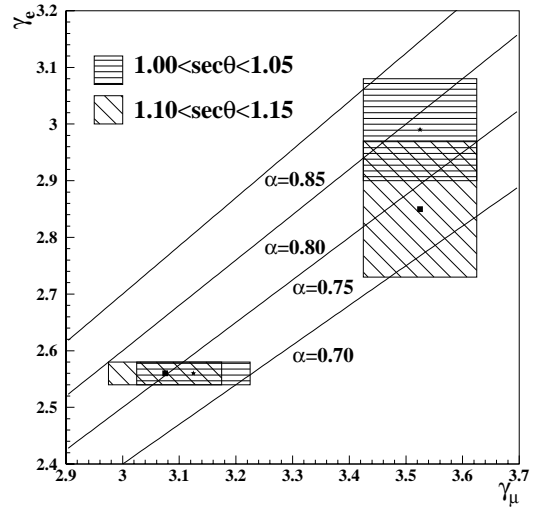Figure 5: *$N_\mu$ spectra measured in two different intervals of zenith angles.*



Figure 6: *Comparison of the slopes of the $N_e$ and $N_\mu$ spectra measured below and above the knee: $\alpha$ is the index of the $N_e - N_\mu$ relation ($N_\mu \propto N_e^\alpha$).*
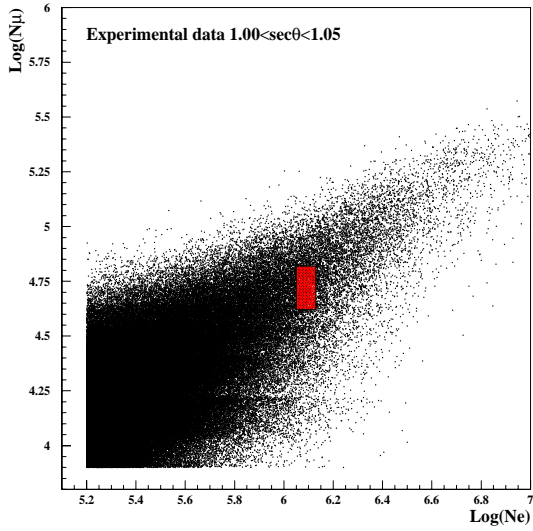


Figure 7: *Scatter plot of $N_\mu$ vs. $N_e$ data for vertical events, with the identification of the knee in the two components shown.*
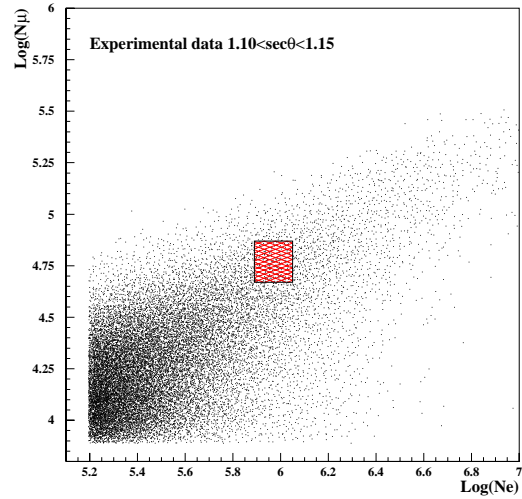


Figure 8: *Same as figure 7 for experimental data for $24.6° < \theta < 29.6°$.*

correspond to very heavy (iron) and light (proton) primaries, so that a break in such components is unlikely. Intermediate mass nuclei ("CNO-Helium like") are thus favoured.

Table 2: *Measured and simulated attenuation lengths* $\Lambda_{\text{obs}}(g/\text{cm}^2)$ . *Different accuracies in the simulations are due to different statistics.*

| $\log N_e^i$ | 6.0 | 6.1 | 6.2 |
|---|---|---|---|
| Exp. Data | $75 \pm 5$ | $76 \pm 6$ | $75 \pm 7$ |
| He correction | $96 \pm 6$ | $93 \pm 7$ | $86 \pm 8$ |
| HDPM | $90 \pm 9$ | $83 \pm 9$ | $80 \pm 10$ |
| VENUS | $78 \pm 7$ | $72 \pm 7$ | $75 \pm 10$ |
| DPMJET | $71 \pm 6$ | $66 \pm 6$ | $66 \pm 7$ |
| QGSJET | $74 \pm 6$ | $69 \pm 6$ | $65 \pm 7$ |
| SIBYLL | $105 \pm 12$ | $89 \pm 10$ | $71 \pm 8$ |

For protons, He and CNO nuclei, the primary energies corresponding to $Ne_k = 1.2$ $10^6$, at the observation depth of $x = 820$ g cm$^{-2}$ are respectively $E_O = (2.7 - 3.4 - 4.1)10^{15}$ eV. Values of $E_O \approx 4.\ 10^{15}$ eV agree with the energy determination of the knee from the TUNKA atmospheric Cherenkov detector (which is independent on the primary composition). Absolute intercalibrations of the detectors, and combined measurements could therefore be of main significance.

# 3 High energy hadron interactions

As already pointed out, the verification of the interaction models used in the analysis (beside its own interest) is a crucial task to proceed further in the composition studies. A particular attention has thus been devoted to such aspect (see also the 1997 Report in which the consistent selection of "light" and "very heavy" primaries was achieved through the $N_e - N_\mu^{GeV} - N_\mu^{TeV}$ data, in agreement with the CORSIKA-HDPM code).

## 3.1 The proton attenuation length

The attenuation length of proton primaries in air (and hence the $p - air$ inelastic cross section) is studied at primary energy $E_o \approx 2.10^6\ GeV$ by selecting EAS near maximum development, through $N_e$ and $N_\mu$ and studying their absorption in the atmosphere.

Events with primary energy $2.10^6$ GeV $< E_0 < 4.10^6$ GeV are selected using expression

$$n_\mu = 1.34 \times 10^{-3} \times \cos^{1.97}\theta \times E_0^{0.9} \times f(r), \tag{1}$$

where $f(r)$ is the muon lateral distribution:

$$f(r) = r^{-0.75} \times (1 + r/320.)^{-2.5}. \tag{2}$$

given their core distance $(50 < r < 150\text{m})$, zenith angle $(\theta)$ and detected muon number in the muon detector $(n_\mu)$.

In order to select proton initiated showers near maximum development, events belonging to the uppermost few percent of the shower size distribution are used. Three cuts $(\log N_e^i = 6.0 \div 6.2)$ are performed, to check the stability of the measurement.

The measured and expected attenuation lengths (obtained from different interaction models included in the CORSIKA code, including the full detectors' responses) are given

in tab. 2. The values corrected for the possible contamination from a primary Helium flux equal to the proton one at the energy of interest is also shown (indicating that the quoted experimental datum could represent a lower limit to the attenuation length).

It results that the experimental values are in better agreement with models predicting longer absorption lengths, as HDPM and VENUS.

The simulated attenuation lengths $\Lambda_{\rm obs}^{\rm sim}$, compared to the interaction mean free path $\lambda_{p-{\rm air}}^{\rm sim}$, provide the factor $k = \Lambda_{\rm obs}^{\rm sim}/\lambda_{p-{\rm air}}^{\rm sim}$. This factor includes shower fluctuations, detectors' response and some features of the interaction model.

From $\lambda_{p-{\rm air}} = \Lambda_{\rm obs}/k$, the measurement of $\lambda_{p-{\rm air}}$ and consequently of $\sigma_{\rm in}^{p-{\rm air}}({\rm mb}) = 2.41 \times 10^4/\lambda_{p-{\rm air}}$ is obtained. The obtained range for $\sigma_{\rm in}^{p-{\rm air}} = (300 \div 400)\,{\rm mb}$ (allowing for the statistical uncertainties, and the differences between the models) is lower than previously reported in literature (as first reported by the EAS-TOP collaboration at the Durban Conference).

## 3.2  The secondary production cross section for $x \approx 0.1$

Data on the discrimination of different interaction models from the point of view of the secondary production cross section for $x = E_s/E_0$ values $\approx 1$ where reported from the "anticoincidence events" from EAS-TOP and MACRO (see 1997 Report).

Concerning the secondary production cross section, the interaction models mainly differentiate in the forward region ($x > 0.1$), which is of difficult access to accelerators, mostly for $p-nucleus$ interactions. The energy spectra of different primaries contributing to TeV muons are shown in fig. 9. At primary energies $E_0 \approx 10$ TeV only primary protons contribute. Muon energies can be selected by deep underground detectors (3400 m $w.e.$ depth in the case of Gran Sasso laboratories) and, in such range, primary energies can be measured by means of atmospheric Cherenkov light observations.

The contemporaneous measurement of these two quantities provides the unique possibility in ground based cosmic ray experiments of obtaining information on the total energy $E_0$ and on the minimum energy per nucleon of the primary ($E_\mu^{th} \propto E_0/A$).

The experiment provides:

a) a measurement of $< N_\mu > (E_\mu \geq 1.3\,{\rm TeV})$ for high energy muons and fixed primary proton energy for $x = E_{sec}/E_0 > 0.1$: since at $E_0 \approx 10$ TeV only proton primaries contribute to TeV muons, this allows to check the models used in H.E. hadron interactions and represent a significant information for the interpretation of deep underground muon measurements.

b) a study of the p/helium ratio at $30 \leq E_0 \leq 100$ TeV which is quite controversial from direct measurements. Helium primaries contribute to the TeV muons flux above $E_0 \simeq 30$ TeV, carbon primaries above $E_0 \simeq 80$ TeV.

The results of a first run performed in $\approx 100$ hours of data taking in coincidence with LVD are shown in fig. 10, together with the results of the calculations by Forti et al. for beams of protons and alfa particles and the expectations from different models and primary protons obtained through the CORSIKA code.

The general trend of expectations over the whole 10 - 100 TeV energy range is confirmed; further statistics (reaching $\approx 10\%$ accuracy) is required to discriminate between different interaction models.
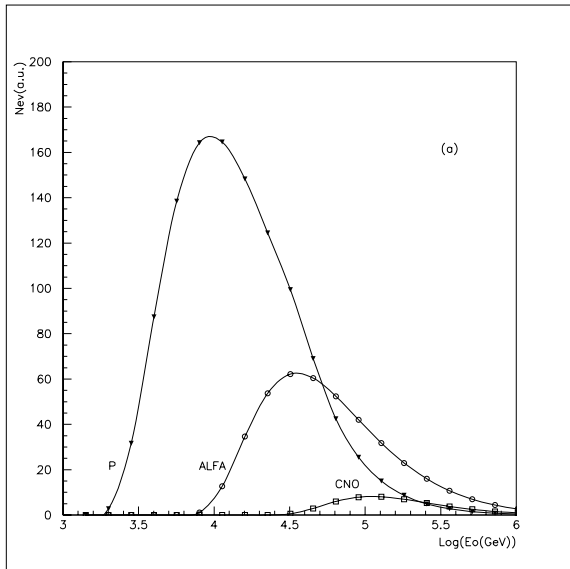
Figure 9: *Energy spectra of primaries contributing to primary muons deep underground ($E_\mu^{th} = 1.3$ TeV, JACEE primary spectra).*



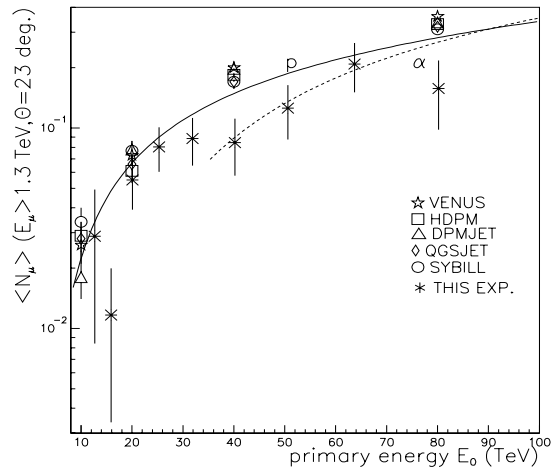Figure 10: *$< N_\mu >$ measured by the combined operation between the EAS-TOP Cherenkov array and the LVD experiment. The continuous and dotted lines show the results of Forti et al..*

## 3.3   Large transverse momenta at $\sqrt{s} \approx 1 - 2\ TeV$

Multicore events (see fig. 11; in fig. 12 the results of the analysis are shown) are selected from the analysis of the e.m. component detected on the uppermost layer of the calorimeter ("quasi proportional" information: pad resolution $38 \times 40\ cm^2$).

For each subcore, the quantities:

$$P9 = \sum_{(i,j)}^{20} N'_{i,j} \quad and \quad S8 = \sum_{k=1}^{8} \sum_{(i,j)}^{20} N'_{i,j,k} \quad (N'_{i,j} = N_{i,j} - \overline{N}_{i,j}) \tag{3}$$

are defined.

The sum involves the 20 most significant pads within $1\ m$ from the subcore position on the uppermost plane ($P9$, i.e. the electromagnetic content) and, for internal ones, around the projected position following the EAS direction ($S8$ integrated over the 8 internal layers, i.e. the hadronic and high energy e.m. contents). $\overline{N}_{i,j}$ for the upper layer is obtained from the NKG fit, for internal ones from the pads at the same distance $r$ from the main core, not belonging to the subcore structure. The resulting scatter plot $P9 - S8$ for physical events is shown in fig. 13. The same plot is shown in fig. 14 for simulated primary proton showers of different energies initiated at the top and at different atmospheric depths ranging from 8 to 10 $km$ a.s.l.. From the comparison of fig. 13 and 14 it results that the patterns of the selected subcore structures fall in the region characterized by intermediate starting levels in the atmosphere. The most natural interpretation for the
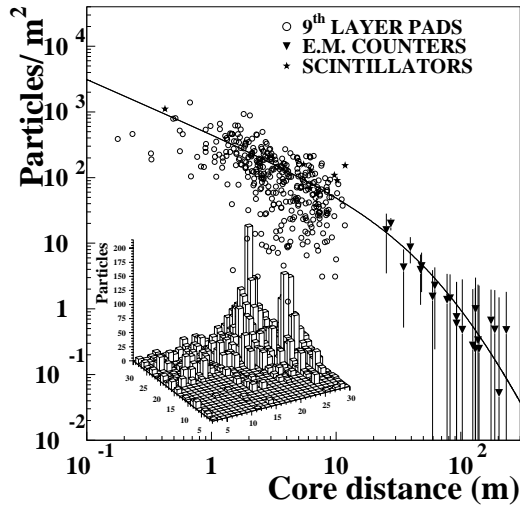
48

Figure 11: *A multicore EAS: the reconstructed lateral distribution function of the main shower and the central region are shown.*
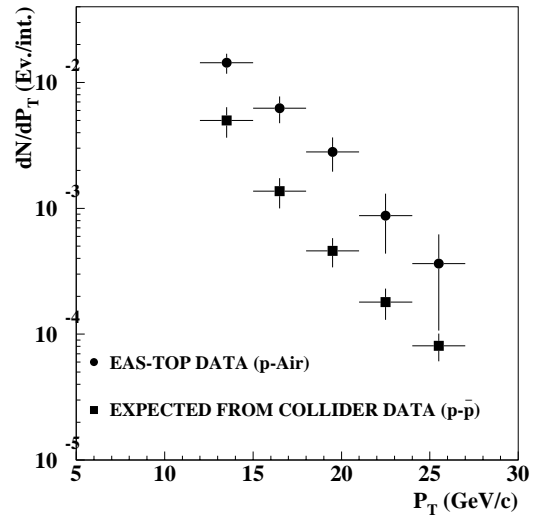


Figure 12: $P_T$ *distribution in multicore EAS (p − Air interactions) compared with the expected one from the p − p̄ collider cross section data.*
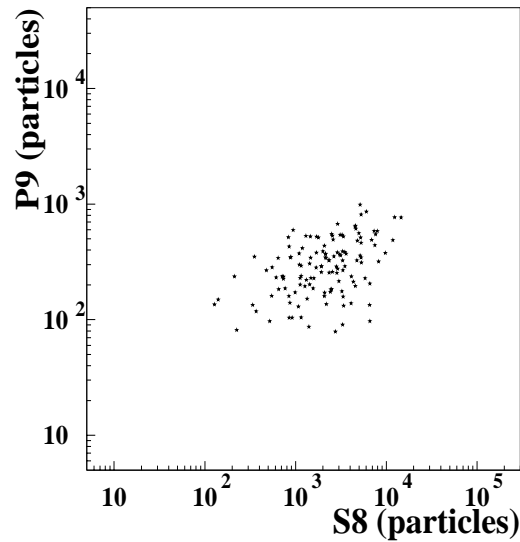


Figure 13: *Scatter plot of cluster patterns (P9,S8) of the detected secondary structures in* 130 *multicore EAS.*
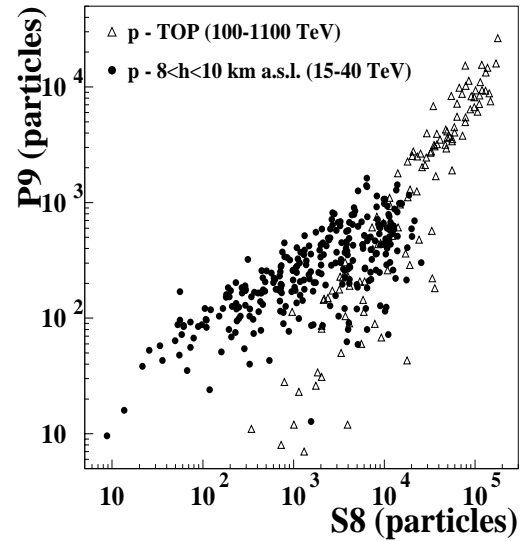


Figure 14: *Scatter plot of cluster patterns (P9,S8), showing the different behaviour between top initiated showers and showers initiated at lower level.*

secondary structures is thus that they are due to jets produced in H.E. "proton-air nuclei" interactions along the shower development. Subcore energies ($E_s$) and production heights ($h$) are obtained through fits to the simulated P9 and S8 quantities. Typical values are: $10 \leq E_s \leq 50\ TeV$ and $5 \leq h \leq 9\ Km$ above the detectors, while the measured distances from axis are $1.5 \leq r \leq 7\ m$.

By means of ad hoc simulations the following quantities have been computed and included in the analysis: a) the correction $\epsilon_E$, due to the jet fragmentation, to be applied to the subcore energy $E_s$; b) the efficiency for subcore detection $\epsilon_D(N_e, E_s, r)$; c) the geometrical rapidity acceptance $\epsilon_R(\eta)$.

The transverse momentum for each subcore has been obtained using expression:

$$P_T = \frac{E_s \cdot r}{\epsilon_E \cdot h}. \tag{4}$$

The uncertainty in the $P_T$ measurements is: $\Delta P_T / P_T \approx 50\%$. At the quoted intermediate interaction levels the projectiles contributing to the events can be associated to the leading particles inside the showers. Their energy spectrum has been derived from the primary one by scaling the corresponding energy to the mean production depth of our events with an attenuation length $\Lambda \approx 100\ gcm^{-2}$. At the mean production height $z \approx 9000\ m\ a.s.l.$, i.e. atmospheric depth $X \approx 270\ gcm^{-2}$, the leading particle energy, averaged over the primary spectrum in the range $500 - 1000\ TeV$ here analysed, is $E_{l.p} \approx 125\ TeV$ corresponding to $\sqrt{s} \approx 500\ GeV$ for $p - p$ interactions. The accepted region of pseudo-rapidity $7.8 \leq \eta \leq 8.8$, where $\epsilon_R(\eta)$ exceeds 40%, corresponds to $1.6 \leq \eta_{c.m.} \leq 2.6$ in the c.m. of the interaction.

The resulting $P_T$ distribution for $1.6 \leq \eta_{c.m.} \leq 2.6$ is shown in figure 12 where the shift due to the uncertainties in the measurements of $P_T$ have been included. In the same figure the $(dN/dP_T)_{p-\bar{p}}$ distribution expected from the cross section $d\sigma/dP_T$ in $p-\bar{p}$ interactions at $\sqrt{s} \approx 500\ GeV$ in the same rapidity interval is shown (collider data). The experimental and expected slopes $\frac{dN}{dP_T} \propto P_T^{-n}$ with $n \approx 7$ are in good agreement. The obtained gap in the absolute values reflects the difference between $p - p$ an $p - N$ collisions. The ratio $R = \sigma_{EAS}^{JET}/\sigma_{p-p}^{JET} = \sigma_{p-N}^{JET}/\sigma_{p-p}^{JET}$ is on average: $R = 3.8 \pm 0.7$. By representing such gap following the usual expression $\sigma_{p-N} = \sigma_{p-p} \cdot A^\alpha$ with $A \approx 14.7$ (mean atomic number of "air" nuclei target) the value $\alpha = 1.53 \pm 0.07$ is obtained. This measurement agrees with the accelerator data obtained in fixed target experiments at $\sqrt{s} \approx 30\ GeV$. It is shown that no change of the value of $\alpha$ occurs between $\sqrt{s} \approx 30\ GeV$ and $\sqrt{s} \approx 500\ GeV$. Such effect can be relevant for experiments studying the c.r. primary composition through the observation of the high energy components in the core region.

# 4  Gamma-ray astronomy

The EAS arrival directions are measured through the times of flight among the different detectors, with accuracy: $\sigma_\alpha = 0.5^o$ for $Ne > 10^5$.

Two data sets (collected between 1st January 1992 and 31st May 1998) corresponding to different primary energy thresholds (LE: $E_1 \approx 25$ TeV and HE: $E_2 \approx 90$ TeV) have been used in the search for UHE $\gamma$-ray continuous and transient (on the time scale of the
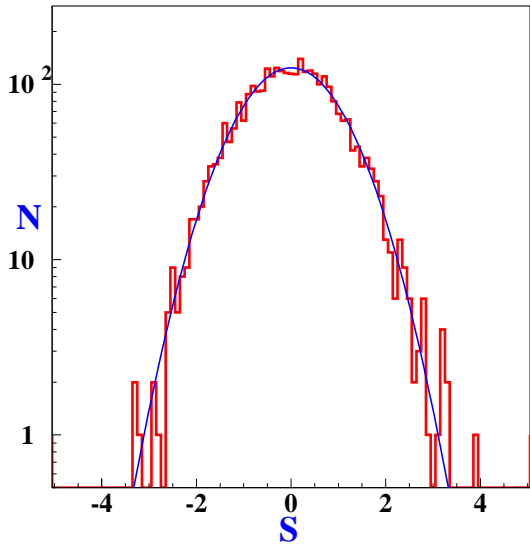
Figure 15: *D.C. emission search: distribution of sky cells significances for H.E. events, superimposed on unit-width gaussian one with zero mean.*
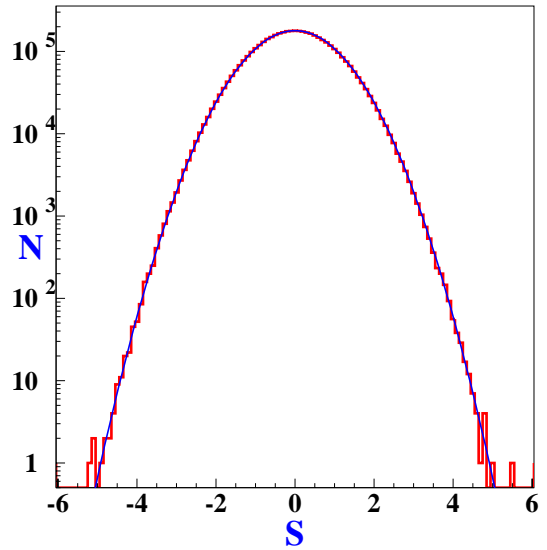


Figure 16: *Transient emission search: distribution of daily significances for H.E. events, superimposed on unit-width gaussian one with zero mean.*
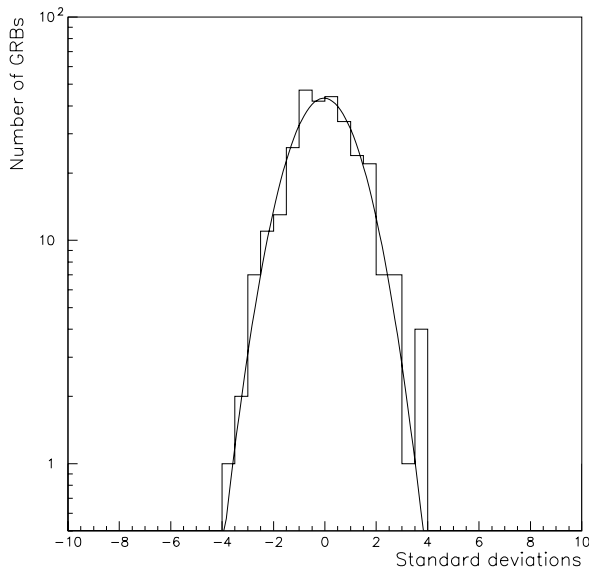


Figure 17: *Distribution of the excesses, in unit of standard deviations, observed in coincidence with 292 BATSE GRBs.*
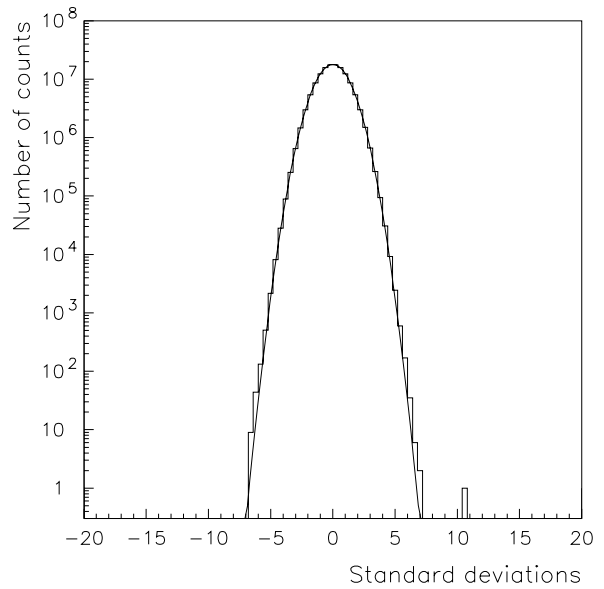


Figure 18: *Distribution of the excesses of duration $\Delta t = 1\ s$ in units of standard deviations, obtained in the "all sky" survey.*

source transit) emissions from unexpected point sources of ultra-high-energy $\gamma$-rays in the northern sky. The distributions of the excesses (Li and Ma statistics) from the 3120 sky cells, integrated over 1433 days of observation, and the 4.470.960 observed "transits"

are shown in figs. 15 and 16 (HE events). The counting rates from all the observed directions in the sky show a behaviour compatible with the expectations from statistical fluctuations, and the agreement between the expected and measured distributions show the excellent stability of the detector.

Derived upper limits (for a source culminating at the zenith, at 90% c.l.) are:

D.C. emission:

$\Phi(> 25 \text{ TeV}) < 4.3 \cdot 10^{-13} \text{ cm}^{-2} \text{ s}^{-1}$,

$\Phi(> 90 \text{ TeV}) < 9.2 \cdot 10^{-14} \text{ cm}^{-2} \text{ s}^{-1}$,

transient emission:

$< 0.6$ evs/year, with duration $< 8$ hrs and

$\Phi(> 25 \text{ TeV}) > 1.8 \cdot 10^{-11} \text{ cm}^{-2} \text{ s}^{-1}$,

$\Phi(> 90 \text{ TeV}) > 5.1 \cdot 10^{-12} \text{ cm}^{-2} \text{ s}^{-1}$.

The search for GRBs of energy $E_\gamma > 10$ GeV has been extended through the single particle counting rate of the EAS array. The excess distributions (see figs. 17 and 18) show again excellent agreement with the statistical expectations. No candidates have been observed in coincidence with 292 BATSE GRBs and the typical upper limits obtained on the energy fluences are $F(10 \text{ GeV} \div 1 \text{ TeV}) \sim 10^{-4} \div 10^{-3}$ erg cm$^{-2}$ for events with zenith angle $\theta < 30°$. A single candidate has been observed in the "all sky" survey mode during $1.5 \ 10^3$ days (see the $> 10$. s.d. excess in fig. 18).

# 5 Conclusions

The status of the EAS-TOP experiment, focousing on the aspects developed in 1998, has been summarized.

The activity has been continued on other items already discussed in previous Reports, namely:

- the study of primary composition and interactions through the coincidences with LVD and MACRO;

- the analysis of primaries by means of the $N_e - N_\mu^{GeV} - N_\mu^{TeV}$ data;

- the anisotropy measurements;

- the Cherenkov light observation program;

- the hadron studies in the calorimeter (uncorreleted and in EAS cores);

- the rate and structure of nearly Horizontal Air Showers.

On such items the improvement of statistics, the comparison with simulations and the interpretation work are in further progress.

A stable and systematic data taking has to be guaranteed to fulfill the experimental program.

# 6 Collaborators and Institutions

M. Aglietta, B. Alessandro, V.V. Alexeenko, P. Antonioli, F. Arneodo, J. Bellandi, V.S. Berezinsky, L. Bergamasco, M. Bertaina, A. Bosio, A. Campos Fauth, A. Castellina, C. Castagnoli, A. Chiavassa, G. Cini Castagnoli, B. D'Ettorre Piazzoli, G. Di Sciascio, W. Fulgione, P. Galeotti, A. Gazizov, P. L. Ghia, R. Granella, M. Iacovacci, L.

B. Konstantinovich, L. Kuzmichev, A.S. Lidvansky, A. Lima de Godoi, G. Mannocchi,
C. Melagrana, N. Mengotti Silva, C. Morello, G. Navarra, H. Nogima, L. Periale, P. Picchi,
V.V. Prosin, L. Riccati, O. Saavedra, M. Serio, G. C. Trinchero, A. Turtelli, P. Vallania,
S. Vernetto, C.Vigorito
Technical staff: G. Giuliani, A. Giuliano, F. Gomez, G. Pirali
*Istituto Nazionale di Fisica Nucleare, Sezione di Torino, Torino, Italy*
*Istituto di Cosmo-Geofisica del CNR, Torino, Italy*
*Dipartimento di Fisica Generale dell' Università di Torino, Torino, Italy*
*INFN, Laboratori Nazionali del Gran Sasso, Assergi (AQ), Italy*
*Dipartimento di Scienze Fisiche dell' Università and INFN, Napoli, Italy*
*Istituto Nazionale di Fisica Nucleare, Sezione di Bologna, Bologna, Italy*
*Instituto di Fisica, Universidade Estadual, de Campinas, Campinas (SP), Brazil*
*Institute of Physics, National Academy of Sciences of Belarus, Minsk, Belarus*
*Institute for Nuclear Research, Russian Academy of Sciences, Moscow, Russia*
*Institute for Nuclear Physics, Moscow State University, Moscow, Russia*
*Universidade de Sao Paulo, Sao Paulo (SP), Brazil*

# 7   List of Publications

1. "The High Energy Muon Spectrum in Extensive Air Showers: First Data from LVD
   and EAS-TOP at Gran Sasso"
   *Astroparticle Physics,* **9***, 185 (1998)*

2. "The hadron calorimeter of EAS-TOP: operation, calibration and resolution"
   *Nuclear Instruments and Methods in Physics Research A,* **420***, 117 (1999)*

3. "The EAS Size Spectrum and the Cosmic Ray Energy Spectrum in the Region
   $10^{15} - 10^{16}$ eV"
   *INFN/AE-98/21*
   *to be published in Astroparticle Physics*

4. "Study of Markarian 421 in the $\gamma - ray$ energy range 30-100 TeV"
   *Nuclear Physics B,* **70***, 506 (1999)*

5. "Experimental Study of Hadronic Interaction Models using Coincident Data from
   EAS-TOP and MACRO"
   *Nuclear Physics B,* **70***, 483 (1999)*

6. "Identification of light and very heavy cosmic ray primaries at $E_0 \approx 10^{15}$ eV from
   surface and deep underground measurements at th Gran Sasso Laboratories"
   *Nuclear Physics B,* **70***, 512 (1999)*

7. "Study of Horizontal Air Showers from EAS-TOP: a possible tool for UHE neutrino
   detection?"
   *Nuclear Physics B,* **70***, 509 (1999)*

# GNO. Gallium Neutrino Observatory

M. Altmann[a], M. Balata[b], P. Belli[c],
E. Bellotti[d], R. Bernabei[c], C. Cattadori[d],
G. Cerichelli[e], M. Chiarini[e], S. d'Angelo[c],
G. Del Re[e], K. Ebert[f], F. von Feilitzsch[a], N. Ferrari[b],
W. Hampel[f], J. Handt[f], E. Henrich[g], G. Heusser[f],
J. Kiko[f], T. Kirsten[f], M. Laubenstein[b], H. Richter[f],
F. Veglio[e], R. Volpe[e], S. Wänninger[a], L. Zanotti[d]

[a] Physik Department E15, Technische Universität München (TUM),
James-Franck Straße, D-85747 Garching b. München, Germany
[b] INFN, Laboratori Nazionali del Gran Sasso (LNGS),
S.S. 17/bis Km 18+910, I-67010 L'Aquila - Italy
[c] Dip. di Fisica, Universitá di Roma "Tor Vergata" and INFN, Sezione di Roma II,
Via della Ricerca Scientifica, I-0133 Roma - Italy
[d] Dip. di Fisica, Universitá di Milano and INFN, Sezione di Milano
Via Celoria 16 - I-20133 Milano Italy
[e] Dip. di Ingegneria Chimica e Materiali, Universitá dell'Aquila.
[f] Max Plank Institut für Kernphysik (MPIK),
Postfach 103980, D-69029 Heidelberg, Germany
[g] Institut für Technische Chemie, Forschungszentrum Karlsruhe (FZK),
Postfach 3640, D-76021 Karlsruhe, Germany

## Abstract

The aim of GNO (Gallium Neutrino Observatory) is to monitor the low energy solar neutrino flux with a gallium detector at LNGS. The experiment is the successor project of GALLEX, which continuously took data with 30 tons of gallium in the time period 1991-1997. The gallium mass in the GNO project will be gradually increased in the next years from the present 30 tons up to 100 tons. In April 1998 GNO started the first series of solar neutrino observations with 30 tons of gallium (GNO30, the first stage of the GNO project).

This report is organized in the following way:

In section 1 we give a short description of the main features of the gallium detector at LNGS; we review the latest results of GALLEX, and summarize the goals and the planned steps of the GNO project.

In section 2 we discuss the experimental activity in 1998 .

Section 3 summarizes the R&D and the future plans.

# 1   Introduction

## 1.1   The gallium solar neutrino detector at LNGS

A gallium solar neutrino detector is installed at Laboratori Nazionali del Gran Sasso (Abruzzo, Italy) since 1990. It looks for solar neutrinos via the reaction $^{71}Ga\,(\nu_e, e\,)^{71}Ge$, which has a threshold of 233 keV. The detector is sensitive mainly to pp-neutrinos.

In the present configuration the target consists of 101 tons solution of $GaCl_3$ in water and HCl, containing 30.3 tons of natural gallium; this amount corresponds to $\sim 10^{29}\,^{71}Ga$ nuclei.

The solar neutrino interaction rate on $^{71}$Ga is deduced from the number of $^{71}$Ge atoms observed. The latter are identified through their decay after chemical separation from the target. In short the experimental procedure is the following [1]:

1. The solution is exposed to solar neutrinos for about 4 weeks; at the end of this exposure about 16 $^{71}$Ge nuclei should be present in the solution if the standard solar model (SSM) is correct and all neutrinos do reach the Earth.

2. The $^{71}$Ge , present in the solution as volatile $GeCl_4$, is chemically extracted into water by pumping $\sim 3,000$ m$^3$ of Nitrogen through the solution.

3. The extracted $^{71}$Ge is converted into $GeH_4$, Germane gas, and introduced into minia-turized proportional counters [2] mixed with Xenon as counting gas. At the end $\sim$ 95 - 98 % of the $^{71}$Ge present in the solution at the time of the extraction is in the counter; extraction and conversion efficiencies are under constant control using non radioactive germanium isotopes as carriers [3].

4. The $^{71}$Ge e-capture (meanlife 16.5 days) $^{71}Ge\,(e^-, \nu_e\,)^{71}Ga$ is observed for a period of 6 months, allowing the complete decay of $^{71}$Ge and a good determination of the counter background.

5. Data are analyzed to obtain the most probable number of $^{71}$Ge introduced in the counter. Counter backgrounds are minimized by rigorous application of low-level technology in counter design and construction. The residual background is mostly rejected through application of amplitude and shape analysis on the recorded pulses. $^{71}$Ge decays produce pulses corresponding to an energy around 10.4 keV (K-captures) or 1.1 keV (L-captures); the ionization produced by the decay is point-like, so that the pulses are fast compared with most of the natural radioactivity back-ground. Counters are calibrated by an external Gd/Ce X-ray source [11], in order to carefully define amplitude and puse shape cuts with known efficiency for each

measurement. The event amplitude and shape selection reduces the mean background rate to less than 0.1 counts per day. Normally, each counter is calibrated 5 times during the 6 month counting time, to check the stability of the gain and of the resolution. In case of instabilities the calibrations are performed every month. The selected data are analyzed with a maximum likelihood method to obtain the most probable number of $^{71}$Ge nuclei at the beginning of counting, which (after correcting for counting, extraction and filling efficiencies) gives the number of $^{71}$Ge produced in the solution during the exposure and, therefore, the $^{71}$Ge production rate.

6. A correction is made to account for contributions to the observed signal from sources other than solar neutrinos, mainly due to interactions in the solution generated by high energy muons from cosmic rays and by products due to natural radioactivity.

7. Another correction is made to account for background signals in the counter that can be confused with $^{71}$Ge decays. The total subtraction for points 6 and 7 is tipically of the order of a few percent of the signal.

## 1.2   The latest results of GALLEX

GALLEX was operating between 1991 and 1997 with a 30 tons gallium detector at LNGS. In 1997, GALLEX completed its scientific program: the achieved results can be summarized in the following way:

- The measured solar neutrino interaction rate on $^{71}$Ga is $77.5 \pm 6.2$ (stat.) $^{+4.3}_{-4.7}(sys.)$ SNU [1] ($1\sigma$) [4]. This result was obtained after 5 years of measurements (65 'solar run' extractions) performed in the time period 1991-1997.

- The target solution was exposed two times to a very intense ($>60$ PBq) $^{51}Cr$ source of monochromatic neutrinos (750 keV, 90%; 430 keV, 10%). The ratio measured signal / expected signal was found to be R=$0.93 \pm 0.08$ [5].

- A test of the systematics on the extraction efficiency was performed at the end of the experiment by introducing in the solution several thousands atoms of radioactive $^{71}As$ (decaying into $^{71}$Ge with a kinematic which closely mimics solar neutrinos); the result confirms that the $^{71}$Ge signal is as expected within 1%[6].

The measured value of the rate is substantially below the predictions of the various standard solar models (about 130 SNU [7]). The results of the two Cr source experiments and of the As experiments validate the GALLEX solar neutrino experiment, and limit any systematic biases to less than a few percent.

Given that the solar luminosity is provided by the pp-fusion reaction in the core of the Sun, and the $^8$B solar neutrino flux is as measured by Superkamiokande, one can conclude from the GALLEX result alone that the $^7$Be solar neutrino flux is much below what is expected from the standard solar model.

For a deeper discussion of the physical implications (both for astrophysics and for particle physics) see [1].

---

[1] 1 SNU (Solar Neutrino Unit) = $10^{-36}$ captures per second and per absorber nucleus

## 1.3 The GNO project

GALLEX completed its experimental program in March 1997. There was then the question if to dismantel the detector or to go on with the observations, possibly with some improvements in the experimental apparatus, and an enlargement of the gallium mass.

The scientific community pushed for a continuation of the observations with the gallium detector at LNGS for a time period of the order of 10 years. The GNO (Gallium Neutrino Observatory) project was then proposed. For an extensive discussion of the overall GNO project see the proposal [8]

The main motivation for GNO is that the only experiments sensitive to the main component of the solar neutrino flux (the p-p neutrinos) which can operate in the next decade are those based on the use of gallium, namely GNO and SAGE. Unfortunately, SAGE suffers of many difficulties related to the present economical and political situation in Russia: thus the gallium detector at Gran Sasso is going to be probably the only low energy solar neutrino detector continuously operating in the next years.

The GNO targets are the following:

- measurement of the interaction rate of low energy solar neutrinos on gallium, with an accuracy of 5 SNU if the central value will be 77 SNU

- study of possible time variation of the rate , with a sensitivity of about 15%.

Three steps are planned:

1. To start a new series of solar runs with 30 tons of gallium using the same but renovated experimental set-up of GALLEX for the extraction and synthesis, and a new electronics and DAQ for counting (GNO30);

2. to increase the target mass to about 66 tons, the maximum amount of gallium that can be accomodated in the two available tanks (GNO66);

3. to further increase the mass up to about 100 tons, with the last 35 tons possibly in metallic form (GNO100).

The first step (GNO30) started data taking in 1998; the status will be discussed in detail in the next section.

The topics concerning the next future of the project are discussed in section 3.

# 2  Experimental activity during 1998

From January to April 1998 the work was devoted to the maintenance of the extraction and synthesis plants, and the renovation of all the electronic instrumentation and the DAQ. Since the end of April the first series of solar neutrino runs within GNO was started.

## 2.1  Extraction system and synthesis line

The activity at the extraction plant and synthesis line in 1998 can be summarized as follows:

1. GNO extraction plant care and maintenance, including the following items:

   - maintenance of the building where the gallium tanks and the extraction plant are located (GNO main building): care of the structure, of the electrical plant, water distribution piping etc., with the help of the different specific services of LNGS;

   - maintenance of gallium tanks, absorber plant, auxiliary plants : standard regular control, repair, replacement of damaged parts, order of spare parts and materials;

   - maintenance of the building safety equipments: building ventilation system, tank leak sensor; HCl leak detector.

2. Carrying out of 9 solar neutrino runs (see section 2.4 for the time schedule): each extraction required the following routine operations:

   - addition and mixing of Ge isotope carrier;

   - Nitrogen stripping of germanium from the gallium solution;

   - absorption into water of tank outlet flow stream;

   - final acidification and concentration of Ge/water acidic solution.

3. Atomic Absorbtion Analysis. Technical LNGS staff was trained for performing the AAS analysis needed for the evaluation of the chemical yield.

4. Synthesis Line. Staff from L'Aquila University was trained for performing the $GeH_4$ synthesis and the counter filling.

## 2.2   Counting system

Presently 19 proportional counters are available at LNGS for measuring the $^{71}$Ge decay. A scheme of one of the counters is shown in figure 1. Each counter is contained in a copper box together with a preamplifier; during the 6 months counting time the box is housed in a special Rn-tight shielding [12].

The electronic chain and DAQ of GNO has been completely redesigned with respect to GALLEX. A simplified scheme of the present hardware situation is shown in figure 2. The new setup has been installed and tested in the underground laboratories between january and march 1998.

The preamplifiers have a 300 MHz bandwidth (in GALLEX it was 150 MHz), to allow a very accurate analysis of the fast part of the signal. The signal from the preamplifier is sent to a main amplifier, where it is split in three parts:
- output 1: gain X4, bandwidth 300 MHz;
- output 2: gain X28, bandwidth 300 MHz;
- output 3: gain X4, bandwidth 50 MHz;

The amplifier also generates a threshold sensitive logical output, which gives the trigger for the DAQ.

Output 1 (low gain) and 2 (high gain) are sent to two independent input channels of a TDF. In that way the same pulse is digitized with two different amplifications: K-capture signals, with energies around 10 keV, are recognized on the low gain TDF channel, and L-capture signals are recognized on the high gain TDF channel. The TDF is operated with a time resolution of 0.2 ns/chan, 2048 channels, and has a 8 bit vertical resolution.
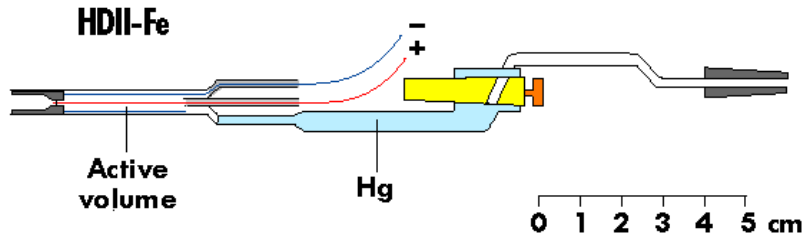
Figure 1: Section of a GNO proportional counter.

The double recording of the pulse on two different scales allows to have a good resolution using an 8 bit instrument. Most background signals are slow (figure 3(b and d)), while genuine $^{71}$Ge e-capure decays are fast (figure 3(a and c))

Presently 4 TDF modules, each with 4 independent channels are available; therefore the system can support at the moment up to 8 counters.

The output 3 of the main amplifier is multiplexed and sent to a slow digitizer with 2048 channels, 400 ns/channel, for studying the trailing edge of the pulse, mainly determined by the preamplifier. This is also important for the rejection of Bi-Po events from the Rn decay chain (see [14] for details)

All in all each event is recorded three times: on two channels of the TDFs (the first with low gain amplification, the other with high gain amplification) and on one channel of the TDS.

The use of the new electronic chain allowed to reach very good noise levels: therefrom we expect positive effects in the data analysis.

A test pulse system is used to check the working condition of the electronic chain. A step-like test pulse is sent to the preamplifiers of each connected counter, at regular time intervals of about 20 min. This allows to check the stability of all the instruments during the counting.

## 2.3   DAQ, Software, data storage and analysis

The DAQ system of GALLEX has been completely changed, owing to the age and scarce flexibility of the components. The GNO DAQ has been designed to meet maximum flexibility and maximum availability:

- Two computers (Digital Alpha server 1000, Digital Unix Operating System) are devoted to the data acquisition and monitor tasks. One of them actually performs the acquisition, while the second is ready as warm-backup and it is also in use for testing upgrades to the system. A third computer (Digital Alpha server 2100, DUnix O.S.), previously of GALLEX, has been updated and acts as computer for program development and data analysis.

- The link with the equipments in the Faraday cage is obtained via a GPIB bus equipped with high speed optical link, to preserve the electrical decoupling inside the cage.

- All the read-out devices (TD's, trigger module, relay units for test pulse switching) are VXI modules; a GPIB VXICC (from National Instr.)  acts as crate controller and
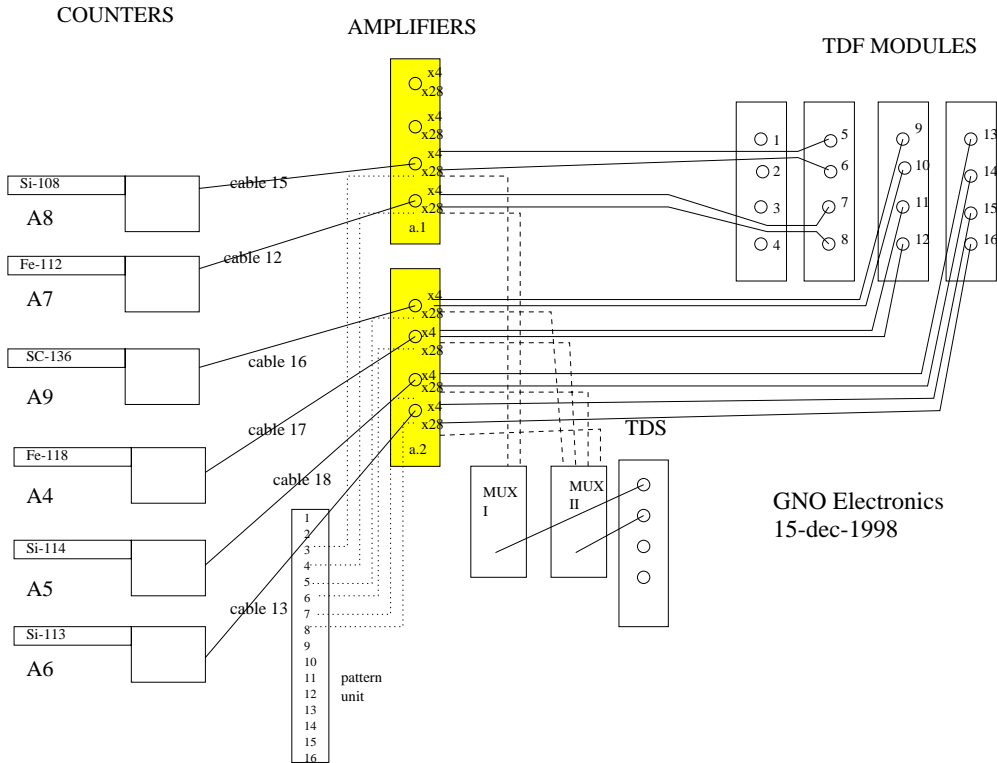
Figure 2: Scheme of the GNO electronics (situation at the end of december 1998).

resource manager and provides the bus conversion among the two standards.

The quality of the data is regularly checked via remote access to the DAQ machine through a user-friendly software. This permits to check daily in real time the status of counting. The new pulses are visually inspected every day and the stability of some parameters of the test-pulses are monitored.

Data are stored on a 20Gb system of 6 hard disks, mounted on the DAQ Alpha station. Backup of the data is made on magnetic tapes.

For the data analysis, we are planning to adopt in a first stage an amplitude/ rise-time approach similar to the one used for GALLEX [9]: in that way it will be possible to have an immediate cross-check between the two different DAQ and electronics.

More sophisticated pulse-shape analyses are under study; they should extract all the information from the pulse recording, using all the benefits of a such extremely fast electronic chain. Some examples of possible techniques to be applied are a pulse fit analysis (already developed for GALLEX as an alternative method to the rise time analysis [10]), and neural networks.

## 2.4   Extractions.

The first GNO extraction was done on April the $23^{rd}$ 1998. Subsequent extractions were performed once every 4-5 weeks: at 31-dec-1998, all in all 9 extractions were successfully
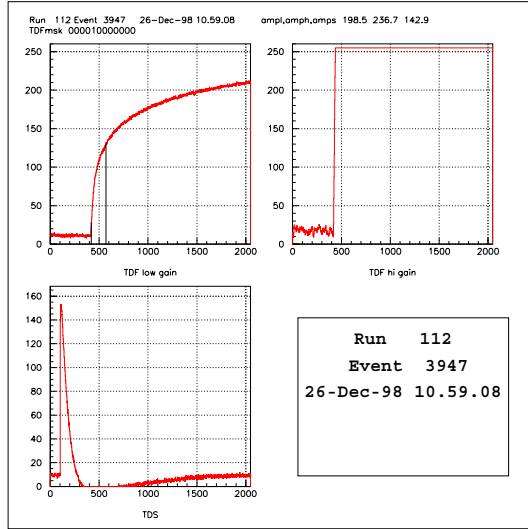
(a)
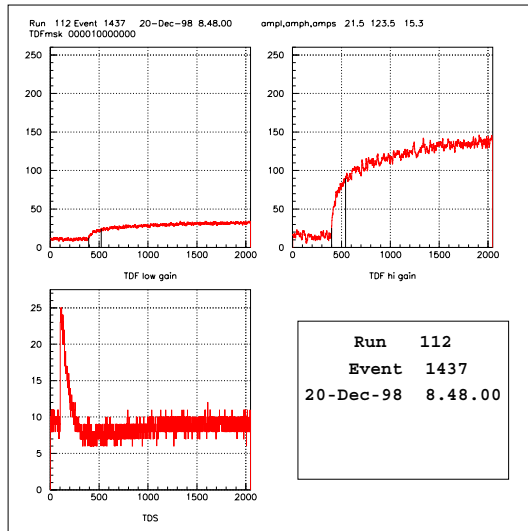
(c)

Figure 3: Examples of 4 pulses recorded during the first extractions of GNO30. Each pulse coming from the counter preamplifiers is recorded on three independent digitizers by the GNO DAQ:
- on a TDF 0.2 ns/chan with amplification X4, 300 MHz bandwidth (low gain TDF);
- on a TDF 0.2 ns/chan with amplification X28, 300 MHz bandwidth (high gain TDF);
- on a TDS 400 ns/chan with amplification X4, 50 MHz bandwidth.
[71]Ge e-capture (both from K and L shells) produce fast pulses, while most background events generate slow pulses from diffuse ionization. (a) fast 'K' pulse, (b) slow pulse in the 'K' region, (c) fast 'L' pulse, (d) slow pulse in the 'L' region. The vertical resolution is for all the instruments 254 channels.

Table 1: Summary of GNO runs performed during 1998. For every extraction the following data are reported: extraction label; extraction date, referred to the end of the extraction (duration 8 hours); exposure time in days; counter type and number used for $^{71}$Ge counting (Fe=Iron cathode, Si=Silicon cathode, SF=Iron shaped cathode, SC=Silicon shaped cathode). Status of counting at 31-dec-1998.

| Extraction | Date (End of extraction) | Exposure time (days) | Counter | Counting (31-dec-1998) |
|---|---|---|---|---|
| A1 | 23-apr-98 | | Fe-112 | completed |
| A2 | 20-may-98 | 27 | Si-106 | completed |
| A3 | 17-jun-98 | 28 | SC-138 | completed |
| A4 | 22-jul-98 | 35 | Fe-118 | ongoing |
| A5 | 26-aug-98 | 35 | Si-114 | ongoing |
| A6 | 23-sep-98 | 28 | Si-113 | ongoing |
| A7 | 21-oct-98 | 28 | SF-093 | ongoing |
| A8 | 18-nov-98 | 28 | Si-108 | ongoing |
| A9 | 16-dec-98 | 28 | SC-136 | ongoing |

performed; the situation is summarized in Table 1.

Three runs have completed the 6 month counting, and 6 are still counting. 30 counter calibrations were performed using the Gd/Ce X-ray source.

According to the present plans the extractions for the next year should go on with a similar time schedule. Preliminary measurements confirm the expected chemical yields (95-98 %) in the 9 extractions.

The statistics accumulated up to now is by far too low to extract a meaningful result: in fact on the average 5-6 $^{71}$Ge per extraction are counted, and 6 month of continous counting are requested for a good evaluation of the background rate. We expect to be able to provide the first results of GNO30 at the end of 1999, if the time schedule will go on as planned.

# 3 R&D, and future plans.

In this section we summarize the status of the R&D under developement, and of the plans for the next future within the GNO project.

Together with the increase of the target mass, the crucial point in the GNO project is to obtain a substantial reduction of systematic error. Thus presently most of the R&D activity has as its final aim the reduction of the various components of the systematic error.

To understand the situation we can refer to table 2, where the different sources of sys-

tematic error for the gallium detector are listed together. A comparison of the GALLEX results with the GNO expected performance [2] shows the following situation:

- Uncertainty on the background from side reactions producing $^{71}$Ge : it will remain unchanged, even with increased target mass, assuming the same purity of the additional gallium;

- Uncertainty on the background from cosmogenic $^{68}Ge$ produced in the gallium solution before transportation underground: it is presently (GNO30) zero because all the activity has decayed away during the 5 years of operation of GALLEX. Concerning GNO66, thanks to the experience gained with GALLEX, we are confident that it will be possible to clean the freshly produced gallium from $^{68}$Ge produced by cosmic rays.

- Presence of Rn in the counters: one of the most dangerous backgroud sources is given by the possible presence of radon inside the counters: the experience with GALLEX has shown that a few Rn atoms are sometime introduced in the counters during the synthesis and counter filling. The decays of Rn and its daughters can produce events which cannot be distinguished from real $^{71}$Ge events, and are time dependent. For that reason a Rn cut was introduced in the GALLEX data analysis, by defining a dead time for each detected Rn decay chain (see [14] for details). The efficiency of this cut was evaluated to be $(91 \pm 5)\%$, and represents one of the major systematic errors in the experiment. A Rn test could lower this error to about 1% or even less. A further reduction will come in GNO66 from the enlargement of the target mass: in fact the presence of Rn in the counters is related to the filling procedure and not to the target solution, so that its weight is inversely proportional to the target mass.

- Uncertainty in the $^{71}$Ge detection efficiency: the main systematic uncertainty in GALLEX comes from the error in the counting efficiency. The latter is the probability that a $^{71}$Ge decay inside a proportional counter is detected and recognized as a good event by the analysis. We expect to lower this uncertainty first of all with some direct $^{71}$Ge calibrations planned for next year. As a further step we plan to adopt a standardization in the counter construction technique.

- The remaining source of error (target mass and chemical yield) is expected to remain constant.

Keeping in mind the situation outlined above, one can understand the importance of the following R&D topics, presently under developement:

New X-ray calibration source.
The energy- and rise-time calibration of the proportional counters is performed with cerium X-rays which are generated by the aid of a radioactive $^{153}$Gd source and a Ce target [11]. Since about 2 years $^{153}$Gd sources are no longer commercially available at the

---

[2]for a detailed explanation of the single components of the systematic error in GALLEX see [8]

Table 2: Systematic errors in GALLEX and GNO

| Source | GALLEX | GNO30 expected | GNO66 expected |
| --- | --- | --- | --- |
| | % | % | % |
| Background from side reactions ( muons, Actinides, $^{69}Ge$) | 1.6 | 1.6 | 1.6 |
| Backgound from $^{68}Ge$ | $^{+0.9}_{-2.6}$ | 0 | 0 |
| Background from Rn in the counter | 1.5 | 1.0 | 0.5 |
| Counting efficiency (including energy and pulse shape cuts) | 4.5 (*) | 3.0 | 2.0 |
| Chemical yield and target Size | 2.2 | 2.2 | 2.2 |
| Total | 5.9 (*) | 4.2 | 3.4 |

(*) A final refined evaluation of the overall GALLEX data is in progress, to be published in a concluding paper in 1999. The uncertainty in the counting efficiency could be lowered to about 3.5 % already at this stage.

needed activity (GBq) and purity level; moreover the halflife of 239.5 d requires frequent replacement of the $^{153}$Gd sources. A solution to this problem is a low power x-ray tube in place of the Gd-source. Fortunately a commercial generator X-ray tube combination became available which is compact enough as to fit in the shield of the proportional counter spectrometer [12]. A system with two stepping motors has been designed and is now under construction which allows to move the tube inside the shield so that each proportional counter can be calibrated in its normal counting position on the passive side of the shield. The Gd source calibration was only possible when the counter was removed from its counting position and when the shield was open. Thus, the new procedure matches better the true measuring condition and allows more frequent calibrations at a much higher comfort. The calibration procedure will be fully software controlled. During normal counting periods the system is completely switched off from electric power in order to maintain the low electronic noise level.

<sup>71</sup>Ge calibrations and Rn tests

$^{71}$Ge calibrations and Rn tests

In the next future we plan to perform at LNGS some calibrations with counters filled with a known amount of active $^{71}$Ge . This will allow to directly measure the efficiencies for the selection criteria to be applied for the data analysis, and hopefully to reduce the uncertainty on the counting efficiency. More measurements with $^{71}$Ge will be necessary after the new calibration system will have been installed. A Rn test measurement is also planned, to reduce the systematic error induced by the Rn-cut.

Enlargement of the counting system.

In the present configuration the electronic chain can support up to 8 counters (see 2.3). We plan to buy the electronics necessary to deal with at least 12 independent lines. This is needed to perform several tests without interfering with the solar neutrino observations: in fact assuming one extraction per month and 6 months counting time per counter, 6 lines are permanently occupied by the solar runs. Supplementary lines are needed for the Rn and $^{71}$Ge calibrations, background measurements for new counters, blanks etc.

New proportional counters.

So far, all the proportional counters used in GALLEX and in GNO30 are individually glass-blown, and therefore their $^{71}Ge$ detection efficiencies differ slightly from counter to counter, leading to a systematic error of the order of 4.5 % in the efficiency determination. In order to reduce the error we have started to investigate a different counter construction procedure. The idea is to fully fabricate the counters mechanically (no glass-blowing involved) so that a mass production is possible. With these counters a systematic error on the counting efficiency not much in excess of 2% should be achievable.

Developement of cryogenic detectors

At TUM an R&D project is ongoing to test the feasibility of low temperature calorimeters as detectors for measuring the $^{71}Ge$-decay in a future phase of GNO and optimize these devices with respect to the technical requirements for implementation into the large-scale experiment at Gran Sasso [13]. The cryogenic calorimetric detectors are made from a superconducting phase transition thermometer evaporated directly onto a dielectric crystal which acts as an absorber for particles and radiation. The energy deposited in this crystal is measured via the resulting temperature rise in the thermometer. The device is operated in the transition region of the superconducting to the normal conducting state of the thermometer, where a small temperature rise $\Delta T$ of the thermometer leads to a large increase $\Delta R$ of its resistance. The readout is done with a Squid-based DAQ-system. First results obtained with test detectors did already show an improvement by about a factor of five in energy resolution, compared to miniaturized low background proportional counters. In 1998 a compound detector setup consisting of two thermally separated sapphire absorber crystals, each of them equipped with a superconducting phase transition thermometer, and the $^{71}$Ge-activity deposited in between has been measured. The next steps are improvements in the Ge-deposition technique, tests of absorber materials other than sapphire, and a several weeks prototype run at TUM.

# 4 Conclusions

GNO (Gallium Neutrino Observatory) started data taking in April 1998, after a major maintenance and renovation of the GALLEX set-up. In the actual configuration it is the first stage of the GNO project, and makes use of 30 tons of gallium as a target for solar neutrinos (GNO30).

9 extractions were performed in 1998 with the expected chemical yield. Counting is ongoing without major problems, and was completed for the first three extractions. A precise evaluation of the performance of the new electronic set-up is in progress. The first reliable data from GNO30 are expected to come for the end of 1999, when the data of about 15 solar runs should be available.

# 5 List of Publications

## 5.1 GNO publications and internal reports

GNO-1 GNO collaboration, "Proposal for a permanent Gallium Neutrino Observatory (GNO) at LNGS", LNGS annual report 1995

GNO-2 A. D'Ambrosio, S.D'Angelo, "GNOsys: the data acquisition system for the Gallium Neutrino Observatory", GNO internal report

GNO-3 E. Bellotti, "The Gallium Neutrino Observatory at Gran Sasso", Proc. IV Int'l. Solar Neutrino Conf., ed. W.Hampel, MPI Kernph., Heidelberg (1997) 173-182

GNO-5 M. Altmann et al., "Development of cryogenic detectors for GNO", Proc. IV Int'l. Solar Neutrino Conf., ed. W.Hampel, MPI Kernph., Heidelberg (1997) 183-191

GNO-5 M. Altmann et al., "Progress in the development of cryogenic detectors for GNO', Proc. Int. Workshop on Topics in Astroparticle and Underground Physics (TAUP97), Nucl. Phys. B (Proc. Suppl.) 70 (1999) 374-376.

GNO-6 T.Kirsten, "Does a CERN-Gran Sasso long base-line experiment constitute a potential risk of disturbing GNO?", GNO internal report.

GNO-7 C.Cattadori, L.Zanotti "Manual for the connection of a new counter to the GNO DAQ", GNO internal report.

GNO-8 GNO collaboration, "Addendum to the GNO proposal", GNO internal report.

GNO-9 GNO collaboration, "GNO progress report for 1997", LNGS annual Report 1997, 69-72.

GNO-10 T. Kirsten, "GALLEX solar neutrino results and status of GNO", Neutrino 98, Takayama (Japan). Proc. XVIII Int. Conf. on Neutrino Physics and Astrophysics, ed. E. Suzuky and Y. Totsuka. Nucl. Phys. (Proc. Suppl.) to appear in 1999.

## 5.2 GALLEX publications, 1998

There is no status report on GALLEX for 1998 (data taking was stopped in March 1997). Nevertheless the GALLEX collaboration was still active, to finalize the data analysis including the overall GALLEX observations. We give here the list of the GALLEX publications appeared during 1998; they are going to complete the reference list appeared in the previous LNGS status reports.

GX112  W.Hampel et al. GALLEX collaboration, "Final results of the $^{51}Cr$ neutrino source experiments in GALLEX", Phys. Lett. B 420 (1998).

GX122  W. Hampel et al., GALLEX collaboration, "Verification tests of the GALLEX solar neutrino detector with $^{71}$Ge produced in-situ from beta decay of $^{71}As$", Phys.Lett. B436 (1998) 158.

GX125  M.Altmann, "GALLEX solar neutrino observations: results from the total data set" Proc. Moriond XXXIII, Les Arcs, March 14-21, 1998.

GX127  W.Hampel et al., GALLEX collaboration, "GALLEX solar neutrino observations: results for GALLEX IV", Phys.Lett B, accepted Dec. 1998.

## References

[1] GALLEX collaboration, Phys.Lett. B285 (1992) 376; Phys.Lett. B314 (1993) 445; Phys.Lett. B327 (1994) 377; Phys.Lett. B342 (1995) 440; Phys.Lett. B357 (1995) 237; Phys.Lett. B388 (1996) 384

[2] R. Wink et al. Nucl. Inst. and Meth. A329 (1993) 541

[3] E.Henrich, K.H.Ebert, Angew. Chemie Int. Ed. (Engl.) 31 (1992) 1283; E.Henrich et al., 'GALLEX, a challange for chemistry', Proc. IV Int'l. Solar Neutrino Conf., ed. W.Hampel, MPI Kernph., Heidelberg (1997) 151-162.

[4] W.Hampel et al. GALLEX collaboration, "GALLEX solar neutrino observations: results for GALLEX IV", Phys.Lett B, accepted Dec. 1998.

[5] W.Hampel et al. GALLEX collaboration, Phys. Lett. B 420 (1998) 114

[6] W.Hampel et al. GALLEX collaboration, Phys.Lett. B436 (1998) 158.

[7] J.N. Bahcall, S.Basu and M.H.Pinsonneault, Phys.Lett. B433 (1998) 1, V. Castellani et al. Phys. Rep. 281 (1997) 309; V.Castellani et al., preprint astro-ph/9712174, A.S.Brun, S. Turck Chiéze and P.Morel, preprint astro-ph/9806272.

[8] E.Bellotti et al., GNO collaboration, LNGS report INFN/AE-96-27, also available at http://kosmopc.mpi-hd.mpg.de/gallex.html

[9] M. Sann 'Data acquisition, calibrations, and data analysis for GALLEX', GALLEX internal report GX114 (1997).

[10] M.Altmann et al., Nucl.Instr. and Meth. A381 (1996) 398-412

[11] U. Schanda and A. Urban, Nucl. Instr. and Meth. A381 (1996) 79-85

[12] G. Heusser, 'Characteristics of the GALLEX Spectrometer, Trends in Astroparticle Physics', ed. P. Ch. Bosetti, (1994) p.33, Teubner, Leibzig

[13] M.Altmann et al., 'Progress in the development of cryogenic detectors for GNO', Proc. Int. Workshop on Topics in Astroparticle and Underground Physics (TAUP97), Nucl. Phys. B (Proc. Suppl.) 70 (1999) 374-376.

[14] H.Lalla, 'Zeitabhängiger Untergrund im GALLEX- Sonnenneutrino-Experiment', thesis, Ruprecht-Karls-Universität Heidelberg (1993).

# HDMS: Dark Matter Search.

L. Baudis, A. Dietz, J. Hellmig, G. Heusser,

H.V. Klapdor–Kleingrothaus, S. Kolb, I.V. Krivosheina, B. Majorovits,

H. Päs, Y. Ramachers, F. Schwamm, H. Strecker

Max–Planck–Institut für Kernphysik, P.O.Box 10 39 80, D–69029 Heidelberg, Germany

### Abstract

The prototype of a new Dark Matter Experiment for the Gran Sasso underground laboratory has been installed. Our HDMS (Heidelberg Dark Matter Search) experiment consists of two germanium detectors in a unique configuration. It is specialized to discriminate the already low background obtained in the Heidelberg–Moscow–Experiment considerably further. The use of anticoincidence between our Ge-detectors reduces the photon background which mainly limits the direct detection of hypothetical dark matter particles (WIMPs). We expect to improve WIMP cross section limits to a level comparable to planned cryogenic experiments. This should, among others, allow to test recently claimed positive evidence for dark matter by the DAMA group.

## 1   Introduction – Motivation

The exciting possibility to detect cold dark matter in our galaxy in the form of WIMPs (weakly interacting massive particles) through direct detection of elastic WIMP–nucleus scattering events (see e.g. [1]) is limited by signal–to–noise ratios due to the very low expected rates [2, 3] in the relevant part of the energy spectrum (typically below 50 keV). Therefore the aim of every experimental attempt to directly detect WIMPs is to optimize the interplay of three important parameters: Threshold energy (as low as possible), detector mass (as high as possible) and background, mainly induced by photon events (as low as possible).

We report about a new dark matter detector using Ge–semiconductor technology [4]. We aim at a further reduction of background compared to our first steps in the field of dark matter research with which we obtained the most stringent limits for WIMPs from essentially raw data [5]. The potential of the new experiment should be similar to that of planned cryogenic experiments like CDMS [6]. It should allow, among others, to test recently reported positive evidence for dark matter signals [7].

## 2   Description of the experiment

A small Ge–crystal (natural Ge for the prototype, isotopically enriched Ge for the second stage) is surrounded by a well–type Ge–crystal and the configuration is run in anticoincidence mode (see Fig. 1). Both crystals are mounted into a common cryostat system. A
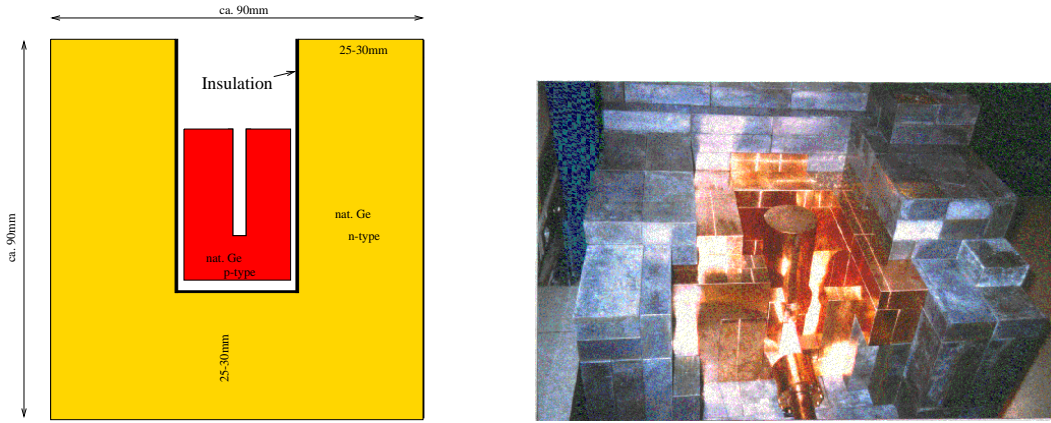
Figure 1: Left: Schematic geometry of our new anticoincidence detector design. The well-type Ge crystal an n–type semiconductor, the small measurement Ge crystal a p–type. The approximate diameter of the well–type is 90mm, height 90mm; the small measurement crystal has about 30mm diameter and height of 40mm. Right: The detector inside the copper and lead box before it's assembly.

thin insulator (about 1mm) is placed between the two crystals in order to shield leakage currents on the surfaces.

We expect two effects to reduce the background: First, the outer well–type will act as an anticoincidence shield for the inner detector, thereby reducing the Compton background from multiple scattered photons. A relative background reduction of the order 10–20 as the anticoincidence efficiency has been estimated from Monte Carlo simulations [4]. Second, the overall background level is expected to be reduced relative to usual Ge ionization detectors, since in the immediate vicinity of the measurement crystal there is one of the radiopurest materials which we know, *i.e.* a second Ge crystal.

# 3   Performance tests in Heidelberg

Before the detector was installed at the Gran Sasso Underground laboratory, extensive tests have been performed in the Low Level Laboratory of the Max-Planck-Institute in Heidelberg.

The detector performances have been checked by measuring energy spectra from standard calibration sources like $^{228}$Th, $^{133}$Ba, $^{241}$Am and $^{60}$Co as well as from background present in the Low–Level laboratory in Heidelberg with the unshielded detectors (for a $^{133}$Ba, $^{60}$Co spectrum, see Fig. 2).

Since our data acquisition system allows us to measure either in a calibration mode (filling a histogram in a memory module) or in an event–by–event mode, where in addition we can choose to record the pulse–shape of an individual event, multiple tests of the detector performance are possible.

We used the calibration mode to determine the optimum energy resolution for both detectors. This procedure then results in an optimum threshold, in our case 2.5 keV measured in Heidelberg. This threshold is basically determined by the baseline noise

after the preamplifier whose stability has been monitored. Please note that thresholds also raise considerably in an ultra–low background environment like the Gran Sasso Laboratory simply due to the exponential shape of electronic noise in an energy spectrum.

The event–by–event (LIST) mode allows to have full control about every event at the expense of slower data acquisition. We divided the preamplifier output from both detectors in order to measure low–energy (threshold to 400 keV) and high energy (100 keV - 8 MeV) signals in different branches using different gains at the spectroscopy amplifiers.

We used the LIST mode to obtain 2-D scatter plots of recorded energies for each detector. Any correlation of recorded energies in one detector with events in the second would be visible in such a scatter plot. Using $^{133}$Ba and $^{228}$Th calibration sources, we found cross talk between the inner and outer detector and vice versa, although in different strength. Clearly visible is the strong linear correlation between energies in the inner and outer detector (see Fig. 2). The width of these correlation lines is determined by the energy resolution of the detectors. The linear correlation can be corrected off–line. According to our expectations for this experiment we tested one of the two effects, the anticoincidence efficiency, before moving the setup to its final location. For the relative background reduction, we measured the anticoincidence efficiency in Heidelberg. A background measurement in the Heidelberg Low–Level laboratory has been corrected for the cross–talk. Afterwards, we produced the original and discriminated energy spectrum, shown in Fig.3. All the analyses are carried out off–line, using the event–by–event mode data. From these measurements, we conclude to obtain a suppression factor in the low–energy region of about 5–6.
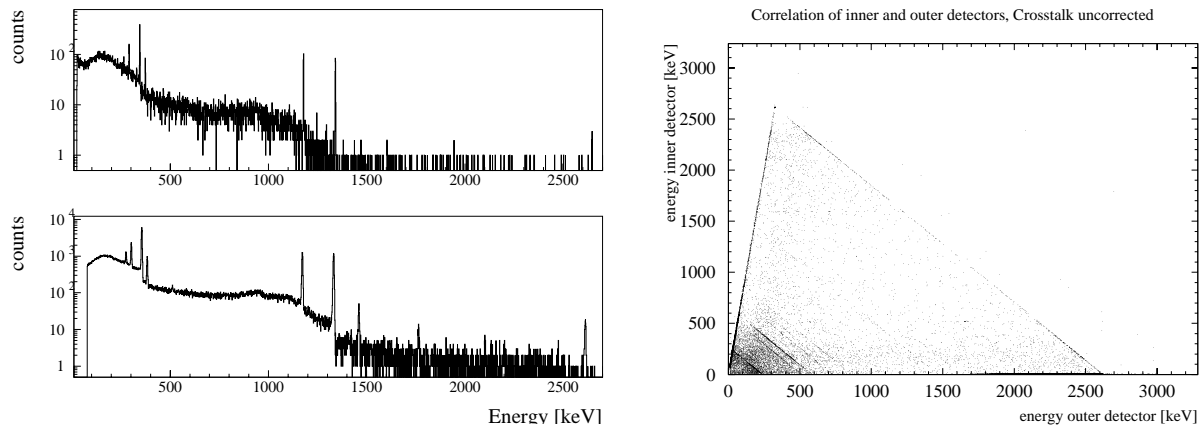


Figure 2: Left: Test measurement using $^{133}$Ba and $^{60}$Co calibration sources to measure spectra from both HPGe–detectors. Upper panel: spectrum obtained with small crystal, lower panel from large crystal. Right: Pick–up between the inner and outer detector crystals measured using a $^{228}$Th source. The linear correlation of the cross–talk can be corrected off–line in order to obtain true anticoincidence spectra.

The detector was moved to the Gran Sasso Underground Laboratory and is taking data since March 1998. The obtained spectrum of the inner detector after 10.1 kg d of measurement with and without the anticoincidence is shown in Fig. 3.

It is seen that the supression through the anticoincidence works well. The obtained overall background level is around 0.7 Counts/(kg d keV) thus still a factor of two worse

| Property | Inner Detector | Outer Detector |
|---|---|---|
| Crystal Type | p–type | n–type |
| Mass [g] | 202 | 2111 |
| Active Volume [cc] | 37 | 383 |
| Crystal diameter [mm] | 35.2 | 84.4 |
| Crystal length [mm] | 40.3 | 86.2 |
| Operation Bias | +2500 | -1500 |
| FWHM (1332 keV) [keV] (Heidelberg) | 1.87 | 4.45 |
| Threshold Heidelberg [keV] | 2.5 | 7.5 |

Table 1: Detector properties for the small inner HPGe–detector and the active veto–shield, the outer well–type HPGe–detector.
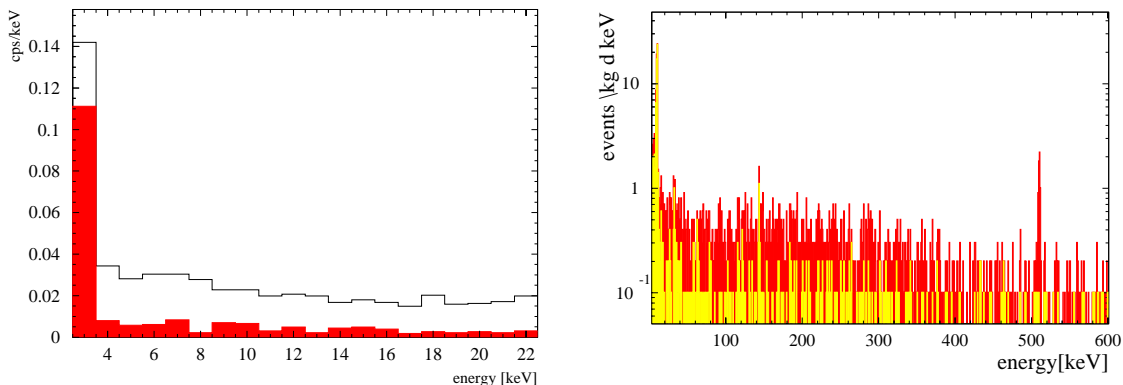


Figure 3: Left: Low–energy part of a background spectrum from Heidelberg, corrected for cross–talk, and the corresponding anticoincidence spectrum (filled histogram). The suppression factor is between 5 and 6, threshold at about 2.5 keV.

than the background reached by the Heidelberg–Moscow–Experiment. This is mainly due to the preliminary crystal-holder mounted in the cryostat system and the high activation of the crystal through cosmic rays. We expect a further reduction of the background level through the installation of a crystal-holder which has been constructed out of specially selected low-level material and further through the deactivation of the cosmogenic activities inside the crystal. In order to reach the aim of background reduction relative to the Heidelberg–Moscow–Experiment of a factor 10–20, our absolute background level has to be a factor 2–4 below the 0.3 Counts/(kg d keV) in the low–energy region from the Heidelberg–Moscow–Experiment.

Using our estimate of a reachable background level we will directly compete with existing or foreseen WIMP–limits from other experiments like large scintillator or new cryogenic experiments (see Fig. 4). In contrast to these mentioned WIMP–detector techniques, we use a well understood technique, namely semiconductor ionization detectors, and use our raw data to obtain limits on WIMPs (in contrast to other limits obtained only after application of pulse–shape discrimination of nuclear recoil events).

A background reduction of a factor of ~2 compared to the Heidelberg–Moscow–Experiment level together with the obtained supression factor of 5-6 through the anticoincidence effect would allow to cover the full range of positive evidence for WIMPs claimed by the DAMA collaborationa [7] using raw data and a HPGe-detector instead of a NaI–scintillator.
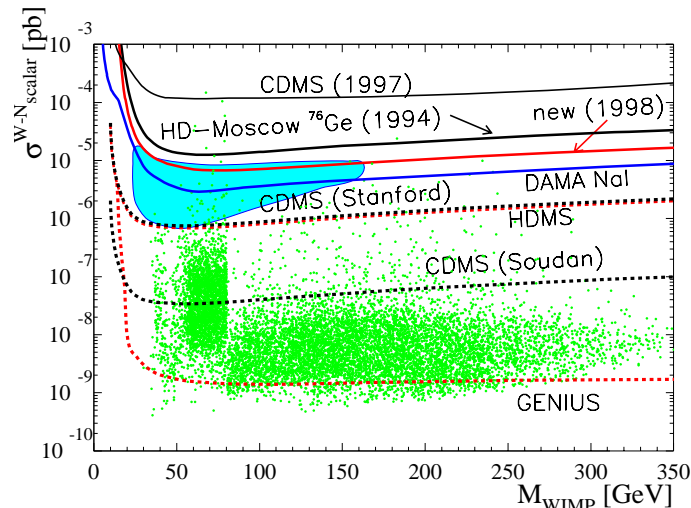


Figure 4: Expected obtainable cross section limits on WIMP–neutron (spin–independent interaction) elastic scattering for the CDMS [6] and the HDMS experiment [4]. For comparison the present lowest–limit results, the Heidelberg–Moscow result [8] and the DAMA result for NaI [7] (including their evidence contour), are also shown, together with expected cross sections for neutralinos in a SUSY–GUT scenario without universal scalar mass unification [2] (points of the scatter plot). Also shown is the expecation for our new proposal, the GENIUS-project [9, 10]

# 4   Conclusion

The new HDMS detector should allow to reach WIMP–limits comparable to results from planned or running cryogenic or large scintillator detectors in the near future (about one or two years from now). HDMS will be similar in sensitivity to the cryogenic detector CDMS under construction, complementary in the energy range to CRESST [11], and will among others, allow to test recently reported positive evidence for dark matter signals.

# References

[1] P.F. Smith and J.D. Lewin, Phys. Rep. **187** (1990) 203

[2] V. Bednyakov, H.V. Klapdor–Kleingrothaus, S.G. Kovalenko, Phys. Rev **D55** (1997) 503, V. Bednyakov, H.V. Klapdor-Kleingrothaus, S. Kovalenko, Y. Ramachers, Z. Phys. A **357**, 339(1997)

[3] V. Berezinsky, A. Bottino, J. Ellis, N. Fornengo, G. Mignola and S. Scopel, Preprint HEP–PH–9508249

[4] L. Baudis, J. Hellmig, H.V. Klapdor–Kleingrothaus, A. Müller, F. Petry, Y. Ramachers and H. Strecker, NIM **A385** (1997) 265

[5] Heidelberg-Moscow Collaboration, Phys. Rev. **D 59** (1999)022001

[6] P.D. Barnes *et al.*, NIM **A370** (1996) 233;

[7] R. Bernabei et al., Phys. Lett. **B 424**, (1998)195, Preprint astro–ph/9710290; R. Bernabei *et al.*, preprint ROM2F/97/33 - August 1st, 1997; P. Belli, talk at TAUP97, Gran Sasso Laboratory, September 7-11, 1997

[8] M. Beck *et al.*, Phys. Lett. **B 336** (1994) 141

[9] H.V. Klapdor-Kleingrothaus, Proc. BEYOND 97, June 8-14, 1997 IOP, Bristol, 1998, eds. H.V. Klapdor-Kleingrothaus and H. Päs, Int. J. Mod. Phys **A 13**, (1998)3593, Proc NEUTRINO 98, Takayama, Japan, June 1998, World Scientific, Singapore, 1999, H.V. Klapdor-Kleingrothaus, Y. Ramachers, Eur. Phys. J. **A3**(1998)85

[10] L. Baudis, G. Heusser,H.V. Klapdor-Kleingrothaus, B. Majorovits, Y. Ramachers, H. Strecker , in press at NIM **A**

[11] W. Seidel *et al.*, J. Low Temp. Phys. **93** (1993) 797; Phys. Lett. **B323** (1994) 95; M. Bühler *et al.*, NIM **A370** (1996) 237

# The Heidelberg–Moscow experiment: Heidelberg-Moscow $\beta\beta$ decay and on dark–matter WIMPs.

V. Alexeev[b], A. Bakalyarov[b], A. Balysh[b], L. Baudis [a], S.T. Belyaev[b],
A. Dietz[a], J. Hellmig[a], G. Heusser[a], H.V. Klapdor–Kleingrothaus[*] [a],
S. Kolb[a], I.V. Krivosheina[a], V.I. Lebedev[b], B. Majorovits[a], H. Päs[a],
Y. Ramachers[a], F. Schwamm[a], H. Strecker[a], S. Zhukov[b]

[a]Max–Planck–Institut für Kernphysik, P.O.Box 10 39 80, D–69029 Heidelberg, Germany

[b]Russian Science Centre Kurchatov Institute, 123 182 Moscow, Russia

* Spokesman of the collaboration

**Abstract**

The Heidelberg–Moscow experiment gives the most stringent limit on the Majorana neutrino mass. After 24 kg yr of data with pulse shape measurements, we set a lower limit on the half-life of the $0\nu\beta\beta$-decay in $^{76}$Ge of $T_{1/2}^{0\nu} \geq 5.7 \times 10^{25}$ yr at 90% C.L., thus excluding an effective Majorana neutrino mass greater than 0.2 eV. The sensitivity of the experiment corresponds to a neutrino mass $\langle m \rangle \leq 0.38$ eV (90% C.L.). New results in WIMP search after 0.69 kg yr of measurement with one of the enriched $^{76}$Ge detector of the Heidelberg–Moscow experiment with an active mass of 2.758 kg are presented. An energy threshold of 9 keV and a background level of 0.042 counts/(kg d keV) in the energy region between 15 keV and 40 keV was reached. The derived limits on the WIMP–nucleon cross section are the most stringent limits on spin–independent interactions obtained to date by using essentially raw data without background subtraction.

## 1 Introduction

The Heidelberg–Moscow experiment, situated in the Gran Sasso Underground Laboratory, operates five p–type HPGe detectors, made of 86% enriched $^{76}$Ge material. The total active mass of the detectors is 10.96 kg, corresponding to 125.5 mol $^{76}$Ge, the presently largest source strength of all double beta experiments. Four detectors are placed in a common 30 cm thick lead shielding in a radon free nitrogen atmosphere, surrounded by 10 cm of boron-loaded polyethylene and two layers of 1 cm thick scintillators on top. The remaining detector is situated in a separate box with 27 cm electrolytical copper, 20 cm lead shielding and 10 cm of boron-loaded polyethylene below the box, flushed with gaseous nitrogen. A detailed description of the experiment and its background is given in [1]. For a further reduction of the already very low background of the experiment, a pulse shape analysis (PSA) method was developed [2]. The analysis distinguishes between

multiple scattered interaction in the Ge crystal, so called multiple site events (MSE) and pointlike interactions, or single site events (SSE). Since double beta decay events belong to the SSE category, the method allows to effectively reduce the background of multiple Compton scattered photons. The probablity of correct detection for a SSE is 75%, and 74% for a MSE [2].

# 2    Results on neutrinoless double-beta-dacay

For the evaluation of the $0\nu\beta\beta$-decay we consider both data sets, with and without pulse shape analysis. We see in none of them an indication for a peak at the Q-value of the $0\nu\beta\beta$-decay. The total spectrum of the five detectors with a statistical significance of 41.21 kg yr contains all the data with exception of the first 200 d of measurement of each detector (see Fig. 1). The extrapolated energy resolution at the energy of the hypothetical $0\nu\beta\beta$-peak is (3.85±0.16) keV. To estimate the expected background in the $0\nu\beta\beta$ region, we take the energy intervall from 2000 to 2080 keV. The number of expected events in the peak region is (78±3) events, the number of measured events in the $3\sigma$ peak interval centered at 2038.56 keV is 68. This is below the expectation and could be due to peaks in the background interval, which are however too weak to be identified. To extract a half-life limit for the $0\nu\beta\beta$-decay we make the assumption, as recommended by [3], that the number of measured events equals the background expectation. With the achieved energy resolution, the number of excluded events in the $3\sigma$ peak region is 15.9 (9.52) with 90% C.L. (68% C.L.), resulting in a half-life limit of:

$$T_{1/2}^{0\nu} \geq 1.3 \times 10^{25} \text{ yr} \quad 90\% \text{ C.L.}$$
$$T_{1/2}^{0\nu} \geq 2.1 \times 10^{25} \text{ yr} \quad 68\% \text{ C.L.}$$

We consider now the data with pulse shape measurements, with a statistical significance of 24.16 kg yr and an energy resolution at 2038.56 keV of (4.2±0.17) keV. The expected number of events from the background left and right of the peak is (13±1) events, the measured number of events in the $3\sigma$ peak region is 7. Taking again the number of expected events instead of the number of measured ones [3], we can exclude 7.17 (4.17) events with 90% C.L. (68 % C.L.). The limit on the half-life is:

$$T_{1/2}^{0\nu} \geq 1.6 \times 10^{25} \text{ yr} \quad 90\% \text{ C.L.}$$
$$T_{1/2}^{0\nu} \geq 2.8 \times 10^{25} \text{ yr} \quad 68\% \text{ C.L.}$$

Obviously the pulse shape data are now not only competitive with the complete data set, but they deliver more stringent lower limits on the half-life of the $0\nu\beta\beta$-decay. The pulse shape analysis reduces the background in the interesting energy region by a factor of 3 [background index without PSA: (0.18±0.02) events/(kg yr keV), with PSA: (0.06±0.02) events/(kg yr keV)]. This reduction factor is due to the large fraction of multiple Compton scattered events in the $0\nu\beta\beta$-decay region.

| | $T_{1/2}^{0\nu}$ [yr] | $\langle m \rangle$ [eV] | C.L. [%] |
|---|---|---|---|
| Full data set | $\geq 1.3 \times 10^{25}$ | $\leq 0.43$ | 90 |
| | $\geq 2.1 \times 10^{25}$ | $\leq 0.33$ | 68 |
| SSE data after [3] | $\geq 1.6 \times 10^{25}$ | $\leq 0.38$ | 90 |
| | $\geq 2.8 \times 10^{25}$ | $\leq 0.29$ | 68 |
| SSE data after [4] | $\geq 5.7 \times 10^{25}$ | $\leq 0.20$ | 90 |
| | $\geq 2.5 \times 10^{26}$ | $\leq 0.10$ | 68 |
| Sensitivity | $\geq 1.6 \times 10^{25}$ | $\leq 0.38$ | 90 |
| | $\geq 2.5 \times 10^{25}$ | $\leq 0.30$ | 68 |

Table 1: Limits on the effective Majorana neutrino mass from the $0\nu\beta\beta$-decay of $^{76}$Ge for the matrix elements from [6].

Figure 1 shows the combined spectrum of the five detectors after 41.24 kg yr and the SSE spectrum in the $0\nu\beta\beta$-region, corrected for the detection efficiency, after 24.16 kg yr. The solid lines represent the exclusion limits for the two spectra at the 90% C.L.
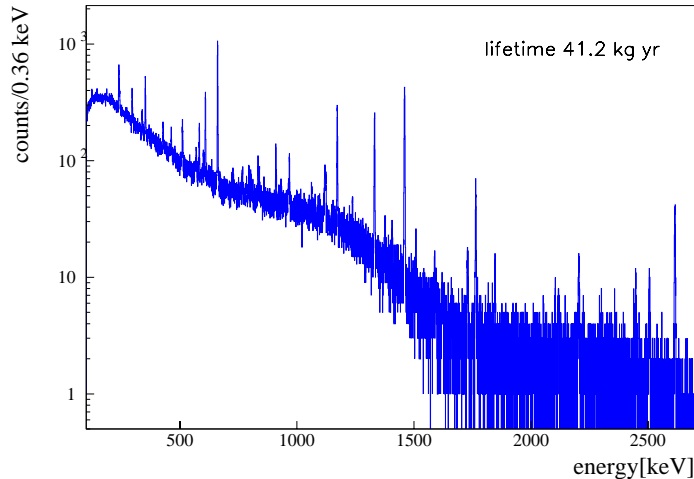


Figure 1: Full spectrum after 41 kg y of measurement of the Heidelberg–Moscow experiment.

In addition we report the limits obtained by evaluating the SSE data with the new method proposed by the Particle Data Group 98 [4]. The number of excluded events for an observation of 7 events and a background expectation of 13 is 2.07 (0.47) with 90% C.L. (68% C.L.) (see Table III and V in [5]). The resulting upper limits for the half-life of the $0\nu\beta\beta$-decay are the following:

$$T_{1/2}^{0\nu} \geq 5.7 \times 10^{25} \text{ yr} \quad 90\% \text{ C.L.}$$
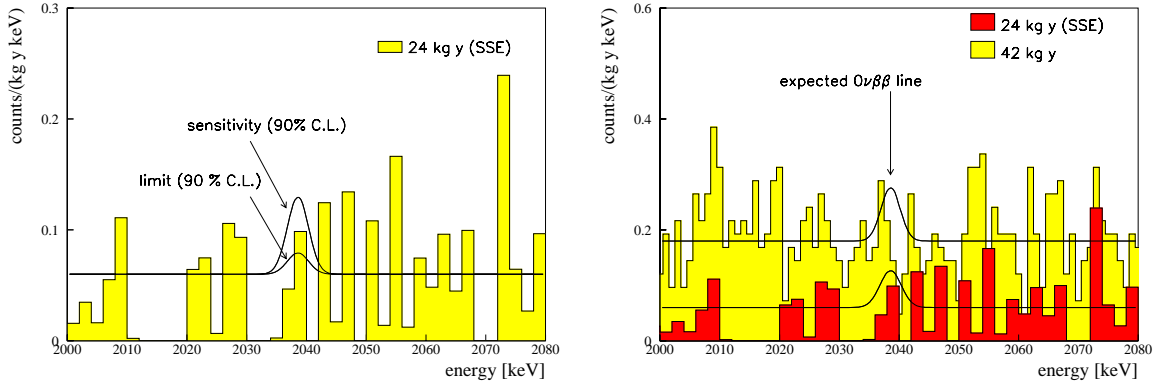$$T_{1/2}^{0\nu} \geq 2.5 \times 10^{26} \text{ yr} \quad 68\% \text{ C.L.}$$

Figure 2: Energy region of the neutrinoless double beta decay. Left: SSE spectrum with the excluded peaks (upper limit and sensitivity) from the method suggested by [4, 5]. Right: SSE spectrum (dark) after 24 kg y and spectrum containing MSE (light) after 42 kg y of data taking analyzed using the procedure given in [3]. Shown is also the excluded peak from these data.

The sensitivity of the experiment, as defined in [5], is again obtained by setting the measured number of events equal to the expected background. With 7.51 (4.71) excluded events at 90% C.L (68% C.L.), the sensitivity is:

$$T_{1/2}^{0\nu} \geq 1.6 \times 10^{25} \text{ yr} \quad 90\% \text{ C.L.}$$
$$T_{1/2}^{0\nu} \geq 2.5 \times 10^{25} \text{ yr} \quad 68\% \text{ C.L.}$$

With the matrix elements of [6], neglecting RHC's, we can convert the lower half-life limit into an upper limit on the effective Majorana neutrino mass. The obtained limits are shown in Table 1. Already in the present stage the Heidelberg-Moscow experiment is setting the most stringent limit on the Majorana neutrino mass, allowing to test the predictions of degenerate neutrino mass models. In models which try to accomodate the solar- and atmospheric neutrino problems while considering the neutrino as a hot dark matter candidate with a few eV, the small angle MSW solution is practically ruled out [7]. For the large angle MSW solution, an effective neutrino mass smaller than 0.2 eV would need an unnatural fine tuning to account for a relevant neutrino mass in a mixed hot and cold dark matter cosmology [8].

The implications for other physics beyond the standard model, like left-right supersymmetric models, supersymmetry, leptoquarks and compositness will be discussed elsewhere.

# 3   New results on dark matter WIMPs

The nature of dark matter in the Universe remains a challenging question. WIMPs (weakly interacting massive particles) and neutrinos are among the most discussed candidates [9].

WIMP detection experiments can decide whether WIMPs dominate the halo of our Galaxy. For this reason, considerable effort is made towards direct WIMP search experiments which look for energy depositions from elastic WIMP–nucleus scattering [10]. The Heidelberg–Moscow experiment gave the most stringent upper limits on spin–independent WIMP interactions [11] until recently. The present best limits on the WIMP–nucleon cross section come from the DAMA NaI Experiment [12].
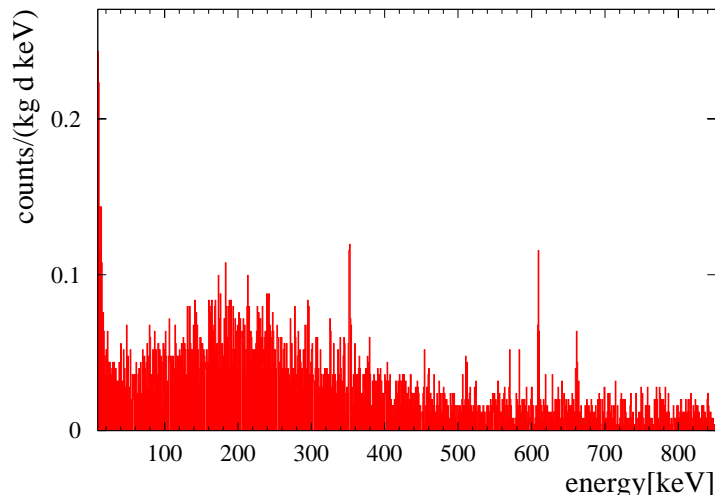


Figure 3: Full recorded sum spectrum with lifetime 0.69 kg yr. Peaks from the $^{238}$U chain can be identified. A $^{137}$Cs peak slowly appears at 662 keV. All structures at low energies are fluctuations so far and therefore not identifiable.

One of the enriched Ge detectors of the Heidelberg–Moscow experiment took new data in a period of 0.249 years in a special configuration developed for low energy measurements. A lower energy threshold and a smaller background counting rate has been achieved with the same detector as used before for this aim [11], mainly due to the lower cosmogenic activities in the Ge crystal and in the surrounding copper after four years without activation.

The utilized detector is a coaxial, intrinsic p–type HPGe detector with an active mass of 2.758 kg. The sensitivity to spin–dependent interactions becomes negligible, since $^{73}$Ge, the only stable Ge isotope with nonzero spin, is deenriched to 0.12% (7.8% for natural Ge). The detector has been in the Gran Sasso Underground Laboratory since September 1991; a detailed description of its background can be found in [2].

The data acquisition system allows an event-by-event sampling and pulse shape measurements. The signals are amplified to record low as well as high–energetic pulses. For details of the experimental setup see [13].

An energy threshold of 9 keV has been reached. This rather high value is due to the large detector size and a 50 cm distance between FET and detector.

We calibrate the detector with a standard $^{152}$Eu–$^{228}$Th source. The energy resolution at 727 keV is $(2.37 \pm 0.01)$ keV.

Figure 3 shows the sum spectrum after a time cut discriminating for microphony. The background counting rate in the energy region between 9 keV and 30 keV is 0.081 cts/(kg d keV) [between 15 keV and 40 keV: 0.042 cts/(kg d keV)]. This is about a factor

of two better than the background level reached by [11] with the same Ge detector. The dominating background contribution in the low–energy region from the U/Th natural decay chain can be identified in Fig. 3 via the 352 keV and 609 keV lines (the continuous beta spectrum from $^{210}$Bi originates from this chain).
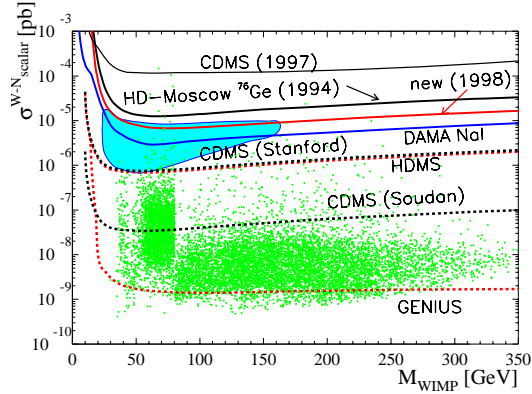


Figure 4: Comparison of already achieved WIMP–nucleon scalar cross section limits (solid lines): the Heidelberg–Moscow $^{76}$Ge [11], the ecent CDMS nat. Ge [16] and the new DAMA NaI result [12], including their evidence contour [14], in pb for scalar interactions as function of the WIMP mass in GeV and of possible results from upcoming experiments (dashed lines for HDMS [17], CDMS (at different locations) and GENIUS [18]). These experimental limits are also compared to expectations (scatter plot) for WIMP neutralinos calculated in the MSSM framework with non–universal scalar mass unification [20] (all curves and dots scaled for $\rho = 0.5$ GeV/cm$^3$ for comparison of published data).

The evaluation for dark matter limits on the WIMP–nucleon cross section $\sigma^{\text{W}-\text{N}}_{\text{scalar}}$ follows the conservative assumption that the whole experimental spectrum consists of WIMP events.

After calculating the WIMP spectrum for a given WIMP mass, the scalar cross section is the only free parameter which is then used to fit the expected to the measured spectrum. According to the underlying hypothesis we check during the fit for excess events above the experimental spectrum (for a one–sided 90% C.L.) using a sliding, variable energy window. The minimum width of this energy window is 5 keV, corresponding to 2.5 times the FWHM of the detector ($6\sigma$ width). The minimum of cross section values obtained via these multiple fits of the expected to the measured spectrum gives the limit.

The new upper limit exclusion plot in the $\sigma^{W-N}_{scalar}$ versus M$_{WIMP}$ plane is shown in Fig. 4. Since we do not use any background subtraction in our analysis, we consider our limit to be conservative. We are now sensitive to WIMP masses greater than 13 GeV and to cross sections as low as $1.12 \times 10^{-5}$ pb (for $\rho = 0.3$ GeV/cm$^3$).

At the same time we start to enter the region (evidence–contour) allowed with 90% C.L. if the preliminary analysis of 4549 kg days of data by the DAMA NaI Experiment [14] are interpreted as an evidence for an annual modulation effect due to a spin independent coupled WIMP. Since the effect was confirmed with much higher statistics (20 000 kg days have been analyzed by the DAMA Collaboration [15]) it has become crucial to test the region using a different detector technique and a different target material.

Also shown in the figure are recent limits from the CDMS Experiment [16], from the

DAMA Experiment [12], as well as expectations for new dark matter experiments like CDMS [16], HDMS [17] and for our recently proposed experiment GENIUS [18]. Not shown is the limit from the UKDM Experiment [19] which lies somewhere between the two germanium limits.

# 4    Acknowledgments

# References

[1] Heidelberg–Moscow Collaboration, M. Günther *et al.*, Phys. Rev. **D 55**, (1997)54.

[2] Heidelberg–Moscow Collaboration, L. Baudis *et al.*, Phys. Lett. **B 407**, (1997)219.

[3] R.M. Barnett *et al.*, Physical Review **D 54**, (1996)1.

[4] C. Caso *et al.*, European Physical Journal, **C 3**, 1998)1.

[5] G.J. Feldman, R.D. Cousins, Physical Review **D 57**, (1998)3873.

[6] K. Muto, A. Staudt, H.V. Klapdor-Kleingrothaus, Europhys. Lett. **13**, (1990)31.

[7] H. Minakata and O. Yasuda, Pys. Rev. **D 56**, (1997)1692

[8] H. Minakata and O. Yasuda, Nucl. Phys. **B 523**, (1998)597

[9] G. Jungman, M. Kamionkowski, and K. Griest, Phys. Rep. **267**, (1996)195.

[10] P.F. Smith and J.D. Lewin, Phys. Rep. **187**, (1990)203.

[11] Heidelberg–Moscow Collaboration, Phys. Lett. **B 336**, (1994)141.

[12] R. Bernabei *et al.*, Phys. Lett. **B 389**, (1997)757.

[13] Heidelberg-Moscow-Collaboration, Phys. Rev. **D 59**, (1999)022001

[14] R. Bernabei *et al.*, Nucl. Phys. [**B** (Proc. Suppl)**70**, (1998)79.

[15] P. Bernabei et al., ROM2F/98/34 august(1998)

[16] D.S. Akerib *et al.*, Nucl. Phys. **B** (Proc. Suppl) **70** , (1998)64.

[17] L. Baudis et al., Nucl. Instrum. Methods **A 385**, (1997)265.

[18] H.V. Klapdor–Kleingrothaus, in *Proceedings of BEYOND 97, the First International Conference on Particle Physics Beyond the Standard Model*, Castle Ringberg, Germany, 8–14 June 1997, edited by H.V. Klapdor–Kleingrothaus and H. Päs, (IOP, Bristol, 1998), H.V. Klapdor–Kleingrothaus, Internat. J. Mod. Phys. **A 13**, (1998)3953 H.V. Klapdor–Kleingrothaus, J. Hellmig and M. Hirsch, J. Phys. **G 24**, (1998)483, L. Baudis, G. Heusser, H.V. Klapdor-Kleingrothaus, B. Majorovits, Y. Ramachers, H. Strecker, in press at Nucl. Instr. Meth. **A**.

[19] P.F. Smith *et al.*, Phys. Lett. B **379**, (1996)299.

[20] V. Bednyakov *et al.*, Z. Phys. A **357** (1997)339.

# ICARUS. Imaging Cosmic And Rare Underground Signals

F.Arneodo[a], A.Badertscher[b], E.Barbieri[c], P.Benetti[d],
A.Borio di Tigliole[f], R.Brunetti[d], A.Bueno[b], E.Calligarich[d],
M.Campanelli[b], F.Carli[c], C.Carpanese[e], D.Cavalli[f],
F.Cavanna[g], P.Cennini[h], S.Centro[e], A.Cesana[f], C.Chen[i], Y.Chen[i],
C.Cinquini[c], D.Cline[j], I.De Mitri[a], R.Dolfini[d], D.Favaretto[e],
A.Ferrari[f], A.Gigli Berzolari[d], P.Goudsmit[b], K.He[i], X.Huang[i],
A.Kruse[b], Z.Li[i], F.Lu[i], J.Ma[i], G.Mannocchi[k], F.Mauri[d],
D.Mazza[g], L.Mazzone[d], C.Montanari[d], G.P.Nurzia[g],
S.Otwinowski[j], O.Palamara[a], S.Parlati[g], D.Pascoli[e], A.Pepato[e],
L.Periale[l], S.Petrera[g], G.Piano Mortari[g], A.Piazzoli[d], P.Picchi[k],
F.Pietropaolo[e], T.Rancati[f], A.Rappoldi[d], G.L.Raselli[d], D.Rebuzzi[d],
J.P.Revol[h], J.Rico[b], M.Rossella[d], C.Rossi[g], A.Rubbia[b],
C.Rubbia[d,h], P.Sala[f], D.Scannicchio[d], F.Sergiampietri[h], S.Suzuki[k],
M.Terrani[f], P.Torre[d], S.Ventura[e], M.Verdecchia[g], C.Vignoli[d],
H.Wang[j], J.Woo[j], G.Xu[i], Z.Xu[d], C.Zhang[i], Q.Zhang[i], S.Zheng[i]

[a] Lab. Naz. del Gran Sasso, S.S. 17 bis Km. 18,910 - Assergi (AQ), Italy
[b] Inst. for Part. Phys. Eidgenössische Tech. Hochschule CH-8093 Zürich, Switzerland
[c] Dip. di Mecc. Strutt. e INFN, Univ. di Pavia, via Abbiategrasso 209, Pavia, Italy
[d] Dip. di Fisica Nucleare e Teorica e INFN, Univ. di Pavia, via Bassi 6, Pavia, Italy
[e] Dip. di Fisica e INFN, Univ. di Padova, via Marzolo 8, Padova, Italy
[f] Dip. di Fisica e INFN, Univ. di Milano, via Celoria, Milano, Italy
[g] Dip. di Fisica e INFN, Univ. dell'Aquila, via Vetoio, L'Aquila, Italy
[h] CERN, CH-1211, Geneva 23, Switzerland
[i] IHEP - Academia Sinica, 19 Yuquan Road, Beijing, People's Republic of China
[j] Dept. of Physics, UCLA, Los Angeles, CA 90024, USA
[k] Lab. Naz. di Frascati dell'INFN, via Fermi 40, Frascati (Roma), Italy
[l] ICGF del CNR di Torino, corso Fiume 4, Torino, Italy

**Abstract**

The main activities of the ICARUS collaboration during the year 1998 are summarised. In particular the 600 ton cryostat construction by AIR LIQUIDE ITALIA, the measurement of the neutron background in Hall C of LNGS, the new detailed design of the complete internal detector and the cryogenic test of a module of the read-out wire chamber system, the complete design and prototyping of all the electronics components, the ongoing $R\&D$ activities and the software studies are reported in some details.

# 1 Introduction

The aim of the ICARUS experiment is to install in the LNGS underground laboratory a multi-kton liquid argon TPC [1]. The ICARUS programme addresses many fundamental issues:

- (i) the nature of neutrinos, in particular the question of the neutrino mass. This is being investigated in ICARUS both through the study of atmospheric neutrinos and through long baseline studies with the foreseen CERN neutrino beam [2];

- (ii) the stability of the nucleon, which is the only way to access phenomena at the energy scale of Grand Unification. ICARUS will be the first high-resolution imaging study of such a phenomenon;

- (iii) the study of solar neutrinos. Even though ICARUS is not optimised to study this kind of events, the issue remains extremely interesting and with a suitable neutron shielding ICARUS can reach a reasonable detection threshold;

- (iv) the detection of astrophysical and cosmological neutrinos from supernova.

As a first practical step the Collaboration proposed in 1996 [3] to build a 600 ton module. The most efficient way to reach the sensitive mass needed to fulfil the ICARUS scientific goals is to proceed through an intermediate step detector between the 3 ton detector [4] operated at CERN and the final multi-kton detector, and to adopt a modular approach to reach the full multi-kton fiducial volume.

A few hundred ton detector at the same time allows an important first step in the ICARUS scientific programme. What the ICARUS technique is providing is a background-free detection of proton decay and neutrino events. While a sensitive mass in excess of few thousands tons of liquid argon is clearly needed to achieve the $10^{34}$ years range in proton decay lifetime, many exotic channels have been only poorly investigated so far or not at all, and would be easily covered in this first phase. Atmospheric and solar neutrinos are areas which could be also investigated with the 600 ton detector. Therefore, a 3 mm wire pitch will be used instead of the 5 mm foreseen for the 5000 ton module, in order to allow for higher precision measurements.

The intermediate step opens in addition the possibility to build the final detector in a modular way: the construction of a number of identical 600 ton detectors installed next to one another.
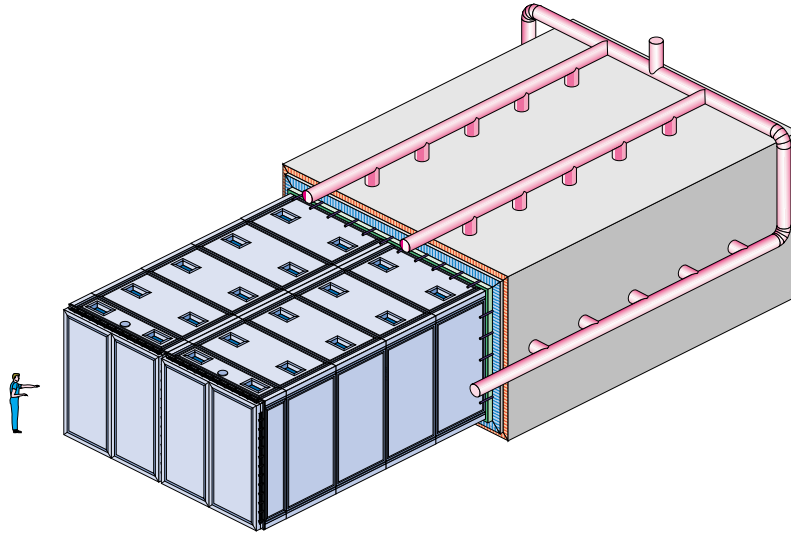
Figure 1: A 3-D sketch of the T600 cryostat.

As a general strategy it was decided that the most time efficient and economical way to have the 600 ton module operative is to build and test it outside the Laboratory and then take it to the Hall C for the final assembly. This implies that the module has to be transportable.

It turns out that the single largest transportable object on the Italian highways and into the Hall C has a volume too small for the physics purposes. Consequently the volume was split into two parts: two identical semi-independent half-vessels with dimensions that correspond to the maximum transportable.

During the year 1998 the ICARUS experiment continued the main activities related to the construction of the 600 ton module.

In particular the construction of the 600 ton cryostat by AIR LIQUIDE ITALIA has continuously evolved and the first half-module is presently being assembled in the AIR LIQUIDE workshop (see Section 2).

The 10 m$^3$ prototype cryostat (Cryogenic Test Facility) has been widely modified and partly rebuilt in order to reflect the final design of the T600 and is now ready for a series of complete tests (see Section 3).

The detector for the measurement of the neutron background in the Hall C of the LNGS has taken data since August 1997 until May 1998. The analysis of the collected data showed that the main source of neutrons is ($\alpha$,n) reactions instead of spontaneous fission as previously supposed (see Section 4).

The internal detector for the 600 ton module has been completely revised, after the realisation of the Test Module and the cryogenic test of a reduced module. The cathodes and the race track system have been designed in details. An assembling ramp (A.R.) has been designed and is now under construction to allow the mounting of the internal detector mechanics in a way suitable to the safety rules (see Section 5).

The complete electronics chain has been designed and tested (see Section 6). For what concerns the system layout, it was decided that all the electronics will be mounted next to

each signal feed-through flange. The decoupling, analogue and digital boards have been completely designed and are now under test to completely qualify the performances. The system of the slow controls for the T600 have been carefully considered and designed.

Many activities were carried out concerning the $R\&D$ studies for the optimisation of the working conditions for some critical items of the apparatus (see Section 7): different approaches to improve the $LAr$ purity monitors, the High Voltage and Signal feed-throughs, scintillation light detection, test on the electrons field emission in $LAr$, new approaches for Argon purification.

The data acquisition studies are in the process of evaluating the requirements for the T600 module. In 1998 a reconstruction code for the detector has started to take shape (see Section 8).

The software activity continued with the simulation of nuclear effects in neutrino interactions, in particular for what concerns the effects on final states kinematics and on acceptances and missing momentum, the simulation of deep inelastic scattering interactions with nuclear effects, the calculations of atmospheric neutrino fluxes and event rates in ICARUS and the LBL CERN-Gran Sasso neutrino beam calculations (see Section 9).

# 2 Cryogenics and purification

The layout of the cryogenics and purification systems for the ICARUS T600 have been described in several documents during the past two years. Here we only report the status of construction as at the end of 1998; for other details see for example the 1997 LNGS Annual Report.

The Contract for the construction of the ICARUS T600 cryogenics and purification systems was formally signed with AIR LIQUIDE ITALIA industry in June 1997. During the second half of 1997 and for all 1998 the project and construction of the T600 module evolved continuously:

- the full engineering design of the cryostat and of all the auxiliary plants was completed;

- all the basic materials needed for the construction were ordered and most of them have been delivered;

- the honeycomb panels for the $LAr$ container (aluminium) and for the insulation (aramid fibre) have been ordered; the aluminium panels have been delivered and are presently ready for the assembly of the cold vessel, the insulation panels will be delivered when the T600 will be ready for the complete installation (after the assembly of the internal detector);

- most of the auxiliary plants have been constructed (cooling units, purifiers and recirculation systems);

- all the tools required for the cryostat assembly (welding machines, lifting and moving devices) have been designed and built;

- all the procedures for testing and for quality check have been defined and agreed.

The first half-module is presently being assembled in the AIR LIQUIDE workshop. The four, 20m long, faces of the cold vessel will be separately assembled by welding together the aluminium panels and the angular profiles on a single, 20m long, positioning and welding tool. The bottom wall is currently in production. The four faces will be then assembled together to form the parallelepiped shape of the cryostat by welding the four angular profiles. The two end caps will be added at the end (one of the two is removable to allow for the installation of the internal detector). When the structure will be complete, all the weldings will be individually tested with helium by pumping inside the panels. The final test will be the vacuum inside the vessel: this will give the overall leak rate, if any, and will provide a mechanical test under the maximum load.

All these operations should take two to three months and the first half-module is expected to be delivered in Pavia for the internal detector assembly in March 1999. The construction of the second half-module will begin immediately after. The complete installation of the T600 module is linked to the internal detector assembly; we expect that all the operations will be completed and the detector will be ready for the first tests around the end of 1999.

# 3  Tests on the $10\,m^3$ prototype

The first series of tests on the $10\,m^3$ prototype was completed at the beginning of 1998 with the successful cryo-mechanical test of a wires chamber module. The overall performance displayed by the prototype was considered satisfactory, however we suffered for some drawbacks which lead to several modifications of the original cryostat design and prevented us from doing part of our testing program (vacuum).

During all 1998 the prototype has been widely modified and partly rebuilt in order to reflect the final design of the T600:

- the cold vessel was completely reconstructed;

- the insulation panels were dismantled and reshaped;

- the expansion vase was removed;

- a cooling unit with forced $LN_2$ circulation and a pre-cooling circuit were added;

- a fast recirculation unit with a $LAr$ pump was added and the purification circuit was modified;

- sensors and electronics for the automatic control of the prototype were also recently added.

The reconstruction of the prototype cryostat allowed to setup and fix the assembly procedures for the T600 (panels positioning, welding procedures and tests, insulation assembly). We performed a vacuum test on the new cold vessel and obtained very positive results: no evident leaks detected with an ultimate vacuum reached in few hours of pumping $\approx 2^{-5}$ mbar. The mechanical stability was also very good with the measured

displacements on the loaded surfaces in good agreement with the results of the finite elements analysis.

The prototype is presently being reassembled with the wires chamber module for a full functional test in working conditions. The prototype is loaded with almost all the instrumentation that we plan to install in the T600:

- several coarse and precision $LAr$ level meters;

- temperature and pressure sensors distributed on the chamber module and inside the volume;

- several $LAr$ purity monitors of different types;

- a precise position sensing device on the chamber tensioning devices for a most sophisticated cryo-mechanical test;

- Ar flow meters, vacuum gauges, etc..

Also few wires ($\approx 100$) of the chamber module are connected to electronic channels in order to test the electronic chain and make some noise measurements in working conditions.

The main goals of the next run are:

- setup and refine the various procedures (vacuum, cooling, filling, run, emptying);

- test cryogenic performances (temperature uniformity, heat losses);

- test the purification procedures and measure the ultimate $LAr$ purity with the chamber module;

- test all the instrumentation and its readout;

- make some noise measurements on the wires and correlate the results with the other active elements of the prototype (pumps, instrumentation, etc.).

The run will start at the beginning of the next year and will continue until the arrival of the first half-module in Pavia.

During 1999 the prototype will be re-installed in the Gran Sasso outside laboratory for a new series of tests mostly dedicated to the chambers readout.

# 4 Neutron background measurement in the Hall C of LNGS

The very low energy and the very low expected rate of solar $\nu$ events, implies that most of the spectrum can be masked by electrons produced by radioactive nuclides present in the environment. This drawback limits in practice the attainable informations, therefore the background noise must be accurately considered. The background components have little

relevance except the one produced by neutron capture in the dewar or in the detector sensitive volume itself.

The neutron field in LNGS halls is produced by Spontaneous Fission (SF), mainly of $^{238}U$, and $(\alpha,n)$ reactions on light elements (O, Al, B, etc.), that are present in the rocks or in the detector material. The $\gamma$-rays following thermal neutron capture can produce, in the sensitive detector volume, Compton electrons which can overcome true solar neutrino events. It follows that the neutron field in the caverns should be well characterised, for what concern both intensity and energy distribution, which is a difficult goal due to its very low intensity.

The fast neutron spectrum has been measured with a 32 litres proton recoil scintillation detector. Data taking lasted about ten months, since August 1997 until May 1998.

We recorded the energy spectrum of particles selected as heavy charged particles and the rate of electron signals, induced by $\gamma$-ray interaction, which turned out to be $\approx 120Hz$ in the whole detector.

We adopted two different experimental setups:

- i) the bare detector to record the environment neutron field (run time $\approx 10^7$s)

- ii) the detector shielded against neutrons by a borated polythene envelope 30cm thick (run time $\approx 3 \cdot 10^6$s), to evaluate the contribution of spurious pulses.

In each run the energy spectra are collected for the following two samples:

- a) single heavy charged particle tracks (p-sample),

- b) one heavy charged particle track in coincidence with an electron track within 10 $\mu$s (p$\gamma$-sample).

At the extremely low neutron flux level in the underground laboratory, the $\alpha$ particles emitted from U and Th impurities, become the dominant fraction (more than 95%) of the p-sample and in practice the unique component in the spectrum collected with the detector shielded against neutrons. For these reasons p-sample is not used for the neutron spectrum determination. However it proved to be pretty useful for the detector energy calibration, and for the evaluation of stochastic coincidences in the p$\gamma$-sample. Once cleaned of the stochastic events contribution, this sample contains 81 events, and it is assumed to represent the proton recoil spectrum induced by the environment neutrons. In order to have a reasonable statistics we chose the binning of Fig. 2 in which the corresponding group intensities are shown.

The neutron spectrum is represented with 36 energy groups, 0.5 MeV wide in the range 0 - 18 MeV.

The counts in each bin of the proton recoil spectrum, $C_i$, are expressed as

$$C_i = \Sigma_j \ S_{ij} \ \Phi_j$$

In this equation:
- $\Phi_j$ is the fluence in the $j^{ij}$ neutron group and
- $S_{ij}$ has the general meaning of a cross section; it represents the number of proton recoils in the i-th bin per unit neutron fluence in the j-th neutron group.
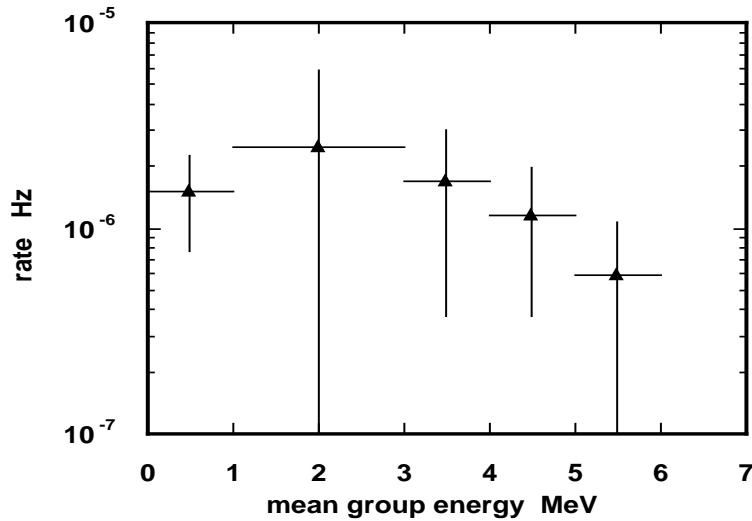
Figure 2: Group proton recoil spectrum.

The set of the previous equations allows in principle the determination of the neutron spectrum if the spectral deconvolution functions $S_{ij}$ , are known. These functions were computed by the FLUKA program and are shown in fig. 3.

The deconvolution of the set of eq.s was performed by an iterative technique with SAND II program [5]. The neutron energy spectrum obtained is shown in the Fig. 4 and compared with the spectrum which should be obtained if the neutrons produced only by spontaneous fission, as was assumed in previous papers [6]. Our results turn out to be consistent with the hypothesis that the main source of neutrons in hall C is $(\alpha,n)$ reactions instead of spontaneus fission as previously supposed.

The results represented in large group fluxes are displayed in Table 1 and compared with the preceding results.

| Energy interval (MeV) | Neutron flux ($10^{-6}\ cm^{-2}\ s^{-1}$) | |
|:---:|:---:|:---:|
| | reference [6] | present measure |
| 1.0 - 2.5 | $0.38 \pm 0.01$ | $0.14 \pm 0.12$ |
| 2.5 - 5.0 | $0.27 \pm 0.14$ | $0.13 \pm 0.04$ |
| 5.0 - 10.0 | $0.05 \pm 0.01$ | $0.15 \pm 0.04$ |
| 10.0 - 15.0 | $(0.6 \pm 0.2){\cdot}10^{-3}$ | $(1.4 \pm 0.4){\cdot}10^{-3}$ |

Table 1: Large group fluxes.

We measured also the proton recoil spectrum in the presence of a calibrated Am/Be source with the bare and shielded detector. From these measurements we estimated the neutron detection efficiency for a point source, used to derive the detector threshold, and the shield effectiveness against neutrons.
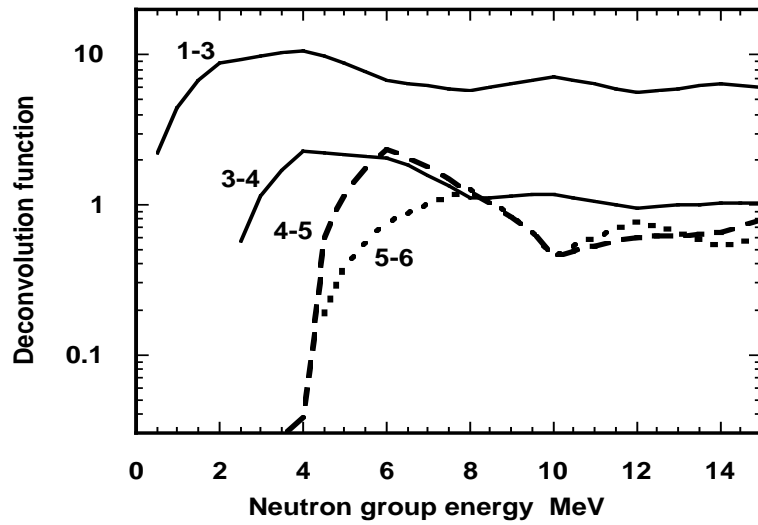
Figure 3: Deconvolution functions for the pg-sample. The energy limits (MeV) of the proton recoil bins are quoted near the corresponding curve.
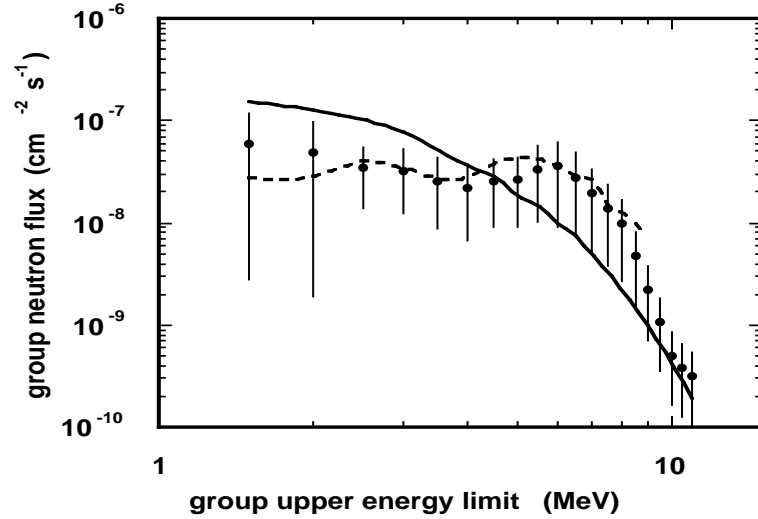


Figure 4: Hall C neutron spectrum (dots), guess spectrum (full line), and computed (a-m) spectrum (dashed line).

# 5 Internal detector

## 5.1 Cryogenic test

The reduced Test Module (2.0 m x 3.9 m x 0.9 m), built in 1997, has been put, at the beginning of 1998, inside the $10\,m^3$ prototype to study the cryogenic behaviour of the mechanics and in particular the thermal stresses during the cooling phase. The results were satisfactory:

- none of the 1,800 wires broken;

- the wire elasticity limit has not been reached;

- the structure was not deformed;

- the wire tension differences between before and after the thermal cycle are limited (from $\approx$25$\pm$6$g$ for the longer wires to $\approx$80$\pm$25$g$ for the shorter ones).

## 5.2 Detailed designs

After analyzing the Test Module results, some minor adjustments were made to the detailed designs:

- to speed the outgassing, all the contact surfaces have been reduced;

- to eliminate the pollution danger of the $LAr$, all the CuBe components have been golded;

- the Peek combs and shells, obtained through a mold, have been revised and improved;

- to speed the outgassing of the closed volumes, holes have been designed whenever possible;

- to enhance the structure rigidity and to improve the cleaning a tubular profile has been chosen. In such a way the computed deformations have been reduced by more than 20%.

The cathode and the electric field shaping electrodes (race tracks) have been designed. The race track system is made by:

- 29 close rectangular rings (per each wire chamber) $18.1m \times 3.2m$;

- $2m$ long stainless steel tubular elements ($\varnothing 34x0.8$) connected by two welded terminals;

- $50mm$ pitch;

- in the upper part, between the race tracks and the Ar gas phase a grounded continuous metallic shielding has been interposed;
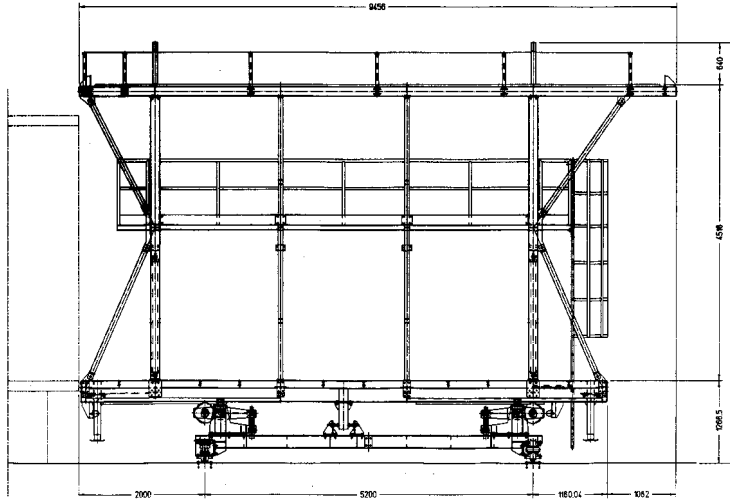
Figure 5: Longitudinal view of the Assembling Ramp.

- the race tracks are held by Vectronite dielectric supports, linked to the structure.

The cathode is made by 9 modular prefabricated panels ($1.95m \times 3.10m$) of stainless steel sheet, 58% pierced to lighten the structure and to allow the transparency for scintillation light collection.

The final designs of all the sustaining structure, the wire chamber system, the cathodes and the drift region field shaping electrodes were finished at the end of April 1998. In May 1998 the formal letters for a call for tenders were sent to various leading industries. The CINEL industry (Vigonza - PD) was chosen for all the sustaining structure and the wire chamber system and the GALLI & MORELLI industry (Acquacalda - LU) for the cathodes and race track system. The first half part of all the mechanical components (for the first half-module) will be delivered in Pavia starting from January 1999.

## 5.3 Assembling ramp

To allow the mounting of the internal detector mechanics in a way suitable to the safety rules, an assembling ramp (A.R.) has been designed and is now under construction in an external factory (see Fig. 5 and 6). It has a twofold functionality:

- to allow the mounting of the chamber modules outside the cryogenic dewar, just in front of the closure flange;

- to get the appropriate tools for shifting the chamber modules in the final position inside the dewar. Lifts and translations are performed by specific chariots, mounted on two iron rails, which connect the platforms basement to the internal dewar plane.

The A.R. operates in a clean room (100,000 class) ($12 \times 12 \times 7 \approx 1000m^3$) and can be translated on iron rails. The clean room is made by polycarbonate and is self carrying.

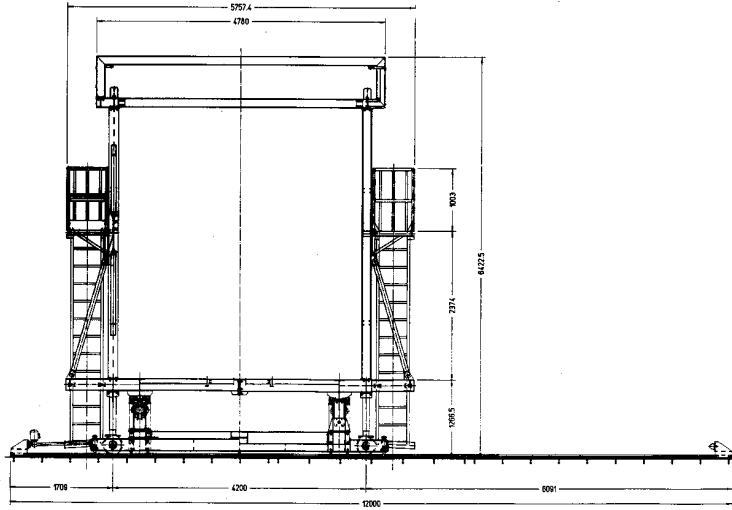The foreseen mounting sequences are as follows:

Figure 6: Transversal view of the Assembling Ramp.

- the A.R. is positioned in front of the closure flange of the first dewar semi-module;

- the closure flange is removed and the mechanical connection is realised by two iron rails;

- the clean room is completed around the operational zone;

- the first $6m$ chamber modules (3 on the right and 3 on the left) are mounted on the platform;

- the chamber modules are translated into the dewar;

- the second $6m$ chamber modules are mounted on the platform and so on.

After complete mounting of the detector (chambers, race tracks and cathodes) in the first half-module (300 ton), the A.R. is translated in front of the second half-module; leaving the first one ready to be operated for vacuum tests.

## 5.4   Wiring table

For the wiring of the 5,000 wires of the Test module and of the 2,000 wires of the reduced module for the cryogenic test, a suitable semi-automatic table has been equipped in the Pavia laboratory. In order to speed up the wiring procedure and to get a better quality, the existing table has been revised, with the use of a new wire tension measurement device. Moreover the storage and cleaning procedures have been studied, with the designs of suitable spools to roll up the 32 wire modules and of special devices to easily mount the wire modules on the frame.

96

# 6  Electronics of the 600 ton module

## 6.1  Introduction

The 1998 activity concerning the electronics can be divided into four main items: system layout (cabling from feedthrough to the electronics crates, electronics modules shielding and crates layout), decoupling board design, analogue board design, and digital board design.

Those specific activities and the status of the DAQ development will be presented in details.

## 6.2  System layout

During 1998 a major decision concerning the system layout has been taken. After the development of the new very compact feedthrough that houses some 576 channel, it was eventually decided that all the electronics needed by the 576 channels will be mounted next to each flange. The rack containing the analogue crate, the digital crate and the power supplies, both low voltage and high voltage, is considered the basic unit of the system layout. This rack is now under development and special care is devoted to the rack cooling that must take into account that racks are on top of the detector and that filter replacement could be a non trivial procedure. An air tight rack with simple heat exchanger is under consideration to avoid any need of filters and the possibility of accumulating dirt on electronics that could cause performance impairment. At the end of the year two prototypes of feedthroughs will be delivered and we intend to mount in the laboratory a complete rack, connected to the flange, to test the system performance.

## 6.3  Decoupling Boards

The decoupling board receives 32 signals from the flange and delivers them to the analogue board. The functions that this unit performs are:
   - $HV$ biasing of the wire;
   - $HV$ decoupling to the amplifiers;
   - delivering of different type of test signals;
   - delivering of calibration signal.

The decoupling board has been completely designed and is now under test to completely qualify its performance under $HV$ biasing. Each board has a metal shield and is housed in the back side of the analogue crate, just behind of the analogue board, in order to have the shortest connection to the amplifiers.

## 6.4  Analogue Boards

The analogue boards have the mechanical size of 6U VME, but they don't use any bus. The bottom back connector is used to input 32 signals from the decoupling board. Another smaller back connector is used for control signals. The 32 signals from 32 channels are

amplified and filtered and then converted to 10 bit by a tree of analogue multiplexers-ADCs-digital multiplexers and sent to the digital board via a serial link (21 bit wide) at the rate of 40MHz. This means that each channel is sampled every 400 ns.

The front end amplifier has been developed under the responsibility of P.Cennini in close collaboration with the electronics laboratory of INFN Padova. It is essentially an unfolded cascode Radekatype integrator with external input jFet, realised in BiCMOS AMS technology [7].

The development of the board has been performed by CAEN spa after the specification defined by the Icarus collaboration. Each board has individual shielding and the prototypes have been tested quite successfully (see later for complete results). The Analogue board functionality is fully described in a CAEN document [8].

## 6.5   Digital Boards

The digital board, named Arianna [9,10], provides selective buffering of 32 input channels in digital form. The buffer length is programmable. The recognition of the ROI (Region of Interest) per each signal is performed by an ASIC designed on purpose (Daedalus) [11,12,13] that serves 16 channel at a time. Two Daedalus chips are required in each Arianna.

The system become operational late spring 1998 and four prototypes are now working.

Early this year the Daedalus chip has been fully redesigned. The old prototype was serving only 4 channel while with the new design 16 channels have included in one chip. This allows a much more compact design of the Arianna board.

## 6.6   Noise performance

The full system made by decoupling, analogue, and digital board has been tested in order to evaluate mainly its noise performance that is the most critical parameter.

The signal to noise ratio before numerical integration of the current signals is S/N= 9.53. The S/N ratio after numerical integration of the current samples is S/N=13.1. This figure is fundamental for precise measurement of the charge deposited in the detector and for track reconstruction. The design figure was set to 10.

## 6.7   Software

As a support to the ongoing prototyping and pre-production batches on the hardware side, this years software development activities have been heavily focussed on providing the testing, debugging and measurement tools needed to qualify the complete readout chain components.

A major concern was to explore and acquire a good knowledge of the development environments and communication technologies - both hardware and software - required to drive a distributed architecture such as the 600T DAQ system.

Therefore, most of the testing setups installed in our lab while working on the hardware qualification, went through dedicated CPUs sitting on the readout crate, remotely

controlled via network following a client/server paradigm. Relying on a widespread supported realtime OS (WindRivers VxWorks) and on standard high level network protocols (udp and tcp/ip based), we achieved some basic building blocks with reduced platform dependence which cover different functionalities foreseen on the daq system.

Those were demonstrated for instance on a Labview-based remote online event display (we ran it from Padova to LNGS) serving 80 channels of the Arianna boards, or on a general purpose multithreaded event builder, easily customizable for different I/O configuration.

As a further step to platform indipendence, we are presently testing the integration of a Java/Web based user interface to control the builder.

## 6.8 Slow controls

### 6.8.1 Cryogenic slow controls - Overview

It is foreseen that the T600 detector life will be subdivided into two regimes:

- Steady state : Normal data taking operation

- Transitory phases : Vacuum pumping, cooling, filling/emptying with Argon, etc...

A certain number of hardware probes, gauges (pressure, temperature, flows, ...) and controllers (pumps, valves, ...) will be installed in order to control and monitor the cryogenic condition of the detector during the steady state and transitory phases.

A proposal for the cryogenic monitoring is been developed in close collaboration with AirLiquide. We are in the process of finishing the definition of the sensors and instrumentation for the T600. It has been agreed that AirLiquide will provide the necessary (minimal) configuration, in order to safely operate the T600 dewar. Additional cryogenic instrumentation not considered as vital by Air Liquide and the instrumentation related to the monitoring of the remaining parts of the detector (chamber structures, HV system, etc.) will be under the responsibility of the Collaboration. Work is on-going. A complete list of sensors has been elaborated. Air Liquide has decided to subcontract the implementation of the slow control (AEI, Grenoble).

The current list of physical parameters to be monitored and controlled is: Vacuum, Pressures (Ar/LN2), Temperatures, Flows (Ar/LN2), $LAr$ purity, levels (Ar, LN2), valves positions, pumps status and various mechanical positions (chambers, ...).

A remote access and control of the parameters will be highly desirable, since it is planned to eventually perform monitoring from outside the GranSasso tunnel and even possibly from remote locations. In view of the modulariry of the detector, the monitoring system should be itself modular, expandable and transportable.

### 6.8.2 Cryogenic instrumentation for the $10m^3$

The $10m^3$ has been equipped with various cryogenic instruments and serves as a good benchmark for the final setup to be installed on the T600. The following instrumentation has been installed on the $10m^3$ prototype:

- level meters (both capacitive and discrete)

- temperature and pressure sensors

- a precise position sensor to attempt to monitor the movements of the readout wires during cooling

- liquid argon purity monitors

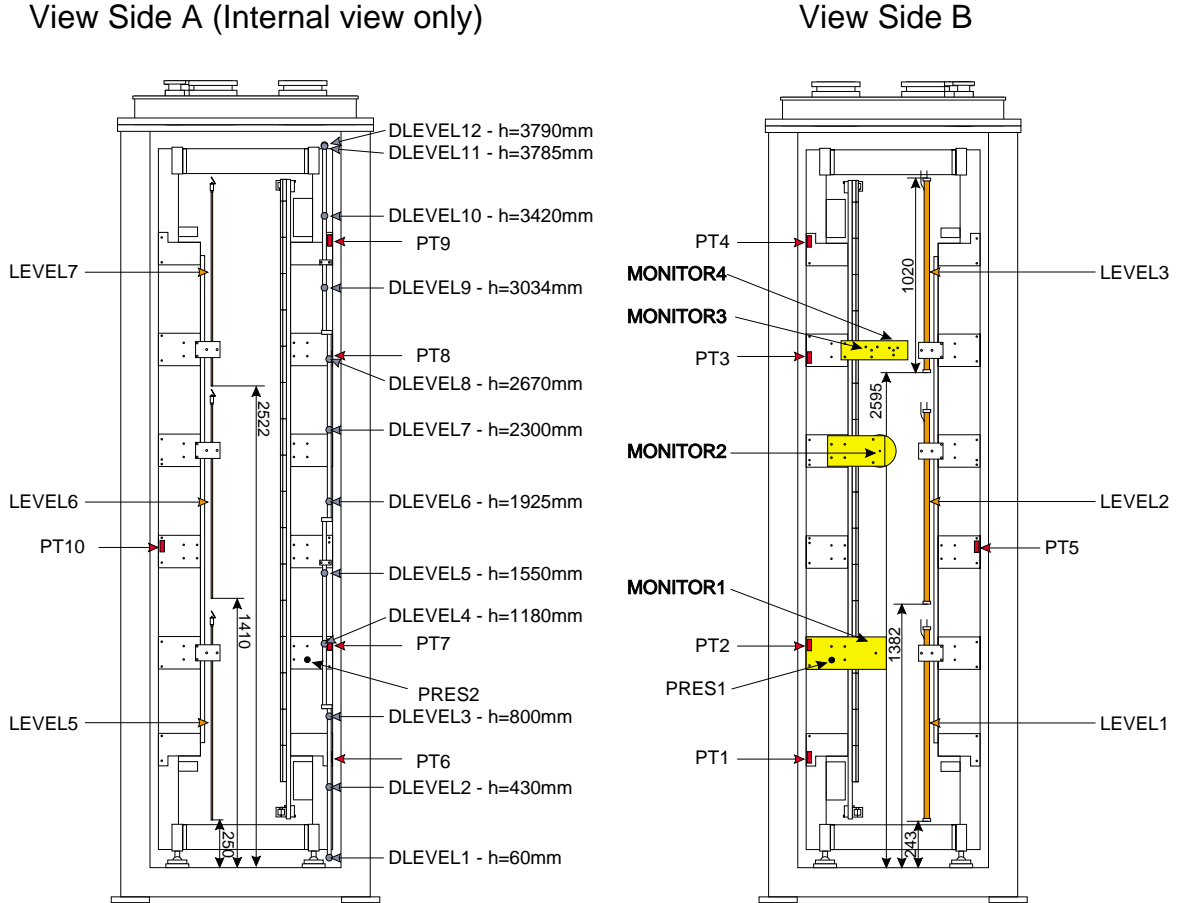A view of the location of the various sensors is shown in Figure 7.



Figure 7: Position of the various sensors installed on the $10m^3$.

### 6.8.3  $LAr$ **Level meters**

A total of seven $LAr$ level meters have been installed in the 10 $m^3$ prototype $LAr$ dewar. Four level meters were designed and built at ETH Zurich and three were purchased from Cryo Anlagenbau GmbH, Germany, as a fallback solution. The principle of the level meters is the measurement of the capacity change when $LAr$, with a dielectric constant of $\varepsilon_{LAr} = 1.54$, is filling the gap of a cylindrical capacitor. The four built level meters consist each of two concentric stainless steel tubes. The outer diameter of the inner tube is 25 mm and the radial gap to the outer tube is 0.5 mm. Three level meters have a length of 1 m

for a coarse determination of the $LAr$ level during the filling procedure and the fourth one is 10 cm long and mounted to precisely monitor the position of the $LAr$ level after the dewar was filled. The level meters were tested with $LN_2$; the measured capacitance and sensitivity (about 7.5 pF/cm) were consistent with the calculated values. The precision of the long level meters is a few centimeters and for the short one a few millimeters ; it is limited by the mechanical properties of the used tubes (straightness, variation of diameter). The three commercial level meters are 1 m long and their sensitivity (not the precision) is about a factor ten less compared to the self-made meters.

### 6.8.4   Position sensor

To measure the contraction of the wires in the wire chamber at the beginning of the cool down process, a position sensor has been built and installed. It is based on a measurement of the capacity change of a cylindrical capacitor when the inner part is moving axially relative to the outer cylinder. The total capacitor consists of ten identical cylindrical capacitors, each 10 mm long and separated by 15 mm from each other. The inner parts are mounted on a 3 m long Invar rod, the end of which is fixed to the spring mechanism compensating the contraction of the wires and mounted to the top part of the wire chamber frame. The outer part is fixed to the bottom part of the wire chamber frame. The sensor has a linear range of about 8 mm. The sensitivity slope in this region is 12.9 pF/mm of displacement.
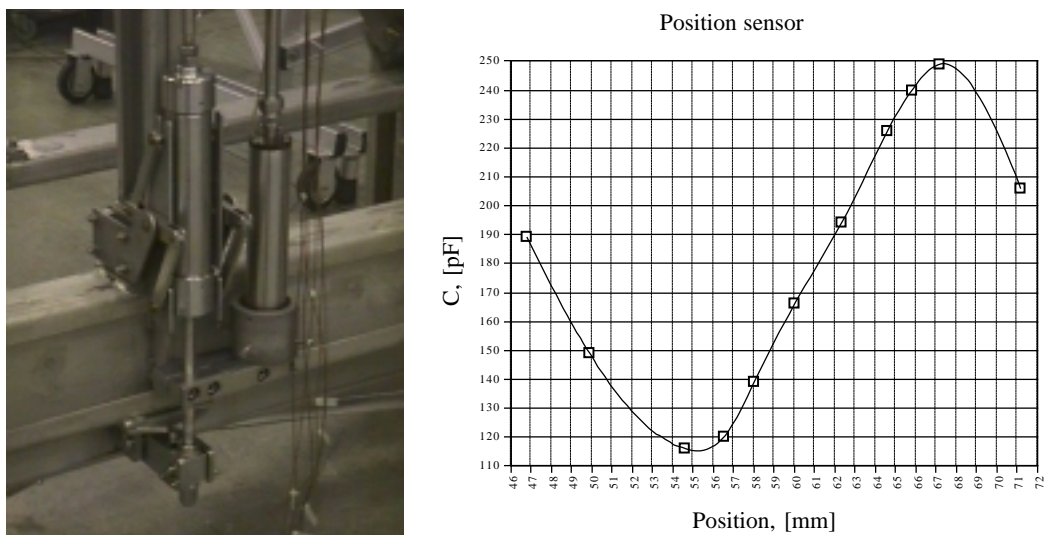


Figure 8: a) Position sensor installed on the $10m^3$; b) measured capacitance as a function of the position of the sensor.

### 6.8.5   4 channels FM-capacimeter

A 4-channel capacimeter was designed to measure the capacitance of the sensors used as indicators of the level of $LAr$. The three sensors Nr. 1,2,3 change their capacitances

101

from 1550 pF (empty) to 2130 pF (full), and the one (Nr 4) which has length of 10 cm, change from 150 pF to 220 pF. The sensors have been connected to the inputs of the capacimeter with RG178BU-Filotex cable, made of teflon. The cables contribute to the total capacitance which is then "zero"-ed out on the capacimeter. The sensors 1N, 2N and 3N (commercially purchased at Cryo Anlagenbau GmbH, Germany) have capacitance of 190 pF (empty) to 265 pF (full). A second capacimeter was built and adjusted accordingly.

The stability of the capacimeter was carefully studied. The following conclusions were drawn:

- all channels behave in a very similar way; differences are within 0.5 pF

- there is some clear correlation with ambient temperature

- the gain (1pF/digit on display) does not depend on the temperature significantly.

### 6.8.6   Charge capacimeter

The charge capacimeter was designed specifically for the position sensor where precision measurement is important. The range of the sensor spans from 110 pF to 250 pF. The principle of operation is as follows: a charge preamplifier is used to integrate the charge coming from the sensor. This charge will be proportional to the amplitude of a driving pulse and to the sensor capacitance. Internal and external cables which appear as parallel capacitances (total is 656 pF after installation) load the generator output but do not play a role (they only increase the effective noise). A driving pulse of amplitude of about 100 mV is generated internally by two monostables. The output signal of the preamplifier pass through a shaper to reduce noise. A semigaussian negative signal on the shaper output is still proportional to the sensor capacitance. It then passes a sample and hold stage. The output of this stage is a quasi-DC signal which is then measured.

The stability of the charge capacimeter was carefully studied. The following conclusions were drawn:

- the channels were adjusted and measured during 30 hours with open inputs. No change in the reading was observed.

- the channels were controlled with 100 pF during 70 hours. Instabilities inside 0.4 pF were observed (equivalent to a sensor displacement of 30 microns!).

### 6.8.7   Temperature monitors

An array of 32 Pt1000 resistors have been placed on the structure of the chamber. A 32 channel multiplexer has been built to interface this resistors to an ADC.

### 6.8.8   Software

The above mentioned sensors installed on the $10m^3$ prototype require a readout system. We developed this readout system based on an Intelligent Instrumentation EDAS-1002E interface box, which provides analog inputs/outputs and digital ports. The monitoring
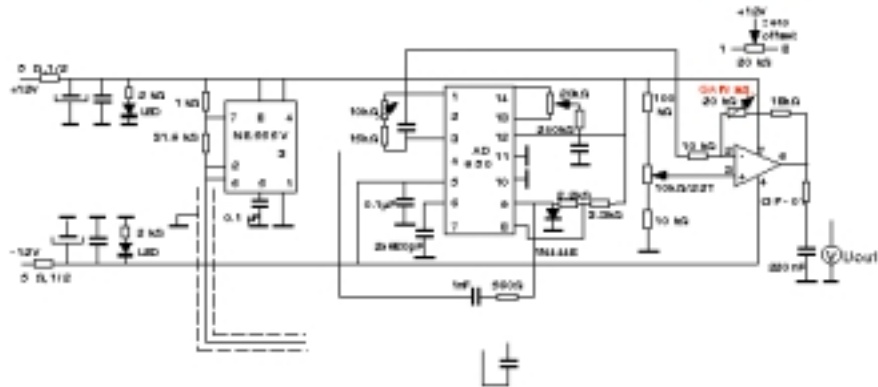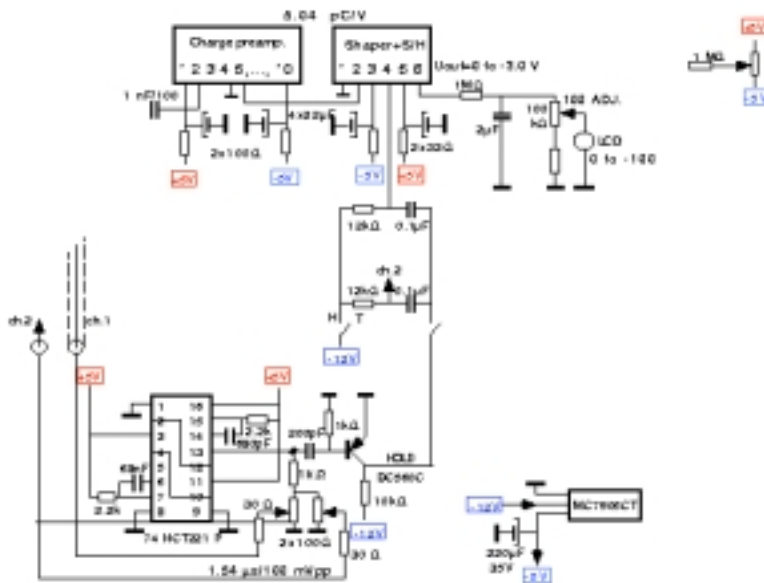
Figure 9: Schematics of the FM-capacimeter and charge-capacimeter.

itself is performed by a Linux-based PC. The monitoring and logging tasks use CORBA based communication. The monitoring facility is developed such that it can be used as a base for the monitoring and control system of the T600 detector.

# 7 $R\&D$ activities

## 7.1 $LAr$ Purity Monitor

A precise measurement of the electron lifetime in $LAr$ is one of the main issues of the working conditions monitoring system of the ICARUS 600-ton detector presently under consideration.

During the long term activity (5 years) of the ICARUS 3-ton detector at CERN the purity of the cryogenic liquid has been routinely checked with two different methods: (1) using dedicated monitor devices and (2) analysing the collected charge attenuation, as a function of distance from the wire chamber, from cosmic muons crossing the detector. These measurements provided an important "on-line" control of the stability of the whole cryogenic apparatus together with necessary information for the collected data handling.

In normal running conditions with the 600-ton module in Hall-C at the GranSasso Laboratory routine measurements of the electron lifetime ($\tau_e$) are as well necessary, possibly with increased accuracy, redundancy and safety margin in operating with dedicated monitor devices. Vertical crossing muon data sample will provide useful information, however due to the limited statistical abundancy in the underground environment, it seems risky to rely on this method alone, to collect prompt information on the purity level of the liquid filling the dewar. Moreover, it seems necessary also to monitor the purity of the GAr exiting the dewar from the recirculation pipes, *before* and *after* the purification systems. Therefore a number of dedicated monitor systems have to be located in different places, inside and outside the dewar. Inside the 600-ton dewar it could be also envisageable to displace several detectors in order to check possible effect of impurity stratification in such a large $LAr$ volume. These detectors must then be simple, accurate, reliable over long term of operation and cheap. A proposal for an improved solution of such devices has been put forward by the ICARUS Aq/LNGS group at the beginning of 1998 [14].

### 7.1.1 The Electron Lifetime Monitor

The monitor systems developed so far for the ICARUS prototypes [15,16] were double gridded chambers where electron clouds are photo-produced by short UV laser pulses impinging a golden cathode via a quartz optical fibre. The ratio of the amount of charge extracted and passing through the cathode grid to that arriving to the anode grid provides information on the electron loss due to attachment to electronegative impurities during the drift time. The electron lifetime, in principle, can thus be calculated on a single laser pulse base.

This technique is well established, however some drawbacks of this solution have been identified, in particular in view of its employ in the 600-ton detector:

- Employ of UV laser

The use of a UV laser ($\lambda = 266nm$), to guarantee metal photo-extraction (the metal quantum efficiency is low, $\sim 10^{-4}$, and the photo-electric threshold is high, $W_{Au} = 4.9eV$), is very expensive in case several (Nd-YAG) laser emitters have to be provided to feed the purity monitors. Moreover, the laser beam has to be focused on the optical fibre by continuously calibrated focusing systems. Thus, a routine measurement of the lifetime from all the monitors needs large, dedicated efforts and expertise. Finally, part of the UV light is reflected by the golden cathode possibly producing further extraction from other metallic parts of the monitor, which perturbs the lifetime measurement.

- Employ of Quartz optical fibre

  The use of Quartz optical fibre is necessary to transmit UV light from the laser generator and the inner monitor device. Quartz fibres are extremely delicate and easily degraded by the high power (intensity) of the laser beam, therefore requiring periodical replacement. Such replacement is not affordable during a steady state operation with the 600-ton detector.

The proposed solution to these inconvenients was:

- the replacement of the metallic photo-cathode with suitable *doped semi-conductors* with enhanced quantum efficiency ($\sim 1-10\%$) and reduced photo-electric threshold (in the $1-2eV$ region);

- the employ of visible light for the photo-extraction, allowed by the use of the selected semi-conductor cathode. Visible laser light can be obtained with cheap laser diodes, directly coupled with normal (plastic) optical fibres. Moreover with visible light pulses also the noise due to the reflected light is eliminated.

Since diodes are normally used at low temperatures in cryogenic liquids, a further improvement may consist in mounting the compact sized laser diode directly on the monitor chamber, in $LAr$, nearby the photo-cathode. This solution allows to eliminate the use of the optical fibres and related feedthroughs.

### 7.1.2  $R\&D$ phase

An $R\&D$ phase immediately appeared necessary to demonstrate the feasibility of the proposed solutions. Two main goals have been identified for this phase, namely the characterization of the electron emission properties of a number of different semi-conductor samples, in order to possibly select a good candidate to be installed in a purity monitor device, and the replacement of the Nd-Yag laser with a cheaper and easy-handling device as light source.

A major fraction of this programme has been completed successfully. The C.R.E.O.[1] company has provided a number of semi-conductor candidates, which have been extensively tested. At least two semi-conductor samples (namely CdZnTe-n type heavily doped, and InSb-p type doped) have been selected for their high quantum efficiency (approximately in the percent range) and reduced energy band gap ($E_{gap} = 0.23eV$ at 80 K in

---

[1]Centro Ricerche Elettro Ottiche-L'Aquila

Figure 10: The *LAr* purity monitor built at LNGS

the InSb case). All preliminary tests have been performed in vacuum showing an electron yield of about $\geq 100$pC/pulse, corresponding to more than $10^9 electrons/pulse$. In the same conditions the standard golden cathode has also been tested obtaining a reduced electron yield of about 1pC/pulse. As evident, the larger electron yield reached with the "non conventional" photo-cathodes strenghtens our proposed solution.

Owing to the enhanced electron emission, the search for a cheaper and easy-handling source of light was preliminary restricted to commercial, pulsed Xenon-lamps emitting UV light. A Hamamatsu Xe flash lamp, equipped with a custom system of lenses focalizing onto an optical quartz fibre, was extensively used during the tests in vacuum reported above. The whole system is very economical, stable and easy handling, in particular compared to more standard solutions with CsI photocathodes. Even though the visible laser diode still represents the optimum solution, the present Xenon-lamp seems at the moment an acceptable intermediate solution.

Further *R&D* studies are under way to improve the system, toward the final visible laser diode solution.

### 7.1.3   Assembling, test and installation of a new purity monitor

A complete purity monitor has been recently built at the GranSasso Mechanical Workshop (fig. 10).

This monitor, equipped with a CdZnTe-Cl doped photocathode, has been carefully tested in vacuum and then in pure liquid Argon. The tests confirmed the good performances in terms of electron emission and mechanichal stability of the crystal at *LAr* temperatures. After these tests the monitor has been installed in the 10m$^3$ cryostat in Pavia, on the wire chamber frame, togheter with other two standard (golden cathode) purity monitors (fig. 11). These monitors are expected to provide accurate and redundant measurements of the electron lifetime in the 10m$^3$ module starting from the first weeks of January, 1999.

Figure 11: Detail of the wire chambers frame of the 10m$^3$ cryostat showing the two purity monitors (above) installed by the LNGS-AQ group

### 7.1.4 A Liquid Argon Cryogenic Facility at LNGS

At the same time, the R&D on semiconductor photocathodes is going on, in order to establish the best setup of light source and photocathode type. In order to perform all the necessary tests in ultrapure Argon, a Liquid Argon Cryogenic Facility (LACF) is presently being assembled at Gran Sasso external laboratory. The LACF (fig. 12) is composed by a 70l stainless steel super-insulated dewar, an Al reservoir used as liquefactor, and an Oxisorb/Hydrosorb purifier. The top flange of the dewar is equipped with all the necessary flanges for the installation of the purity monitor, of the electrical and optical feedthroughs. The top flange and the liquefactor have been manufactured by a specialised company. The purifier cartridge has been manufactured by the LNGS mechanical workshop, and has been sent to Messer Griesheim, Germany, for filling with Oxisorb and Hydrosorb. The first operation of the LACF was expected in September 1998, but the huge delays of the suppliers have shifted this term to January 1999. Presently the LACF is routinely used for purity measurements.

## 7.2 High Voltage feed-through

After experimentation with different insulating techniques (Teflon, ceramic plus high vacuum, polyethylene) a high voltage feed-through, with a coaxial structure and polyethylene insulation, suitable for high voltage up to $150kV$ has been designed and built. A test cryostat has been assembled to allow long- term test in controlled and stable thermodynamic conditions. After a successful preliminary test at $150kV$ in $LN_2$, at present, the feed-through is under a long-term test in $LAr$ to verify the stability of the dielectric rigidity,
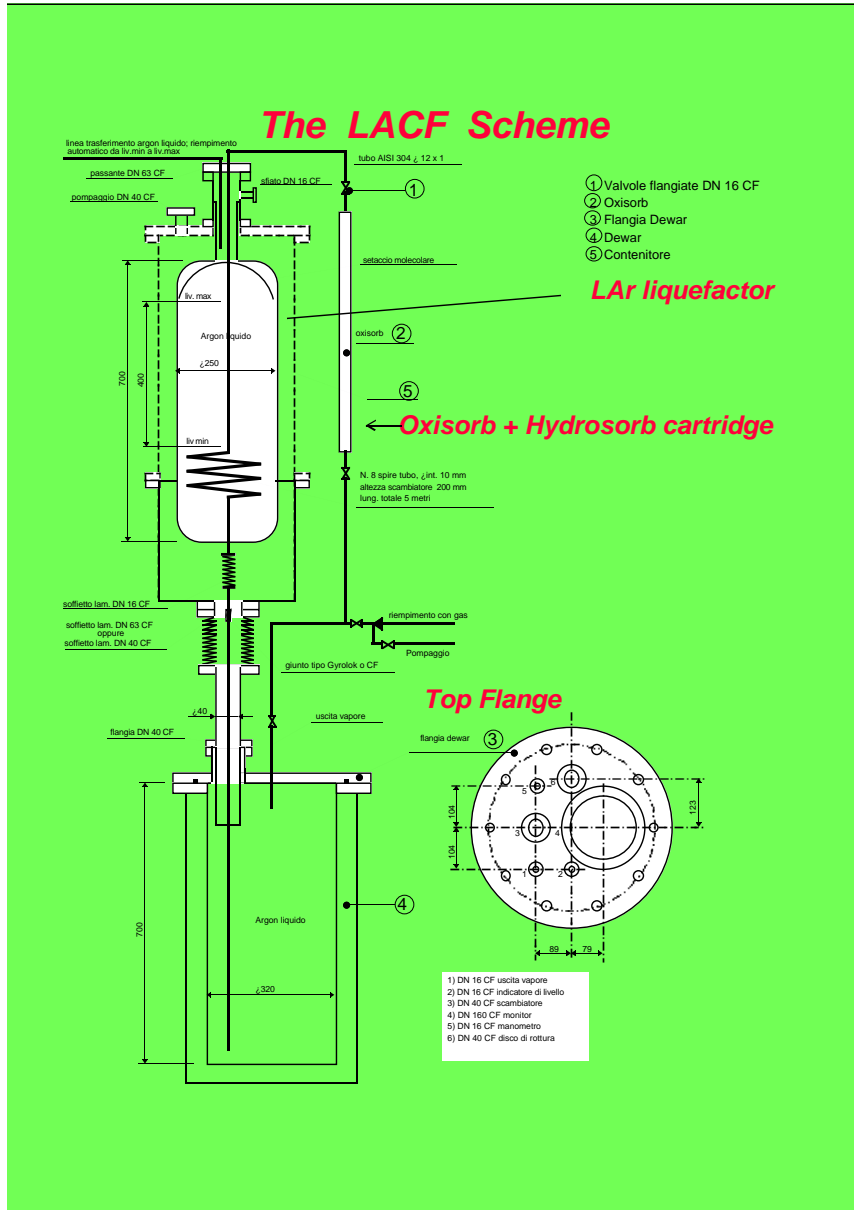
Figure 12: Design of the Liquid Argon Cryogenic Facility at LNGS

the tightness of the polyethylene-to-stainless steel seals and the absence of leakage currents.

A simpler $HV$ feed-through, suited for lower voltages, has also been developped. It is essentially a rigid coaxial structure, $80cm$ long, where the inner conductor ($HV$) is a thin copper tube and the outer one (ground) is a inox cylinder ($2.54cm$ in diameter). The insulator is epoxy-resin poured into the inox cylinder and slowly solidified under controlled conditions. The vacuum tightness is ensured by the length of the metal-to-epoxy interface. Cryogenic stresses are avoided because at least top half of the feed-through is meant to work at room temperature. We successfully tested it on the *50 litre LAr TPC* for $HV$ up to $70kV$. Longer and thicker versions of this design could stand higher voltages.

## 7.3   High voltage system

The high voltage system, including cathode, field electrodes and voltage divider has been designed to optimize the field uniformity across the drift volumes and to guarantee its long-+term operation. A resistive voltage divider based on 4 parallel-connected chains of $HV$ resistors insures acceptable field uniformity even in case of breakdown of one or two resistors in the chain. The design has been checked by electrostatic finite element analysis and the resistor insertion has been verified with a full-scale prototype. After the production of the full set of mechanical drawings ($BremeTecnica$) the production of all details has been commissioned and their delivery is expected for March 1999.

## 7.4   Layout of the read-out connections

The schematics of signal read-out, voltage biasing of the wire planes and injection of calibration signals has been conceived in order to avoid any delicate electronic components inside the cryostat. All the signal cables (2x34 conductor flat ribbon twisted pairs) connected to wires are biased (in both signal and shield conductors) at the high voltage requested for the wires. They connect the wires to the signal feed-through and then, outside the cryostat, to a set of $HV$ de-coupling boards at the input of the front-end electronics. The signal cables are grouped in modular sets, each with 18 cables (32 channels/cable). In each of the four chambers of the $ICARUS - 600T$ detector there are 18 equal cable sets for the wires at $+-30^o$ with respect to the vertical direction, and ending on the top/horizontal side of the frame (A). For the wires at $+-30^o$, ending on the vertical sides of the frame (B), there are 4 cable sets (two with 18 and two with 16 cables). For the horizontal wires (C) there are 4 cable sets (2 with 18 cables and 2 with 15 cables). Each cable set is connected to a low voltage feed-through flange. The flanges are arranged along four rows on the top platform of the detector, each row including 18 flanges, for the cable sets of A, and 4 flanges for the cable sets of B and C.

In correspondence of each flange there will be a mini-rack with the de-coupling boards and the front-end analog and digital electronics.

## 7.5 Signal feed-throughs

The low voltage feed-through flanges are built of a cylindrical thick body welded on $UHV$ flange (DN200CF). The cylindrical body is machined with 11 pass-through grooves, 9 of which host the printed circuit boards ($PCB$s) for signals and the remaining 2 for the $PCB$s for calibration. The interstice between the flange body and the $PCB$s is filled, for tightness, with a high thermal conductivity, low shrinkage resin (Stycast 2850-FT). Each flange hosts 18x68=1224 contacts in the signal $PCB$s and 8 coaxial ways in the calibration $PCB$s. The total number of signal feed-through flanges needed for $ICARUS - 600T$ is 88.

## 7.6 Wire-to-cable connections

Depending on the orientation and position of the chamber wires, four different types of $PCB$s have been designed (and their production is underway) for the wire-to-cable connections:

   - UP-3.46, (n. 1296, wire pin pitch = 3.46 mm) for the connection of wires at $\pm60°$ on the top side of the chamber frame;

   - DOWN-3.46, (n. 1296, wire pin pitch = 3.46 mm) for the connection of wires at $\pm60°$ on the bottom side of the chamber frame;

   - SIDE-6, (n. 136, wire pin pitch = 6 mm) for the connection of wires at $\pm60°$ on the vertical sides of the chamber frame;

   - SIDE-3, (n. 264, wire pin pitch = 3 mm) for the connection of wires at $0°$ on the vertical sides of the chamber frame.

## 7.7 Scintillation light

We are studying a new concept of photocathode able to work at $LAr$ temperature with high collection efficiency for the Argon scintillating light.

   It consists of a large area $GEM - like$ detector (a metallized thin insulator foil thoroughly punched accordingly to a regular patter) where a thick layer ($500nm$) of Cesium Iodate ($CsI$) is deposited on one face. This detector is meant to work in gas phase with the $CsI$ deposited side facing the $LAr$ volume.

   The $CsI$ acts as a photocathode with high quantum efficiency ($\approx20\%$), at $LAr$ temperature, for the $128nm$ scintillating light of argon. A proper voltage applied across the GEM attracts the photo-electrons into the $GEM$ holes where they are multiplied (factors 100 to 1000 are easily obtained with few hundreds volts applied) and collected on the non-deposited side of the $GEM$.

   If these fast signals result to be large enough, they would be available for $T = 0$ and trigger purposes.

## 7.8 Electrons field emission in liquid argon

A test has been performed to verify the electron field emission in $LAr$. Field ionization in noble liquids, known and extensively studied since more than 30 years ago, is used for high-current injection, for estimation of electron mobility, for understanding of electrical

breakdown in liquids. The test was made with a stainless steel tip, 1 micrometer radius facing, at 3 mm distance, a large radius (r = 16 mm) spherical electrode. The conduction current was measured in function of the $HV$ (from $-5.9kV$ to $5.9kV$) applied to the tip with the sphere at ground. The results show a negligible increasing current from $-5.9kV$ to $5.2kV$ followed by a sharp rise from $5.3kV$ to$5.9kV$. At $5.9kV$ the surface electric field is approximately $E = 5.9 \cdot 10^7 V/cm$ and the corresponding current density is $1.6 \cdot 10^2 A/cm^2$. This behavior is well in agreement with the Fowler-Nordheim equation on the field emission.

This phenomenon could be exploited to purify argon in liquid phase at an extremely high level. In fact electrons copiously produced by field emission could be forced to drift in liquid argon where they are eventually captured by the residual electronegative impurities. This method should by highly efficient because it acts only on the impurities that affect the electron lifetime in $LAr$. Lifetimes longer that tens of milliseconds could in principle be at reach.

## 7.9    Argon purification

The standard purification/recirculation scheme adopted up to now in the tests of the ICARUS prototypes has the drawback that the initial electron lifetime after filling with purified $LAr$ is never above few hundreds microseconds. This is due to the impurities produced by the degassing of the detector materials that diffuse in $LAr$ during filling when the materials are still in gas phase and at high temperature. Several cycles of recirculations are then needed to reach a purity corresponding to a lifetime of several millisecond (necessary to run the detector without excessive charge losses). This process could require some weeks depending on the recirculation speed.

In order to shorten this time interval, we developed a simple method to obtain electron lifetime of the order of few milliseconds immediately after filling.

The idea consists in connecting a small empty container in series with the detector vessel. Both containers are roughly evacuated (about 0.1 mbar just by means a rotative pump) and then cooled down at $LAr$ temperature (the small container could be directly immersed in a $LAr$ bath).

When we start filling, $LAr$ mixed with Argon gas flows through the purifier into the detector vessel; the Argon gas, together with most of the impurities due to degassing, is then sucked into the second vessel where it is condensed.

As the detector temperature decreases, less and less Argon gas (and degassing impurities) is produced and condensed into the second container until the latter is no more needed.

We tested this method with the 50 liter $LAr\ TPC$ in December 1998. The electron lifetime reached soon after filling was better than 2 ms and no decrease was observed during the following 10 days (with recirculation system active).

We believe that this method could be easily implemented in the future ICARUS detectors ($10 m^3$ and 600 ton).

## 7.10 Three wire plane chamber

A 200-liter (100 liter sensitive volume) $LAr$ detector has been designed. The detector, with a $LAr\ TPC$ structure, has a cylindrical drift volume, 28.8 cm in diameter and 154 cm long, with a 3 wire plane chamber at one end and a $HV$ cathode at the other end. The drift volume is contoured by a stack of rings biased at voltages linearly degrading from the cathode voltage to ground. The chamber is built with a stack of three equal circular frames ($PCB$s) on which 96 wires are soldered at a 3-mm pitch. Each frame is rotated with respect to the other ones by 120°. The total number of channels results 288. The layout of the chamber $PCB$ is such to allow the use of the same read-out schematics and the same kind of cables and signal feed- throughs developed for $ICARUS - 600T$. One mini-rack of front-end electronics, $ICARUS - 600T - like$, is needed for the read-out. The detector is inserted in an existing cryostat, with vacuum insulation and $LN_2$ cooling.

## 7.11 A back-up design for the read-out electrodes

We studied, built and tested a new read-out chamber where the electrode structure is not based on wires but on a multi-layer printed circuit board.

The aim of this test was to provide a back-up solution for the read-out system with performance similar to that with the wires. The design is based on the consideration that the wire structure could be immersed into a solid dielectric (the PC board support), with clear advantage for the mechanics of the project, if we provide the path for the drifting electrodes through it.

This idea can be easily implemented with the technique of the multi-layers $PCB$ where the wires are replaced by strips drawn on various layers; the electron trajectories through the $PCB$ are ensured by grooves and holes drilled in the $PCB$ support exactly where the electrons are expected to drift across.

We built a three layer $PCB$ to be mounted in the 50 liter $LAr\ TPC$.

- On the first layer (the one facing the drift volume) the focusing grid is drawn with a pitch of 2.54 mm, acting also as first induction plane; grooves, 1 mm wide, are excavated parallel to the grid direction as deep as the spacing between first and the second $PCB$ layers (2 mm). Electron trajectories are forced into the grooves by the electric potential applied to the grid strips.

- At the bottom of each groove, at the level of the intermediate $PCB$ layer, pads are drawn spaced 2.54 mm. They are connected by strips, in rows running along a direction orthogonal to that on the first layer. They form the second induction plane. Holes are drilled, as deep as the spacing between second and the third $PCB$ layers (2 mm), in the middle of each pad where electron trajectories are forced to funnel into. Field shaping strips are also foreseen between induction strips to enhance the funneling effect.

- The last layer acts as collection plane. It has a design similar to that of the second layer. The pads, located exactly beneath those on the previous layer, are connected along a different direction to provide the third 2D imaging projection. The holes, drilled from the second layer, allow the electrons to reach these pads where they are collected.

The prototype for the 50 liter $LAr\ TPC$ has a surface of $32x32cm^2$ and 128 channels per read-out plane. Is has been coupled with the electronic chain used for the test of the
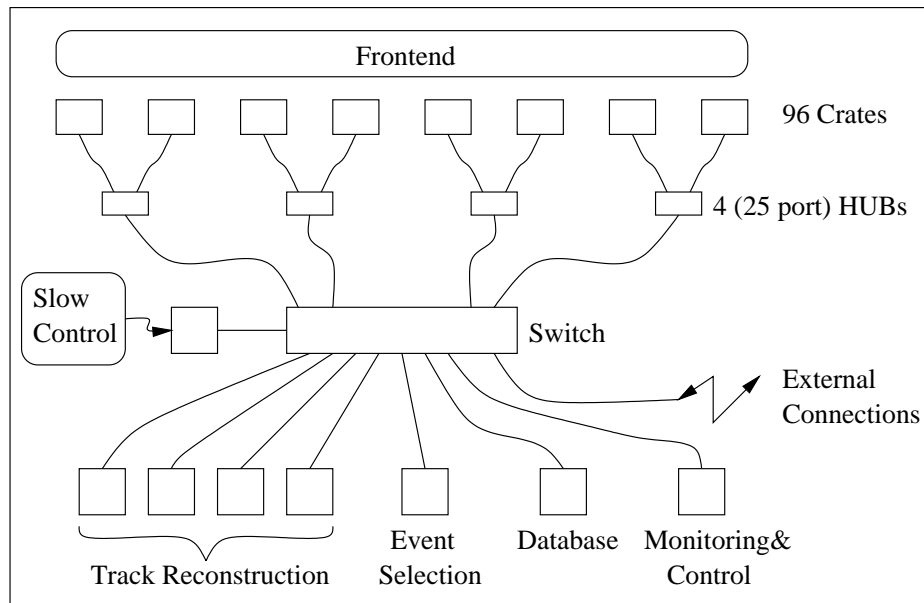
Figure 13: Possible hardware architecture for the daq.

50 liter $TPC$ exposed in 1997 at the CERN neutrino beam (with the front-end amplifiers immersed in $LAr$). It is presently under test with cosmic rays.

First preliminary results indicate that the signal shapes on each plane do not differ from those of the wire structure. The electronic noise is also comparable (this comparison need deeper investigation because the electrode length of 32 cm implies a low input capacitance in both cases hence small differences in noise).

# 8 Data aquisition studies

The ETHZ group is in the process of evaluating the requirements for the ICARUS data acquisition system and propose an architecture for the system. The proposal is characterised by two main ideas:

- it should be possible to base the online filtering solely on hit and track information. For offline purposes all data are required.

- the architecture should have a continuous data flow to reflect the nature of the raw data itself which arrives continously.

This foresees an implementation of the system architecture in a tree-like structure. Only the hits of a sub-volume of the full detector are transported to processors for track reconstruction while the raw data are buffered on the crates. ¿From the processors performing the track reconstruction only the reconstructed tracks are then transported to a single processor which performs the filtering. For positively identified events all detector data of that drifttime is stored in the output database.

We have identified several advantages of this system:

- The amount of data that need to be transported is minimized, thus allowing for cheap networking hardware to be used.

- The continous data flow will be required by some rejection algorithms running the online filter (low energy events)

We are studying this proposal and in particular the question of processing power that is required for data processing.

We also architect the software for the data acquisition system in order to break it down into components and identify parts which can be purchased or have to be developed internal to the Collaboration.

## 8.1 Reconstruction software

In 1998 a reconstruction code for the detector has started to take shape, having as a first goal the comparison of the data taken with the 50 liters chamber with the Monte Carlo simulation. The program is based on the ROOT environment, recently developed at CERN, and can also be used as a scan program, giving the possibility of displaying recostructed objects together with the raw data.

Hits (charge clusters) are reconstructed in both collection and induction planes, having as coordinates the wire number (for the x or y axis) and the drift time (for the z axis). When one value of the drift time is assigned only to a hit on the collection plane and to another on the induction plane, it is assumed that the two are projections of the same 3-dimentional hit, with x and y coordinates defined by the wire numbers, and z coordinate defined by the common drift time.

In some cases, the 3D information for the single hits cannot be extracted due to ambiguities. In order to perform a three-dimensional reconstruction, tracks are made in two dimensions, using the collection and induction projections, and then 3D tracks are built using pairs of 2D ones. Hits belonging to the projected tracks are then reassigned to those 3D tracks, allowing the determination of the third dimension also for the ambiguous ones.

A particle identification of the reconstructed tracks, based on the dE/dx information, has been included, and vertices in two or three dimensions are found at the track intersections.

Current work includes the search for optimized algorithms for hit and track finding, as well as the study of calorimetry reconstruction, with the separation of the electromagnetic and hadronic components of the showers in mind (software compensation).

# 9 Software activity

## 9.1 Simulation of Nuclear Effects in neutrino interactions

The final state kinematics in a neutrino-nucleus interaction is in principle different from the free neutrino-nucleon one. The extent of this difference has never been investigated in details, although it can heavily affect the results of neutrino experiments.
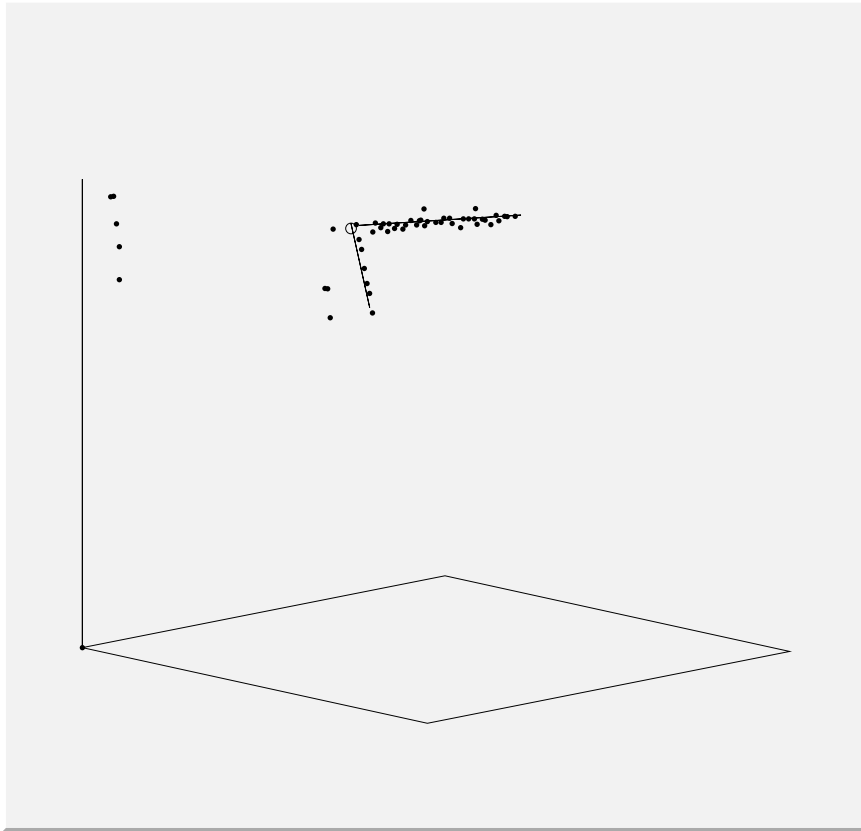
Figure 14: Preliminary reconstruction of a quasi-elastic neutrino interaction. The dots show the reconstructed clusters. Two fitted tracks and a vertex are also displayed. The scanning program display is three dimensional and the view can be easily rotated on the screen.

Nuclear effects include initial state effects, essentially related to nucleon Fermi motion, and final state effects, due to reinteractions of the scattered hadrons in the nucleus, to deflections in the nuclear and Coulomb fields, and to reaction Q-values.

All these factors have been taken into account in the calculations using the nuclear interaction model already developed for the FLUKA code [17]

Comparisons of the free and the bound final states have been performed for quasielastic interactions and interactions with $\Delta^+$ and $\Delta^{++}$ resonance production [18].

### 9.1.1 Effects on final states kinematics

The kinematics of the final states of the free nucleons and bound nucleons QE neutrino interactions have been compared. The free nucleon interactions of the three neutrino species give a lepton and a proton ($< p_p > \sim 800$ MeV) in the final state, while the bound nucleons interactions have in the final state a lepton, one (or more) residual nucleus ($< p_{res\ nucleus} > \sim 250$ MeV) and some protons, neutrons, $\gamma$-rays (1.46, 1.3 and 2.36 in average respectively) and few charged and neutral pions.

The kinematics of the final states of the free nucleons and bound nucleons $\Delta^+$ and $\Delta^{++}$ production neutrino interactions have also been compared. The free nucleon interactions of the three neutrino species with $\Delta$ resonances production give a lepton, a charged or neutral pion ($< p_\pi > \sim 400$-600 MeV) and a nucleon (proton or a neutron) ($< p_{nucleon} > \sim 800$-1000 MeV) in the final state, while the bound nucleons interactions have in the final state a lepton, one (or more) residual nucleus ($< p_{res\ nucleus} > \sim 300$ MeV) and charged and neutral pions and some protons, neutrons, $\gamma$-rays.

### 9.1.2 Effects on acceptances and missing momentum

Defining a "QE $\nu$ event in Icarus" as an event satisfying the following criteria: presence of a lepton and one proton with $T_p > 150$ MeV (with no pions with $T_\pi > 15$ MeV), the acceptance of these criteria applied to free and bound nucleon interactions for the three neutrino species are very similar and goes from $\sim 60\%$ for free nucleon interactions to $\sim 42\%$ for bound nucleon interactions.

The most important nuclear effect is an apparent missing momentum in the interaction, due to the unseen energy, taken away by the residual nucleus, by neutrons and by undetected low energy particles ($\gamma$, p, $\pi$). For that reason , while in the free nucleon $\nu_e$ and $\nu_\mu$ interactions the missing momentum is zero, in the bound nucleon interactions the missing momentum is different from zero.

If a criterium to recognize $\nu_\tau$ events (where a real missing momentum ($< p_{miss} > \sim 700$ MeV) is present also in free nucleon interactions) from $\nu_e$ interactions were to have a missing momentum $> 400$ MeV, the acceptance would be $\sim 4.\%$ for $\nu_e$ and $\nu_\mu$ and $\sim 33\%$ for $\nu_\tau$. So there will be a contamination of $\nu_e$ events in the selected $\nu_\tau$ events sample: this contamination can be reduced applying other cuts for example on lepton momentum and direction.

Defining a "$\Delta^{++} \rightarrow p\pi^+\nu$ event in Icarus", a" $\Delta^+ \rightarrow p\pi^0$ event in Icarus" and a "$\Delta^+ \rightarrow n\pi^+$ event in Icarus" as an event satisfying respectively the following criteria: presence of a lepton and one charged pion with $T_\pi > 15$ MeV and a proton with $T_p > 60$ MeV, a lepton and one neutral pion with $T_\pi > 15$ MeV and a proton with $T_p > 60$ MeV and

a lepton and one charged pion with $T_\pi > 15$ MeV and no protons with $T_p > 60$ MeV, we find that the acceptance of these criteria applied to free and bound nucleons interactions for the three neutrino species are very similar. The acceptance is $\sim 95\%$, $\sim 95\%$ and $\sim 100\%$ respectively for the three resonances produced in free nucleon interactions, due to the request on the proton energy; the acceptance is lower for bound nucleons interactions, where a $\nu$ event with $\Delta$ production can be classified as a QE event (according to the criteria described in previous section: a lepton and one proton with $T_p > 150$ MeV) or as an event with more than one fast proton ($T_p > 150$ MeV) or as an event with a pion with a different charge or with more than 1 pion or as an event with only very slow protons ($T_p < 60 MeV$) accompanied by neutrons and $\gamma$-rays.

In particular a not negligible percentage (10-20%) of $\Delta^+$ and $\Delta^{++}$ events are classified as QE events.

The most important nuclear effect is again an apparent missing momentum in the $\nu_e$ and $\nu_\mu$ interactions where there is no real missing momentum ($\Delta^{++} \to p\pi^+$and $\Delta^+ \to p\pi^0$), due to the unseen energy, taken away by the residual nucleus, by neutrons and by undetected low energy particles ($\gamma$, p, $\pi$). In the $\Delta^+ \to n\pi^+$events there is a real missing momentum due to the neutrons, that are detected with difficulty.

If a criterium to recognize a $\Delta^{++} \to p\pi^+$or a $\Delta^+ \to p\pi^0 \nu_\tau$ events from the equivalent $\nu_e$ interactions would be to have a missing momentum $> 400$ MeV, the acceptance would be 11(5)% for $\nu_e$ $\Delta^{++} \to p\pi^+$and 46(35)% for $\nu_\tau$ $\Delta^{++} \to p\pi^+$and 10(4)% for $\nu_e$ $\Delta^+ \to p\pi^0$and 53(43)% for $\nu_\tau$ $\Delta^+ \to p\pi^0$, simply asking for 1 charged or neutral pion (or also asking for a proton with $T_p > 60$ MeV); but with other cuts the contamination can be reduced.

## 9.2 Simulation of Deep Inelastic Scattering interaction with nuclear effects

During 1998 the FLUKA nuclear interaction model has been successfully coupled with the NOMAD version of the LEPTO deep inelastic scattering event generator. The combined model has been used for computing the background for the recent Super-Icarus proposal submitted to the joint SPSC-LNGS committee meeting [19]. The predictions of this model are currently being benchmarked against available NOMAD results. The outcome if these tests, if positive, will represent an important milestone in the assessment of the ultimate Icarus performances for $\tau$ appearance with a possible beam from CERN.

## 9.3 Calculations of Atmospheric Neutrino Fluxes

A new calculation of atmospheric neutrino fluxes has been performed using the FLUKA Montecarlo code, that contains a particularly accurate interaction model.

In a first phase the $\mu$-fluxes predicted by FLUKA have been compared with the measured $\mu$-fluxes, showing a good agreement.

The $\nu$-fluxes predicted by FLUKA are typically 10-15 % lower than those computed by the Bartol group for the same input primary cosmic ray spectra.

The $\nu$-fluxes in the present calculation using FLUKA are calculated using a 3-D approach instead of the 1-D approach used in the other calculations. Fig. 15 shows the difference between the 3-D and the 1-D calculation, with respect to the angular

distribution of neutrino in the energy range where most of the interactions occurs; there are striking differences, whose impact on a given analysis is strongly dependent on the detector ability in determining the actual neutrino direction.

## 9.4   Preliminary Study of Atmospheric Neutrino Events

Using $\nu_\mu$, $\bar{\nu}_\mu$, $\nu_e$ and $\bar{\nu}_e$ fluxes calculated by FLUKA, an atmospheric neutrino event study has been started. Supposing to work with an *ideal resolution* detector, the number of quasielastic (QE), resonance (RS) and deep inelastic (DIS) CC and NC events has been computed, corresponding to 1 year of exposure of 1 kton $LAr$ detector. The results are shown in Table 1.

|         | $\nu_\mu$ | $\bar{\nu}_\mu$ | $\nu_e$ | $\bar{\nu}_e$ |
|---------|-----------|-----------------|---------|---------------|
| **CC QE**  | 83   | 14.7 | 53   | 6.6  |
| **CC RS**  | 17   | 5.7  | 9.2  | 2.3  |
| **CC DIS** | 15   | 7.0  | 5.8  | 2.4  |
| **NC QE**  | 37   | 19.9 | 19.4 | 7.9  |
| **NC RS**  | 6.3  | 2.8  | 3.1  | 1.1  |
| **NC DIS** | 5.0  | 3.0  | 1.8  | 0.95 |

Table 2: Number of CC and NC events expected in 1kton $LAr$ detector during 1 year of exposure computed using FLUKA.

The FLUKA code was used to simulate the QE interactions of neutrinos with Ar nuclei. Since the atmospheric neutrino flux matrices, folded with the respective cross sections[2] are used, the simulated QE events have the correct direction and energy distribution of the atmospheric neutrino events with fixed $\Delta m^2$ as oscillation frequency.

Using tabulated values for ranges in $LAr$ at different energies, an evaluation of the number of contained particles outcoming from CC neutrino events in the 600ton detector is possible. A detailed study of the events topologies taking into account the nuclear effects is also possible. Preliminary results have already been obtained for QE charged currents $\nu_\mu$ and $\bar{\nu}_\mu$ interactions.

The analysis, complete with nuclear effects, of resonance and deep inelastic events in Ar is in progress.

The work will continue with the simulation of $\nu_e$ and $\bar{\nu}_e$ interactions, where a complete simulation of the EM showers in the detector will be done using FLUKA.

## 9.5   LBL CERN-Gran Sasso neutrino beam

### 9.5.1   NGS beam design improvements

During the second half of 1998 the design of the neutrino beam from Gran Sasso to CERN has been optimized and significantly improved, with a significant contribution of members of the Collaboration.

---

[2]The flux matrices *do not yet include* the geomagnetic field cut-off over primary cosmic rays.
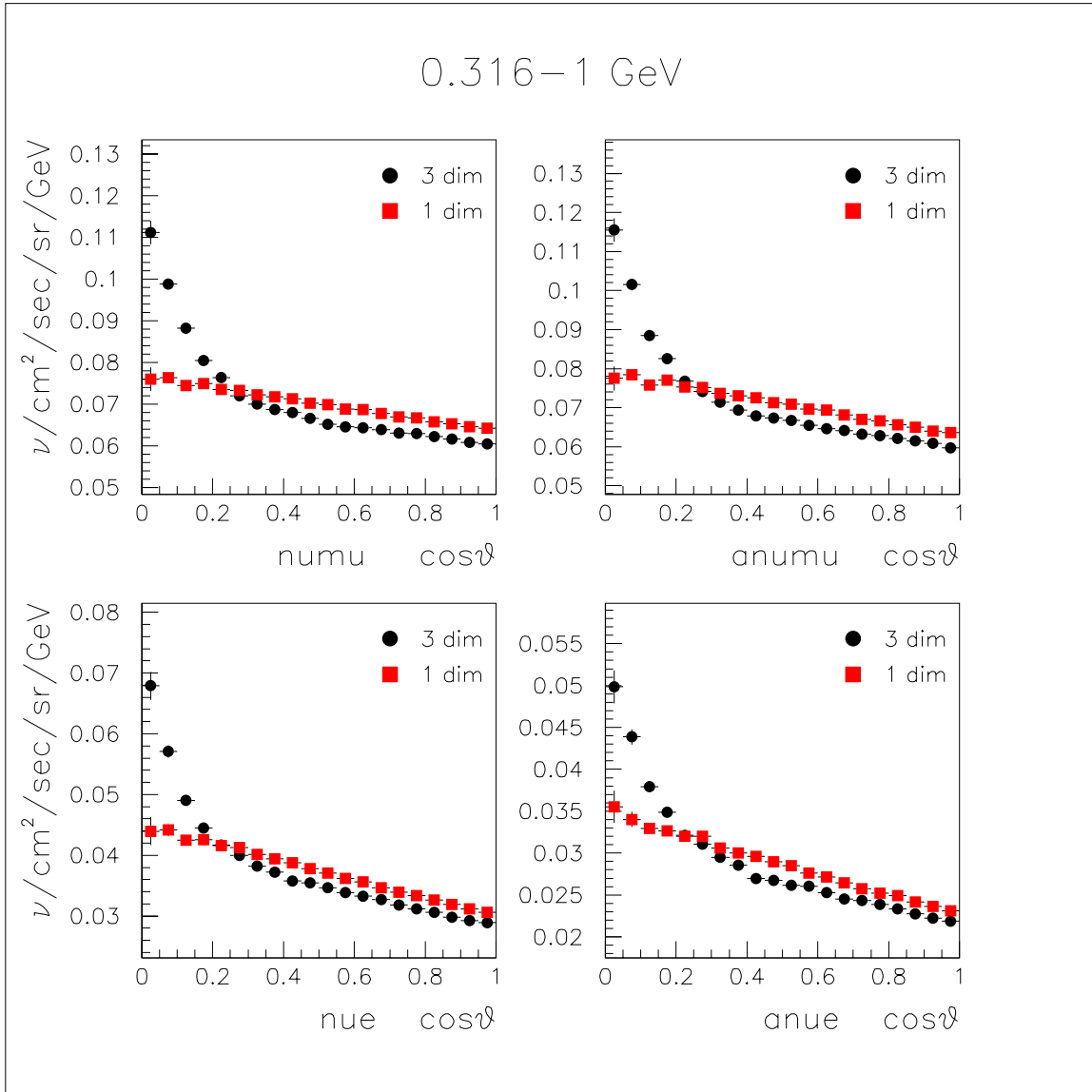
Figure 15: Comparison between the $\nu$ fluxes obtained using the 1-D and the 3-D calculations
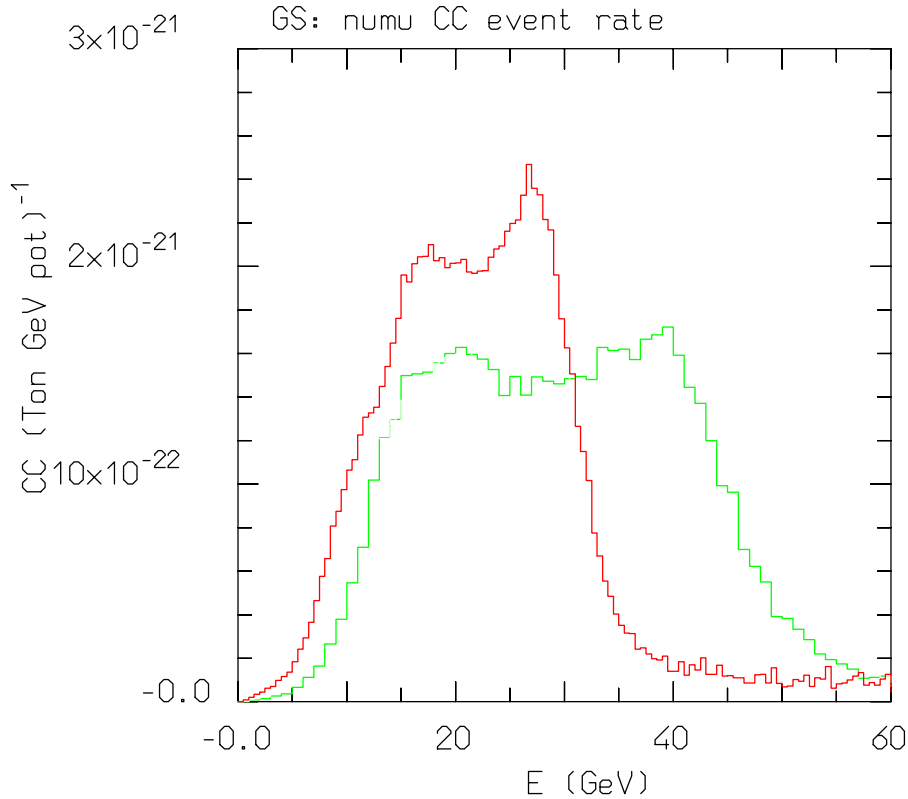
119

Figure 16: Calculated spectra of muon neutrino charged current interactions at Gran Sasso. The old baseline NGS spectrum and the improved one are shown

The amount of material in the beam line has been reduced, according to technical improvements in the design, and the optics has been changed to focus the energy range that matches at best the convolution of the oscillation probability (low-energy peaked), the $\nu_\mu$ spectrum (rapidly dropping at low energies) and the $\nu_\tau$ CC cross section.

The angular acceptance of the optics has also been improved, by placing the horn very close to the target. A low energy beam option, for disappearance studies, has also been investigated. Results are shown in figs. 16 and 17.

This optimization resulted in an increase of the expected number of $\nu_\tau$ charged current interactions from 1.7 to 2.9 events per kiloton per $10^{19}pot$. The new spectrum is peaked at lower energies with the additional benefit that the bulk of $\nu_\tau$ CC interactions is now below 30 GeV, in a range which is optimal for detector efficiency. The expected $\nu_e$ contamination of the beam is 0.8 %.

Furthermore, the beam parameters have been reconsidered, and the design intensity is now assumed to be $4 \cdot 10^{19}$ protons per year in shared mode.
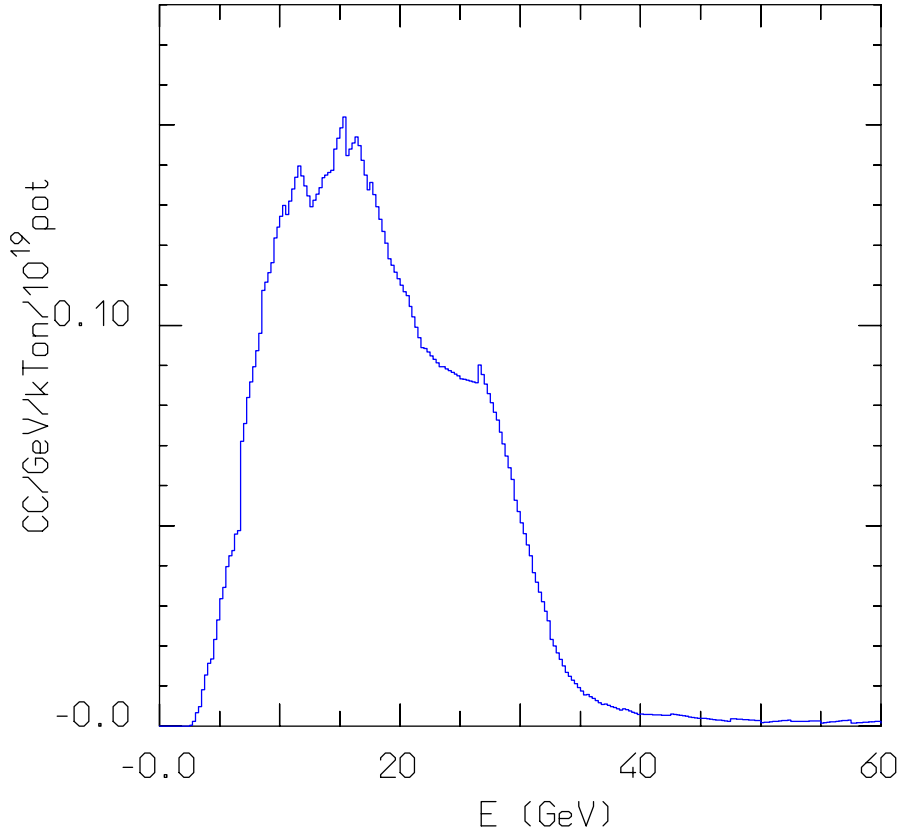
Figure 17: Computed spectrum of $\nu_\tau$ CC interactions at Gran Sasso, for $\Delta m^2 = 2.5 10^{-3} eV^2$

### 9.5.2 Tau apperance studies

The long baseline $\nu_\tau$ appearance experiment using as a neutrino source the high energy configuration of the Neutrino to Gran Sasso (NGS) beam appears as the most appealing possibility, to confirm the SuperKamiokande atmospheric result, in an environment where better controlled background and signal conditions exist and where tau neutrinos can be positively identified.

The expected sensitivities in ICARUS for various fiducial masses are continuously being updated and refined and to reflect the latest changes in the beam design. Work included improvements in the event generation (in particular at low $Q^2$ and updated simulation of the detector response). Comparisons with the results obtained within the NOMAD experiment are being pursued.

In order to fully cover the parameter space suggested by the on-going atmospheric neutrino experiments, large fiducial masses coupled to good $\nu_\tau$ detection efficiencies are needed. By means of kinematical criteria, a Liquid Argon ($LAr$) detector provides high
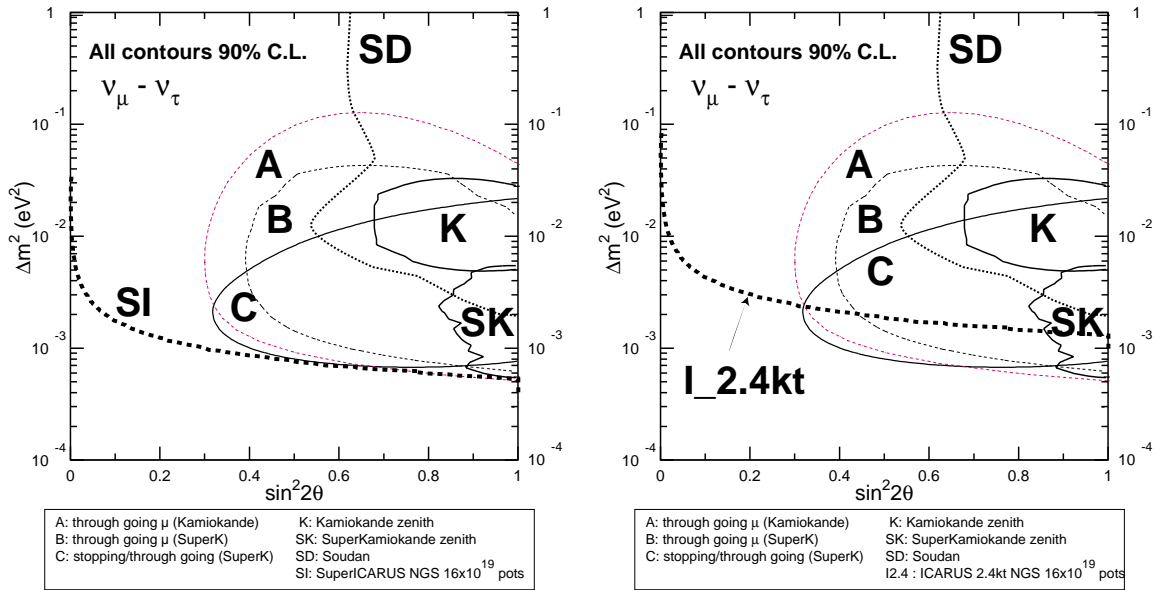
121

Figure 18: 90% C. L. exclusion region in case we see no evidence for oscillations with the SuperI detector and 2.4 kton ICARUS. Favoured regions obtained by other atmospheric neutrino experiments are also shown.

background rejection for high $\nu_\tau$ detection efficiencies. The large mass required (of the order of 30 Kton) can be realised in a single $LAr$ module by scaling up the parameters of the alreday approved 600 tonnes ICARUS detector. We call this scaled-up detector SuperI.

The $\nu_\tau$ appearance is searched for through the electronic and hadronic decays of the $\tau$ lepton produced via the Charged Current (CC) interaction of the $\nu_\tau$ with a nucleon. The event total momentum is reconstructed using the $LAr$ as an homogeneuous calorimeter. The resolution of this measurement is excellent thus allowing the use of kinematical criteria as the basis of the oscillation search.

The main background to the $\tau \to e$ channel comes from $\nu_e$ CC. The oscillated neutrinos show a softer energy spectrum and larger missing momentum due to the presence of two neutrinos among the tau decay products. Remaining backgrounds are rejected requiring the electron candidate to be isolated from the rest of the event (the angle between the momentum of the electron and the event total momentum should be large).

The appearance search is also carried out using the hadronic decays of the $\tau$: $\pi$, $\rho$, $3\pi$. Here the main background corresponds to neutrino Neutral Current (NC) events. Requiring the tau candidate to be well isolated from the hadronic jet (large $P_T$ of the tau candidate with respect to the total reconstructed momentum), the NC background is largely reduced. Another source of background comes from $\nu_\mu$ CC events where the prompt muon is not the most isolated track and therefore not considered as the tau candidate. Given the large dimensions of the SuperI detector and the nuclear interaction length (84cm), we consider every track leaving the active target without interacting as a muon and therefore the event is rejected. This muon veto renders the $\nu_\mu$ CC contamination

neglible while reducing the final $\tau$ efficiency by less than 10%.

Figure 18 shows the 90% C. L. exclusion region in case no evidence for oscillation is observed, together with the favoured parameter space obtained by other atmospheric neutrino experiments, assuming an exposure of $16 \times 10^{19}$ p.o.t.

We also performed a $\tau$ search using the final mass configuration (2.4 Kton) of the ICARUS detector. The analyses are similar to those described for the SuperI detector.

# 10   List of Publications

1. F.Arneodo et al., "Performance evaluation of a hit finding algorithm for the ICARUS detector", Nucl. Instr. and Methods A412, 440 (1998).

2. P. Cennini, S. Centro, D. Favaretto, S. Motto, A. Puccini, C. Tintori, "Low-noise BICMOS front-end and fast analogue multiplexer for ionisation chamber", Nucl. Instr. and Methods A409 (1998), 300.

3. C. Carpanese, S. Centro, M. Lippi, D. Pascoli, F. Pietropaolo, G.Pratali, S. Ventura, "ARIANNA: the Icarus experiment readout module", IEEE Trans. Nucl. Sc., 45, n.4 (1998) 1804.

4. C. Carpanese, S. Centro, M. Lippi, D. Pascoli, F. Pietropaolo, G.Pratali, S. Ventura, "Daedalus:a hardware signal analyser for Icarus", Nucl. Instr. and Methods A409 (1998), 294.

5. F.Sergiampietri, "Resistive voltage divider for ICARUS 600T and electric field uniformity inside the drift volume", ICARUS-TM-98/02 (1998).

6. F.Cavanna, A.Rubbia, F.Sergiampietri, "Complementary activities required for the setting up of the first ICARUS 600T detector module", ICARUS TM-98/03 (1998).

7. ICARUS Aquila-LNGS Group, "Proposal for an improved electron lifetime monitor for the ICARUS 600-ton detector", ICARUS-TM-98/04 (1998).

8. S.Bricola et al., "Report on the tests of the $10m^3$ cryostat", ICARUS-TM-98/05 (1998).

9. C.Carpanese et al., "ARIANNA: the readout module for ICARUS, prototype version", ICARUS-TM-98/07 (1998).

10. C. Carpanese, S. Centro, M. Lippi, G. Meng, D. Pascoli, F. Pietropaolo,G. Pratali, S. Ventura, "Daedalus: a feature extractor for Icarus signals", ICARUS-TM-98/08 (1998).

11. P. Benetti et al., "Detection of Scintillation Light in Coincidence with Ionizing Tracks in a $LAr$ TPC", ICARUS-TM-98/10 (1998).

12. A.Ereditato, A.Ferrari, P.Migliozzi, F.Pietropaolo, J.P.Revol, P.Sala, "Towards the optimization of the NGS neutrino beam for $\nu_\mu$- $\nu_\tau$ appearence experiments", ICARUS-TM-98/13 (1998).

13. C.Montanari, M.Rossella, C.Vignoli, "Measurements of outgassing rates of signals cables", ICARUS-TM-98/14 (1998).

14. D.Cline, S.Otwinowski, "Detection of $\nu_\mu$-$\nu_e$ at $\delta^2 m \approx 10^{-3} eV^2$ from 3 neutrino mixing in ICARUS", ICARUS-TM-98/15 (1998).

15. ICARUS Collaboration,"ICARUS-like technology for long baseline neutrino oscillations" ICARUS-TM-98/16, CERN/SPSC 98-33 (1998).

# References

[1] P.Cennini et al., "ICARUS II: second generation proton decay experiment and neutrino observatory at the Gran Sasso Laboratory", LNGS-94/99 Vol. I & II, Proposal (1994).

[2] J.P.Revol et al., "A search programme for explicit neutrino oscillations at the long and medium baselines with ICARUS detectors" - ICARUS-TM-97/01 (1997).

[3] P.Cennini et al., "A first 600 ton ICARUS detector installed at the Gran Sasso Laboratory", Proposal, Addendum to LNGS-94/99 (1996).

[4] P.Cennini et al., Nucl. Instr. and Methods A345 (1994) 230.

[5] W.N.McElroy, S.Berg and G.Gigas, Nucl. Sci. Eng. 27 (1970), 533.

[6] P. Belli et al., Il Nuovo Cimento, 101A, n.6 (1989), 959.

[7] P. Cennini, S. Centro, D. Favaretto, S. Motto, A. Puccini, C. Tintori, Nucl. Instr. and Methods A409 (1998), 300.

[8] CAEN spa "32 CH. ICARUS ANALOG BOARD MOD. V791", Viareggio 1998.

[9] C. Carpanese, S. Centro, M. Lippi, D. Pascoli, F. Pietropaolo, G.Pratali, S. Ventura, IEEE Trans. Nucl. Sc., 45, n.4 (1998) 1804.

[10] CAEN spa " 32 CH. DIGITAL BOARD MOD. V789" Viareggio 1998.

[11] C. Carpanese, S. Centro, M. Lippi, D. Pascoli, F. Pietropaolo, G.Pratali, S. Ventura, Nucl. Instr. and Methods A409 (1998), 294.

[12] C. Carpanese, S. Centro, M. Lippi, G. Meng, D. Pascoli, F. Pietropaolo,G. Pratali, S. Ventura, "Daedalus: a feature extractor for Icarus signals", ICARUS-TM-98/08 (1998).

[13] F.Arneodo et al., Nucl. Instr. and Methods A412 (1998), 440.

[14] The Icarus Aq/LNGS Group, "Proposal for an improved electron lifetime monitor for the ICARUS 600-ton detector", ICARUS/TM-98/04 (1998).

[15] G. Carugno et al., Nucl. Instr. and Methods A292 (1990) , 580.

[16] A. Bettini et al., Nucl. Instr. and Methods A305 (1991) , 177.

[17] A. Ferrari, and P. R. Sala, Proc. of the *Workshop on Nuclear Reaction Data and Nuclear Reactors Physics, Design and Safety*, ICTP Trieste, Italy, (1996).

[18] D. Cavalli, A. Ferrari, P. R. Sala, "Simulation of nuclear effects in neutrino interactions", ICARUS TM-97/18 (1997).

[19] ICARUS Collaboration, ICARUS TM-98/16, CERN/SPSC 98-33 (1998).

# LUNA:Laboratory for Underground Nuclear Astrophysics

R. Bonetti[1], C. Broggini[2], L. Campajola[3], P. Corvisiero[4],
A. D'Alessandro[5], M. Dessalvi[4], A. D'Onofrio[3], A. Fubini[6], Z. Fulop[7],
G. Gervino[8], L. Gialanella[2], U. Greife[9], A. Guilielmetti[1], C. Gustavino[5],
M. Junker[5], A. Kiss[7], P. Prati[4], V. Roca[3], C. Rolfs[9], M. Romano[3],
F. Schümann[9], F. Strieder[9], E. Somorjai[7], F. Terrasi[3],
H.P. Trautvetter[8], S. Zavatarelli[4]

[1] Universitá di Milano, Dipartimento di Fisica and INFN, Milano
[2] INFN, Padova
[3] Universitá di Napoli, Dipartimento di Fisica and INFN, Napoli
[4] Universitá di Genova, Dipartimento di Fisica and INFN, Genova
[5] Laboratori Nazionali Gran Sasso, Assergi
[6] ENEA, Frascati and INFN, Torino
[7] ATOMKI, Debrecen, Hungary
[8] Politecnico di Torino, Dipartimento di Fisica and INFN, Torino
[9] Institut für Experimentalphysik III, Ruhr–Universität Bochum

### Abstract

The reaction $^3$He($^3$He,2p)$^4$He has been studied for the first time over the whole thermal energy region of the sun using the 50 kV accelerator facility at the LNGS. The measurements have been concluded in fall 1998. Since then the electron screening effect is being studied at the 50 kV accelerator by measuring the cross section of the reaction D($^3$He,p)$^4$He at low energies. Also the work on the new 400 kV accelerator, which will be installed in the underground laboratories, is in progress. The collaboration is preparing a reinvestigation of the reaction $^7$Be(p,$\gamma$)$^8$B at energies as near as possible to the solar energies.

# 1   Introduction

The low-energy studies of thermonuclear reactions are hampered by exponentially dropping cross sections at energies which are below the Coulomb barrier (see for example *LNGS Annual Report 1997, p. 106*) [1]. Typical cross sections in the range of stellar energies – called the Gamow Peak – are smaller than 1 fbarn. The reaction rate in a nuclear physics experiment involving such low cross sections is thus often less than one event per day. In consequence the studies of thermonuclear reactions in a laboratory at the earth's surface are hampered by the background induced in the detectors by cosmic rays.

Passive shielding around the detectors provides a reduction of gammas and neutrons from the environment, but it produces at the same time an increase of gammas and neutrons due to the cosmic-ray interactions in the shielding itself. A $4\pi$ active shielding can only partially reduce the problem of cosmic-ray activation. The best solution is to install an accelerator facility in a laboratory deep underground [2].

But still due to the extremely low counting rates mentioned above the experiments are very time consuming. For this reason the facility must be very reliable and should not require a lot of maintenance.

The worldwide first underground accelerator facility has been installed at the Laboratori Nazionali del Gran Sasso (LNGS), based on a 50 kV accelerator [3]. This pilot project is called LUNA and has been supported since 1992 by INFN, BMBF, DAAD-VIGONI and NSF/NATO.

# 2   Measurements of $^3$He($^3$He,2p)$^4$He at the LNGS

The major aim of the LUNA project has been to measure the cross section of $^3$He($^3$He,2p)$^4$He which is one of the major sources of uncertainties for the calculation of the neutrino source power of the sun. It has been studied previously [4] down to about $E_{cm}$=25 keV, but there remained the possibility of a narrow resonance at lower energies that could enhance the rate of path I of the pp-chain at the expense of the alternative paths that produce the high-energies neutrinos ($E_\nu > 0.8$ MeV). The LUNA–facility has allowed to study this important reaction over the full range of the solar Gamow peak ranging from 20 keV down to 16 keV, where the cross section is as low as 8 pbarn at $E_{cm}$=25 keV and about 20 fbarn at $E_{cm}$=17 keV [5].

While the upper part of of the solar Gamow Peak has been scanned in 1997 the cross section in the lower part has been investigated in 1998. To achieve this goal the LUNA Collaboration has changed the previously used detector setup consisting of four $\Delta$E-E telescopes (see *LNGS Annual Reports 1996 and 1997*) with a new detector setup. The new system is based on the detection of pp-coincidences from the reaction $^3$He($^3$He,2p)$^4$He. The setup is shown in Fig. 1. It consists of eight 1000 $\mu$m thick silicon particle detectors with a surface of 5 cm x 5 cm each, which are covered by 10 $\mu$m Nickel foils that stop the alpha particles emitted in the reactions $^3$He($^3$He,2p)$^4$He and $^3$He(d,p)$^4$He. With the present configuration the beam induced background from the reaction $^3$He(d,p)$^4$He can be suppressed very efficiently as only the reaction $^3$He($^3$He,2p)$^4$He emits two protons
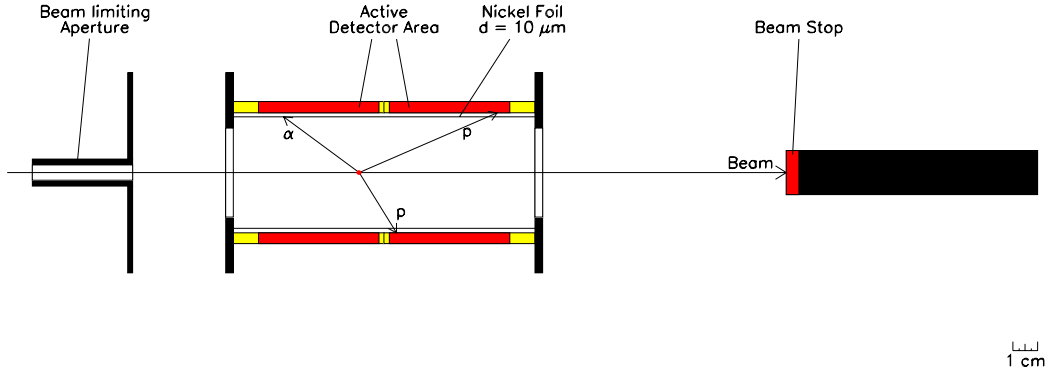
Figure 1: Schematic design of the new detector setup.

simultaneously.

To test the systematic consistency of the data obtained with the telescope setup and the new detection system, measurements have been carried out at overlapping energies. As can be seen in Fig. 2 the data determined with the two different detector arrangements are in quite good systematic agreement.

After these systematic tests data have been taken down to $E_{cm} = 16.5$ keV. At the lowest energy of 16.5 keV the cross section is as low as 0.02 pbarn corresponding to a count rate of about 2 events/month, rather low even for the 'silent' experiments under ground. The data are still under evaluation but preliminary results are given in Fig. 2. The energy dependence of the astrophysical $S(E)$ factor is consistent with the predictions based on an extrapolation from higher energies. In addition it is possible to obtain conclusions on the effect of the tail of a hypothetical narrow resonance lying in the not measured low-energy region. Upper limits for the strength of such a resonance have been calculated. A detailed description of the calculations is given in [5]. Fig. 2 shows the calculated ratio

$$r = < \sigma v >_{\text{res}} / < \sigma v >_{\text{SSM}}$$

as a function of the resonance energy for some values of the total resonance width $\Gamma$. A central temperature of the sun of $15 \cdot 10^6$ K has been assumed. $< \sigma v >_{\text{res}}$ and $< \sigma v >_{\text{SSM}}$ are the reaction rates due to the hypothetical resonance and the non-resonant rate used in Standard Solar Model (SSM) calculations respectively.

The $< \sigma v >_{\text{res}}$ values obtained with this procedure are upper limits for the reaction rate due to the hypothetical resonance. At energies $E_R \leq 9$ keV one concludes that the presence of a resonance cannot account for even a partial nuclear solution of the solar neutrino puzzle [6, 7]. The same conclusion applies in the energy region between 9 and 20 keV for resonance widths $\geq 0.5$ keV. Resonances with width below 0.05 keV do not contribute significantly.
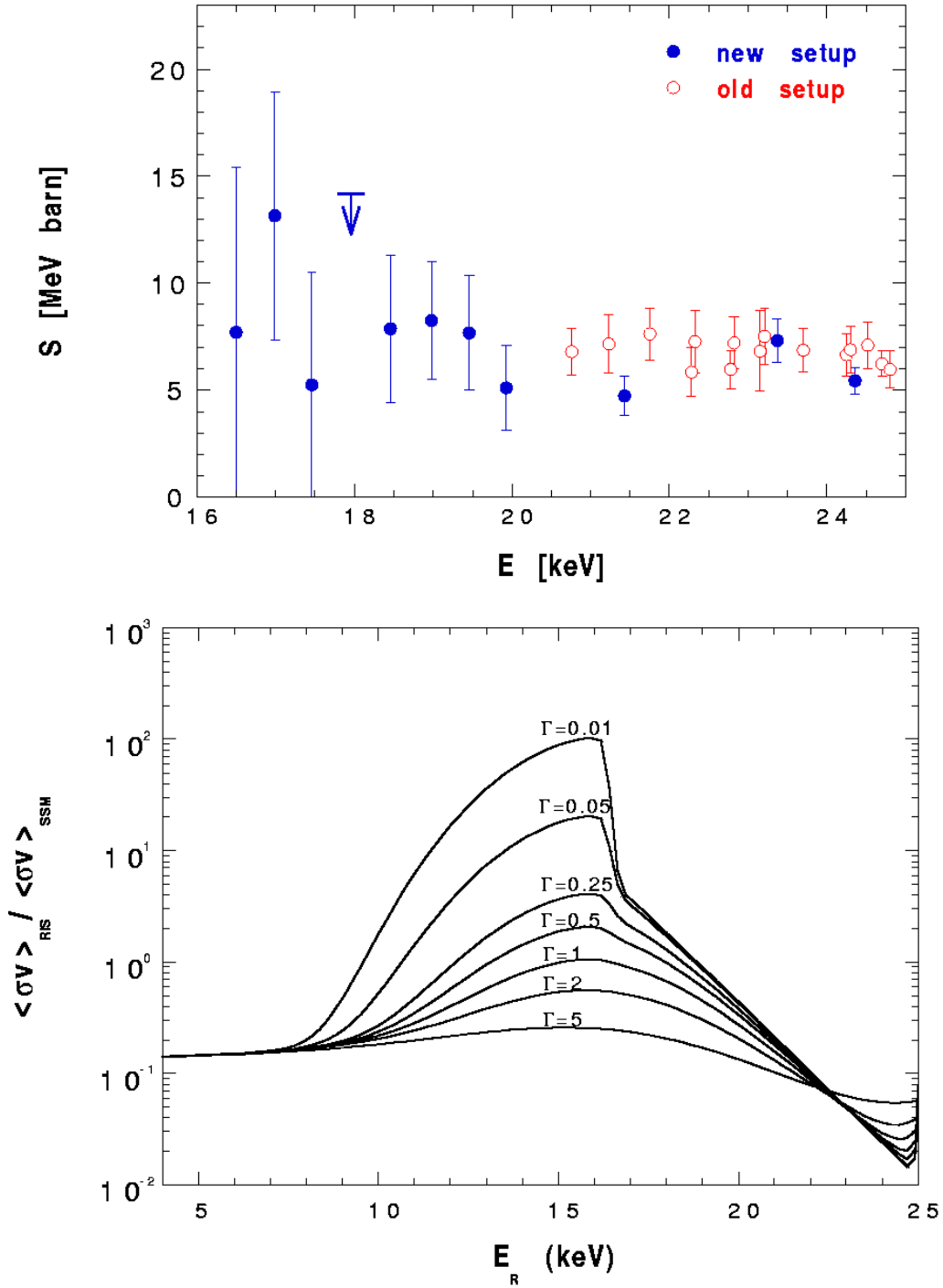
Figure 2: Top: The astrophysical $S(E)$ factor of $^3\text{He}(^3\text{He},2p)^4\text{He}$ measured with the telescope setup (full points) [5] and the preliminary results obtained with the new detector system (open cycles).
Bottom: The ratio $< \sigma v >_{\text{res}} / < \sigma v >_{\text{SSM}}$ of the resonance and non resonance reaction as a function of the resonance energy $E_\text{R}$ for some values of the total width $\Gamma$ given in units of keV.

# 3   Studies of Electron Screening at the LNGS

For nuclear reactions studied in the laboratory, the target nuclei and the projectiles are usually in the form of neutral atoms/molecules and ions, respectively. The electron clouds surrounding the interacting nuclides act as a screening potential: the projectile effectively sees a reduced Coulomb barrier. This leads to a higher cross section than would be the case for bare nuclei (*LNGS Annual Report 1997, p. 106*). For a stellar plasma the cross section of the bare nuclei must be known because the screening in the plasma can be quite different from that in laboratory studies [10], and the bare nucleus cross section must be explicitly included in each situation. Thus, a good understanding of electron-screening effects is needed to arrive at reliable data at low energies. Low-energy studies of several fusion reactions involving light nuclides [11, 12, 13, 5] showed the exponential enhancement of the cross section at low energies. The observed enhancement was in all cases close to or higher than the adiabatic limit derived from atomic-physics models.

The reaction $^3$He(d,p)$^4$He has been studied in the past by the LUNA-Collaboration using a Deuterium beam and a $^3$He gas target at the University of Bochum (Germany) [12]. Theses data are the most precise experimental data for electron screening available at the moment. As the electron screening effect depends on the molecular status of the projectile and the target it is quite interesting to study the low-energy cross section of the reaction D($^3$He,d)$^4$He thus sending a $^3$He beam on a $D_2$ target. The experimental setup for this measurement is almost identical to the system used for the $^3$He($^3$He,2p)$^4$He experiment. Only minor modifications had to be done in the vacuum system. The Ni-foils in front of the detectors had to be removed. First data taken in fall 1998 look very promising. The experiment will be continued in 1999.

# 4   Status of the LUNA – Phase II

While investigating the reaction $^3$He($^3$He,2p)$^4$He at very low energies the LUNA Collaboration has started to prepare for the second phase of Underground Nuclear Astrophysics.

LUNA – Phase II will concentrate initially on the other key reactions of the pp–chain like $^3$He($\alpha,\gamma$)$^7$Be and $^7$Be(p,$\gamma$)$^8$B and the key reaction of the CNO–cycles, $^{14}$N(p,$\gamma$)$^{15}$O, which have never been studied in or even near their solar Gamow peaks. All these reactions are critical to the solar neutrino puzzle. The reaction rate of $^{14}$N(p,$\gamma$)$^{15}$O is also one of the ingredients needed to determine the theoretical scenario used to constrain both the age and the distance of the oldest stellar system in our galaxy, namely the Globular Clusters.

In 1998 the LUNA–Collaboration obtained the funding needed in order to buy the accelerator and to prepare the infrastructure in the underground laboratories of LNGS. By the end of 1998 the invitations for tenders for the infrastructure and for the accelerator have been officially approved and first works at the future site of the experiment are already in progress.

In addition detailed tests of gamma-detectors, which could be used for the experiments, are going on in the underground laboratory of LNGS and a new Monte Carlo Code for the simulation of gamma cascades originating from nuclear reactions is being developed.

## Studies of the reaction $^7$Be(p,$\gamma$)$^8$B

The reaction $^7$Be(p,$\gamma$)$^8$B is of particular importance in the framework of neutrino astrophysics. For this reason the LUNA-Collaboration is aiming to investigate this reaction as near as possible to its solar Gamow peak [14] using the LUNA II accelerator at the LNGS. In order to prepare these measurements the collaboration has settled a hot chemistry laboratory at the University of Bochum (Germany). In this facility activities up to 35 GBq can be handled at a time. Up to now about 40 GBq of $^7$Be-activity produced at the Cyclotron at ATOMKI in Debrecen (Hungary) have been transformed to hot targets for test purposes.

Also a target chamber has been developed in Bochum. In the chamber the $^7$Be-target is first irradiated with protons. After some seconds the target is transfered to the counting chamber where the $\beta^+$-delayed alpha decay of the $^8$B recoils is observed as the signature of the reaction $^7$Be(p,$\gamma$)$^8$B. The target chamber has intensively been tested at the 4MV tandem accelerator in Bochum by measuring the cross sections of the reaction $^6$Li(d,p)$^8$Li (which produces the same $\beta^-$ -delayed alphas) and the reaction $^7$Be(p,$\gamma$)$^8$B) at high energies, where the reaction rate is still quite high.

At the moment the work is mainly focused on the choice of the detectors for the detection of the $\beta$-delayed alphas. In alternative to the traditionally used silicon particle detectors track etch detectors are being tested.

## Studies of systematic errors in literature data of $^7$Be(p,$\gamma$)$^8$B

The target chamber described above has already been used in order to investigate the loss of $^8$B recoils from the reaction $^7$Be+p due to scattering of the recoils in backwards direction. The recoils would consequently not be transfered to the detector resulting in an underestimation of the cross section. This mechanism has been found recently in TRIM calculations by Weissmann et al. [15]. The measurements of the LUNA–Collaboration carried out at the 4MV accelerator in Bochum clearly confirm the recoil loss [16]. Especially the energy dependence of the cross section of $^7$Be+p might be affected by the recoil losses. This could severely influence the extrapolation of the existing data to the solar Gamow peak producing a non-negligible influence on the Solar Neutrino Puzzle. As the existing data can hardly be corrected for this recoil loss these measurements clearly indicate the necessity of new low energy measurements of the cross section of $^7$Be(p,$\gamma$)$^8$B.

# 5 Acknowledgements

# 6 Publications and Conferences

- M. Junker et al, Phys. Rev. **C57** (1998) 2700;

- F. Strieder et al, Eur. Phys. J. A3, (1998) 1;

- M. Junker, invited talk at International Workshop XXXVI on Gross Properties of Nuclei and Nuclear Excitations, Hirschegg, Austria, January 11 – 17, 1998

- M. Junker, talk at SNEC98, Padua, Italy, March 31 – April 4, 1998

- A. D'Alessandro, Talk at 5th International Symposium on Nuclei in the Cosmos, Volos, Greece, June 6 – 11, 1998;

- F. Strieder, Talk at 5th International Symposium on Nuclei in the Cosmos, Volos, Greece, June 6 – 11, 1998;

- P. Prati, Talk at INPC/98, International Nuclear Physics Conference, Paris, France, August, 24 – 28, 1998;

- P. Corvisiero, invited talk at LXXXIV Congresso Nazionale Societá Italiana di Fisica, Salerno, Italy, September 28 – October 2, 1998

# References

[1] C. Rolfs and W.S. Rodney, Cauldrons in the Cosmos (University of Chicago press, 1988);

[2] G. Fiorentini, R. W. Kavanagh, and C. Rolfs, Zeitsch. Phys.**A350** (1995) 289;

[3] U. Greife et al., Nucl.Instr.Meth. **A350** (1994) 327;

[4] A. Krauss et al., Nucl.Phys. **A467** (1987) 273;

[5] M. Junker et al., Phys. Rev. **C57** (1998) 2700;

[6] V. Castellani,S. Degl'Innocenti and G. Fiorentini Astron. Astrophys. **271** (1993) 601;

[7] V. Berezinsky,G. Fiorentini and M. Lissia, Physics Letters **B365** (1996) 185;

[8] H.J. Assenbaum et al., Z. Phys. **A327** (1987) 461;

[9] L. Bracci et al., Nucl. Phys. **A513** (1990) 316;

[10] B. Ricci et al., Phys. Rev. **C52** (1995) 1095;

[11] U. Greife et al., Z.Phys. **A351** (1995) 107;

[12] P. Prati et al., Z.Phys. **A350** (1994) 171;

[13] K. Langanke et al., Phys.Lett. **B369** (1996) 211;

[14] The Luna Collaboration, "Future research aims of LUNA 1997 — 2002", INFN internal report, 1997;

[15] L. Weissmann et al., Nucl. Phys. **A 630** (1998) 678;

[16] F. Strieder et al., Eur. Phys. J. A3, (1998) 1

# LVD. Large Volume Detector

M.Aglietta[16], B.Alpat[13], E.D.Alyea[7], P.Antonioli[1], G.Badino[16], G.Bari[1], M.Basile[1], V.S.Berezinsky[10], F.Bersani[1], M.Bertaina[16], R.Bertoni[16], G.Bonoli[1], A.Bosco[2], G.Bruni[1], G.Cara Romeo[1], C.Castagnoli[16], A.Castellina[16], A.Chiavassa[16], J.A.Chinellato[3], L.Cifarelli[1,†], F.Cindolo[1], G.Conforto[17], A.Contin[1], V.L.Dadykin[10], A.De Silva[2], M.Deutsch[8], P.Dominici[17], L.G.Dos Santos[3], L.Emaldi[1], R.I.Enikeev[10], F.L.Fabbri[4], W.Fulgione[16], P.Galeotti[16], C.Ghetti[1], P.Ghia[16], P.Giusti[1], R.Granella[16], F.Grianti[1], G.Guidi[17], E.S.Hafen[8], P.Haridas[8], G.Iacobucci[1], N.Inoue[14], E.Kemp[3], F.F.Khalchukov[10], E.V.Korolkova[10], P.V.Korchaguin[10], V.B.Korchaguin[10], V.A.Kudryavtsev[10], K.Lau[6], M.Luvisetto[1], G.Maccarone[4], A.S.Malguin[10], R.Mantovani[17], T.Massam[1], B.Mayes[6], A.Megna[17], C.Melagrana[16], N.Mengotti Silva[3], C.Morello[16], J.Moromisato[9], R.Nania[1], G.Navarra[16], L.Panaro[16], L.Periale[16], A.Pesci[1], P.Picchi[16], L.Pinsky[6], I.A.Pless[8], J.Pyrlik[6], V.G.Ryasny[10], O.G.Ryazhskaya[10], O.Saavedra[16], K.Saitoh[15], S.Santini[17], G.Sartorelli[1], M.Selvi[1], N.Taborgna[5], V.P.Talochkin[10], J.Tang[8], G.C.Trinchero[16], S.Tsuji[11], A.Turtelli[3], I.Uman[13], P.Vallania[16], G. Van Buren [8], S.Vernetto[16], F.Vetrano[17], C.Vigorito[16], E. von Goeler[9], L.Votano[4], T.Wada[11], R.Weinstein[6], M.Widgoff[2], V.F.Yakushev[10], I.Yamamoto[12], G.T.Zatsepin[10], A.Zichichi[1]

[1] *University of Bologna and INFN-Bologna, Italy*
[2] *Brown University, Providence, USA*
[3] *University of Campinas, Campinas, Brazil*
[4] *INFN-LNF, Frascati, Italy*
[5] *INFN-LNGS, Assergi, Italy*
[6] *University of Houston, Houston, USA*
[7] *Indiana University, Bloomington, USA*
[8] *Massachusetts Institute of Technology, Cambridge, USA*
[9] *Northeastern University, Boston, USA*
[10] *Institute for Nuclear Research, Russian Academy of Sciences, Moscow, Russia*
[11] *Okayama University, Okayama, Japan*
[12] *Okayama University of Science, Okayama, Japan*
[15] *Ashikaga Institute of Technology, Ashikaga, Japan*
[16] *Institute of Cosmo-Geophysics, CNR, Torino, University of Torino and INFN-Torino, Italy*
[17] *University of Urbino and INFN-Firenze, Italy*
[†] *now at University of Salerno and INFN-Salerno, Italy*

**Abstract**

The Large Volume Detector (LVD) in the Gran Sasso Underground Laboratory is a $\nu$ observatory mainly designed to study low energy neutrinos from gravitational stellar collapses. The experiment is sensitive to collapses in our Galaxy since June 1992, nowaday with an active mass of about 670 tons.

The detector performances and the method used to search for Supernova events and to identify different neutrino interactions is presented. During 1998 the online and offline analysis for burst identification continued with no positive results.

Duirng 1998, some cosmic ray muons studies presented to the 1997 International Cosmic Ray Conference have been completed and published on international reviews: they include new results regarding prompt muons search, muon energy spectrum, neutrino-induced muons and cosmic ray composition.

# 1    Introduction

The Large Volume Detector in the Gran Sasso underground Laboratory is a multipurpose detector consisting of a large volume of liquid scintillator interleaved with limited streamer tubes in a compact geometry.

A major purpose of the LVD experiment is to search for neutrinos from stellar collapses in our Galaxy. The main results about this item are reviewed in section 3 of this report.

Other LVD physics items are: measurements of atmospheric muon and neutrino-induced flux; study of events detected in time coincidence with the EAS-TOP array at the surface of the mountain. The main results about these issues are reviewed in section 3 of this report.

# 2    The LVD detector

The LVD detector, operating since June 1992, has a modular structure that consists of aligned towers of 38 modules each. In any tower the scintillator / tracking modules are stacked in five columns.

Every module contains 8 liquid scintillation counters of dimensions $1.5 \times 1 \times 1\ m^3$ seen by three photomultipliers. The density of the scintillator is about $0.8\ g/cm^3$ and the energy resolution is about 15% for a 10 $MeV$ energy release, where for electrons it begins to be dominated by leakage effects in the counter.

The tracking system consists of L-shaped detectors for each module. Each element contains two staggered layers of 6.3 $m$ long limited streamer tubes. The bidimensional read-out is made by means of 4 $cm$ strips, parallel and perpendicular to the tubes, providing high detection efficiency and an angular resolution better than 4 milliradians.

# 3 Neutrino physics

## 3.1 Neutrinos from collapsing stars

In the picture of all existing detectors of neutrinos from Gravitational Stellar Collapses (G.S.C.), the LVD scintillator detector has two peculiarities: it can operate at lower energy thresholds as compared to Čerenkov light detectors (because of a higher light yield and a better light collection), and it can detect both products ($e^+$ and n) of the dominant interaction of $\bar{\nu}_e$ with free protons.

The detection of low energy neutrinos, of the order of a few MeV, gives the possibility to study objects emitting at low temperatures $\nu$-sphere. Low temperatures, corresponding to neutrino average energies of a few MeV, are difficult to detect but surely cannot be excluded: neither by theoretical models, nor from the phenomenological point of view; indeed our experimental knowledge of the neutrino signal from G.S.C. is based on an single event with poor statistics and controversial energy spectrum.

Moreover a poor knowledge of the $\bar{\nu}_e$ spectrum in the low energy region (where the deviation from the standard Fermi-Dirac distribution could be strong) induces errors in determining the total $\bar{\nu}_e$ luminosity.

On the other hand the possibility to identify $\bar{\nu}_e$ interactions with protons by a stringent signature (and not simply by the absence of directionality as for light water Cherenkov detectors) gives us the chance to play with pure $\bar{\nu}_e$ energy spectrum and to separate the rare, but very interesting, charged and neutral current interactions with C nuclei from the most common $\bar{\nu}_e$ interactions. Most theoretical models agree in predicting the total energy emitted as $\nu$ 's during the stellar collapse, the energy equipartition among the different $\nu$ flavours and the time duration of the $\nu$ burst. Precisely, for a collapsing star at the distance of 10 Kpc, with $\nu$-sphere temperatures $T_{\nu_e} = 3$ MeV and $T_{\nu_\mu} = 6$ MeV we have computed a total of $\approx 400$ interactions, in agreement within 5% with other calculations.

For any scintillator detector the bulk of events (about 90% of the total number of interactions) is due to the capture reaction:

$$\bar{\nu}_e + p \rightarrow n + e^+ \qquad\qquad n + p \rightarrow d + \gamma_{2.2MeV}. \qquad (1)$$
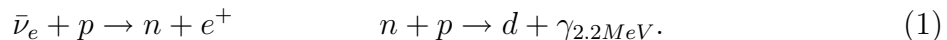
The possibility of detecting both products of reaction (1): $e^+$ and $n$, allows LVD to identify $\bar{\nu}_e$ interactions, and thus to measure the temperature of the $\bar{\nu}_e$ neutrino-sphere.

Further, we wish to recall that in LVD about 5% of the events are due to neutral current interactions with $^{12}C$ which deexcites emitting a 15.1 MeV $\gamma$. The detector efficiency on detecting these signals has been evaluated. Because $\mu$ and $\tau$ neutrino-spheres are located deeper in the collapsing stellar core, and because of a temperature gradient, their energy spectra have higher temperatures as compared with the electron neutrino spectra. As a consequence more then 90% of the n.c. interactions with Carbon nuclei are produced by $\nu_\mu$ and $\nu_\tau$.

Moreover, 3% of events in LVD, are due to elastic scattering of all neutrino flavours on electrons, and less then 1% to c.c. interactions of $\nu_e$ and $\bar{\nu}_e$ with $^{12}C$ nuclei. These reactions could easily be separated by subsequent $\beta$ decay, but because of their relative high thresholds they are few. If energetic $\mu$ and $\tau$ neutrinos oscillate in electron neutrinos, the $\bar{\nu}_e$ spectrum will be distorced and c.c. interaction channel will open.

In the search for $\nu$ bursts from gravitational stellar collapses, the most important performances of LVD are the following.

- The information related to each signal is stored in a temporary memory buffer which is shared by 8 scintillator counters. This buffer can store up to $2 \cdot 10^5$ pulses, which corresponds to the signal from a standard supernova at a distance closer then 1 Kpc from the Earth.

- The total deadtime corresponds to a maximum detectable frequency (per counter) of 500 kHz. The read out procedure does not introduce any additional deadtime.

- The time of each event, relative to the U.T. time ( $\pm 1$ $\mu$s from the Gran Sasso facility), is measured with an accuracy of $\pm 12.5$ ns.

- The experiment duty cycle averaged since June '92, when the first LVD tower started taking data, is 76% and during 1997 is better than 95%.

## 3.2 Neutrino interactions

The search for $\nu$ burst candidates is performed by studying the trigger time sequences and searching for signal clusterization. The background due to cosmic ray muons is rejected by the tracking system. The total counting rate of the experiment after $\mu$ rejection is 0.2 Hz tower$^{-1}$, dominated by the internal counters which operate at a lower energy threshold (E $\geq 3-4$ MeV ). At E $\geq 7$ MeV all LVD counters are active and the total counting rate is 0.06 Hz tower$^{-1}$, the ratio between the counting rate of external and internal counters is 3 (in LVD about 1/2 of the total mass belongs to the detector core). The technique we use to select burst candidates and to evaluate their significance, is operating (on-line on the experimental data stream) since June '92. We call this the Supernova On-line Monitor (SOM).

The detector sensitivity as a function of the burst duration for the LVD mass active at present (560 tons) is shown in Fig. 3.2 The two lines are obtained by setting the imitation frequency to 1 event/100 years, for the detector as a single telescope, and to 1 event/month for the detector inserted into a network. With the present LVD active mass, a complete survey of our Galaxy is guaranteed, the Large and Small Magellanic Clouds will eventually become observable with LVD in the final configuration (5 towers).

After the selection of any cluster of pulses, by means of a pure statistical analysis based on their temporal sequence, the burst candidate is analysed to test its consistency with a $\nu$ signal. Three independent tests are performed:

a) presence of signals due to n-capture, from reaction (1);

b) event topology;

c) energy spectra.

a) The efficiency in detecting the 2.2 MeV photons from n-capture, measured on some counters by using a n-source ($^{252}$Cf), was found to be $\approx 60\%$. The average counting rate per counter for E $\geq 1$ MeV is 120 s$^{-1}$. On the average in a time window of 600 $\mu$s the signal to noise ratio is about 10. Moreover the time distribution of these delayed signals is different in the case of background (flat distribution) or n-capture (exponential with mean life $185\mu$s).
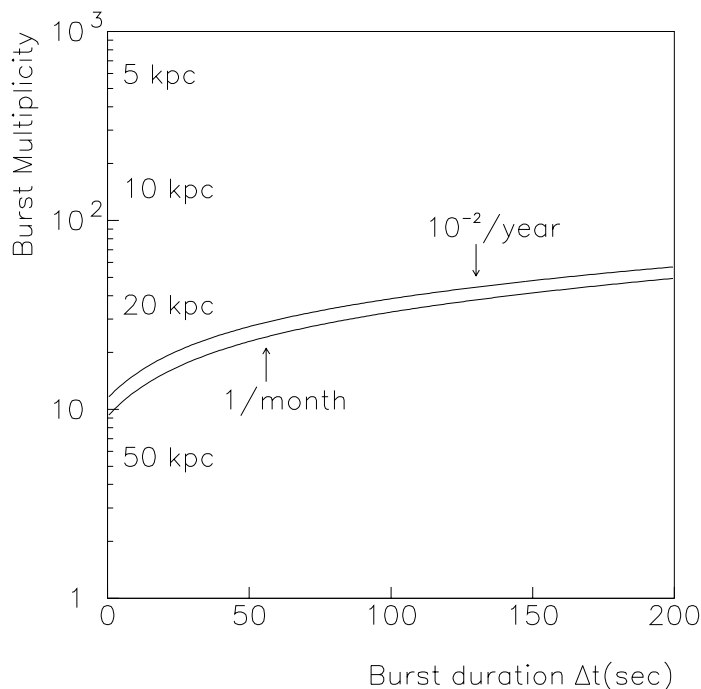
Figure 1: Detector sensitivity for different durations of the $\nu$ emission (560 tons)

b) Background events are concentrated in scintillation counters more exposed to natural radioactivity. Neutrino interactions must be uniformly distributed inside the volume of the detector. Thus we study the spatial distribution of events inside the experiment for each burst candidate by two independent methods. Both methods, if we exclude the background contamination (that depends on the burst duration), are completely independent on the time features of the cluster, and they are very effective in rejecting burst candidates produced by non Poissonian fluctuation of the noise, namely electronic troubles.

c) The expected energy distribution of $e^+$ from $\bar{\nu}_e$ interactions strongly differs from the background energy spectrum. By studying the measured spectra one can also determine the temperature of the $\bar{\nu}_e$-sphere and the number of n.c. interactions on $^{12}C$.

The LVD experiment detects neutrinos of different flavours through different interaction channels. The most effective is the c.c. $\bar{\nu}_e$ interaction with free protons, but a significant amount of $\nu$'s can be detected through charged and neutral current interactions with $^{12}C$ nuclei. All these channels, besides the $\nu_i + e^-$ scattering, are characterized by stringent signatures and hence can be separated.

In order to estimate the number of expected interactions in the different $\nu$ channels we assume energy equipartition among flavours and Fermi-Dirac spectra with eventually non zero chemical potential, in agreement with most models.

The temperature of the $\nu$-sphere is given by: $T_{\nu_e} = T_{\bar{\nu}_e}$ and $T_{\nu_\mu} = T_{\bar{\nu}_\mu} = T_{\nu_\tau} = T_{\bar{\nu}_\tau}$ $= \alpha \, T_{\bar{\nu}_e}$ for the different flavours, where $\alpha$ affects the number of n.c. interactions with $C$ nuclei but only marginally acts on the total number of interactions. In our calculation we

used $\alpha=2$.

In Fig.3.2 the total number of interactions expected in LVD for a G.S.C. at 10 Kpc emitting $E_{\nu_{tot}} = 3\ 10^{53}$ erg is shown versus the average $\bar{\nu}_e$ energy.
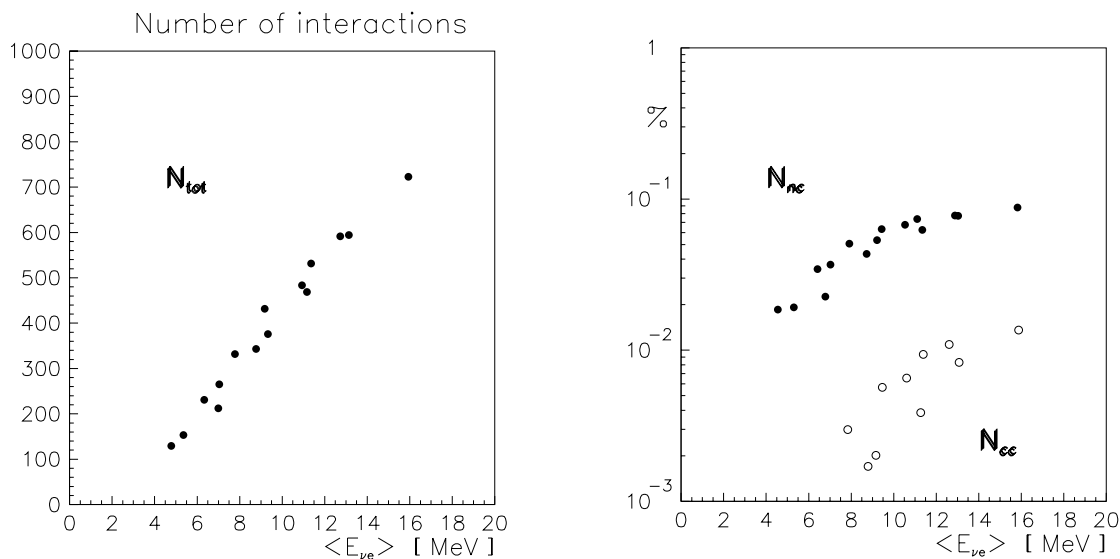


Figure 2: Total number of expected interactions vs. the $\bar{\nu}_e$ average energy.

Figure 3: Percentage of interaction in n.c. and c.c. channels with $^{12}C$ with respect to the total number of interactions vs. the $\bar{\nu}_e$ average energy.

We tested different parameters of the $\bar{\nu}_e$ spectrum with $T_{\bar{\nu}_e}$ ranging between 1.5 and 3.5 MeV and $\eta = \mu/$T ranging between 0 and 4; this corresponds to an average $\bar{\nu}_e$ energy between 4.7 and 15.6 MeV.

In order to avoid the dependence on the distance $(D)$ and the luminosity $(L_{\nu_i})$ of the source, the ratio between the number of interactions in the n.c. and c.c. channels with C to the total number of interactions has been plotted in Fig.3.2 for the same range of spectral parameters, carefully taking into account detector efficiency.

During 1998 the third tower construction has been continued, in particular the production of liquid scintillator, using the facility established at LNGS during 1997. At the end of 1998 $\approx 2/5$ of scintillator needed for third tower has been produced and tested.

# 4 Cosmic ray muons

## 4.1 Muon intensity and search for prompt muons

During 1998 we have performed a more detailed evaluation of the characteristics of the muon spectrum at the sea level, including the ratio of the prompt muon flux to that of pions, using the depth – zenith angle distributions of measured muon intensities $(I_\mu(x,\theta))$.

The analysis is based on an increased statistics.

The measured angular distribution of muon intensity has been converted to the 'depth – vertical intensity' relation in the depth range from 3 to 12 km w.e.. The analysis of this relation allowed to derive the power index, $\gamma$, of the primary all-nucleon spectrum: $\gamma = 2.78 \pm 0.05$.
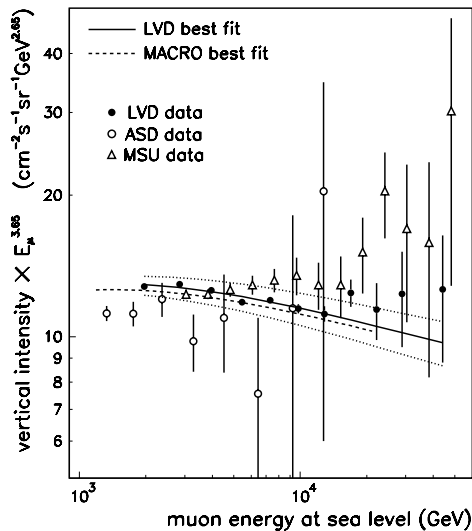


Figure 4: Energetic spectrum of vertical muon at sea level. $\bullet$ – LVD data; $\circ$ – ASD data [4]; $\diamond$ – MSU data [7]; continuous curve: LVD best fit together curves representing parameter errors and absolute flux normalization; dashed curve MACRO best fit

The data analysis has included the procedure of fitting of the measured depth – zenith angle distribution of muon intensity with the distributions calculated using the known muon survival probabilites modified for a new muon bremsstrahlung cross-section and muon spectrum at sea level with three free parameters: normalization constant, $A$, power index of primary all-nucleon spectrum, $\gamma$, and the ratio of prompt muons to pions, $R_c$. Results about vertical intensity have been published during 1998 on Phys. Rev. D. In Fig. r̃effi:livmare the energetic spectrum at sea level, as derived by LVD data, is shown, compared with other experiments. Upper and lower curves represent errors on fitted parameters plus a 10% error from absolute flux normalization uncertainties.

To obtain this result, the muon spectrum at sea level has been taken according to:

$$\frac{dI_{\mu 0}(E_{\mu 0}, \cos \theta)}{dE_{\mu 0}} \quad = \quad A \cdot 0.14 \cdot E_{\mu 0}^{-\gamma}$$

141

$$\times \quad \left( \frac{1}{1 + \frac{1.1 E_{\mu 0} \cos \theta^\star}{115 GeV}} + \frac{0.054}{1 + \frac{1.1 E_{\mu 0} \cos \theta^\star}{850 GeV}} + R_c \right) \qquad (2)$$

where the values of $cos\theta$ have been substituted by $cos\theta^\star$ which have been taken from either explicit calculations or a simple consideration of the curvature of the Earth atmosphere.

The study of muon flux intensity over different ranges of depth (shown in Fig. 5) allowed to finally check for a prompt muon component.
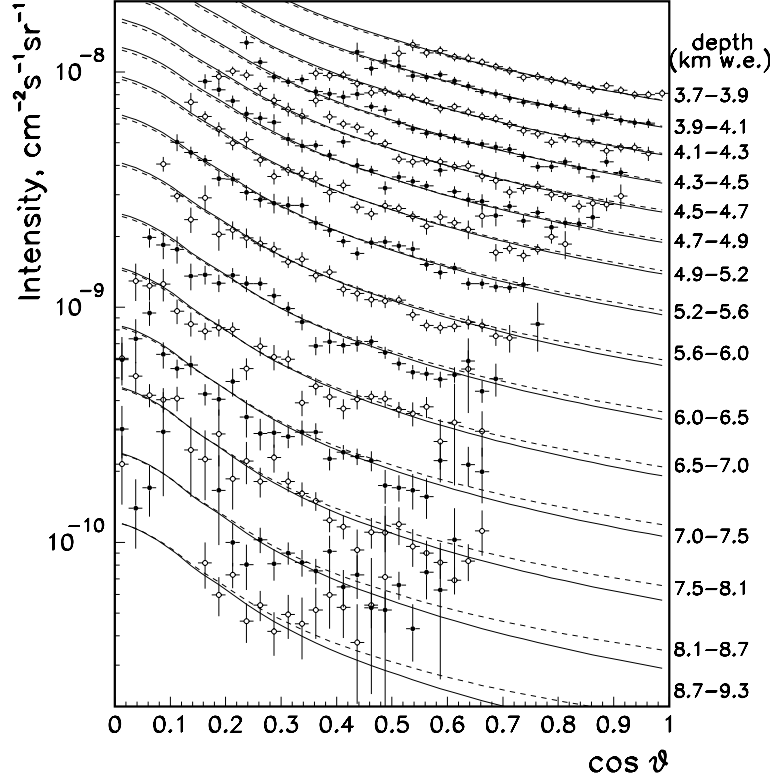


Figure 5: Muon intensity dependency fron zenithal angle at different depths. Continuous curve: calculations with $\gamma = 2.77$ e $R_c = 0$ (better fit for LVD data). Dashed curve: calculations with $\gamma = 2.77$ e $R_c = 2 \cdot 10^{-3}$ (upper limit of LVD). Errors include statistics and systematics.

As a result of the fitting procedure we have obtained the values of the free parameters: $A = 1.84 \pm 0.31$, $\gamma = 2.77 \pm 0.02$ and the upper limit (95% C.L.) $R_c \leq 2 \cdot 10^{-3}$. This upper limit to the prompt muon flux favours the models of charm production based on QGSM and the dual parton model. This result, presented to ISVHECRI Conference '98, has been submitted to Phys. Rev. D.

Always during 1998, finally results related to correlated events with EAS-TOP have been published on Astroparticle Physics, introducing a new observable in composition studies, e.g. the energy losses per unit path length. This measurement is done by the LVD with good precision, combining information from tracking system and from scintillation counters. For correlated events energy losses have been examined for different size intervals of the EAS correlated, measured by EAS-TOP.
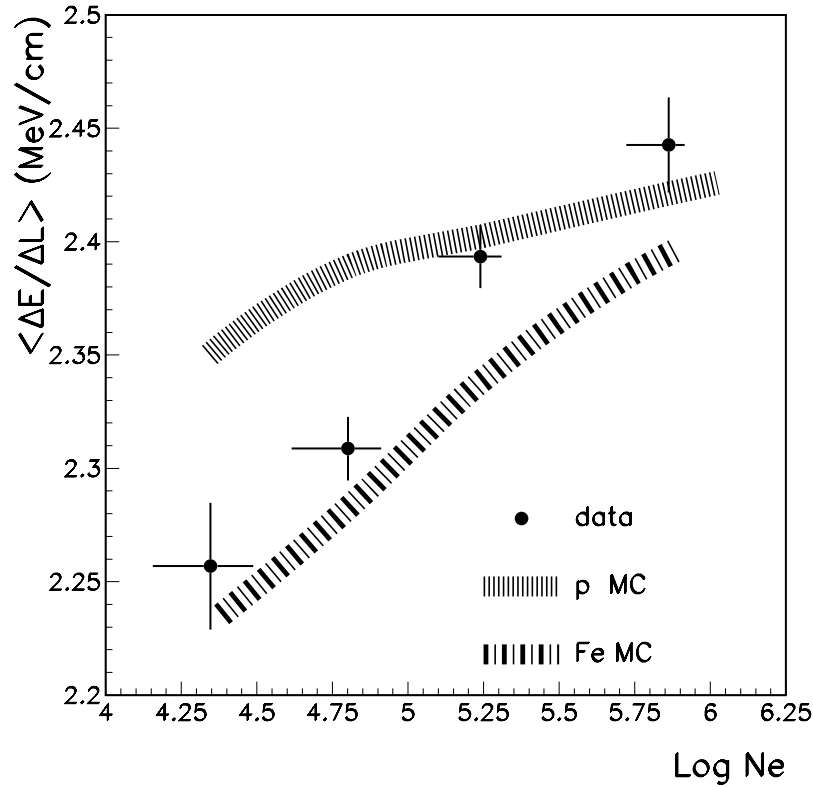


Figure 6: $< \Delta E/\Delta L >$ as a function of shower size: LVD data are compared wiht pure proton and iron compositions

In Fig. 6 the comparison between simulated average beahviors for primary composition of pure iron and protons and LVD is shown.

# 5 Conclusions

The LVD detector is operating has a Supernova Neutrino Observatory since 1992.

During 1998 the liquid scintillator production is continued at LNGS, producing approximately 2/5 of scintillator needed for third tower completion.

The tracking system design of LVD provides good detection efficiency even for tracks near horizontal. This feature allows the LVD to study the muon vertical intensity over a

large range of slant depth, give an upper limit to the prompt muon component and study the "plateau" region e.g. the deepest component. These results have been published on Phys. Rev. D.

Muon energy losses study has been used as a tool in composition studies for correlated events with the EAS-TOP. The results of this analysis have been published on Astroparticle Physics.

# 6 List of Publications

1. EAS-TOP and LVD Collaborations, Astrop. Phys. 9, 185 (1998)

2. LVD Collaboration, Phys. Rev. D58, 2005, (1998)

# MACRO. Monopole Astrophysics Cosmic Ray Observatory

M. Ambrosio[12], R. Antolini[7], C. Aramo[7,n], G. Auriemma[14,a], A. Baldini[13],
G. C. Barbarino[12], B. C. Barish[4], G. Battistoni[6,b], R. Bellotti[1], C. Bemporad[13],
E. Bernardini[7], P. Bernardini[10], H. Bilokon[6], V. Bisi[16], C. Bloise[6], C. Bower[8],
S. Bussino[14], F. Cafagna[1], M. Calicchio[1], D. Campana[12], M. Carboni[6],
M. Castellano[1], S. Cecchini[2,c], F. Cei[11,13], V. Chiarella[6], B. C. Choudhary[4],
S. Coutu[11,o], G. De Cataldo[1], H. Dekhissi[2,17], C. De Marzo[1], I. De Mitri[9],
J. Derkaoui[2,17], M. De Vincenzi[14,e], A. Di Credico[7], O. Erriquez[1], C. Favuzzi[1],
C. Forti[6], P. Fusco[1], G. Giacomelli[2], G. Giannini[13,f], N. Giglietto[1], M. Giorgini[2],
M. Grassi[13], L. Gray[4,7], A. Grillo[7], F. Guarino[12], C. Gustavino[7],
A. Habig[3], K. Hanson[11], R. Heinz[8], Y. Huang[4], E. Iarocci[6,g], E. Katsavounidis[4],
I. Katsavounidis[4], E. Kearns[3], H. Kim[4], S. Kyriazopoulou[4], E. Lamanna[14],
C. Lane[5], T. Lari[7], D. S. Levin[11], P. Lipari[14], N. P. Longley[4,l], M. J. Longo[11],
F. Loparco[7], F. Maaroufi[2,17], G. Mancarella[10], G. Mandrioli[2], S. Manzoor[2,m],
A. Margiotta[2], A. Marini[6], D. Martello[10,], A. Marzari-Chiesa[16], M. N. Mazziotta[1],
C. Mazzotta[10], D. G. Michael[4], S. Mikheyev[4,7,h], L. Miller[8], P. Monacelli[9],
T. Montaruli[1], M. Monteno[16], S. Mufson[8], J. Musser[8], D. Nicoló[13,d], C. Orth[3],
G. Osteria[12], M. Ouchrif[2,17], O. Palamara[7], V. Patera[6,g], L. Patrizii[2],
R. Pazzi[13], C. W. Peck[4], S. Petrera[9], P. Pistilli[14,e], V. Popa[2,i], A. Rainó[1],
A. Rastelli[7], J. Reynoldson[7], F. Ronga[6], U. Rubizzo[12], C. Satriano[14,a],
L. Satta[6,g], E. Scapparone[7], K. Scholberg[3], A. Sciubba[6,g], P. Serra[2],
M. Severi[14], M. Sioli[2], M. Sitta[16], P. Spinelli[1], M. Spinetti[6], M. Spurio[2],
R. Steinberg[5], J. L. Stone[3], L. R. Sulak[3], A. Surdo[10], G. Tarlé[11], V. Togo[2],
D. Ugolotti[2], M. Vakili[15], C. W. Walter[3] and R. Webb[15]

145

1. Dipartimento di Fisica dell'Università di Bari and INFN, 70126 Bari, Italy

2. Dipartimento di Fisica dell'Università di Bologna and INFN, 40126 Bologna, Italy

3. Physics Department, Boston University, Boston, MA 02215, USA

4. California Institute of Technology, Pasadena, CA 91125, USA

5. Department of Physics, Drexel University, Philadelphia, PA 19104, USA

6. Laboratori Nazionali di Frascati dell'INFN, 00044 Frascati (Roma), Italy

7. Laboratori Nazionali del Gran Sasso dell'INFN, 67010 Assergi (L'Aquila), Italy

8. Depts. of Physics and of Astronomy, Indiana University, Bloomington, IN 47405, USA

9. Dipartimento di Fisica dell'Università dell'Aquila and INFN, 67100 L'Aquila, Italy

10. Dipartimento di Fisica dell'Università di Lecce and INFN, 73100 Lecce, Italy

11. Department of Physics, University of Michigan, Ann Arbor, MI 48109, USA

12. Dipartimento di Fisica dell'Università di Napoli and INFN, 80125 Napoli, Italy

13. Dipartimento di Fisica dell'Università di Pisa and INFN, 56010 Pisa, Italy

14. Dipartimento di Fisica dell'Università di Roma "La Sapienza" and INFN, 00185 Roma, Italy

15. Physics Department, Texas A&M University, College Station, TX 77843, USA

16. Dipartimento di Fisica Sperimentale dell'Università di Torino and INFN, 10125 Torino, Italy

17. L.P.T.P., Faculty of Sciences, University Mohamed I, B. P. 524 Oujda, Morocco

a Also Università della Basilicata, 85100 Potenza, Italy

b Also INFN Milano, 20133 Milano, Italy

c Also Istituto TESRE/CNR, 40129 Bologna, Italy

d Also Scuola Normale Superiore di Pisa, 56010 Pisa, Italy

e Also Dipartimento di Fisica, Università di Roma Tre, Roma, Italy

f Also Università di Trieste and INFN, 34100 Trieste, Italy

g Also Dipartimento di Energetica, Università di Roma, 00185 Roma, Italy

h Also Institute for Nuclear Research, Russian Academy of Science, 117312 Moscow, Russia

i Also Institute for Space Sciences, 76900 Bucharest, Romania

l Swarthmore College, Swarthmore, PA 19081, USA

m RPD, PINSTECH, P.O. Nilore, Islamabad, Pakistan

n Also INFN Catania, 95129 Catania, Italy

o Also Department of Physics, Pennsylvania State University, University Park, PA 16802, USA

## Abstract

The status of the MACRO detector is described and results are presented on atmospheric neutrinos and neutrino oscillations, high energy neutrino astronomy, searches for WIMPs, search for low energy stellar gravitational collapse neutrinos, searches for magnetic monopoles, nuclearites and lightly ionizing particles, high energy downgoing muons and primary cosmic ray composition.

146

# 1   Introduction

MACRO is a large area multipurpose underground detector designed to search for rare events in the cosmic radiation. It has been optimized to look for supermassive magnetic monopoles as predicted by Grand Unified Theories (GUT) of the electroweak and strong interactions; it can also perform measurements in areas of astrophysics, nuclear, particle and cosmic ray physics. These include the study of atmospheric neutrinos and neutrino oscillations, high energy ($E_\nu \gtrsim 1$ GeV) neutrino astronomy, indirect searches for WIMPs, search for low energy ($E_\nu \gtrsim 7$ MeV) stellar collapse neutrinos, studies of various aspects of the high energy underground muon flux (which is an indirect tool to study the primary cosmic ray composition, origin and interactions), searches for fractionally charged particles and other rare particles that may exist in the cosmic radiation. The mean rock depth overburden is $\simeq 3700$ m.w.e. while the minimum is 3150 m.w.e. This defines the minimum muon energy at the surface at $\sim 1.3$ TeV in order to reach MACRO. The average residual energy and the muon flux at the MACRO depth are $\sim 310$ GeV and $\sim 1$ m$^{-2}$ h$^{-1}$, respectively. The detector has been built and equipped with electronics during the years $1988 - 1995$. It was completed in August 1995 and since the fall of 1995 it is running in its final configuration.

The 1998 highlights have been presented at the 1998 summer conferences and in one paper dedicated to the anomaly on atmospheric neutrinos, suggestive of neutrino oscillations.

# 2   The Detector

The MACRO detector has a modular structure: it is divided into six sections referred to as supermodules. Each active part of one supermodule has a size of $12.6 \times 12 \times 9.3$ m$^3$ and comes with separate mechanical structure and electronics readout. The full detector has global dimensions of $76.5 \times 12 \times 9.3$ m$^3$ and provides a total acceptance to an isotropic flux of particles of $\sim 10,000$ m$^2$ sr. The total mass is $\simeq 5300$ t.

Redundancy and complementarity have been the primary goals in designing the experiment. Since no more than few monopoles can be expected, multiple signatures and ability to perform cross checks among various parts of the apparatus are important.

The detector is composed of three sub-detectors: liquid scintillation counters, limited streamer tubes and nuclear track detectors. Each one of them can be used in "stand-alone" and in "combined" mode. A general layout of the experiment is shown in Fig. 1.

Each supermodule contains 77 scintillation counters, divided into three horizontal (bottom, center, and top) and two vertical (east and west) planes. The bottom and center horizontal planes, along with the lower seven scintillators of the east and west planes, occupy the lower section of each supermodule which is frequently referred to as the *lower* MACRO. The mass of the *lower* MACRO is $\simeq 4200$ t. The top and upper seven scintillators of the east and west planes occupy the upper section of the detector, often referred to as the *Attico*. The lower part of the north and south faces of the detector are covered by vertical walls with seven scintillation counters each. The upper part of these
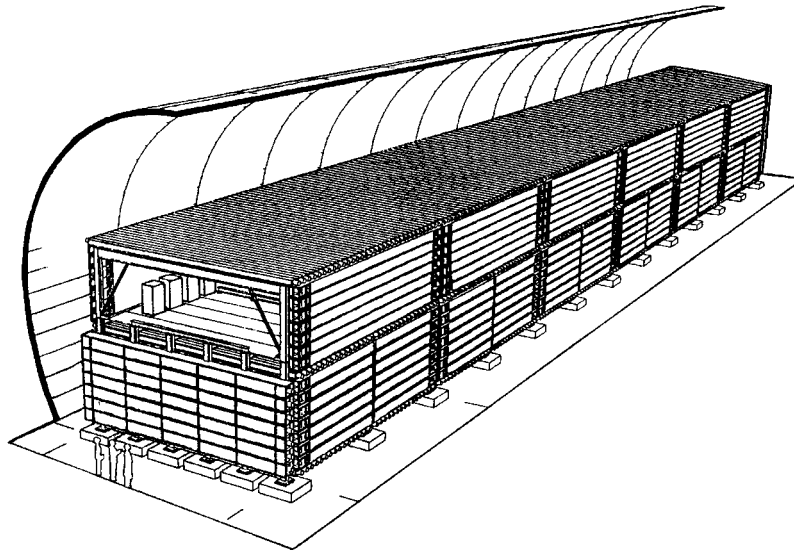
147

Figure 1: General layout of the MACRO detector installed in Hall B of the LNGS. Overall dimensions of the active part are $76.5 \times 12 \times 9.3$ m$^3$.

faces is left open in order to allow access to the readout electronics. The scintillation counters of the horizontal planes measure $11.2 \times 0.73 \times 0.19$ m$^3$, while the vertical ones measure $11.1 \times 0.22 \times 0.46$ m$^3$. All are filled with a mixture of mineral oil (96.4 %) and pseudocumene (3.6 %), with an additional 1.44 g/l of PPO and 1.44 mg/l of bis-MSB as wavelength shifters. The horizontal counters are seen by two 8″ phototubes (PMTs) and the vertical counters by one 8″ PMT at each end. Each PMT housing is equipped with a light collecting mirror. The total number of scintillators is 476 (294 horizontal and 182 vertical) with a total active mass of almost 600 tons. Minimum ionizing muons when crossing vertically the 19 cm of scintillator in a counter release $\simeq 34$ MeV of average energy and are measured with a timing and longitudinal position resolution of $\simeq 700$ ps and $\simeq 10$ cm, respectively.

The scintillation counters are equipped with specific triggers for rare particles, muons and gravitational collapse neutrinos: the Slow Monopole Trigger (SMT) is sensitive to monopoles with velocities from about $10^{-4}c$ to $10^{-2}c$, the Fast Monopole Trigger (FMT) is sensitive to monopoles with velocities from about $5 \times 10^{-3}c$ to $5 \times 10^{-2}c$, the Lightly Ionizing Particle (LIP) trigger is sensitive to fractionally charged particles, the Energy Reconstruction Processor (ERP) and "CSPAM" are primarily muon triggers (but used also for relativistic monopoles) and finally the gravitational collapse neutrino triggers (the Pulse Height Recorder and Synchronous Encoder –PHRASE– and the ERP), optimized to trigger on bursts of low energy events in the liquid scintillator. The scintillator system is complemented by a 200 MHz wave form digitizing (WFD) system that is used in rare particle searches but also on any occasion where knowledge of the PMT waveform is useful.

The lower part of the detector contains ten horizontal planes of limited streamer tubes, the middle eight of which are interleaved by seven rock absorbers (total thickness $\simeq 360$ g cm$^{-2}$). This arrangement sets a $\simeq 1$ GeV energy threshold for muons vertically

crossing the lower part of the detector. In the *Attico* there are four horizontal streamer tube planes, two located above and two below the top scintillator layer. On each lateral wall six streamer tube planes sandwich the corresponding vertical scintillator plane (three streamer planes on each side). Each tube has a $3 \times 3$ cm$^2$ cross section and measures 12 m in length. The total number of tubes is $55,200$ and are all filled with a gas mixture of $He$ (73%) and n-pentane (27%). They are equipped with 100 $\mu$ $Cu/Be$ wires and stereo pickup strips at an angle of 26.5°. The intrinsic position and tracking resolutions of the streamer tube system are $\simeq 1$ cm and $\simeq 0.2°$, respectively. The overall angular resolution is limited to $\simeq 1°$ by the multiple scattering in the rock above the detector. The streamer tubes are read by 8-channel cards (one channel for each wire) which discriminate the signals and send the analog information (time development and total charge) to an ADC/TDC system (the QTP). The discriminated signals are used to form two different chains (Fast and Slow) of TTL pulses, which are the inputs for the streamer tube Fast and Slow Particle Triggers.

The nuclear track detector is deployed in three planes, horizontally in the center of the lower section and vertically on the East and North faces. The detector is divided in $18,126$ individual modules, which can be individually extracted and changed upon need. Each module ($\sim 24.5 \times 24.5 \times 0.65$ cm$^3$ in sizes) is composed of three layers of CR39, three layers of Lexan and 1 mm Aluminium absorber to stop nuclear fragments.

In addition to the three detection elements already described, a Transition Radiation Detector (TRD) was installed in part of the *Attico*, right above the central horizontal plane of the main detector. It is composed of three individual modules (overall dimensions $6 \times 6 \times 2$ m$^3$) and it is made of 10 cm thick polyethylene foam radiators and proportional counters. Each counter measures $6 \times 6 \times 600$ cm$^3$ and is filled with $Ar$ (90%) and $CO_2$ (10%). The TRD provides a measurement of the muon energy in the range of 100 GeV $< E <$ 930 GeV. Although the energy measurement with the TRD saturates at $\sim 930$ GeV, muons of higher energies can still be detected and counted.

# 3   Selected Physics Results

In 1998 six papers were published and in addition two were submitted for publication. The papers concerned the supernova real time neutrino monitor [M1], the detection of upward going charged particles produced by downward going cosmic ray muons [M2], the measurement of the atmospheric neutrino-induced muon flux [M3], the observation of the shadowing of cosmic rays by the moon [M4], the energy spectrum of underground muons measured with the Transition Radiation Detector [M5], the search for dark matter WIMP annihilations in the Earth and the Sun [M6], the measurement of the underground muon pair separation [M7], the search for nuclearites [M8]. Several results appeared in preliminary form in 15 paper contributions that were published in various physics conference proceedings [M9, M23]. They concern the study of atmospheric neutrinos, neutrino astronomy, rare particle searches and the study of muon interactions in the rock above the detector. Three MACRO/Pubs update our results on dark matter WIMPs [M24], on neutrino astronomy [M25] and on searches for magnetic monopoles and nuclearites [M26].
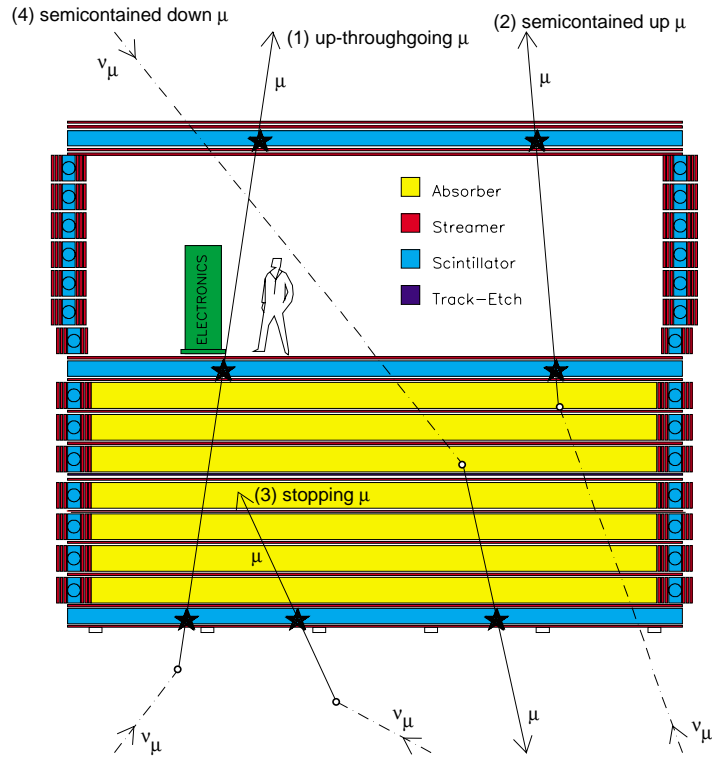
Figure 2: Sketch of different event topologies induced by $\nu_\mu$ interactions in or around MACRO. The stars represent scintillator hits. The time-of-flight of the muon can be measured for *Up Semicontained* and *Up throughgoing* events.

## 3.1 Neutrino-induced Upward Going Muons

Upward going muons are identified using the streamer tube system (mainly for tracking) and the scintillator system (mainly for time-of-flight measurement). A rejection factor of at least $10^5$ is needed in order to separate the up-going muons from the large background coming from the down-going muons. Fig. 2 shows a sketch of the three different topologies of neutrino events analyzed until now: up throughgoing muons, semicontained upgoing muons and up stopping muons+semicontained downgoing muons. Fig. 3 shows the muon-neutrino energy spectra for the three event topologies, computed with Monte Carlo methods. The number of events measured and expected are given in Table 1.

## 3.2 Upgoing charged particles produced by downgoing muons

The background on upgoing muons arising from downgoing muons interacting in the rock around MACRO and giving an upward going charged particle was studied in detail in [M2]. This background is small at MACRO depths when using a tracking system; it is large at lower depths and if no tracking system is present.
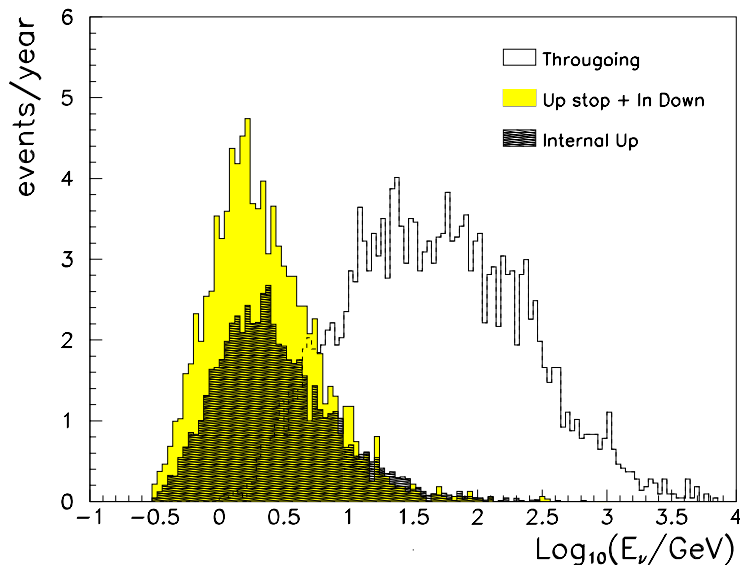
Figure 3: Distribution of the parent muon neutrino energy giving rise to the three different event topologies.

## 3.3    Upgoing $\mu$ flux. Neutrino oscillations

The *up throughgoing muons* come from $\nu_\mu$ interactions in the rock below the detector, with $\overline{E}_\nu \sim$ 100 GeV. The muons ($E_\mu > 1$ GeV) cross the whole detector. The time information provided by the scintillation counters allows the determination of the direction by the time-of-flight (T.o.F.) method. The data presented in Fig. 4a correspond to $\sim 3.5$ live years. In 1997 and 1998 we studied a large number of possible systematic effects that could affect our mesurements. We have shown that no significant systematic problems exist in the detector or in the data analyses. One of the most significant checks was performed using the Wave Form Digitizer of the PHRASE system, completely independent of the ERP system.

The *semicontained upgoing muons* come from $\nu_\mu$ interactions inside the lower apparatus. Since two scintillation counters are intercepted, the T.o.F. is applied to identify the upward going muons. The average parent neutrino energy for these events is $\sim 4$ GeV. If the atmospheric neutrino anomalies are the results of $\nu_\mu$ oscillations with maximum mixing and $\Delta m^2$ between $10^{-3}$ and $10^{-2}$ eV$^2$ one expects a reduction of about a factor of two in the flux of these events, without any distortion in the shape of the angular distribution. This is what is observed in Fig. 5a.

The *up stopping muons* are due to external $\nu_\mu$ interactions yielding upgoing muon tracks stopping in the detector; the *semicontained downgoing muons* are due to $\nu_\mu$ induced downgoing tracks with vertex in the lower MACRO. The events are found by means of topological criteria; the lack of time information prevents to distinguish the two sub samples. An almost equal number of up stopping and semicontained downgoing events is expected, and the average neutrino energy for these events is around 4 GeV. In case of oscillations with the quoted parameters, a similar reduction in the flux of the up stopping events as the semicontained upgoing muons is expected. No reduction is instead expected for the semicontained downgoing events (from neutrinos having path lengths of $\sim 20$ Km).
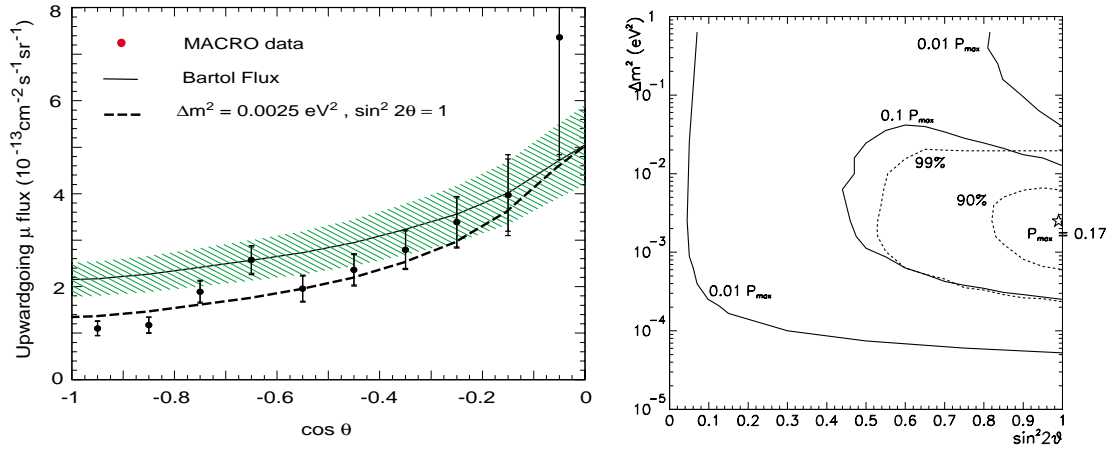
151

Figure 4: MACRO data. (a) Flux of the up throughgoing muons with $E_\mu > 1$ GeV vs. zenith angle $\Theta$. The solid line is the expectation for no oscillations and the shaded region is a 17 % scale uncertainty. The dashed line is the prediction for an oscillated flux with maximum mixing and $\Delta m^2 = 0.0025$ eV$^2$. (b) Probability contours for $\nu_\mu \rightarrow \nu_\tau$ oscillations. The dashed lines are 90 % and 99 % CL contours. The best probability is 17 %; iso-probability contours are shown for 10 % and 1 % of this value (i.e. 1.7 % and 0.17 %).
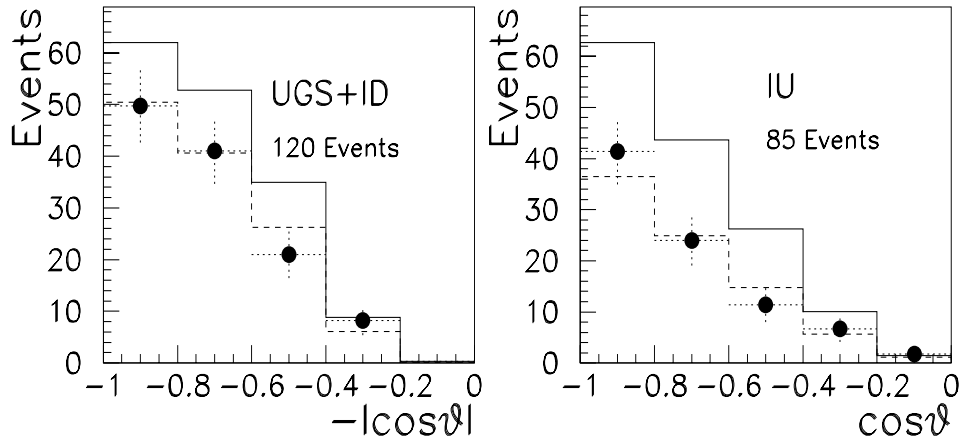


Figure 5: MACRO data. Measured and expected number of low energy events versus zenith angle; left: up stopping plus down semicontained; right: up semicontained. The solid lines are the predictions without oscillations; the dashed lines are the predictions assuming neutrino oscillations with the parameters suggested by the Up throughgoing sample.

|  | Events | Predictions (Bartol neutrino flux) | |
|  | selected | No Oscillations | With oscillations |
| --- | --- | --- | --- |
| Up Through | 451 | $612 \pm 104_{th} \pm 37_{sys}$ | $431 \pm 73_{th} \pm 26_{sys}$ |
| Internal Up | 85 | $144 \pm 36_{th} \pm 14_{sys}$ | $83 \pm 21_{th} \pm 8_{sys}$ |
| In Down+Up Stop | 120 | $159 \pm 40_{th} \pm 16_{sys}$ | $123 \pm 31_{th} \pm 12_{sys}$ |

Table 1: Event summary for the MACRO neutrino flux analysis. The predicted number of events with oscillations are for maximum mixing and $\Delta m^2 = 0.0025$ eV$^2$.

The measured data have been compared with Monte Carlo simulations. In the up throughgoing muon simulation the neutrino flux computed by the Bartol group is used. The cross sections for the neutrino interactions have been calculated using the Morfin and Tung parton distribution set S1. The propagation of muons to the detector has been done using the energy loss calculation by Lohmann *et al.* in standard rock [M3]. The total theoretical uncertainty from neutrino flux, cross section and muon propagation on the expected flux of muons is ~17 %. Fig. 4a shows the zenith angle distribution of the measured flux of up throughgoing muons with energy greater than 1 GeV; the Monte Carlo expectation for no oscillations is shown as a solid line, and for a $\nu_\mu \to \nu_\tau$ oscillated flux with $\sin^2 2\theta = 1$ and $\Delta m^2 = 0.0025$ eV$^2$ is shown by the dashed line. The systematic uncertainty on the up throughgoing muon flux is mainly a scale error that doesn't change the shape of the angular distribution. The ratio of the observed number of events to the expectation without oscillations is $0.74 \pm 0.036_{stat} \pm 0.046_{sys} \pm 0.13_{theor}$ [M3].

The shape of the angular distribution of Fig. 4a has been tested with the hypothesis of no oscillation, giving a $\chi^2$ of 26.1 for 8 degrees of freedom. Assuming $\nu_\mu \to \nu_\tau$ oscillations, the best $\chi^2$ in the physical region of the oscillations parameters is 15.8 for $\Delta m^2 = 0.0025$ eV$^2$ and $\sin^2 2\theta = 1$.

To test oscillation hypotheses, the independent probability for obtaining the number of events observed and the angular distribution for various parameter values have been calculated. The value of $\Delta m^2$ suggested from the shape of the angular distribution is similar to the value needed to obtain the observed reduction in the number of events in the hypothesis of maximum mixing. Fig. 4b shows probability contours for oscillation parameters using the combination of probability for the number of events and the $\chi^2$ of the angular distribution. The maximum probability is 17 %. The probability for no oscillations is 0.1 %.

The MC simulation for the low energy data uses the Bartol neutrino flux and the neutrino low energy cross sections of ref. [1]. The number of events and the angular distributions are compared with the predictions in Table 1 and Fig. 5. The low energy data show a uniform deficit of the measured number of events over the whole angular distribution with respect to the predictions; there is good agreement with the predictions based on neutrino oscillations using the parameters obtained from the up throughgoing muon sample.

Using the double ratio $R = (Data/MC)_{IU}/(Data/MC)_{ID+UGS}$ between data and MC of the two low energy data sets, the theoretical uncertainties on neutrino flux and cross sections almost disappear (a residual 5 % uncertainty remains due to small differences
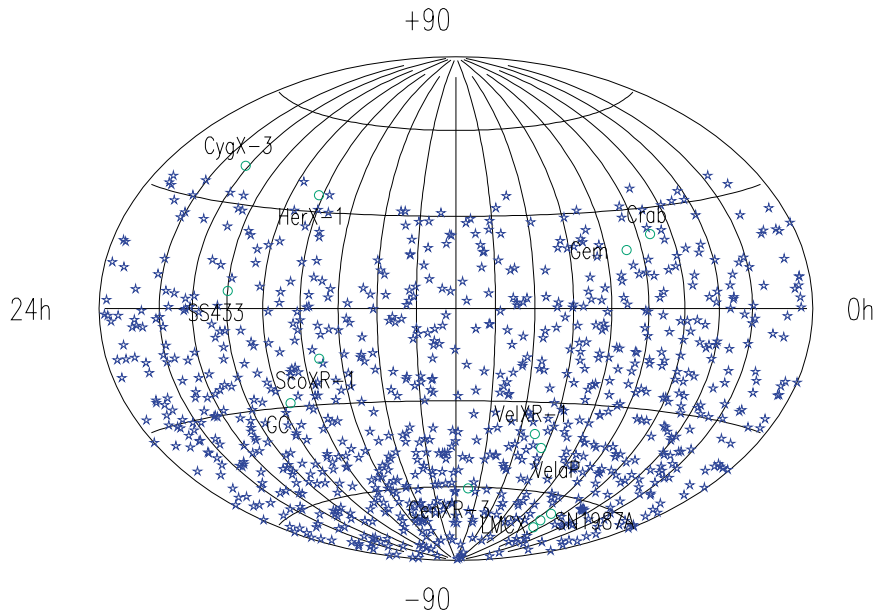
Figure 6: Upgoing muon distribution in equatorial coordinates.

between the energy spectra of the two samples). The systematic uncertainty is reduced to about 5 %. The average value of the double ratio over the measured zenith angle distribution is $R \simeq 0.73$ (with a statistical uncertainty of about 0.12). $R = 1$ is expected in case of no oscillation, also assuming a reduction of the neutrino flux and neutrino cross sections.

These data and the analyses were presented by P. Bernardini at the may 1998 Vulcano workshop [M10], by F. Ronga at the june Neutrino 98 meeting at Takayama [M11], by M. Spurio and A. Surdo at the July 1998 European Cosmic Ray Conference, in Madrid [M15, M16], by T. Montaruli at the July meeting in Heidelberg [M19] and the August meeting in Erice [M20], by D. Michael at the 29th ICHEP in Vancouver, Canada [M17], and in other meetings [M21], [2], [3].

**Search for Astrophysical Point Sources (Neutrino Astronomy)**

The excellent angular resolution of the MACRO experiment allows a sensitive search for up-going muons produced by neutrinos coming from celestial sources, with a negligible atmospheric neutrino background. An excess of events was searched around the positions of known sources in 3° (half width) angular bins. This value was chosen so as to take into account the angular smearing produced by the multiple scattering in the rock below the detector and by the energy-integrated angular distribution of the scattered muon, with respect to the neutrino direction. A total of 909 events observed with MACRO until now was used in this search, see Fig. 6. No excess was observed and the 90 % c.l. limits on the neutrino fluxes from specific celestial sources are in the range of $\sim 10^{-14}$ cm$^{-2}$ s$^{-1}$ and are reported in the papers submitted to the 1998 conferences [M22, M23, M25].

**Indirect Search for WIMPs**

Weakly Interacting Massive Particles (WIMPs) could be part of the galactic dark matter; WIMPs could be intercepted by celestial body, slowed down and trapped in their centers. WIMPs and anti-WIMPs could annihilate and yield up-throughgoing muons.
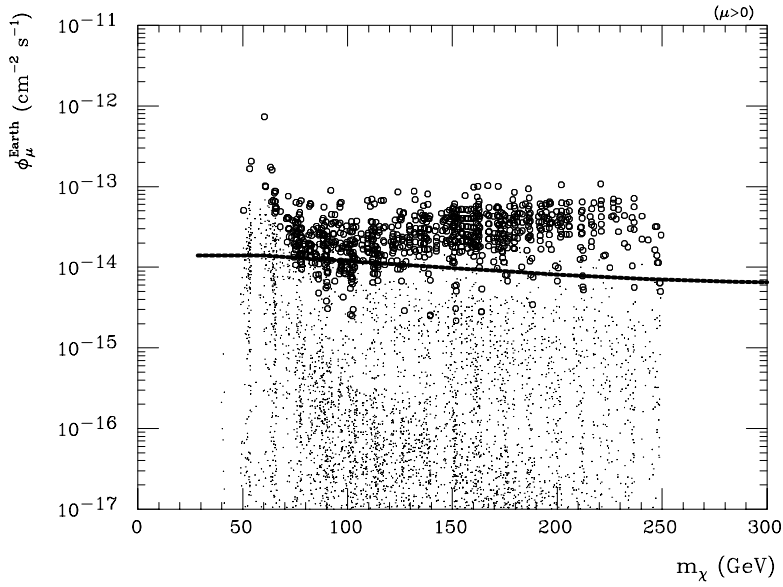
Figure 7: Upward-going muon flux vs neutralino mass $m_\chi$ for $E_\mu{}^{th} = 1$ GeV from the Earth [M6]. Each dot is obtained varying model parameters, leaving $\mu > 0$ ($\mu$ is the higgsino mass parameter); similar results are obtained for $\mu < 0$ [4]. Solid line: MACRO flux limit (90 % c.l.). The solid line representing the flux limit for the no-oscillation hypothesis is indistinguishable in the log scale from the one for the $\nu_\mu \to \nu_\tau$ oscillation hypothesis, but the expectations could be about two times lower. The open circles indicate the models *excluded* by direct measurements (particularly the DAMA/NaI experiment [5]) and assume a local dark matter density of 0.5 GeV cm$^{-3}$.

WIMPs annihilating in these celestial bodies would produce neutrinos of GeV or TeV energy, in small angular windows around their centers. The 90 % c.l. MACRO limit for the flux from the Earth center is $\sim 10^{-14}$ cm$^{-2}$ s$^{-1}$ for a 10° cone around the vertical. For the same cone searched for around the Sun direction, the limit stands at $\sim 1.4 \times 10^{-14}$ cm$^{-2}$ s$^{-1}$ [M6].

If the WIMPs are identified with the smallest mass neutralino, the MACRO limit may be used to constrain the stable neutralino mass, see Figures 7, 8, [M6].

## 3.4    Magnetic Monopoles and Nuclearites

The search for magnetic monopoles (MM) is one of the main objectives of our experiment. Supermassive ($m \sim 10^{17}$ GeV) GUT monopoles are expected to have typical galactic velocities ($\sim 10^{-3}c$) if trapped in our Galaxy. MMs trapped in our solar system or in the supercluster of galaxies may travel with typical velocities of the order of $\sim 10^{-4}c$ or $\sim 10^{-2}c$, respectively. Monopoles in the presence of strong magnetic fields or lighter monopoles in general may reach relativistic velocities. The reference mark in the sensitivity level for a significant MM search is the Parker bound, the maximum monopole flux compatible with
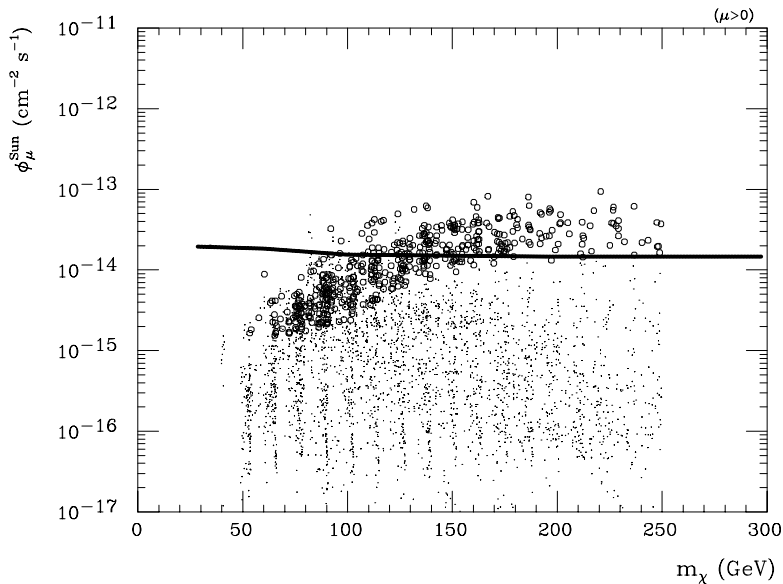
Figure 8: Upward-going muon flux vs $m_\chi$ for $E_\mu^{th} = 1$ GeV from the Sun [4]. In this plot values of $\mu > 0$ are considered. Solid line: MACRO flux limit (90 % c.l.). The open circles concern the regions excluded by direct measurements [5].

the survival of the galactic magnetic field. This limit is $\Phi \lesssim 10^{-15}$ cm$^{-2}$ s$^{-1}$ sr$^{-1}$, but it can be reduced by almost an order of magnitude when considering the survival of a small galactic magnetic field seed. Our experiment was designed to reach a flux sensitivity well below the Parker bound, in the MM velocity range of $4 \times 10^{-5} < \beta < 1$. The three MACRO sub-detectors have sensitivity in wide $\beta$-ranges with overlapping regions, thus allowing multiple signatures of the same rare event candidate. No candidates were found in several years of data taking by any of the various subdetectors.

The limits set by different analyses were combined to obtain a global MACRO limit. For each $\beta$ value, the global time integrated acceptance was computed as the sum of the independent portions of each analysis. The MACRO limit is shown in Fig. 9 together with those set by other experiments [M18, M26], [6].

The searches based on the scintillator and the nuclear track subdetectors were also used to set new limits on the flux of cosmic ray nuclearites, see Fig. 10, [M8, M18, M26], [6].

Finally, work is in progress in order to compute the energy losses of magnetic monopoles and dyons in the Earth and in the MACRO subdetectors for various particle masses and velocities [7]. This will allow a complete interpretation of all limits for monopoles of multiple charges, monopole composites as well as for monopoles of any given mass.

## 3.5 Neutrinos from Stellar Gravitational Collapses

A stellar gravitational collapse (GC) is expected to produce a large burst of $\bar{\nu}_e$'s with energy $7 - 30$ MeV and with a duration of $\sim 10$ s. These $\bar{\nu}_e$'s can be detected via the process $\bar{\nu}_e + p \to n + e^+$ in the liquid scintillator. About $100 \div 150$ $\bar{\nu}_e$ events should be detected in MACRO for a stellar collapse at the center of our Galaxy. We employ
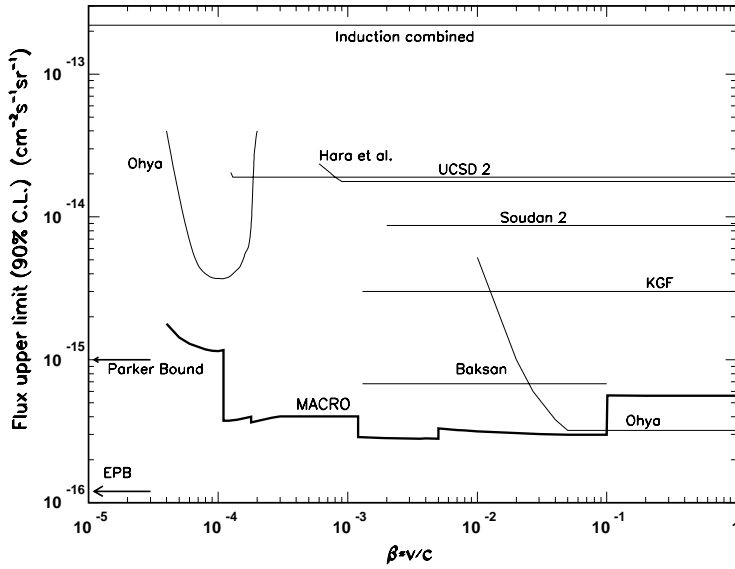
Figure 9: Magnetic monopole flux upper limits at the 90 % c.l. obtained by MACRO and other experiments. The limits apply to singly charged ($g = g_D$) monopoles assuming that catalysis cross sections are smaller than a few mb.
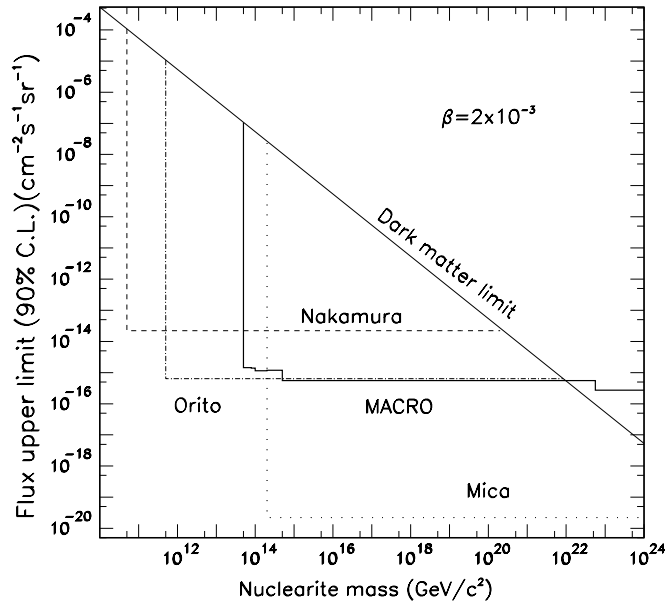


Figure 10: 90 % c.l. flux upper limits vs mass for nuclearites with $\beta = 2 \cdot 10^{-3}$ at ground level. Nuclearites of such velocity could have galactic or extragalactic origin. The MACRO direct limit (solid line) is shown along with the limits of Refs [8] (dashed line), [9] (dot-dashed line) and the indirect mica limits of Refs. [10], [11] (dotted line). The MACRO limit for nuclearite masses larger than $5 \cdot 10^{22}$ GeVc$^{-2}$ corresponds to an isotropic flux

157

two electronic systems that provide sensitivity to GC neutrinos. One is based on the dedicated PHRASE trigger and the other one on the ERP trigger. Both systems have an energy threshold of $\sim 7$ MeV and record pulse shape, charge and timing information. After a $\sim 7$ MeV trigger, the PHRASE system lowers its threshold for $\simeq 800\ \mu$s to detect (with a $\simeq 25\,\%$ efficiency) the 2.2 MeV $\gamma$ released in the reaction $n + p \rightarrow d + \gamma_{2.2\ \mathrm{MeV}}$ induced by the neutron of the primary process. A redundant supernova alarm system is in operation, alerting immediately the physicists on shift. We have defined a general procedure to alert the physics and astrophysics communities in case of an interesting alarm [M1]. Finally, a procedure to link the various supernova observatories around the world (MACRO, SuperKamiokande, LVD, SNO and other neutrino observatories able to generate a prompt alarm) was set up. The MACRO active mass is $\sim 560$ t; the live-time fraction in the last three years was $\simeq 97.5\,\%$. No stellar gravitational collapses were observed in our Galaxy since 1989.

## 3.6   Cosmic Ray Muons

MACRO large area and acceptance ($\sim 10000\ m^2$ sr for an isotropic flux) allow to study many aspects of physics and astrophysics of cosmic ray muons. We have recorded $\sim\ 47 \times 10^6$ muons and we keep collecting them at the rate of $\simeq 18,000/$day.

**Intensity**

The underground muon intensity vs. rock thickness provides information on the high energy ($E \gtrsim 1.3$ TeV) atmospheric muon flux and on the all-particle primary cosmic ray spectrum. The results can be used to constrain the models on cosmic ray production and interaction. The analysis performed in 1995 covered the overburden range $2200 \div 7000$ hg/ cm$^2$; a new analysis is under development to extend the results to larger rock thicknesses.

**Decoherence**

The decoherence function is the distribution of the distance between pairs of muons in a multimuon event. This function is the result of the convolution of separate and competing factors: the production height of the muon parent mesons (and hence the primary Cosmic Ray cross section), the muon multiple scattering through the rock, the earth magnetic field and the muon parent mesons transverse momentum ($P_t$) distribution. The shape of the decoherence function has a weak dependence on primary mass composition. In MACRO, muon pair separations up to 70 m can be measured, corresponding to parent mesons with $P_t \leq 1 \div 2$  GeV/c. The resolution of the apparatus allows an accurate study of the low distance separation region: the accuracy of the measurement is such that the possible contribution of rare processes, such as $\mu^\pm + N \rightarrow \mu^\pm + N + \mu^+ + \mu^-$, can be experimentally studied.

The measured decoherence function is compared with the predictions of the hadronic interaction model of the HEMAS Monte Carlo code. Good agreement is obtained. We interpret this agreement to indicate that no anomalous $P_\perp$ components in soft hadron-Nucleus and Nucleus–Nucleus collisions are required by our experimental data. A new unfolding procedure has been designed and implemented to minimize systematic errors in the numerical algorithm [M7]. Fig. 11a shows the comparison between unfolded experi-
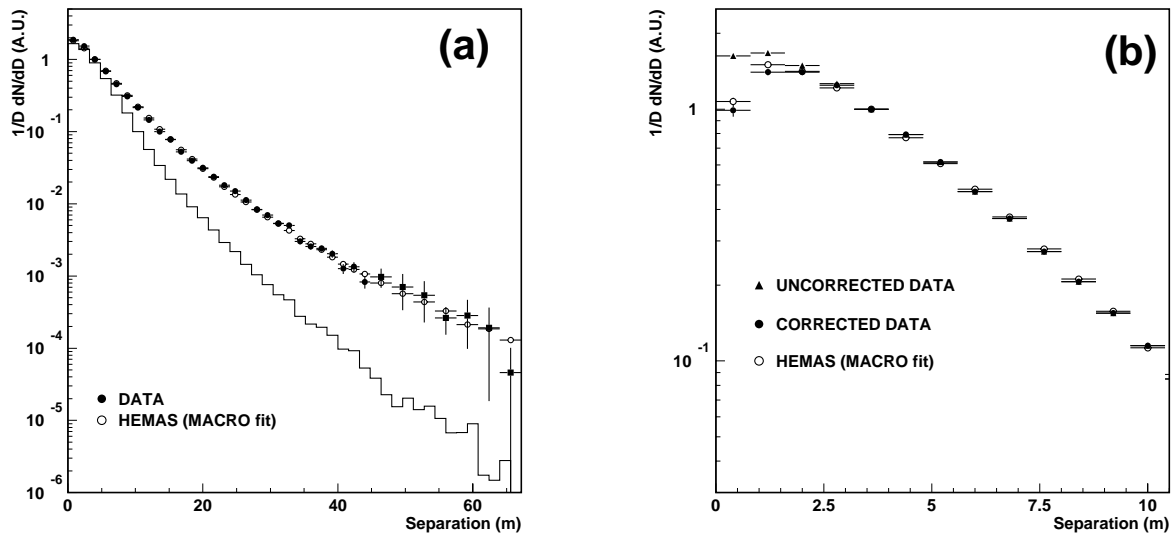
Figure 11: (a) True unfolded experimental decoherence distribution for an infinite detector (black points) compared with Monte Carlo expectation (white points). For comparison, the measured decoherence distribution without unfolding (histogram) is superimposed to the plot. (b) The low distance region of the experimental decoherence function, before and after the subtraction of the secondary muon sample, and comparison with the Monte Carlo simulation.

mental data and the Monte Carlo simulation. The discrepancy which existed in previous analyses in the first bins of the distributions is due to the muon pair production process. This is shown in Fig. 11b, where the low distance region is shown in more detail. The discrepancy is completely eliminated if such a process is taken into account. With these final corrections, we obtain an average detector-independent separation between muons of $\simeq 10.1$ m.

### Muon Astronomy

In the past some experiments have reported possible excesses of muons from the direction of known astrophysical sources, expecially Cyg X-3. Our data has not indicated any significant excess above the statistical background, both for steady dc fluxes and for modulated ac fluxes. These results can be used to constrain some spectral parameters of $\gamma$ fluxes from selected sources. Our most recent analyses reported muon flux limits from various sources (Crab Nebula, Cyg X-3, MRK 421 etc.) at the level of $(0.4 \div 8) \times 10^{-14}$ cm$^{-2}$ s$^{-1}$. For several sources (e. g. Vela Pulsar) our limits are the best existing.

A search for sidereal anisotropies (modulations in arrival times introduced by the galaxy's rotational motion through the extragalactic cosmic rays) is also in progress. The muon data sample is analyzed searching for periodic modulations. The amplitude of the modulations are at the level of $\sim 0.2\%$. We are increasing the statistics and improving the systematics in order to obtain a significant result by adding a few more years of data to our current sample.

### Seasonal Variations

Underground muons are produced by mesons decaying in flight in the upper atmosphere. The muon flux thus depends on the ratio between the decay and the interaction
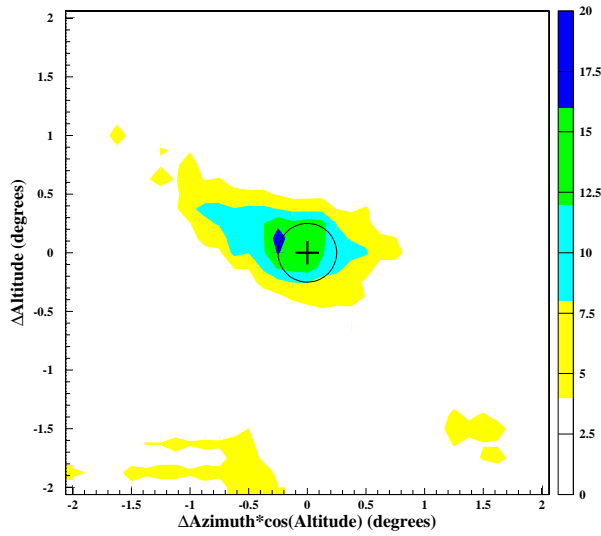
Figure 12: Muon event density map in angular coordinates; the Moon is at (0,0). The various regions of increasing gray scale indicate various levels of deficit in percent. The darkest one corresponds to the maximum deficit.

probability of the parent mesons, which is sensitive to the atmospheric density, and so, to its average temperature. The flux is expected to decrease in winter, when the temperature is lower and the atmosphere more dense, and to increase in summer. This correlation leads to variations at the level of 2 % to 3 %.

**Moon Shadow**

The pointing capability of MACRO was demonstrated searching for the shadow of the Moon, which produces a "shield" to the cosmic rays. We used a sample of $\sim 40 \times 10^6$ muons, looking at the density of the events as a function of the angular distance from the center of the Moon position [M4]. In Fig. 12 we show a two-dimensional plot of the significance of the muon deficit caused by the Moon. The Moon is placed at coordinates $(0,0)$; the darkest region corresponds to a maximum observed deficit of $\simeq 200$ events in the bin of coordinates $(-0.25, +0.125)$. The observed displacement of the maximum deficit is consistent with the displacement of the primary protons due to the geomagnetic field. The Moon shadow has been observed by several EAS, see [12]. We have started an analysis to observe the shadow from the sun; it requires more statistics, which can be obtained in few more years of data taking.

**Photonuclear interactions of downgoing muons in the rock above MACRO**
Fig. 13 shows an example of one muon photonuclear interaction in the rock above MACRO. The process was studied in detail and the frequency of such events relative to the number of downgoing single muons, $R_{\mu+h} = N_{\mu+h}/N_\mu$, was measured. The predictions of the FLUKA Monte Carlo ($R_{\mu+h}(MC\ FLUKA) = (1.89\pm0.16_{stat}\pm0.02_{syst})\cdot10^{-4}$) are in good agreement with the measured rates ($R_{\mu+h}(DATA) = (1.91\pm0.05_{stat}\pm0.03_{syst})\cdot10^{-4}$), while those of the hadronic interface of the GEANT code ($R_{\mu+h}(MC\ GEANT) = (1.31\pm 0.14_{stat} \pm 0.02_{syst}) \cdot 10^{-5}$) are inadequate [M9, M13].
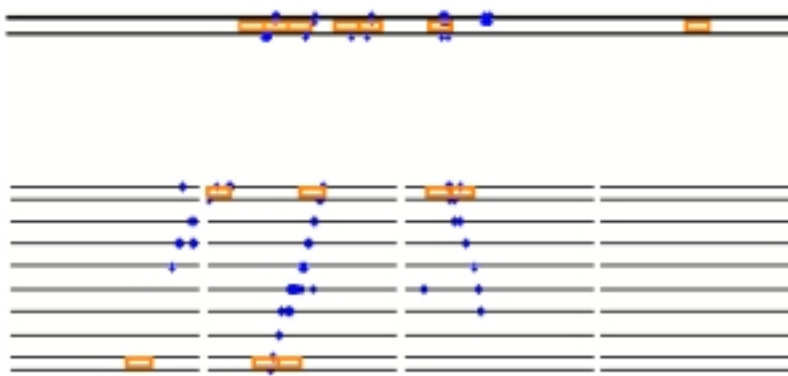
Figure 13: An example of a muon photonuclear interaction in the rock above MACRO [M9, M13].

### Measurement of the Muon Energy with the TRD Detector

The differential energy spectrum of single muons reaching MACRO was measured by the TRD detector and is shown in Fig. 14 [M5]. The systematic errors, mainly due to calibration uncertainties, are included in the error bars. The average single muon energy is $320 \pm 4_{stat} \pm 11_{sys}$ GeV. More data with the three TRD modules will improve significantly the data of Fig. 14. Moreover it may yield a significant number of upgoing high energy muons which may be of help in neutrino astronomy.

## 3.7  Cosmic Ray Composition

One of the most important aspects of the cosmic ray physics with MACRO is the indirect study of the primary composition through the detection of muons. This study of composition is particularly interesting in the region of the "knee" ($10^3$ TeV $\lesssim E \lesssim 10^4$ TeV) as it may lead to a better understanding of the cosmic rays origin.

The basic idea used in this study is that the multiplicity of the muons observed in an underground experiment is sensitive to the primary composition. If one fixes the energy of the primary cosmic ray, the multiplicity of the pions produced by heavy nuclei is higher than that of the pions produced by protons.

The underground muon data were simulated with a detailed HEMAS-based Monte Carlo code, which includes a hadronic interaction model, the air shower development, the propagation of the muons in the rock, the detector response, etc. Since the HEMAS hadronic model is not completely satisfactory in explaining the MACRO/EAS-TOP data, an independent code based on the DPMJET hadronic model is under development.

### MACRO/EAS-TOP Correlations

New types of studies have been started with the events detected in coincidence with the EAS-TOP surface array. Besides the usual sample of events consisting of $N_\mu$(MACRO)–$N_e$(EAS-TOP) coincidences (1.7 yrs of live time in coincidence are now fully analysed), two other new activities have been started:

1. Coincidences between the underground muons and the Cherenkov light detectors by EAS-TOP.
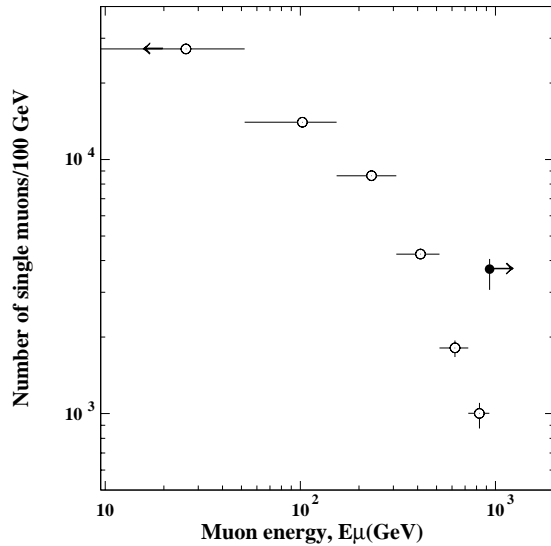
161

Figure 14: Differential energy spectrum of single muons reaching MACRO measured with the TRD detector. The arrow indicates the TRD response saturation at 930 GeV [M5].

2. 3–fold coincidences, including e.m. size, and GeV muons detected at the surface by EAS-TOP and TeV muons detected underground by MACRO.

The sample of events in coincidence with the Cherenkov detectors (about 1 event/hour in the dark night runs) allows to lower the threshold of the coincidence to few TeV of primary energies (in the range 5÷ 10 TeV of protons). In that case, MACRO can study the yield of underground muons as a function of primary energy. This helps in the discrimination of the hadronic interaction models used for the shower simulation.

The 3–fold coincidences instead, should allow a better discrimination of events produced by the heavy primary component, thus allowing a determination of the evolution of this fraction of primaries as a function of shower size.

In order to study these new categories of events, new simulations have being started, with the aim of testing a variety of composition and interaction models. For this purpose, the migration of event generation from the HEMAS and HEMAS/DPMJET packages to CORSIKA is now in progress. The latter allows the simulation of low energy components at the surface, including Cherenkov light, and is interfaced to different hadronic interaction models. Among them, also DPMJET is included, so that these coincident data can be also used to check the predictions of different codes based on the same interaction model.

Results on these topics will be available next year.

# 4   Nuclear Track Detector Calibrations

We have continued the calibrations of the nuclear track detector with both slow and fast ions. In all measurements we have seen no deviation of its response from the restricted
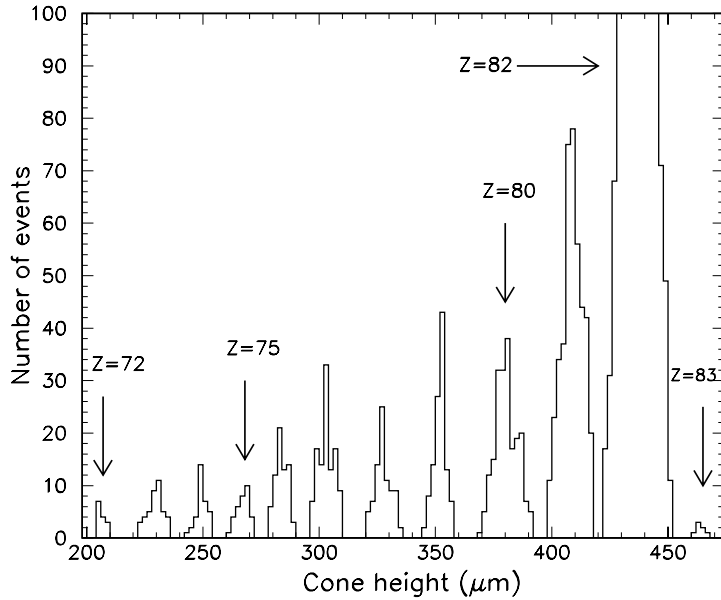
162

Figure 15: Cone height distribution for the fragmentation products of 160 GeV/nucleon $^{208}Pb$ ions hitting a lead target and detected in CR39.

energy loss (REL) model. To complete the calibration, nuclear track detector stacks made of CR39 and Lexan foils were exposed to $^{207}Pb$ ions of 160 GeV/nucleon at the CERN SPS before and after various targets. In traversing the target, the lead ions produce nuclear fragments with $Z < 82$ thus allowing a measurement of the response of the detector in a $Z$ regime most relevant to the detection of fast, relativistic monopoles. For the calibration in the range $75 < Z < 83$ we have used the etched cone height technique in order to separate the nuclear fragments. An example of distribution is shown in Fig. 15, where the various groupings of cone heights are identified with the $Z$ of the fragment. One may appreciate the very good resolution of the detector even at high $Z$ which complements its low threshold ($Z \sim 5$) and excellent resolution at low $Z$ which we have reported previously [13].

# 5   Conclusions

The MACRO detector is running smoothly in its final configuration. The experiment is now in a long-term running and data analysis phase. In 1998 we have extended most of our analyses and searches. We obtained important results on atmospheric neutrinos and more stringent limits on monopoles, nuclearites, WIMPs, astrophysical point sources, sidereal anisotropies, etc. Analyses sensitive to detector and Monte Carlo systematics have been refined and improved to yield solid results in many fields of high energy neutrino physics and of cosmic ray physics. No stellar gravitational collapse neutrinos have been observed since 1989; our on-line monitor is now integrated in a world supernova watch system.

The present data rate for high energy muon neutrinos is (in parentheses is the number

163

of events we have up to Jan 31, 1999):
- Muon neutrinos for neutrino astronomy: 215 / yr ($\sim$ 1000);
- Up throughgoing muons: 140 / yr ($\sim$ 640);
- Semicontained events: 25 / yr ($\sim$ 115);
- Upstopping plus down semicontained: 45 / yr ($\sim$ 180).
These rates are approximate since they depend on the cuts used for the different analyses.

# 6 List of MACRO publications, conference proceedings and memos MACRO/PUBs during 1998

[M1] MACRO Collaboration, M. Ambrosio et al., "Real time supernova neutrino burst detection with MACRO", Astropart. Phys. **8** (1998) 123 and INFN-AE **97/44** (1997).

[M2] MACRO Collaboration, M. Ambrosio et al., "The observation of upgoing charged particles produced by high energy muons in underground detectors", Astropart. Phys. **9** (1998) 105; INFN-AE **97/55** (1997) and hep-ex/9807032.

[M3] MACRO Collaboration, M. Ambrosio et al., "Measurement of the atmospheric neutrino-induced upgoing muon flux using MACRO", Phys. Lett.**B434** (1998) 451; INFN/AE **98/13** (1998) and hep-ex/9807005.

[M4] MACRO Collaboration, M. Ambrosio et al., "Observation of the shadowing of cosmic rays by the moon using a deep underground detector", accepted for publication on Phys. Rev. D; INFN/AE **98/14** (1998) and hep-ex/9807006.

[M5] MACRO Collaboration, M. Ambrosio et al., "Measurement of the energy spectrum of underground muons at Gran Sasso with a Transition Radiation Detector", Astropart. Phys. **10** (1999) 11; INFN/AE **98/15** (1998) and hep-ex/9807009.

[M6] MACRO Collaboration, M. Ambrosio et al., "Limits on dark matter WIMPs using upward-going muons in the MACRO detector", submitted to Phys. Rev. D and hep-ex/9812020.

[M7] MACRO Collaboration, M. Ambrosio et al., "High statistics measurement of the underground muon pair separation at Gran Sasso", submitted to Phys. Rev D; INFN/AE **99/04** (1999) and hep-ex/9901027.

[M8] MACRO Collaboration, M. Ambrosio et al., "Nuclearite search with the MACRO detector at Gran Sasso", submitted to Europhys. Jour.

[M9] G. Battistoni, "Study of photonuclear interaction of muons in rock with the MACRO experiment", hep-ex/9809006, Vulcano Workshop on Frontier Objects in Astrophysics and Particle Physics, May 25-30 1998.

[M10] P. Bernardini, "Atmospheric neutrino induced muon flux measurement with MACRO", hep-ex/9809003, Vulcano Workshop on Frontier Objects in Astrophysics and Particle Physics, May 25-30 1998.

[M11] F. Ronga, "Measurements of the atmospheric neutrino-induced muon flux using MACRO", hep-ex/9810008, Neutrino 98, Takayama, Japan, 4-9 June 1998.

[M12] O. Palamara, "Relevance of the hadronic interaction model in the interpretation of the multiple muon data as detected in the MACRO experiment", Int. Symp. on Very High Energy Cosmic Ray Interactions, Laboratori Nazionali del Gran Sasso, 12-17 July 1998.

[M13] G. Battistoni and E. Scapparone, "Hint of $\mu + n \rightarrow \mu + n + \mu^+ + \mu^-$ process observation with the MACRO detector at Gran Sasso", hep-ex/990218, International Symposium on Very High Energy Cosmic Ray Interactions, Laboratori Nazionali del Gran Sasso, 12-17 July 1998.

[M14] E. Scapparone, "Study of photonuclear interaction of muons in rock with the MACRO experiment", hep/ex-990216, International Symposium on Very High Energy Cosmic Ray Interactions, Laboratori Nazionali del Gran Sasso, 12-17 July 1998.

[M15] M. Spurio, "Measurements of the atmospheric neutrino-induced muon flux using MACRO", hep-ex/9808001, European Cosmic Ray Conference, Madrid, 20-25 July 1998.

[M16] A. Surdo, "Measurement of the atmospheric neutrino-induced upward-going muon flux with the MACRO detector", European Cosmic Ray Conference, Madrid, 20-25 July 1998.

[M17] D. Michael, "Measurements of atmospheric neutrinos with MACRO", 29th ICHEP, Vancouver, Canada, 22-30 July 1998.

[M18] F. Cei, "Search for rare particles with the MACRO detector", hep-ex/9810012, 29th ICHEP, Vancouver, Canada, 23-29 July 1998.

[M19] T. Montaruli, "Atmospheric and astrophysics neutrinos with MACRO", hep-ex/9810017, Dark Matter in Astrophysics, Heidelberg, 20-25 July 1998.

[M20] T. Montaruli, "Atmospheric neutrinos with MACRO", Erice Summer School, August 1998.

[M21] M. Spinetti, "Measurements of the atmospheric neutrino-induced muon flux using MACRO", Neutrino Oscillation Workshop, Amsterdam, 7-9 September 1998.

[M22] T. Montaruli, F. Ronga, "Search for a possible space-time correlation between high energy neutrinos and gamma-ray bursts", astro-ph/9812333, Proc. of Gamma-Ray Bursts in the Afterglow Era, Rome, November 3-6 1998, Submitted to Astronomy and Astrophysics (Supplement Series).

[M23] F. Ronga, "Neutrino astronomy", 1997 ICRC, Durban, South Africa; A. Di Credico, "Neutrino Astronomy", WIN99, Capetown.

[M24] MACRO/Pub 98/1 - Limits on dark matter WIMP particles using upward-going muons in the MACRO detector - MACRO Collaboration, M. Ambrosio et al.

[M25] MACRO/Pub 98/2 - Neutrino astronomy with the MACRO detector - MACRO Collaboration, M. Ambrosio et al.

[M26] MACRO/Pub 98/3 - Search for magnetic monopoles and for nuclearites with the MACRO detector at Gran Sasso - MACRO Collaboration, M. Ambrosio et al.

[M27] Posters presented at the 1998 Meeting of the Italian Physical Society (SIF) and at the Fifth School on Particle Astrophysics, Trieste 29 june-10 july 1998; see also: **http://infn-bo-macro1.bo.infn.it:8080/macro_pict.htm**.

# 7 References

[1] P. Lipari et al., Phys. Rev. Lett. **74** (1995) 384.

[2] G. Giacomelli and M. Spurio, "Atmospheric neutrinos and neutrino oscillations", Lecture at the Fifth School on Particle Astrophysics, Trieste 29 June-10 July 1998; hep-ph/9901355.

[3] M. Spinetti, "Recenti risultati e prospettive dello studio dei neutrini atmosferici", 1998 Meeting of the Italian Physical Society (SIF).

[4] A. Bottino, N. Fornengo, F. Donato and S. Scopel (private communication). N. Fornengo, to appear in the Proceedings of the Ringberg Euroconference "New Trends in Neutrino Physics" (Ringberg Castle, Tegernsee, Germany, May 1998), edited by B. Kniel (World Scientific, Singapore).

[5] R. Bernabei et al., Phys. Lett. B **389** (1996)757.

[6] G. Giacomelli and L. Patrizii, "Magnetic monopoles", Lecture at the Fifth School on Particle Astrophysics, Trieste 29 June-10 July 1998, DFUB 98/30.

[7] J. Derkaoui et al., Astropart. Phys. **9** (1998) 173; "Energy losses of magnetic monopoles and dyons in scintillators, streamer tubes and nuclear track detectors", DFUB 98/13 (1998), to be published on Astrop. Phys.;

[8] S. Nakamura et al., Phys. Lett. **B263** (1991) 529.

[9] S. Orito et al., Phys. Rev. Lett. **66** (1991) 1951.

[10] P. B. Price, Phys. Rev. **D38** (1988) 3813.

[11] D. Ghosh and S. Chatterjea, Europhys. Lett. **12** (1990) 25.

[12] M. Aglietta et al., N.I.M.**A336**(1993) 310.

[13] MACRO Coll.,"Annual Report 1996 - Laboratori Nazionali del Gran Sasso"; P. Serra et al., "Total charge changing cross section of 158 A GeV *Pb* ions in different targets with nuclear track detectors", proceedings of the XXV ICRC Conference, Durban (South Africa), 28 july - 8 August 1997 and DFUB **10/97** (1997)

# MIBETA. A cryogenic experiment on double beta decay and search for rare event

A.Alessandrello[a], C.Brofferio[a], C. Bucci[b], O.Cremonesi[a],
E.Fiorini[a], A.Giuliani[a], A. Nucciotti[a], M.Pavan[a],
G.Pessina[a], S. Pirro[a], E.Previtali[a], M.Vanzini[a],
L.Zanotti[a]

[a]Dipartimento di Fisica dell'Università di Milano e INFN, Sezione di Milano

[b]INFN - Laboratori Nazionali del Gran Sasso

### Abstract

The activity of the group has been mainly carried out with the two dilution refrigerators operating in Hall A and C and with the Ge detectors operating in the low background laboratory. The main achievements have been the full operation of the 20 crystal arrays in Hall A and the tests carried out in Hall C with crystals of $TeO_2$ enriched in $^{128}Te$ and $^{130}Te$ and with new large crystals of natural $TeO_2$ . These last results are essential for the planning on the experiment CUORICINO, recently approved by the Gran Sasso Scientific Committee. We would like to stress that these are the largest thermal detectors operating underground. The results obtained with the enriched crystals will be essential for the determination of the two neutrino double beta decay of $^{130}Te$.

## 1 Operation and first results of the array of twenty $TeO_2$ thermal detectors

In the first months of 1998 the array of twenty $TeO_2$ detectors of 340 g each was successfully starting its operation. We would like to note that with its mass of 6.8 kg it represents by far the most massive thermal detector operating in the world. After a few months this preliminary run was interrupted in order to improve the performance of the detectors and of the read out electronics and to install, in addition to the previously mounted cylinders of Roman lead above and below the array, a lateral internal shield of 1 cm thickness of the same lead. This operation allowed a substantial reduction of the background especially in the low energy region, which is essential for searches on Dark Matter Particles and on solar axions. The operation of the array restarted in summer and at the end of the year the collected

statistics allowed to set the following lower limits on the lifetimes for various channels of double beta decay:

a. 4 x $10^{20}$ years for two neutrino double beta decay

b. $10^{21}$ for neutrinoless double beta decay with the emission of a majoron

c. $10^{23}$ years for neutrinoless double beta decay.

We would like to note that the first limit is already very near to the values obtained indirectly by geochemical experiments, and already excludes the predictions of some theoretical models. The limits on the majoron induced and neutrinoless double beta decay are the most sensitive after the most recent experiments carried out with germanium diodes.

# 2 Measurements carried out in hall C

In the dilution refrigerator in Hall C we have carried out a series of measurements leading to technical developments of the detectors to be operating in Hall A. Two of them seem to us of particular importance:

a. we have operated two crystals of $TeO_2$ of 3x3x6 $cm^3$ produced from powder enriched in $^{130}$Te and two similar crystals produced from powder enriched in $^{128}$Te. The good operation of these crystals, which could have been endangered by the enrichment process, is essential for a planned measurements by our group of the two neutrino double beta decay of $^{130}$Te. As it is well known the only existing results on double beta decay of this isotope are based from geochemical experiments, which strongly disagree among themselves. In addition geochemical experiments cannot obviously distinguish among the various channels of double beta decay. We are convinced that the best way to determine the rate for two-neutrino double beta decay is based in the comparison between spectra obtained with materials enriched in two different , but near, Tellurium isotopes. The four enriched crystals have been successfully tested and are going to be inserted in the 20 crystal array operating in Hall A.

b. we have successfully operated in Hall C crystals of 5x5x5 $cm^3$ of natural $TeO_2$. Their mass (770 g) is the largest for any underground thermal detector. These crystals are in fact planned for the recently approved CUORICINO experiment, as well as for the planned experiment CUORE. The results obtained with these very massive detectors have been excellent: their resolution has been found to be the same as for the 3x3x6 $cm^3$ crystals despite the much larger mass. This is mainly due to a better suspension and to a more appropriate choice of the thermistors.

# 3 References

[1] A. ALESSANDRELLO, C. ARPESELLA, C. BROFFERIO, C. BUCCI, C. CATTA-DORI, O. CREMONESI, E. FIORINI, A. GIULIANI, S. LATORRE, A. NUCCIOTTI, E. ORVINI, M. PAVAN, S. PARMEGGIANO, M. PEREGO, G. PESSINA, S. PIRRO, E. PREVITALI, B. ROMUALDI, A. ROTILIO, and L. ZANOTTI: Measurements of the internal radioactive contamination in samples of Roman lead to be used in experiments on rare events, Nucl. Instrum. and Meth. B 142 (1998) 163

[2] A. ALESSANDRELLO, C. BROFFERIO, D.V. CAMIN, O. CREMONESI, E. FIORINI, A. GIULIANI, A. NUCCIOTTI, M. PAVAN, G. PESSINA, S. PIRRO, E. PREVITALI, L. ZANOTTI and C. BUCCI: Preliminary results on double beta decay of $^{130}$Te with an array of twenty cryogenic detectors, Phys. Lett. B 433 (1998) 156

[3] E. FIORINI: CUORE: a Cryogenic Underground Observatory for Rare Events, Physics Reports 307 (1998) 309

[4] E.FIORINI et al.: Cryogenic Detectors, in Progress in Detectors, Ed.by H.Morsi, N. Kroo and C. Ayache, Brussels 1998, page 58

# THEORY

Components of the group:  V.Berezinsky, A. F. Grillo, M.P. Lombardo
R. Aloisio [a], G. Di Carlo[b], A. Galante [a,b] and M.Kachelriess [c].
Visitors: B.Hnatyk[d], V. Dokuchev[e], A. Gazizov[f].
The group worked in close collaboration with
V. Azcoiti[g], P. Blasi[h], E. Follana[g],
A.Vilenkin [i], M. Lissia[l].


[a] Physics Department, University of L' Aquila, Italy;
[b] Laboratori Nazionali di Frascati, Italy;
[c] Bochum University, Germany; [d] Lviv University, Ukraine;
[e] Institute for Nuclear Research, Moscow, Russia; [f] Institute of Physics, Minsk, Belarus;
[g] Physics Department, University of Zaragoza, Spain; [h] Chicago University, USA;
[i] Tufts University, USA; [l] Physics Department, University of Cagliari, Italy;

### Abstract

The activity of the group has concerned research in two main areas:  Astroparticle
Physics and Cosmology, and Lattice Gauge Theory.

## 1 Astroparticle Physics

The Astroparticle group of LNGS in 1998 included V.Berezinsky, M.Kachelriess and visitors B.Hnatyk, V.Dokuchev, and A.Gazizov.  The group worked in close collaboration with A.Vilenkin, P.Blasi, with Ferrara group (G.Fiorentini et al) and with M.Lissia


**Scientific work**

The main field of the work is astroparticle physics, including solar neutrinos, ultra high energy cosmic rays, topological defects and relativistic astrophysics.

From several works finished in 1998 or in progress now, the following results can be singled out.

V.Berezinsky, G.Fiorentini and M.Lissia have analyzed the high energy excess in the boron solar neutrino spectrum recently found in Superkamiokande experiment.  This excess was thought to be impossible to explain by both MSW effect and vacuum oscillations. It was shown that vacuum oscillations describe well this excess if the boron neutrino flux is 20% less than the SSM prediction and the chlorine signal is 30% higher than measured

in the Homestake experiment. The anomalous seasonal variation of $Be$ neutrino signal is very specific in this case: it has a half-year period and large amplitude. There is an indication to such variation in the GALLEX signal.

V.Berezinsky and M.Kachelriess studied the QCD cascades at very high energies with supersymmetric effects taken into account. The analitic limiting spectrum of partons in MLLA approximation was obtained. Now the Monte Carlo simulation for the hadrons produced in these cascades is in progress. These results are important for calculations of spectrum of Ultra High Energy Cosmic Rays produced at the decays of superheavy particles.

V.Berezinsky, P.Blasi and A.Vilenkin have analyzed Topological Defects as sources of Ultra High Energy Cosmic Rays. It was demonstrated that ordinary and superconducting cosmic strings are disfavored as the possible sources of observed UHECR, that monopolonia behave like superheavy particles, concentrating in the halo of our galaxy, and that a presence of UHE photons in the primary radiation is an inevitable signature of all Topological Defects. Necklaces are shown to be more reliable sources of UHECR than any other Topological Defects, known so far.

**Theoretical Activity in LNGS and Participation in Conferences**
The theoretical group participated in the organization of the LENS workshop in LNGS. The members of the theoretical group participated in the International conferences and gave the talks: V. Berezinsky presented a plenary talk at 19th International Texas Symposium on Relativistic Astrophysics and gave the invited talks at the CAPP meeting at CERN, at 10th Int. Symposium on very high energy cosmic rays at LNGS, and concluding talk at Astroparticle conference in Liebezell (Germany). M. Kachelriess gave the talks at 10th Int. Symposium on very high energy cosmic rays, at the Kazimierz conference (Poland): From the Planck scale to the electromagnetic scale" and at Astroparticle Physics Summer Institute , Aspen, USA.

### Journal and Proceedings publications of 1998

1. V.Berezinsky and M.Kachelriess, Ultra High Energy LSP.
Phys. Lett. B 422 (1998) 163.

2. V.Berezinsky and M.Kachelriess, Limiting SUSY QCD spectrum and its application for decays of superheavy particles.
Phys. Lett. B 434 (1998) 61.

3. V.Berezinsky, A.S.Joshipura and J.W.F. Valle, Gravitational violation of R-parity.
Phys. Rev. D 57 (1998) 163.

4. V.Berezinsky, P.Blasi and A.Vilenkin, Signatures of Topological Defects
Phys. Rev. D 58 (1998) 103515

5. V.Berezinsky (as a member of LVD collaboration), Muon-depth intensity relation
Phys.Rev. D 58 (1998) 092005

6. V.Berezinsky, Baryonic and Cold Dark Matter

Yadernaya Fizika 61 (1998) 1138

7. V.Berezinsky, M.Kachelriess and A.Vilenkin, Ultra High Energy Cosmic Rays from decaying relic particles.
Nucl Phys. B (Proc. Suppl) 70 (1999) 500.

8. V.Berezinsky, Ultra High Energy Cosmic Rays
Nucl. Phys. B (Proc. Suppl) 70 (1999) 419.

9. V.Berezinsky (in EASTOP collaboration), Study of horizontal air showers as a possiblr tool for UHE neutrino detection
Nucl. Phys.B (Proc.Suppl) 70 (1999) 509

10. V.Berezinsky, Solar neutrinos as highlight of astropartcle physics
Proc. 25th ICRC v.8 (1998) 59

11. V.Berezinsky, Ultra High Energy Cosmic Rays from decaying superheavy particles.
Workshop on observing giant cosmic ray airshower, AIP conf. proc. 433 (eds J.F.Krismanic, J.F.Ormes and R.E.Streitmatter) (1998) 279

12. G.Fiorentini, V.Berezinsky, S.Degl'Innocenti and B.Ricci, Bounds on hep neutrinos
Phys. Lett. B

13. M.Kachelriess, Are strongly magnetized degenerate stars cooling by axion emission?
Proc. Beyond the Desert 1997 (eds H.V.Klapdor-Kleingrothaus and H.Paes) (1998) 829.

14. M.Kachelriess, Neutrino self-energy and pair creation in neutron stars.
Phys. Lett. B 426 (1998) 89.

# 2 Lattice Gauge Theory

This activity has involved A. F. Grillo, M. P. Lombardo, R. Aloisio, G. Di Carlo, A. Galante, V. Azcoiti and E. Follana.

**Scientific work**

During last years the group has developed an approach to lattice simulations involving fermionic degreess of freedom based on a microcanonical approach (MFA) allowing the study of fermion-gauge system using computer resosurces far smaller than other methods. In 1997 this approach has been generalized in order to describe frmion-gauge systems at non zero baryonic density.

During 1998 the group has studied the phase diagram of the finite density QCD both in the small and large mass regions.

At small quark masses, the results show that the approach to the finite density normally used, namely the one that uses the Grand Canonical Partition Function (GCPF), suffers from subtle and dangerous numerical effects that in general make the results totally unreliable. This problem is present in all the approches to non zero density QCD. In addition, once these effects are properly accounted for, we have shown that the statistics needed to obtain sensible results in the parameter region where the qurk-gluon plasma transition is expected exponentially exceeds any reasonable computing resource. Namely,

the GCPF approach seems to be inadequate, independently from the numerical approach.

On the other hand, finite density QCD in the large mass region has been analytically solved using an approximation for gluon dynamics; numerical results have been obtained in the general case which are intersting and are being published.

Since September 1998, M. P. Lombardo joined the Laboratory, having her activity partly within the theoretical group. The research, devoted in general to phase transitions in particle physics, in the last four months of the year was concentrated on simple, yet significant models, for finite density theory, which are amenable to lattice calculations, in particular, the thermodynamics of four fermion models, which are well known within the nuclear physics community as relevant models for QCD. Further, a lattice study of the symmetries, transitions and thermodynamic of two color QCD, was carried on, the emphasis being on the nature of the microscopic vacuum and its relation with the physical observables. The insight provided by these simpler models can inspire QCD developments. In addition, as these models have real actions which can be implemented exactly on the lattice, they are also ideal testbeds for lattice QCD algorithms.

### Publications

1. "Continuous chiral transition in strongly coupled compact QED with the standard torus topology" , V. Azcoiti, G. Di Carlo, A. Galante, A.F. Grillo, V. Laliena; Phys. Lett. B416(1998)409.
2. " First Order Phase Transition in Finite Density QCD using the modulus of the Dirac Determinant" , R. Aloisio, V. Azcoiti, G. Di Carlo, A. Galante, A.F. Grillo; Phys. Lett. B428(1998)166
3. "Frustration in Finite Density QCD", R. Aloisio, V. Azcoiti, G. Di Carlo, A. Galante, A.F. Grillo; Phys.Lett. B435 (1998) 175-180.
4. "Investigation of a Toy Model for Frustration in Abelian Lattice Gauge Theory" , V. Azcoiti, G. Di Carlo, E. Follana; Int. J. Mod. Phys. **A**14 (1999) 1125
5. "Rigorous arguments against current wisdoms in finite density QCD", R. Aloisio, V. Azcoiti, G. Di Carlo, A. Galante, A.F. Grillo; Phys. Lett. B453 (1999) 275.

### Conferences

1. "Finite density QCD in the chiral limit" , R. Aloisio, V. Azcoiti, G. Di Carlo, A. Galante, A.F. Grillo; (Lattice 97), Nucl. Phys. B(Proc.Suppl)63(1998)442.
2. "Frustration in lattice gauge theory" , V. Azcoiti, G. Di Carlo, E. Follana; (Lattice 97), Nucl. Phys. B(Proc.Suppl)63(1998)688.
3. "Phase Transition(s) in Finite Density QCD", R. Aloisio, V. Azcoiti, G. Di Carlo, A. Galante, A.F. Grillo; Workshop on QCD at Finite Density: a Complex System with a Complex Action, Bielefeld 27-30 Apr 1998; Nucl.Phys. A642 (1998) 263-268.
4. "Finite density QCD with heavy quarks" , R. Aloisio, V. Azcoiti, G. Di Carlo, A. Galante, A.F. Grillo; (Lattice 98), HEP-LAT 9809186 to appear in Nucl. Phys.

B(Proc.Suppl).

**Publications of M.P. Lombardo**

1. "QCD at Finite Baryon Density", Proceedings of the workshop QCD at Finite Density:a Complex System with a Complex Action, Bielefeld, 27-30 Apr 1998, editor with F. Karsch, Nucl.Phys. **A642** ,1998.

**Conferences** 1. "Idee per un centro di fisica computazionale integrato nel territorio", Seminario Internazionale Attività Spaziali, Scuola Superiore Guglielmo Reiss Romoli, l'Aquila, October 16 1998 [2c]; 2. "The Phase Diagram of Two Colors QCD", invited talk at the RIKEN/BNL workshop on QCD Phase Transitions, Brookhaven, November 4 1998;

# GIGS.The Interferometric Station at LNGS

Antonella Amoruso[1,3], Luca Crescentini[2,3], Roberto Scarpa[1,3]

[1]Dip.to di Fisica, Univ.dell'Aquila, L'Aquila, Italy
[2]Dip.to di Scienze della Terra, Univ. di Camerino, Camerino (MC), Italy
[3]INFN - Gruppo collegato dell'Aquila , L'Aquila, Italy

## 1   Introduction

A geodetic interferometer is working in the underground laboratories since May 1994, apart from some interruptions due to system improvements. From December 1995 it is measuring the difference in deformation between two baselines (each 90-m long): the former is iso-oriented with the Apennines, while the latter is orthogonal to them. From February 1996 strain is continuously recorded at 0.5 Hz. The signal is dominated by long-term and seasonal deformations, Earth tides, and occasionally local and distant earthquakes. The instrument has already been described in previuos LNGS reports. At the beginning of 1997 new signals (strain changes with rising times up to 40 minutes) appeared. Tens of such events have been recorded from March 1997: a typical example of them is shown in the Figure 1.

The analyses of the whole 1996 and more than half 1997 show that slow strain changes are almost completely gathered in at least one sequence (Figure 2). In the same time period, after more than one year of usual diffused seismicity, four relevant *regular* seismic swarms occurred within a radius of 200 Km from the interferometer. The shown part of the Colfiorito swarm occurred in the same area of and preceded the main Umbria-Marche 1997-1998 seismic sequence.

The maximum magnitude of the events was about 4.1. The similarity between *slow* and *regular* cumulative number of events is impressive (see Figure 3) but the lack of direct causal connections between the occurrence of each *slow* event and any *regular* earthquake is suggested by the lack of correlation between the sequences, and, if the *slow* events occurred on a fault close to the interferometer, by the extremely small local amplitude of the static stress drop and of the elastic waves produced by the *regular* earthquakes.

There is no correlation between the *slow* events and meteorological data (such as pressure and precipitation, see Figure 4) or between *slow* events and water table.

Occurrence times of regional, shallow, intermediate, and deep world-wide events show no correlation with the *slow* events. For the sake of brevity, only data about deep earthquakes (having magnitude $\geq 5$ and depth $\geq 200$ Km) are shown (Figure 5).
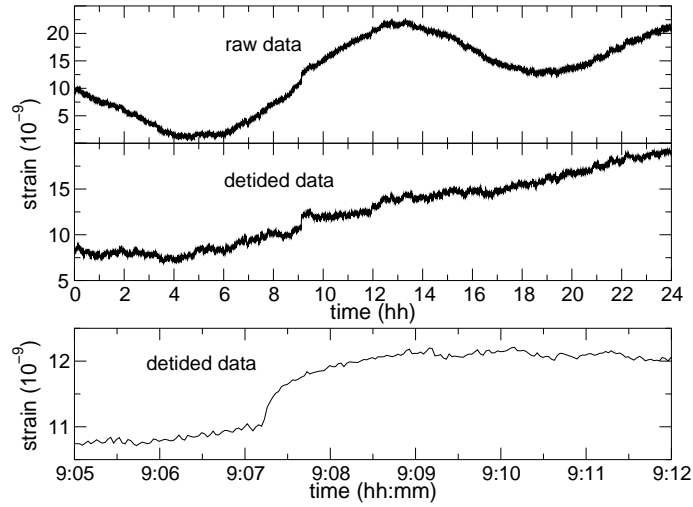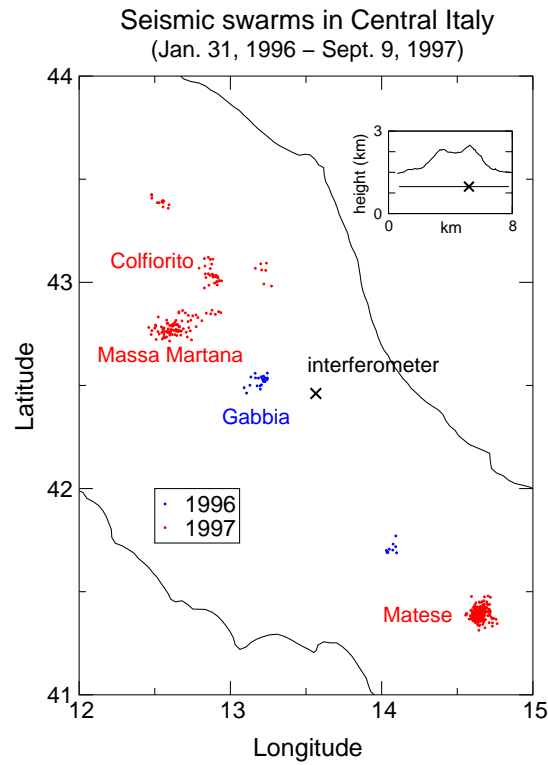
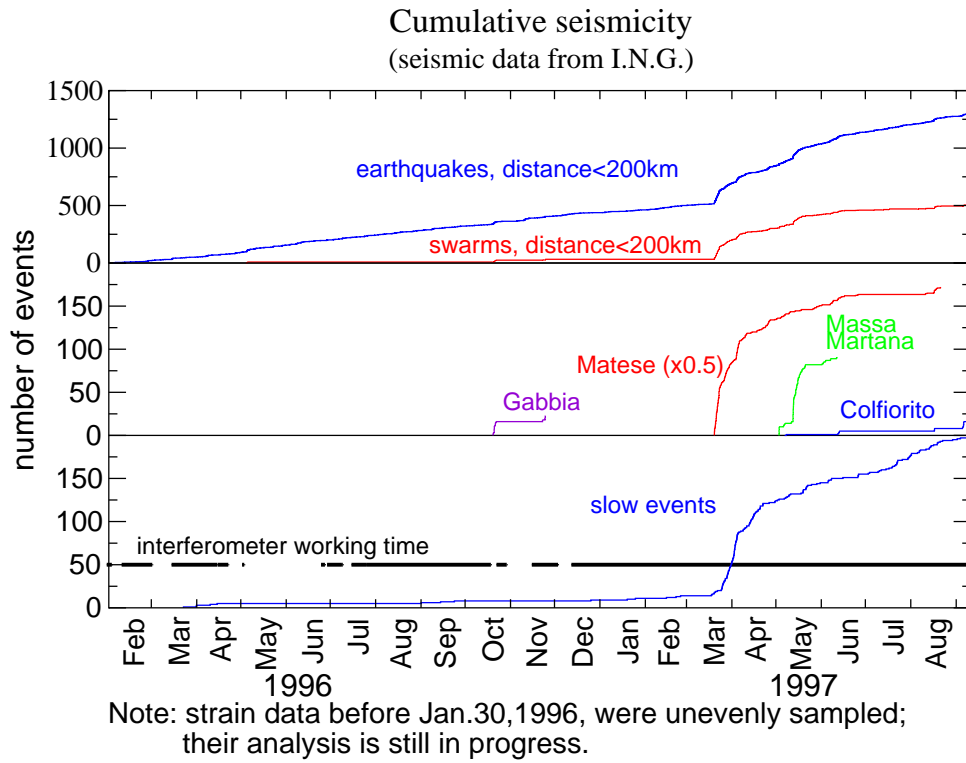Figure 1: Note the characteristic exponential shape of the signal.
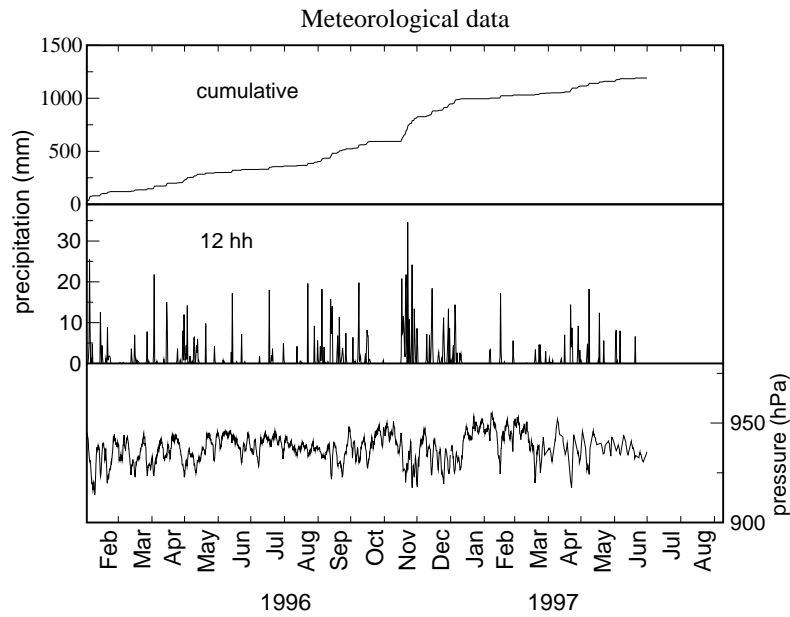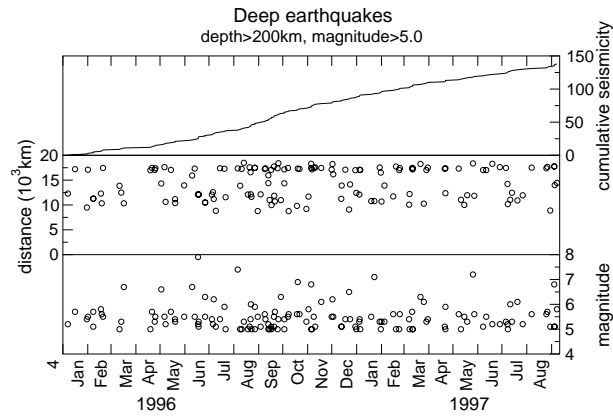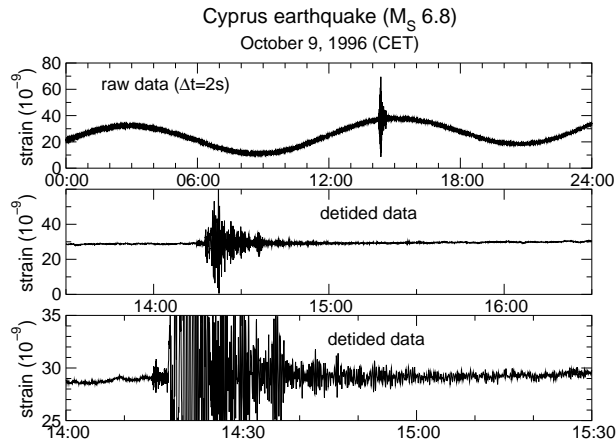


Figure 2

Figure 3



Figure 4

Figure 5



Figure 6

To exclude any ill-working of the instrument, permanent effects following the transit of wide seismic waves have been checked. In the Figure 6 an example of the response of the instrument is shown.

Amplitudes of the *slow* events are plotted vs their 1/e rising times (obtained by the exponential fit of each event) in the Figure 7. The existence of a scaling law suggests that sources are homogeneuous and clustered in space. Whatever its interpretation is, this scaling law can put a strong constrain in modelling slow earthquakes.

Strain signals produced by the *slow* events are compatible with missing *regular* earthquakes having magnitude about 6 at a distance of 150 Km (Matese area), and magnitude about 4 at a distance of 30 Km. Work is still in progress to go deep into and to extend our analyses. We think that if the *slow* events are actually small and originated locally, *slow* and *regular* earthquake sequences could be different aspects of a unique strain release episode affecting a large area in Central Italy, where *slow* seismicity could be a common way to release stress. If sources are located in the Matese area, the stress drop due to the *slow* events is by far larger than that caused by the *regular* events, maybe affecting the onset of northerly sequences, like the Massa Martana sequence and the Umbria-Marche
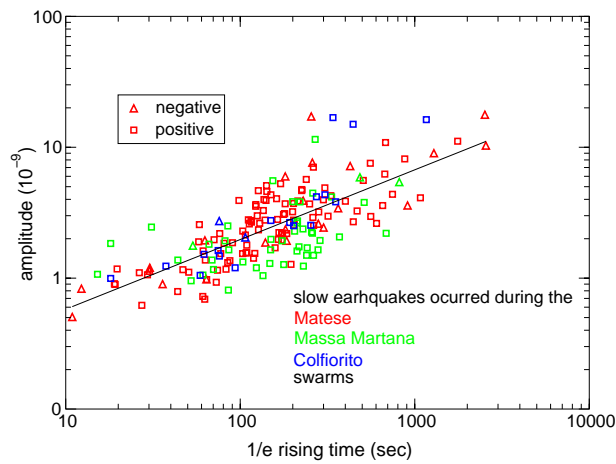
180

Figure 7

sequence.

Methodologies and procedures developed for analysing interferometric data have been improved and successfully applied to other problems, such as the 1915 Fucino earthquake and the 1908 Messina earthquake, whose fault mechanisms have been object of strong debates among researchers in the past.

# Publications and communications during 1998

1. Amoruso, A., L. Crescentini e R. Scarpa, "Inversion of source parameters from near- and far-field observatios: an application to the 1908 Messina and 1915 Fucino earthquakes, Italy", International Workshop "The resolution of geological analysis and models for earthquake faulting studies", Camerino, 3-6 giugno 1998.

2. Amoruso, A., L. Crescentini, and R. Scarpa, "Inversion of source parameters from near- and far-field observations: an application to the 1915 Fucino earthquake, central Appennines, Italy, " J. Geophys. Res., **103**, 29989-30000 (1998).

3. Amoruso, A., L. Crescentini, and R. Scarpa, "Inversione dei parametri sorgente del terremoto di Messina del 1908 mediante dati sismici e geodetici", XVII Convegno del Gruppo Naz. di Geofisica della Terra Solida, 1998.

4. Amoruso, A., L. Crescentini, and R. Scarpa, "Sismicit recente e possibili terremoti lenti in Italia centrale," XVII Convegno del Gruppo Naz. di Geofisica della Terra Solida, 1998.

5. Amoruso, A., L. Crescentini, and R. Scarpa, "Removing tidal and atmospheric effects from Earth deformation measurements", Geophysical Journal International (under revision).

6. Amoruso, A., L. Crescentini, and R. Scarpa, "Slow earthquakes and seismicity in Central Italy," American Geophysical Union Fall Meeting, S. Francisco, CA, Dec. 6-10, 1998.

# Tectonic deformation events and local seismicity in the Gran Sasso area of the central Apennines

Francesco Bella[a], Giuseppe Della Monica[a], Wolfango Plastino[a],
Roberto Scandone[a], Vittorio Sgrigna[a]

[a] Dipartimento di Fisica "E. Amaldi",
Università degli Studi "Roma Tre",
Via della Vasca Navale, 84, I-00146 Roma, Italy.

## Abstract

Geophysical equipment and investigations at LNGS concerning deformation phenomena of seismotectonic interest are described. Results obtained in 1998 are also reported.

## 1 Introduction

Investigations concerning deformation events of tectonic interest detected at three sites of the LNGS are carried out and correlated to local earthquakes. Deformation phenomena are studied through the continuous monitoring of some geophysical and geochemical parameters. Observations deal with the possibility to study the time and space earthquake occurence by the study of rock microfracturing process which takes place in the preparation focal area during preseismic period.

Such process gives rise to a nonelastic rock behaviour (dilatancy) in which volumetric strain increases relative to what would be expected from the elasticity. At the LNGS, the intermediate-term volumetric strain increase, involved in the thrust and deeper fault systems of the Gran Sasso chain, is studied by continuous ground tilt measurements. Shorter-term secondary effects, such as the emission of radioactive and nonradioactive gases during rock microfracturing, are also investigated through the monitoring of their content in groundwater by an automatic multiparametric equipment. In particular, temperature, electric specific conductivity, pH and $^{222}$Rn are also analyzed by this equipment, which performs a discrete sampling of the water collected in the interferometric area. Tiltmeters and automatic equipment for groundwaters analysis are also installed at the Gran Sasso area, outside the LNGS, for a better investigation of the above-mentioned phenomena of tectonic interest.

# 2  Results

During 1998, results obtained at LNGS and in the surrounding area (or related to the same investigations) have been summarized in the following.

## 2.1  Multiparametrical investigations in the Gran Sasso area

We have shown that new seismological data from the Latium-Abruzzi carbonatic platform, which includes the Gran Sasso chain, fit a block tectonic modelling previously proposed for this area on the basis of structural and paleomagnetic evidences [1]. A migration of earthquake foci has been also observed. Velocity values are similar to those obtained in other seismic regions (0.1 cm/s), demonstrating the slow propagation of a stress-strain field in such areas[1].

Aquifer-induced seismicity has been revealed in the Gran Sasso area [2]. It has been demonstrated that the cyclic ground water level changes may trigger small earthquakes in a region with high seismic potential. We observed a similar triggering but on the occasion of a sudden increase in such water table changes which were superimposed to the normal seasonal variations.

Some evidence of hydogeochemical anomalies obtained before strong earthquakes have been observed in Kamchatka (Russian Federation) [3].

## 2.2  Multiparametrical investigations in the LNGS

### 2.2.1  Experimental apparatus

The experimental apparatus consist of three tiltmeters and an automatic equipment for groundwater analysis.

The tilt sensors consist of two-component-horizontal-pendulum tiltmeters with a Zőllner bifilar suspension. They have been made using super Invar. The analog detecting system is constituted by an infrared laser beam and a 1024-photodiodes linear array of 0.5 inch long. The resolution is of 0.05 $\mu$rad. A digital acquisition system allows the tilt data to be collected hourly.

The multiparametric equipment for groundwater analysis has been made by stainless steel with pneumatic valves. It is monitored by a computer. The automatic equipment consists of a system for water geochemical analysis and gas extraction. This system includes the sensors, a cylindrical container (where the water flows) and an expansion chamber where the stripped gases are gathered from the water. A detecting system includes a Lucas cell made in perspex having an external shape of truncated cone where in the inside surface is spread ZnS(Ag), with tickness of 8-10 mg/cm$^2$[4]. The water sampling period is of 12h.

### 2.2.2  Ground tilt

A 2-D model for slow crustal movements, including creep-related tilt and strain anomalies associated to earthquakes, has been proposed [5]. The model describes the earth-

quake preparation through the rheological properties of viscoelastic fault gouge (separating crustal rigid blocks) studied by constitutive equations of standard linear solid [1].

Ground tilt as well as electromagnetic emissions and groundwater level variations have been correlated to a small earthquake (M=3.0) occurred in the Gran Sasso chain[6]. Actually, we are trying to determine the direction of local stress field through the evaluation of the principal stresses $\sigma_1$, $\sigma_2$, $\sigma_3$ obtained from the ground tilt trends. Moreover, tilt data are under study to reveal variations possibly correlated with the Umbria-Marches seismic sequence of 1997-1998.

Finally, a new 2-D model for the real geodynamic structures of the Gran Sasso is also in preparation.

### 2.2.3   Radon content in groundwater

During 1998, the monitoring of hydrogeochemical parameters in the LNGS (started since August 1995), has pointed out the gradual return of the signals to the background level already obtained in 1997, just before the Umbria-Marches seismic sequence which started on September 1997.

In the period May 1996 - September 1997 the hydrogeochemical parametrs emphasized a correlation with the aquifer dynamics. During this period, the electric specific conductivity showed an anomalous decrease on the occasion of some earthquakes occurred in October 1996 at 40 km N-NW from LNGS [4].

From May 1997 to September 1997 it was observed an anomalous oscillation in the radon content which decreased slowly up to the normal background of autumn 1998. In this sense, this anomaly can be associated both to the earthquake preparation and postseismic deformation of the above mentioned Umbria-Marches seismic sequence.

The phenomenology appears to be justfied by a variation in the gas concentration in groundwater, particularly $CO_2$ which is a well known radon gas-carrier.

The radon relaxtion time, due to the pertubation related to the seismic sequence of the Umbria-Marches earthquake, has been estimated to be 14 months.

# 3   Conclusions

Experimental and theoretical results at LNGS obtained during 1998, as well as the ongoing investigations reveal a good agreement between geodynamic, rheological, hydrogeochemical and seismological data.

These correlations are also confirmed by the same investigations carried out in the Gran Sasso area of the carbonatic platform.

# References

[1] F. Bella, M. Caputo, G. Della Monica, A. Lisi, W. Plastino, R. Scandone, V. Sgrigna, *Crustal blocks and seismicity in the central Apennines*, il Nuovo Cimento C, 21, 6, 1998.

[2] F. Bella, P.F. Biagi, M. Caputo, E. Cozzi, G. Della Monica, A. Ermini, W. Plastino, V. Sgrigna, *Aquifer-induced seismicity in the central Apennines (Italy)*, Pure appl. Geophys., 153, 1, 179-194, 1998.

[3] F. Bella, P.F. Biagi, M. Caputo, E. Cozzi, G. Della Monica, A. Ermini, E.I. Gordeev, Y.M. Khatkevich, G. Martinelli, W. Plastino, R. Scandone, V. Sgrigna, D. Zilpimiani, *Hydrogeochemical anomalies in Kamchatka (Russia)*, Physics and Chemistry of the Earth, 23, 9/10, 921-926, 1998.

[4] F. Bella, C. Azzi, R. Bella, G. Della Monica, W. Plastino, R. Scandone, V. Sgrigna, *Tectonic deformation events and local seismicity in the Gran Sasso area of the central Apennines*, LNGS Annual Report, 169-178, 1997.

[5] F. Bella, M.Caputo, G. Della Monica, W. Plastino, V. Sgrigna, Yu. P. Vaveluk, T. B. Yanovskaya, *A 2-D model for tilt and strain fields associated to earthquakes in crustal block structures*, Phys. Earth and Planet. Int., 106 (1-2), 155-164, 1998.

[6] F. Bella, P.F. Biagi, M. Caputo, E. Cozzi, G. Della Monica, A. Ermini, W. Plastino, V. Sgrigna, *Anomalies in different parameters related to the M=3.0 Gran Sasso earthquake (1992)*, Physics and Chemistry of the Earth, 23, 9/10, 959-964, 1998.

# TRIS. A search for distortion in the spectrum of the Cosmic Microwave Background

R.Baselli[c], G.Boella[a], G.Bonelli[b], P.Buratti[c],
F.Cavaliere[a], M.Gervasi[a], A.Lagostina[a], A.Passerini[a],
G.Sironi[a], A.Vaccari[a], M.Zannoni[a]

[a] Physics Dept. G.Occhialini - GIFCO Unit - Universita' di Milano Bicocca - Italy
[b] IFCTR / CNR - Milano - Italy
[c] Universita' degli Studi di Milano - Italy

**Abstract**

TRIS is a set of three absolute radiometers we use to measure the temperature of the Cosmic Microwave Background at 0.6, 0.82 and 2.5 $GHz$. Goal of the experiment is the detection of a deviation from a Planck distribution in a frequency region close to 1 $GHz$. A positive detection should provide direct information on $\Omega_b$, the baryon density of the Universe. We discuss the improvements of the system we recently completed: sensitivity is sufficient to detect distortions with a minimum amplitude of 8%, in a region where the limits presently available are close to 30%.

## 1 Introduction

The scientific goal of TRIS is to find out spectral distorsions (deviations form a Plank distributions) in the spectrum of the Cosmic Microwave Background (CMB) in the frequency region close to 1 $GHz$. A positive detection in fact should allow a direct measurement of $\Omega_b$, the baryon density of the Universe (for a general discussion see [1] and references therein). To achieve this goal, we measure the absolute temperature of the sky at three frequencies, 600 MHz, 820 MHz and 2.5 $GHz$ using a set of three absolute radiometers installed at Campo Imperatore and disentangle the CMB from other components of the diffuse background (galactic synchrotron and bremstrahlung emission, blend of unresolved extragalactic radiosources) taking advantage of the different spatial and frequency distribution of the various components. Details of the experiment and its scientific motivations have been already presented ([3], [2], [5]) in various occasions and can be found also in the LNGS annual reports of past years. Here we give a description of the step forward we made in 1998.

187

# 2 Modes of operation of TRIS

The radiometers at Campo Imperatore are used in two *modes*.

## 2.1 Drift scan Mode

Drift scans are differential measurements of the sky temperature made with an angular resolution of 15°, at 600 MHz, 820 MHz and 2.5 $GHz$, while the sky transits through the antenna beams of the three radiometers set on the meridian at zenith angle $\theta$ (this is equivalent to analyze the sky temperature along a strip of right ascension $0 \le \alpha \le 24$ h at declination $\delta = \lambda_{CI} - \theta$, where $\lambda_{CI} = 42^0$ is the latitude of Campo Imperatore).

To get sufficient statistics at least five, clean (no radionterferences, no antenna mismatch caused by dew, rain or snow), 24 h long, drift scans must be recorded at each zenith angle. Observations are repeated six months apart to recognize and cut the sun contribution.

This is a mode of operation which does not require the use of liquid helium to produce a known reference level comparable to the sky temperature and to fix the zero level of the scale of temperature. When TRIS is in this mode data are recorded automatically by a PC, therefore the system can run unattended for long periods. The quality of the data can be checked and the recorded files are transferred to Milano via a phone link and modem.

## 2.2 Absolute measurements

. The absolute temperature of the sky is measured at various points along the strips previously studied with the *drift scans* mode, using *primary* calibrators which require large quantities of liquid helium ($\sim$300 l/week/radiometer) for cooling the system front end and fixing the zero level of the scale of temperature. Absolute measurements are made preferentially at nightime to cut completely the sun contribution and require many sorts of ancillary observations, dedicated to the evaluation of the environment contributions (atmosphere, ground, radio interferences).

# 3 Present Status of the experiment

In 1998 the following activities have been performed:

i)all the receivers have been completely refurbished and their thermal stabilization improved,

ii)the construction of a dedicated 820 MHz primary calibrator began (so far at 820 MHz we used a modified 600 MHz unit)

iii)the construction of *secondary* calibrators, less accurate but portable has been decided and is now unserway. These calibrators can be brought at Campo Imperatore in winter when the road is closed by snow and the transportation of large quantities of liquid helium impossible,

iv)a system for measuring the level of olinear polarization of the sky diffuse radiation has been tested and is now ready for implementation

v)a stable data link, (phone plus modem), has been established between Campo Imperatore and Milano.

The refurbished 820 MHz system is now running continously since November 1998. Data are collected and transferred by phone twice a week in Milano where the analysis is performed. In spite of the heavy snow which this year covered Campo Imperatore we have been able to get useful data. The refurbished systems at 600 MHz and 2.5 GHz are now being completed and will be brougth to Campo Imperatore respectively by mid February and mid March 1999

In October 1998 a description of TRIS and preliminary sample of data have been presented at the 3K Cosmology Euroconference held in Rome.

# 4   Future plans for TRIS

Considering that the system is now running regularly we have the following plans:

- January - May 1999: drift scans along $\delta = +42^o$ at 600 Mhz, 820 MHz and 2.5 GHz. Absolute measurements using the secondary calibrator

- June - July 1999: first run of absolute measurements at the same frequencies

- September - October 1999: second run of absolute measurements

- November 1999: modification of the mounts of the antennae: the beam axis will oscillate along the meridian between $\theta = 48^0 N$ and $\theta = 22^o S$ allowing to scan in 24 h the sky between $\delta = 12^o$ and the North Celestial Pole

- December 1999 - May 2000: drift scans between $\delta = 20^0$ and $\delta = 90^o$

- June-July 2000: absolute measurements

- September-October 2000: absolute measurements and measurements of the environmental contributions

- December 2000 - April 2001: drift scans

- May 2001: end of TRIS observations

- June 2001 - December 2002: analysis of the data

# 5   List of Milano Publications related to TRIS

1. G. Sironi, M. Limon, G. Marcellino, G. Bonelli, M. Bersanelli, G. Conti, K. Reif 1990: *The Absolute Temperature of the Sky and the Temperature of the Cosmic Background Radiation at 600 MHz*, Ap. J. **357**, 301

2. G. Sironi 1990: *A Search for Distortions in the Spectral distribution of the Cosmic Background Radiation at Low Frequencies*, Memorie S.A.It. **61**, 161

3. G. Sironi, L. Celora 1990: *Absolute measurements of the Cosmic Background Radiation at low frequencies*, Nuovo Cimento B **105**, 1031

4. G. Sironi, P. Inzani, M. Limon, C. Marchioni 1990: *Evaluation of small signals with a differential radiometer (with application to radio observations at 2.5 GHz)*, Measur. Sci. Tech. **1**, 1119

5. G.Sironi, G.Bonelli, M.Limon 1991: *Measured temperature of the South Celestial Pole and the temperature of the CBR at 36 and 12 cm wavelength*, in Physical Cosmology (A.Blanchard Ed.) - Editions Frontieres - Gif sur Yvette - pag. 559

6. G.Sironi, G.Bonelli, M.Limon 1991: *The Low Frequency Spectrum of the CBR*, Annals N.Y. Acad. Sci. **647**, 791

7. G.Sironi, G.Bonelli, M.Limon 1991: *The Brightness Temperature of the South Celestial Pole and the Temperature of the Cosmic Background Radiation measured at 36.6 and 12 cm wavelength*, Ap. J. **378**, 550

8. G.F. Smoot, G. De Amici, M. Bensadoun, A. Kogut, S. Levin, M. Limon, G. Sironi, M. Bersanelli, G. Bonelli 1991: *The Long Wavelength Spectrum of the Cosmic Microwave Background*, Antarctic J. : **XXVI**, 286

9. G.Sironi, G.Bonelli, M.Gervasi 1992: *The CBR frequency Spectrum below 1 GHz. Recent Results and new observations*, Highlights in Astronomy **9**, 297

10. G.Sironi, G.Bonelli, M.Gervasi 1993: *Spectral Distortions in the Frequency Distribution of the Cosmic Background Radiation*, PASP : **51**, 541

11. G.Sironi, G.Bonelli, M.Limon 1992: *Measurements of the absolute temperature of the Relic Radiation - Observations at 0.6, 0.82 and 2.5 GHz from Alpe Gera and the South Pole*, Nuovo Cimento **15 C**, 983

12. M. Bensadoun, G.F. Smoot, M. Bersanelli, G. De Amici, A. Kogut, S. Levin, M. Limon, A. Vinje, G. Sironi, G. Bonelli 1993: *Low Frequency Measurements of the Cosmic Microwave Background Spectrum*, Ann. N.Y. Acad. Sci. **688**, 792

13. M. Bersanelli, G. Bonelli, G. Sironi, S. Levin, G. Smoot, M. Bensadoun, G. De Amici, M. Limon, W. Vinje 1993: *Absolute measurements of the Cosmic Microwave Background from the Amundsen - Scott South Pole Station*, Antarctic J. **XXVIII**, 306

14. G. De Amici, G. Smoot, M. Bensadoun, M. Limon, W. Vinje, M. Bersanelli, G.Bonelli, G. Sironi 1993: *Low Frequency Maps of the galactic radio emission*, Antarctic J. **XXVIII**, 308

15. G. De Amici, S. Torres, M. Bensadoun, M. Bersanelli, G. Dall' Oglio, M. Limon, G. Smoot, G. Sironi, T. Villela, C. Witebsky 1994: *A research program to map the Galactic emission at low frequencies*, Astrophysics Space Sci. **214**, 151

190

16. G. Sironi, G. Bonelli, G. Dalloglio, E. Pagana, M. Perelli 1995: *Measurements of the CBR frequency spectrum at low frequencies. Ground and Space Observations*, Ap. Lett. Comm.: **32**, 31

17. G. Bonelli, M. Gervasi, G. Giardino, G. Sironi, M. Zannoni 1995: *Low frequency observations of the cosmic microwave background radiation: the Campo Imperatore Experiment*, Ap. Lett. Comm.: **32**, 15

18. C. Ajello, G. Bonelli, G. Sironi 1995: *Evaluation of the Earth's Atmospheric Brightness Temperature at Decimetric Wavelengths*, Ap. J. Suppl. : **96**, 643

19. M. Gervasi, G. Bonelli, G. Sironi, S. Casani, F. Cavaliere, A. Passerini 1995: *An absolute cryogenic calibration source for a 2.5 GHz radiometer*, Rev. Sc. Inst. : **66**, 4789

20. G. Bonelli, F. Cavaliere, G. Giardino, M. Gervasi, F. Monforti, S. Mussio, A. Passerini, G. Sironi, F. Villa, M. Zannoni 1997: *Observations of the Cosmic Background Radiation. Search for spectral distortions and residual polarization*, Nuovo Cimento **20C**, 673

21. M.Zannoni, G.Boella, G.Bonelli, F.Cavaliere, M.Gervasi, A.Lagostina, A.Passerini, G.Sironi, A.vaccari 1998: *TRIS EXPERIMENT: a search for spectral distortions in the CMB spectrum close to 1 GHz*, Proc. 3 K Cosmology Euroconference - Rome October 1998, AIP Conf. Proc. : in press

22. G.Boella, G.Bonelli, M.Gervasi, A.Passerini, G.Sironi, A.Vaccari, M.Zannoni 1998: *TRIS: a search for distortion in the spectrum of thje Cosmic Microwave Background - a brief description*, LNGS Report

# 6   Acknowledgements

# References

[1] B.Partridge : 3 K: The Cosmic Microwave Background Radiation - Cambridge University Press, Cambridge (UK), 1995.

[2] G.Sironi et al. 1995: Astro. Lett. and Communications **32**, 31.

[3] G.Bonelli et al. 1995: Astro. Lett. and Communications **32**, 15.

[4] G.Sironi et al. 1993: PASP **51**, 541.

[5] M.Zannoni, G.Boella, G.Bonelli, F.Cavaliere, M.Gervasi, A.Lagostina, A.Passerini, G.Sironi, A.vaccari 1998: TRIS EXPERIMENT: a search for spectral distortions in the CMB spectrum close to 1 GHz, Proc. 3 K Cosmology Euroconference - Rome October 1998, AIP Conf. Proc. : in press